XXII Congreso de Física Estadística

FisEs'18

Libro de Resúmenes

Book of Abstracts

Madrid, 18 - 20 de octubre de 2018

XXII Congreso de Física Estadística

FisEs'18

Libro de Resúmenes

Book of Abstracts

Madrid, 18–20 de Octubre de 2018

Preparado por los autores usando el sistema de composición LaTeX/
Typesetting by the authors using LaTeX document preparation system

XXII Congreso de Física Estadística (FisEs'18) – Libro de Resúmenes/*Book of Abstracts*
Editado por/*Edited by*: F. J. Arranz (Universidad Politécnica de Madrid)
`https://fises18.gefenol.es/`

La Reunión de Física Estadística se viene celebrando, con intervalos de año y medio, desde 1987, año en el que tuvo lugar la primera edición en Barcelona. Desde el año 1996 esta reunión es conocida también como FisEs. Con FisEs'18 se cumplirán, por tanto, 31 años de reuniones.

Ha sido organizado siempre por distintos grupos de investigación, repartidos por toda la geografía nacional, y ha reunido a una media de 150 investigadores y a conferenciantes invitados de primera talla mundial.

En torno a FisEs se creó, en el año 2001, el Grupo Especializado de Física Estadística y No Lineal (GEFENOL), dentro del marco de la Real Sociedad Española de Física. Su principal objetivo es promover la Física Estadística y No Lineal en España y el intercambio científico y académico entre los grupos que investigan en estas disciplinas.

The Statistical Physics Conference takes place every one a half years since 1987, when the first edition was held in Barcelona. Since 1996 the Conference is also known as FisEs (Statistical Physics acronym in Spanish). Therefore, with the current FisEs'18, it will reach 31 years of conferences.

The Conference has always been organized by different nationwide research groups, gathering about 150 researchers on average, including world-class invited speakers.

Around FisEs Conferences it was created in 2001 the Specialized Group of Statistical and Nonlinear Physics (GEFENOL, acronym in Spanish), under the aegis of the Royal Spanish Society of Physics. Its main aim is to promote the Statistical and Nonlinear Physics in Spain and the scientific and academic exchange between the groups that research in these disciplines.

Reuniones de Física Estadística previas/*Previous Statistical Physics Conferences*

I Física Estadística'87	Barcelona, mayo de 1987/*May 1987*
II Física Estadística'88	Palma de Mallorca, septiembre de 1988/*September 1988*
III Física Estadística'90	Badajoz, mayo de 1990/*May 1990*
IV Física Estadística'91	Gijón, septiembre de 1991/*September 1991*
V Física Estadística'93	El Escorial, mayo de 1993/*May 1993*
VI Física Estadística'94	Sevilla, octubre de 1994/*October 1994*
VII Física Estadística (FisEs'96)	Zaragoza, mayo de 1996/*May 1996*
VIII Física Estadística (FisEs'97)	Getafe, septiembre de 1997/*September 1997*
IX Física Estadística (FisEs'99)	Santander, mayo de 1999/*May 1999*
X Física Estadística (FisEs'00)	Santiago de Compostela, septiembre de 2000/*September 2000*
XI Física Estadística (FisEs'02)	Tarragona, mayo de 2002/*May 2002*
XII Física Estadística (FisEs'03)	Pamplona, octubre de 2003/*October 2003*
XIII Física Estadística (FisEs'05)	Madrid, junio de 2005/*June 2005*
XIV Física Estadística (FisEs'06)	Granada, septiembre de 2006/*September 2006*
XV Física Estadística (FisEs'08)	Salamanca, marzo de 2008/*March 2008*
XVI Física Estadística (FisEs'09)	Huelva, septiembre de 2009/*September 2009*
XVII Física Estadística (FisEs'11)	Barcelona, junio de 2011/*June 2011*
XVIII Física Estadística (FisEs'12)	Palma, octubre de 2012/*October 2012*
XIX Física Estadística (FisEs'14)	Ourense, abril de 2014/*April 2014*
XX Física Estadística (FisEs'15)	Badajoz, octubre de 2015/*October 2015*
XXI Fisica Estadística (FisEs'17)	Sevilla, marzo de 2017/*March 2017*

Comité organizador

Organizing Committee

Francisco Javier Arranz
Rosa María Benito (coordinadora/*coordinator*)
Florentino Borondo
Javier Ricardo Galeano
Juan Carlos Losada
Juan Manuel Pastor
Fabio Revuelta
Ana María Tarquis

Comité científico

Scientific Committee

Rosa María Benito (Universidad Politécnica de Madrid)
Javier Burguete (Universidad de Navarra)
Mario Castro (Universidad Pontificia de Comillas)
Pablo Ignacio Hurtado (Universidad de Granada)
Cristina Masoller (Universitat Politècnica de Catalunya)
Juan José Mazo (Universidad de Zaragoza)
María del Carmen Miguel (Universitat de Barcelona)
Alberto Pérez Muñuzuri (Universidad Santiago de Compostela)
José Manuel Romero Enrique (Universidad de Sevilla)
Miguel Ángel Rubio (Universidad Nacional de Educación a Distancia)
Juan Jesús Ruiz Lorenzo (Universidad de Extremadura)
Tomás Miguel Sintes (Universitat de les Illes Balears)

CONTENIDOS/*CONTENTS*

Conferencias invitadas

Invited Conferences

Random walks, flocking, large deviations and Bose-Einstein transition

Raúl Toral
Instituto de Física Interdisciplinar y Sistemas Complejos (IFISC), UIB-CSIC, 07122 Palma de Mallorca, Spain

Persistent random walks have been used to model self-propelled particles that are able to move with almost constant speed while randomly changing their direction of motion. Under the effect of interactions these self-propelled particles might exhibit self-organized motion where the majority of the particles move in the same direction, a behavior known as flocking.

In this talk I will first analyze a simple model of continuous-time persistent random walkers from the point of view of the large deviation theory, and I will show that it displays a phase transition that bears many similarities with the Bose-Einstein condensation. I will also present a mathematical model (taking ingredients from some well-known models of collective behavior in social systems) for self-propelled particles that under appropriate conditions are capable of collective motions.

---

[1] D. Escaff, R. Toral, C. Van den Broeck, K. Lindenberg, A continuous-time persistent random walk model for flocking, Chaos **28**, 075507 (2018).

[2] K. Proesmans, R. Toral, C. Van den Broeck, Bose-Einstein phase transition in persistent and run-and-tumble walks, arXiv: 1808.09715.

Statistical physical approach to ionic channels

José María Sancho
Dep. Física de la Matèria Condensada, Facultat de Física, Universitat de Barcelona, Martí i Franquès 1, 08028 Barcelona, Spain

Experiments on single ionic channels have contributed to a large extent to our current view on the function of cell membrane. In these experiments the main observables are the physical quantities: ionic concentration, membrane electrostatic potential and ionic fluxes, all of them presenting large fluctuations.

Real molecular channels are active pores with open and close dynamical states. By skipping their molecular complexity, here we present a simpler modeling based on statistical physics. These models present a minimum set of degrees of freedom, specifically ion positions and gate states, which follow Langevin equations constructed from a unique potential energy functional and by using standard rules of statistical physics. Numerical simulations are implemented and the results show that they have dynamical properties very close to those observed in experiments of Na and K molecular channels.

In particular, a significant effect of the external ion concentration on gating dynamics is predicted, which is consistent with previous experimental observations. Within this approach the excitability and oscillatory properties of a cell membrane have been studied.

Statistical physics of viral self-assembly

David Reguera[1,2]
[1]Departament de Física de la Matèria Condensada, Universitat de Barcelona, Martí i Franquès 1, 08028 Barcelona, Spain
[2]Universitat de Barcelona Institute of Complex Systems (UBICS), Barcelona, Spain

Viruses are fascinating biological entities, in the fuzzy frontier between life and inert matter. Despite the lack of sophisticated biological machinery viruses have found the way to efficiently infect the host, replicate, and egress the cell using, in most cases, a coordinated sequence of passive and spontaneous physical mechanisms. The understanding of those mechanisms and their thriving potential applications has stirred the appearance of the emerging field of Physical Virology.

The efficient construction of their protective protein shell, or *capsid*, is one of the most crucial steps in the replication cycle of a virus. The formation of the capsid typically proceeds by the spontaneous assembly of identical building blocks that can be achieved *in vitro* even in the absence of viral genetic material, thus opening the door to the production of artificial viral cages for innovative applications.

In this talk, I will summarize how ideas and techniques from statistical physics can help us understand how viruses work. In particular, I will discuss the remarkable physical principles behind the architecture, self-assembly, and mechanical properties of viruses. The understanding of the physical mechanisms that are common to a wide class of viruses could lead to the development of novel broad-spectrum routes to attack viral infections, based on interfering with their assembly. In addition, I will briefly summarize how this knowledge is opening the door to innovative biomedical and nanotechnological applications of viruses.

Más allá del "compendio del desorden": desde flujos granulares hasta el empaquetamiento de granos

Beyond the "epitome of disorder": From granular flows to grain packings

Diego Maza
Laboratorio de Medios Granulares, Depto. de Física y Matemática Aplicada, Universidad de Navarra, Navarra, España

Al comienzo de este siglo la aparición del concepto de "estado atascado" introdujo un nuevo paradigma sobre el porque sistemas de naturaleza muy dispar podían comportarse de forma comparable bajo la acción de cargas externas [1]. De este modo, sistemas diversos como dispersiones coloidales, pilas de arena, geles y espumas, o incluso el tráfico de vehículos, podrían quedar enmarcados bajo un enfoque singular que describiría sus propiedades comunes. Tal idea se desarrolló de forma sistemática definiendo estados como "estructuralmente atascados", introduciendo así un escenario común que los englobara a todos. Una de las características presente en todo sistema atascado sería por tanto la ausencia de una escala espacial donde poder acotar las variables macroscópicas cuyos valores medios pueden medirse en el laboratorio. Además, podría asumirse que muchos de ellos son "atérmicos", es decir, que las fluctuaciones térmicas a las que están sometidos son despreciables comparadas con a las energías de interacción entre sus componentes [2].

Sin embargo nuestro grupo ha demostrado recientemente que no todos los sistemas aparentemente atascados pueden ser descritos mediante este enfoque. Así, cuando los estados de atasco o bloqueo se alcanzan de forma súbita (sin que se aplique un proceso de "recocido" o envejecimiento), también existen propiedades comunes entre sistemas diversos pero que deben ser descritas de otra manera. Denominamos el pasaje a este nuevo estado como transición por embotellamiento o *cloggin transition* para diferenciarla de la *jamming transition* mencionada anteriormente [3].

En esta comunicación se resumirán algunos de los resultados numéricos y experimentales desarrollados por el Laboratorio de Medios Granulares para definir esta nueva calificación.

Early in this century, the introduction of the "jammed state" idea provides a new paradigm about how systems of a very diverse nature could behave similarly under the action of different types of loads [1]. Hence, systems as sand piles, colloidal dispersions, gels, foams or even vehicular traffic could be encompassed under a single framework that highlights their characteristic features systematically. If these jammed systems would be considered as formally equivalent, a unified description of all of them could be introduced. Importantly, almost all these systems lack an evident spatial scale where to calculate mean values that can be measured in the lab. Moreover, these systems are usually considered "athermic" because its thermal fluctuations are negligible compared with the interactions energies between its components [2].

However, our group has recently shown that not all seemingly jammed states can be described by this approach. Accordingly, when these states of blockage are suddenly reached (without there being an "annealing" process), there are common features between systems of a very different nature that can be compared using a new type of description. We have named this new regime as "clogging transition" to distinguish it from the jamming transition mentioned above [3].

In this presentation, we summarize some of the numerical and experimental results developed by the Granular Media Lab to introduce this denomination.

---

[1] A. J. Liu and S. R. Nagel (Eds.), *Jamming and Rheology – Constrained Dynamics on Microscopic and Macroscopic Scales*, (Taylor & Francis, London and New York, 2001).

[2] C. S. O'Hern, L. E. Silbert, A. J. Liu, and S. R. Nagel, Jamming at zero temperature and zero applied stress: the epitome of disorder, Phys. Rev. E **68**, 011306 (2003).

[3] I. Zuriguel, D. R. Parisi, R. C. Hidalgo, C. Lozano, A. Janda, P. A. Gago, J. P. Peralta, L. M. Ferrer, L. A. Pugnaloni, E. Clément, D. Maza, I. Pagonabarraga, and A. Garcimartín, Clogging transition of many-particle systems flowing through bottlenecks, Sci. Rep. **4**, 7324 (2014).

Critical regimes driven by recurrent mobility patterns of reaction-diffusion processes in networks

Àlex Arenas
Departament d'Enginyeria Informàtica i Matemàtiques, Universitat Rovira i Virgili, 43007 Tarragona, Spain

Reaction-diffusion processes have been widely used to study dynamical processes in epidemics and ecology in networked metapopulations. In the context of epidemics, reaction processes are understood as contagions within each subpopulation (patch), while diffusion represents the mobility of individuals between patches. Recently, the characteristics of human mobility, such as its recurrent nature, have been proven crucial to understand the phase transition to endemic epidemic states.

Here, by developing a framework able to cope with the elementary epidemic processes, the spatial distribution of populations and the commuting mobility patterns, we discover three different critical regimes of the epidemic incidence as a function of these parameters. Interestingly, we reveal a regime of the reaction-diffussion process in which, counterintuitively, mobility is detrimental to the spread of disease.

We analytically determine the precise conditions for the emergence of any of the three possible critical regimes in real and synthetic networks.

Relay synchronization in multiplex networks

I. Sendiña-Nadal[1,2], I. Leyva[1,2], R. Sevilla-Escoboza[3], V. P. Vera-Avila[3], P. Chholak[4], and S. Boccaletti[5]
[1]Complex Systems Group and GISC, Universidad Rey Juan Carlos, 28933 Móstoles, Madrid, Spain
[2]Center for Biomedical Technology, Universidad Politécnica de Madrid, 28223 Pozuelo de Alarcón, Madrid, Spain
[3]Centro Universitario de los Lagos, Universidad de Guadalajara, Jalisco 47460, Mexico
[4]Department of Mechanical Engineering, Indian Institute of Technology Bombay, Powai, Mumbai 400076, India
[5]CNR-Institute of Complex Systems, via Madonna del Piano 10, 50019 Sesto Fiorentino, Italy

Synchronization is one of the most important collective phenomena in many natural, social and technological systems becoming a very active research topic in network science. The modeling of complex systems using graph theory has improved our understanding of the interplay between the topology of the arrangement of the interacting units and the emerging dynamics [1]. The huge amount of new data collected in the last years has permitted a higher resolution network representation of real systems. In particular, the inclusion of new features shaped multi-layer representations, i.e., approaches in which the network units are arranged in several layers, each one accounting for a different kind of interactions among the nodes [2]. Multi-layer structures determine scenarios where novel forms of synchronization are relevant, as unidirectional coordination between layers [3], intra-layer or inter-layer [4, 5] synchronization.

Very recently, relay and remote synchronization (two very well known phenomena in chains, or small motifs, of coupled oscillators) have captured the attention of researchers [6]. This form of synchronization is observed when two units of a network (identical or slightly different) synchronize despite not being directly linked, and due instead to the intermediation of a relay mismatched unit. Relay synchronization is of outstanding relevance in the brain: The thalamus acts as a relay between distant cortical areas through the thalamo-cortical pathways, playing the role of a coordination hub that maintains the information flow. Recently, remote synchronization has been addressed in the context of complex networks revealing the extremely important role of network structural and dynamical symmetries in the appearance of distant synchronization as it was already suggested by the observation of zero-lag delays between mirror areas of the brain. Nevertheless, the interplay between symmetry, dynamics and xsmulti-layer structure remains still unexplored.

In this talk, we report on the realization of relay synchronization in multiplex networks, where inter-layer synchronization occurs between distant layers mediated by a relay layer that acts as a transmitter (see Fig. 1). We show that this transmission can be extended to higher order relay configurations, provided symmetry conditions are preserved. By first order perturbative analysis, we identify the dynamical and topological dependencies of relay synchronization in a multiplex. We find that the relay synchronization threshold is considerably reduced in a multiplex configuration, and that such synchronous state is mostly supported by the lower degree nodes of the outer layers, while hubs can be demultiplexed without affecting overall coherence. Finally, we experimentally validated the analytical and numerical findings by means of a multiplex of three layers of electronic circuits.

[1] S. Boccaletti, V. Latora, Y. Moreno, M. Chavez, and D.-U. Hwang, Complex networks: Structure and dynamics, Phys. Rep. **424**, 175 (2006).

[2] S. Boccaletti, G. Bianconi, R. Criado, C. I. del Genio, J. Gómez-Gardeñes, M. Romance, I. Sendiña-Nadal, Z. Wang, and M. Zanin, The structure and dynamics of multilayer networks, Phys. Rep. **544**, 1 (2014).

[3] R. Gutiérrez, I. Sendiña-Nadal, M. Zanin, D. Papo, and S. Boccaletti, Targeting the dynamics of complex networks, Sci. Rep. **2**, 396 (2012).

[4] R. Sevilla-Escoboza, I. Sendiña-Nadal, I. Leyva, R. Gutiérrez, J. M. Buldú, and S. Boccaletti, Inter-layer synchronization in multiplex networks of identical layers, Chaos **26**, 065304 (2016).

[5] I. Leyva, R. Sevilla-Escoboza, I. Sendiña-Nadal, R. Gutiérrez, J. M. Buldú, and S. Boccaletti, Inter-layer synchronization in non-identical multi-layer networks, Sci. Rep. **7**, 45475 (2017).

[6] V. Nicosia, M. Valencia, M. Chavez, A. Díaz-Guilera, and V. Latora, Remote synchronization reveals network symmetries and functional modules, Phys. Rev. Lett. **110**, 174102 (2013).

[7] I. Leyva, I. Sendiña-Nadal, R. Sevilla-Escoboza, V. P. Vera-Avila, P. Chholak, and S. Boccaletti, Relay synchronization in multiplex networks, Sci. Rep. **8**, 8629 (2018).

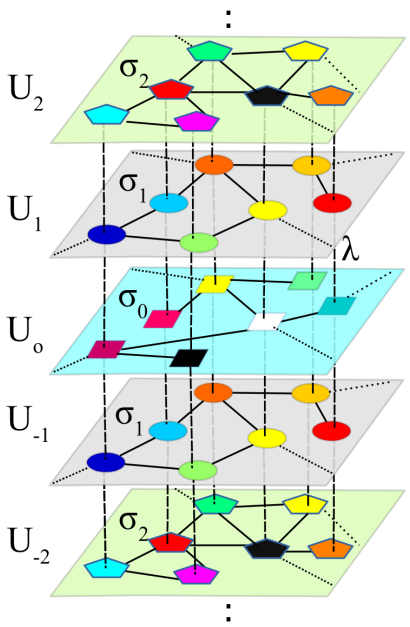

Fig. 1. Schematic representation of a multiplex of 5 layers, where each pair of layers k and $-k$ with $k = -2, -1, 0, 1, 2$, (painted with the same color) are networks of identical oscillators with the same topology and coupling strength and whose dynamical state is described by the variable $\mathbf{U}^k$ and $\mathbf{U}^{-k}$, respectively. The multiplex is symmetric with respect to the layer $k = 0$ that acts as the relay layer and the nodes are coupled to their replicas in the rest of layers with a different coupling strength.

Modelling the gut microbiota ecosystem

Rosa del Campo[1,2], Manuel Ponce-Alonso[1,2], Rafael Vida[3], Lucía García-Regueiro[3], Fernando Baquero[1,2], and Javier Galeano[3]

[1]Servicio de Microbiología, Hospital Ramón y Cajal, 28034 Madrid, Spain
[2]Instituto Ramón y Cajal de Investigación Sanitaria (IRYCIS), 28034 Madrid, Spain
[3]Grupo de Sistemas Complejos, Universidad Politécnica de Madrid, 28040 Madrid, Spain

The application of the recent molecular techniques based on massive nucleotide sequencing for the study of the composition of the intestinal microbiota has allowed us to discover an exciting and completely unknown ecosystem. In addition, it has been demonstrated that alterations in their composition or functionality are linked to numerous gastrointestinal and systemic diseases. In recent years, numerous studies have shown the influence of gut microbiota on human health and, consequently, numerous research lines have been established to optimize health influencing this ecosystem. However, the regulation rules of this bionetwork have not yet been deciphered, and this knowledge is crucial to be able to modulate the ecosystem.

The modulation of the microbiota needs not only physician approximations, but also biological, ecological, biochemical and physical. The microorganisms maintain a close relationship with the host and this complicates the restoration of the ecosystem.

In Spain, our group has been a pioneer in the use of faecal microbiota transference to cure the diarrhoea caused for *Clostridium difficile*. In this pathology, the therapy is completely successful, but has not shown efficacy in other pathologies such as Ulcerative Colitis. The recently publications show that the success of the microbiota transference for the replacement of the gut ecosystem in Ulcerative Colitis patients depends on numerous factors such as the composition of the donor's microbiota, the density of the patient's bacterial ecosystem, the technique of transference, etc. Our proposal is to optimize the management of the gut microbiota modulation to the incorporation of the knowledge of other scientific areas such as mathematical modelling.

Temporal organisation of extreme events: Data analysis and modelling

Annette Witt
Max Planck Institute for Dynamics and Self-Organization, 37077 Göttingen, Alemania

Extreme events as floods or draughts do often occur in temporal clusters. In this talk I will present the analysis and modelling of the timings of observed series of extreme events.

The data series are presented as binary symbol sequences where the symbol "1" presents time intervals with an extreme event and the symbol "0" time intervals without. The symbol sequences are characterised by the following measures from statistical physics and time series analysis: the Shannon entropy which is estimated in terms of the Lempel-Ziv complexity, the shape parameter of the Weibull distribution that best fits the event return times, and the strength of long-range correlations quantified by detrended fluctuation analysis (DFA). The event series will be modelled by peaks over threshold models, where the background signal will be chosen appropriately.

These methodical concepts will be applied to two sets of observational data: (i) to heart beat annotations obtained from 24-h electrocardiogram recordings of post-infarction patients where the symbol sequences represent arrhythmic and normal beats, and (ii) to a record of palaeofloods which occurred over a period of 9.3 thousand years in the southern Alps.

What lies beyond the surface tension?

Andrew Parry
Imperial College London, South Kensington Campus, London SW7 2AZ, United Kingdom

It is well known that near a free liquid-gas interface the pair correlation function contains a long-wavelength, Goldstone mode divergence, due to the fact that the position of a free interface can be translated without energy cost.

In the 1970s and 1980s, after much initial debate between proponents of microscopic and mesoscopic approaches, everyone came to agree that at these long wavelengths the energy cost of fluctuations is controlled by the surface tension which of course resit any increase in the surface area –this is the famous capillary-wave picture of an interface behaving like a taut drum skin. However the debate as to what happens beyond the long wavelength limit, that is what, if anything, lies beyond the surface tension, has continued and indeed escalated in recent years.

We discuss these issues and present results of a new microscopic approach based on the idea that, in addition to a Goldstone mode, the correlation function must also exhibit a hierarchy of resonances at specific wavelengths, the consequences of which are discussed in depth.

Using Lagrangian coherent structures to understand dynamics in multiphase flows with chemical reactions

Alexandra von Kameke, Sven Kastens, and Michael Schlüter
Institute of Multiphase Flows, Hamburg University of Technology, Eißendorfer Straße 38, 21073 Hamburg, Germany

Reactive bubbly flows are essential for many chemical industrial applications, e.g., hydrogenation, oxidation and chlorination reactions in bubble column and loop reactors. The efficiency of these reactors is mostly described by the yield and selectivity of the products and side products, which can be measured and estimated globally by various methods [1]. However, to achieve more reliable estimations it has to be taken into account that yield and selectivity depend sensitively on the coupling of the fluidic and microscopic transport processes and the reaction kinetics [2].

To study the dependency between local hydrodynamics, mass transfer and a chemical reaction at a single gas bubble we use Taylor bubbles which are a helpful simplification. This enables us to obtain quasi steady conditions with well-defined and reproducible flow structures. It also allows us to adjust the hydrodynamics in the bubble wake by changing the hydraulic diameter of the capillary and accordingly the Reynolds number of the flow. Taylor bubbles are elongated gas bubbles in channels, where the gas volume is forced into a bullet shape by the channel geometry and the continuous liquid which wets the glass wall. The rising velocity of Taylor bubbles is independent of the bubble volume and can be predicted by the dimensionless Eötvös number $\mathrm{Eo}_D = (\rho_L - \rho_G) g D_h^2 / \sigma$ of the fluidic system [3], where σ is the interfacial tension, ρ_L and ρ_G are the densities of the liquid and gaseous phases, g is the magnitude of the gravitational acceleration, and D_h is the hydraulic diameter of a channel.

In order to analyse the hydrodynamics in our reactor we calculate the Lagrangian coherent structures (LCS) and the finite-time Lyapunov exponent fields (FTLE-fields) from the measured two-dimensional velocity and concentration fields (PIV-LIF). LCS are defined to be the most repelling, attracting or shearing material lines of the tracer field in finite-time [4]. Here we focus on the so called hyperbolic LCS which correspond to the most attracting and repelling material lines. The LCS give us new insights into the flow topology for the finite time τ: imagine an artificial tracer released at some point in the fluid inside or outside the red repelling LCS in Fig. 1. After a time τ the tracers released inside the red LCS will still largely remain in the vortical structures close to the bubble bottom while tracers released below the red LCS will have been flushed away rapidly. This affects the local residence times of the chemical molecules dramatically. Especially the dissolved gas is thus highly dependent on the local hydrodynamics and thus prone to chemical reactions with longer timescales. This fact can have undesired effects on overall yield and selectivity of the targeted reaction. We find that the local residence times vary strongly for different Reynolds numbers of the flow. We show that these local effects of mixing intensity and residence times should be taken into account for the design and operation of bubbly flows in multiphase reactors. These local effects on residence behaviour analyzed by LCS might also play a role in other multiphase and chemical reactors where wake flow is the main cause for mixing.

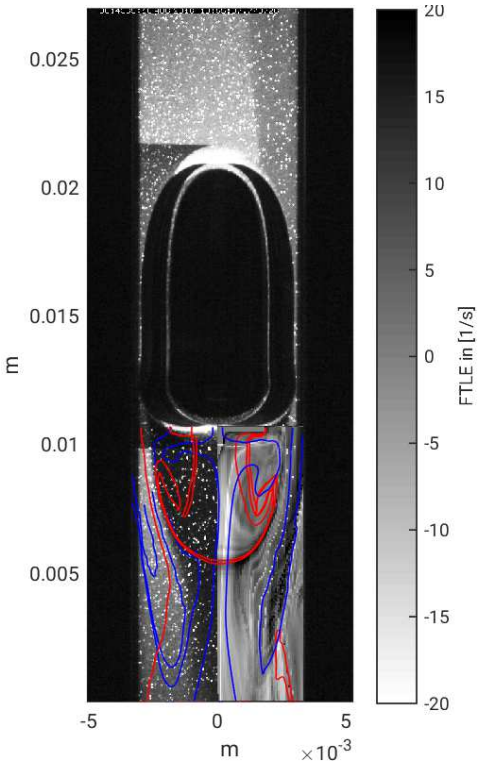

Fig. 1. LCS calculated from the velocity fields derived from Particle Image Velocimetry (PIV) data for a pipe channel diameter of $D = 6$ mm. The mean free velocity (sufficiently ahead of the bubble) is 6 mm/s. The red lines denote the repelling- and the blue lines the attracting LCS. On the right side below the bubble a combination of the forward and the backward FTLE-field $\Lambda_+ - \Lambda_-$ is shown in the background. The liquid is an aqueous solution of fluorescein sodium salt which shows a decrease in fluorescence intensity for higher amounts of dissolved carbon dioxide gas released from the bubble. This decrease is visualized using Laser Induced Fluorescence (LIF) [1].

[1] S. Kastens, J. Timmermann, F. Strassl, R. F. Rampmaier, A. Hoffmann, S. Herres-Pawlis, and M. Schlüter, Chem. Eng. Technol. **40**, 1494-1501 (2017).

[2] J. Baldyga and J. R. Bourne, *Turbulent Mixing and Chemical Reactions* (John Wiley and Sons Ltd., Chichester, UK, 1999).

[3] K. Hayashi, R. Kurimoto, and A. Tomiyama, Int. J. Multiphase Flow **37**, 241-251 (2011).

[4] K. Onu, F. Huhn, and G. Haller, J. Comput. Sci. **7**, 26-36 (2015).

Statistical characterization and control of nonlinear dynamics of semiconductor lasers

Jordi Tiana-Alsina, Carlos Quintero-Quiroz, M[a] Carme Torrent, and Cristina Masoller
Nonlinear Dynamics, Nonlinear Optics and Lasers (DONLL), Department of Physics (DFIS),
Universitat Politècnica de Catalunya (UPC), 08222 Terrassa, Spain

Semiconductor lasers with optical feedback are important and widely used devices. Because of the complex output signals that they generate can be exploited for several applications, including sensors, ultra-fast random number generation, reservoir computing and life science applications. In absence of external perturbations, semiconductor lasers show an stable output while subject to optical feedback or injection exhibits a rich variety dynamical behaviors.

The research in our lab is focused on the influence of optical feedback over semiconductor laser dynamics. We mainly study the low-frequency fluctuations (LFFS) and coherence collapse (CC) regimes. While the LFFs regime, in its slow time scale, is characterized abrupt and sudden dropout of the laser intensity followed by a gradual recovery, the CC collapse regime consists of fast and chaotic intensity fluctuations [1]. With the aim of quantitatively characterize the dynamical response of the system we apply new statistical tools based on information theory.

In this talk we aim to address the following questions: Can these regimes be quantitatively distinguished? Can the onset of each regime be quantitatively identified? We show that, by using three diagnostic tools applied to experimental intensity time-series we are able to quantify these transitions [2]. We use these tools to analyze how noisy fluctuations (close to lasing threshold) gradually transform into well-defined and apparently randomly distributed dropouts (i.e., LFFs regime, at higher pump currents), which then merge into fast and irregular fluctuations (i.e., CC regime at even higher pump currents). We also establish the coexistence region, where the dropouts alternate with stable noisy emission and find a region of pump currents where occasionally, extremely depth dropouts occur.

In the second part of the talk we investigate if a semiconductor laser with optical feedback is able to adapt its natural rhythm to an external weak periodic signal. Entrainment or locking phenomenon [3] between the natural frequency of the system and the external perturbation is typically achieved by increasing the amplitude of the forcing signal until the system adjusts its frequency to that of the forcing signal. However, it is not always possible to achieve the locked state by increasing the forcing amplitude, since too strong forcing might damage the system that one aims to control. Optimal conditions for entraining the system have been studied, and methods for achieving entrainment with minimum forcing power, minimum transient time, maximum coherence, and widest locking range will be discussed [4, 5]. To that end, the role of the modulation amplitude and frequency, and the role of the DC value of the laser pump current (that controls the natural spike frequency) in the entrainment quality will be analyzed.

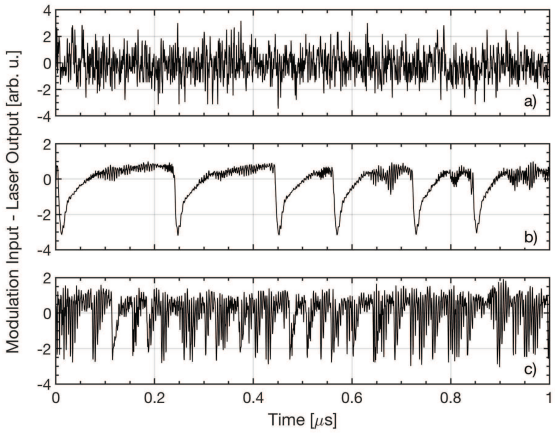

Fig. 1. Normalized to zero-mean and unit variance time-series for a semiconductor laser with optical feedback. (a) Noisy fluctuations, (b) low frequency fluctuations, and (c) coherence collapse regimes. The DC pump current normalized to the solitary lasing threshold is $I/I_{\rm th} = 0.95$, 1.02, and 1.20, respectively.

We are currently working in tuning of the system to a region where the laser spikes are rare and at the same time highly sensitive to an external perturbation. Find this region parameters could be significant for sensing applications.

[1] J. Ohtsubo, *Semiconductor Lasers. Stability, Instability and Chaos* (Springer, 2013), 3th edition.

[2] C. Quintero-Quiroz, J. Tiana-Alsina, J. Roma, M. C. Torrent, and C. Masoller, Characterizing how complex optical signals emerge from noisy intensity fluctuations, Sci. Rep. **6**, 37510 (2016).

[3] A. Pikovsky, M. Rosenblum, and J. Kurths, *Synchronization. A Universal Concept in Nonlinear Sciences* (Cambridge University Press, 2001).

[4] J. Tiana-Alsina, C. Quintero-Quiroz, M. Panozzo, M. C. Torrent, and C. Masoller, Experimental study of modulation waveforms for the entrainment of the spikes emitted by a semiconductor laser with optical feedback, Opt. Express **26**, 9298-9309 (2018).

[5] J. Tiana-Alsina, C. Quintero-Quiroz, M. C. Torrent, and C. Masoller, Experimental characterization of transitions between locking regimes in a laser system with weak periodic forcing, arXiv:1806.08950.

Comunicaciones orales

Oral Communications

The vaccination dilemma: A mean field analysis

Benjamin Steinegger[1], Alessio Cardillo[2,3], Paolo De Los Rios[1], Jesús Gómez-Gardeñes[3,4], and Alex Arenas[5]

[1]Laboratory for Statistical Biophysics, École Polytechnique Fédérale de Lausanne (EPFL), CH-1015 Lausanne, Switzerland
[2]Institut Català de Paleoecologia Humana i Evolució Social (IPHES), E-43007 Tarragona, Spain
[3]GOTHAM Lab, Institute for Biocomputation and Physics of Complex Systems (BIFI), University of Zaragoza, E-50018 Zaragoza, Spain
[4]Department of Condensed Matter Physics, University of Zaragoza, E-50009 Zaragoza, Spain
[5]Department d'Enginyeria Informática i Matemátiques, Universitat Rovira i Virgili, E-43007 Tarragona, Spain

Vaccination, whenever possible, is the most effective way to harness and prevent the spreading of a disease. Besides the protection bestowed at individual level, vaccination hinders as well the spreading at whole population level. Optimally, the individual decisions to vaccine would lead to the immunization of the entire population. However, instead of taking the vaccine, individuals may also rely on the others will to vaccinate. However, if too many of these *free riders* are present in the population, herd immunity is lost. This social *dilemma* characterizes the voluntary vaccination problem.

For analyzing social dilemmas, game theory is an adequate tool. Previous studies have combined game theory and epidemic spreading, developing coevolutionary models, in order to study the vaccination uptake [1]. Nevertheless, the analytical work has mainly focused on vaccination against pediatric diseases, such as measles, for example. In contrast, most of the articles having tackled the vaccination uptake against the seasonal influenza relied heavily on numerical simulations [2, 3, 4, 5], which makes it difficult to understand the underlying processes. For this reason, we set up a model incorporating the main features of the previous work, but that in addition allows for an analytical mean field solution [6].

The model is organized in the following way. We consider the fraction of infected agents in the previous year's influenza outbreak as an input of the model. From there, we set up a vaccination game, whose stationary state will define the vaccination coverage of the population. A subsequent outbreak of the disease with transmission probability β is then considered in the population. We obtain analytical expressions for the vaccine coverage y^* and the epidemic thresholds.

A crucial property of vaccines against the seasonal influenza is their effectiveness. The constant mutation of the virus strains makes it difficult to anticipate the subsequent season's form of the virus. Vaccine efficiency is usually only between 30% and 60%. Interestingly, the system shows a big tolerance regarding the vaccine quality, γ. As a matter of fact, a decrease in the effectiveness of the vaccine can even promote vaccination as one can see in Fig. 1. At first glance, the increase in vaccine uptake as effectiveness decreases may seem counterintuitive. However, this phenomena stems from the fact that the probability of getting infected becomes non negligible. In other words, as the vaccine efficiency decreases there is a competition between the increasing risk of getting infected and the reduced protection bestowed by the vaccine itself. Furthermore, we are able to show that the maximal vaccination coverage is reached when a further decrease in the vaccine effectiveness increases the infection probability by a larger amount for vaccinated than for not vaccinated agents. Hence, what may look as an irrational act at first sight is —instead— a rational individual decisions of agents striving to mitigate the infection pressure. In this sense, the corresponding effectiveness of the vaccine $(1-\gamma)$ as the maximal vaccine coverage $y^*_{\max}$ is reached, may be seen as a tolerance threshold of the system.

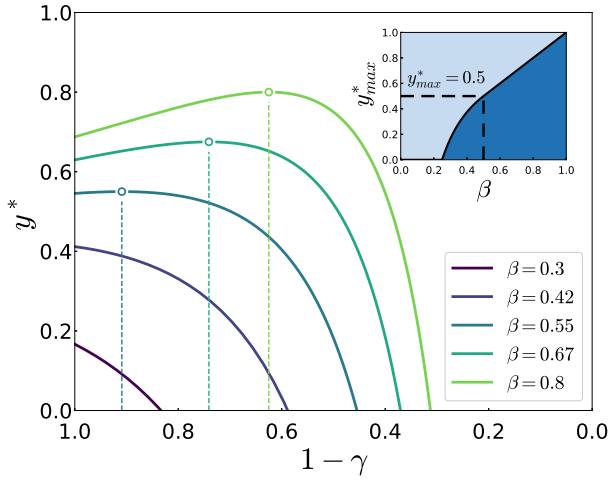

Fig. 1. Vaccination coverage at equilibrium y^* as a function of vaccine effectiveness $(1-\gamma)$. A perfect vaccine corresponds to $\gamma = 0$. Each line represents a different value of infection probability β. The maximum coverage $y^*_{\max}$ is denoted by a point and the dashed line delimits the tolerance range. The inset presents the maximum coverage $y^*_{\max}$ as a function of infectivity β. The color highlights the region where vaccination takes place or not.

Additionally to the high relevance of vaccine effectiveness in the voluntary vaccine uptake, we are recently witnessing the emergence of widespread anti-vaccine movements, which are mainly fueled by misconceptions and mischievous news about vaccines. A way for incorporating these movements in the model is the introduction of *zealots*; agents who unconditionally do not take the vaccine. Interestingly, the presence of the zealots has a non trivial detrimental effect on the aforementioned tolerance to decreasing vaccine quality.

[1] Z. Wang, C. T. Bauch, S. Bhattacharyya, A. d'Onofrio, P. Manfredi, M. Perc, N. Perra, M. Salathé, and D. Zhao, Phys. Rep. **664**, 1-113 (2016).

[2] F. Fu, D. I. Rosenbloom, L. Wang, and M. A. Nowak, Proc. R. Soc. B **278**, 42-49 (2011).

[3] B. Wu, F. Fu, L. Wang, PLoS ONE **6**, e20577 (2011).

[4] A. Cardillo, C. Reyes-Suárez, F. Naranjo, and J. Gómez-Gardeñes, Phys. Rev. E **88**, 032803 (2013).

[5] L. G. Alvarez-Zuzek, C. E. La Rocca, J. R. Iglesias, and L. A. Braunstein PLoS ONE **12**, e0186492 (2017).

[6] B. Steinegger, A. Cardillo, P. De Los Rios, J. Gómez-Gardeñes, and A. Arenas, Phys. Rev. E **97**, 032308 (2018).

Teoría cinética de sistemas confinados

Pablo Maynar, J. Javier Brey y María Isabel García de Soria
Área de Física Teórica, Universidad de Sevilla, España

En este trabajo abordamos el estudio de la dinámica de un sistema de esferas duras confinadas desde el punto de vista de la Teoría Cinética. Las colisiones entre las partículas pueden ser elásticas o inelásticas. Admitiendo caos molecular y que el sistema está confinado por paredes rígidas, se obtiene una ecuación de evolución para la función de distribución que tiene en cuenta los efectos del confinamiento [1] y que es válida para bajas densidades. Para densidades moderadas, también se puede formular una ecuación tipo Enskog teniendo en cuenta las correlaciones de posición entre las partículas que van a colisionar [2].

En el caso elástico se puede demostrar un teorema H para ambas ecuaciones: en el límite de tiempos largos, el sistema alcanza un estado caracterizado por una función de distribución Maxwelliana con el perfil de densidad que da la Mecánica Estadística de equilibrio. En el caso inelástico, se estudia una inestabilidad que aparece en el contexto de un medio granular confinado entre dos placas planas y paralelas separadas una distancia menor que el doble del diámetro de las partículas (para que el sistema sea casi bidimensional) al que se le inyecta energía por medio de una pared vibrante.

[1] J. J. Brey, P. Maynar, and M. I. García de Soria, Kinetic equation and nonequilibrium entropy for a quasi-two-dimensional gas, Phys. Rev. E **94**, 040103(R) (2016).

[2] P. Maynar, M. I. García de Soria, and J. J. Brey, The Enskog equation for confined elastic hard spheres, J. Stat. Phys. **170**, 999-1018 (2018).

Field theory for recurrent mobility

José J. Ramasco[1] , Mattia Mazzoli[1], Alex Molas[1], Maxime Lenormand[2], and Pere Colet[1]
[1]Instituto de Física Interdisciplinar y de los Sistemas Complejos (IFISC), CSIC-UIB, Campus UIB, 07122 Palma de Mallorca, Spain
[2]Irstea, UMR TETIS, 500 rue JF Breton, FR-34093 Montpellier, France

Mobility flows are mathematically encoded using the so-called Origin-Destination (OD) matrices. Given a set of geographical areas, such matrices can be seen as weighted networks in which the nodes are the unit areas and the links point from the origin to the destination of the flow (see [1] for a recent review). Since these are recurrent mobility flows, these areas correspond to home and work locations, and besides the morning direction the flows also occurs on the opposite direction in the afternoon. These are therefore spatially embedded networks for which factors like the population density, job opportunities, location and distance play a fundamental role. Several models have been proposed in order to obtain the flows from these basic variables. The bet is high since determining transport demand is fundamental for infrastructure building and urban planning.

In this work, we introduce a new approach to the topic. It is based on the observation that the flows can be represented as vectors pointing from the origin to the destination, and that these elementary vectors can be summed to produce an average field in every unit area. This mechanism is illustrated for London in Fig. 1 with ODs coming from Twitter data, where each unit cell of 1×1 km^2 is depicted with its corresponding average vector. Furthermore, we found that this vector field fulfills the Gauss (divergence) theorem and also that its rotational is nearly zero in all the space. The first feature allows us to study the flux around different closed perimeters, we used essentially circles of different radius around the center of the cities. The classical models to reproduce OD matrices are then employed to generate fields and their results are tested against the empirical fields. The flux produced by a gravity model with an exponentially decaying deterrence function with the distance fits much better than the same model with other deterrence functions or the radiation model.

Additionally, the fact that the rotational is almost zero everywhere allows us to define a potential in the space reducing, thus, the dimensionality of the problem. The maximum of the potential is located in the center of the cities, and then it decays as one gets further. Interestingly, the extrema of the potential can be used to define different mobility attraction areas and to delimit the areas of influence of different cities as it can be seen in the case of the Manchester-Liverpool conurbation (Fig. 2). The results of this work will appear soon in a coming paper [2].

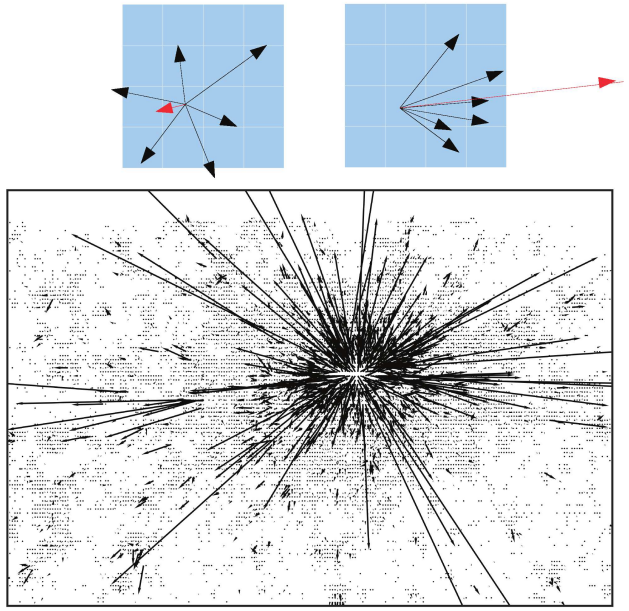

Fig. 1. Top row, two examples with the definition of the average vector in every cell (red vector). In the bottom, the vector field in an area comprehending the Greater London.

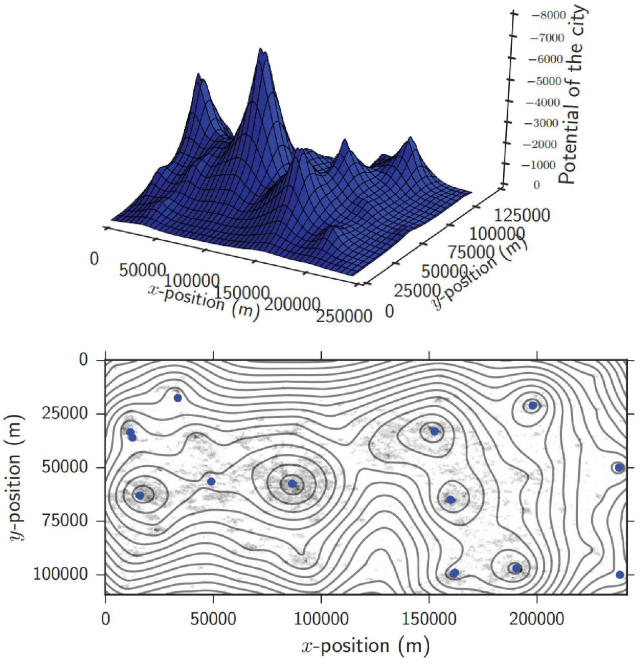

Fig. 2. The potential field calculated using the gravity model with an exponential deterrence function in the area of Manchester an Liverpool. We find 13 centers (local maxima).

[1] H. Barbosa, M. Barthelemy, G. Ghoshal, C. R. James, M. Lenormand, T. Louail, R. Menezes, J. J. Ramasco, and F. Simini, M. Tomasini, Human mobility: Models and applications, Phys. Rep. **734**, 1-74 (2018).

[2] M. Mazzoli, A. Molas, M. Lenormand, P. Colet, and J. J. Ramasco, Field Theory for recurrent mobility, (in preparation).

Ageing-induced continuous phase transition

Oriol Artime, Antonio F. Peralta, Raúl Toral, José J. Ramasco, and Maxi San Miguel
Instituto de Física Interdisciplinar y Sistemas Complejos (IFISC), CSIC-UIB, Campus UIB, 07122 Palma de Mallorca, Spain

Ageing is an ubiquitous effect in nature. It has different meanings, depending on the strand of research considered. Classical examples range from non-equilibrium statistical mechanics [1], where its effects are studied on spin glasses, to biology [2], considered as the increase of mortality with age of a species, to chemistry [3], where the properties of a material change over time without any external forces. In any case, ageing can be seen as the dependence of the dynamics of a system on an internal time, often heterogeneously distributed, of the individual components that form such a system. Specifically, we take the approach of considering ageing as the influence that persistence times, i.e., the time without changing state, have on the state transitions: it constrains the transitions in a way that the longer an element remains in a given state, the smaller is the probability to change it. The inclusion of this effect in the modelling part adds a realistic component into the description of a given problem and unveils new and rich phenomenology.

In this work [4] we investigate the effects of including heterogeneous time-dependent transitions on the critical properties of a stochastic model. We add ageing into the noisy voter model (also known as the Kirman model), a paradigmatic binary-state stochastic model appeared in several contexts: percolation, surface-catalytic reactions, probability theory, opinion dynamics, ... The agents modify their binary state by means of noise and pair-wise interactions. Interestingly, due to ageing the system passes from a finite-size discontinuous transition between ordered (ferromagnetic, bimodal) and disordered (paramagnetic, unimodal) phases to a second order phase transition, well-defined in the thermodynamic limit, belonging to the Ising universality class (see top and middle panels in Fig. 1). We characterize it analytically by finding the stationary solution of an infinite set of mean field equations. The theoretical predictions are tested with extensive numerical simulations in low dimensional lattices and complex networks. In addition, the ageing properties are employed to understand the symmetries broken in the phase transition (bottom panel in Fig. 1).

In summary, by adding a realistic ingredient in the modelling framework, we prove that ageing plays a central role in modifying the critical properties of a stochastic model. The studied phenomenology can occur in other complex systems beyond opinion dynamics models, with potential impact on a wide range of disciplines.

[1] M. Henkel and M. Pleimling, *Non-Equilibrium Phase Transitions. Volume 2: Ageing and Dynamical Scaling Far from Equilibrium* (Springer Netherlands, 2011).

[2] M. Y. Azbel, Phenomenological theory of mortality, Phys. Rep. **288**, 545-574 (1997).

[3] A. L. Robinson, N. M. Donahue, M. K. Shrivastava, E. A. Weitkamp, A. M. Sage, A. P. Grieshop, T. E. Lane, J. R. Pierce, and S. N. Pandis, Rethinking organic aerosols: Semivolatile emissions and photochemical aging, Science **315**, 1259-1262 (2007).

[4] O. Artime, A. F. Peralta, R. Toral, J. J. Ramasco, and M. San Miguel, Ageing-induced continuous phase transition, (under review).

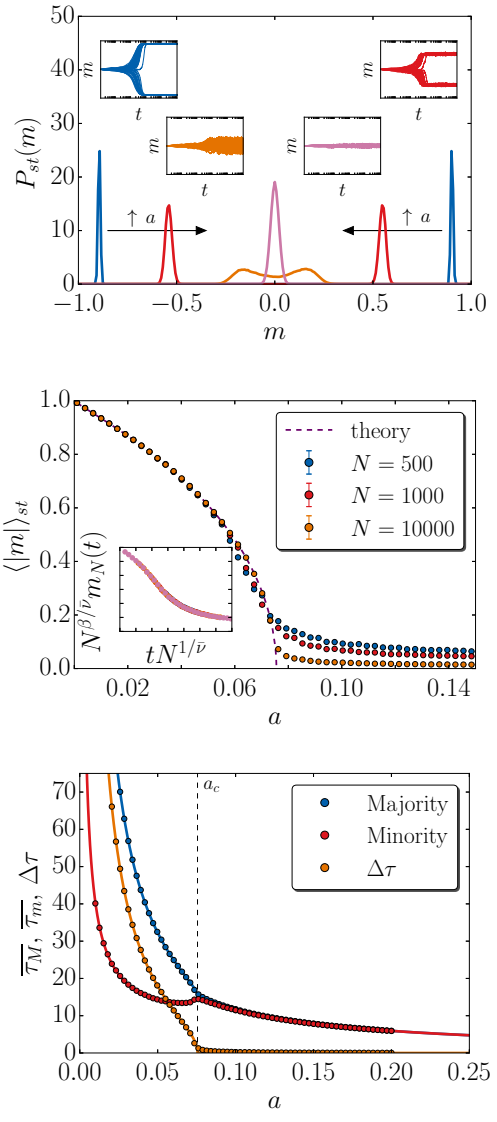

Fig. 1. (Top) Stationary probability distribution for the magnetization. Different curves correspond to different values of noise a. In the insets, the individual trajectories of the dynamics. (Middle) Phase diagram for the stationary value of the magnetization for different system sizes, together with the analytical curve. In the inset, collapse of the magnetization curves using the mean field Ising critical exponents. (Bottom) Mean internal times for the majority and minority population, and their difference, in function of the noise. Points are simulations and solid line is the analytical curve.

Sorting of flocking active particles using asymmetric obstacles

Raul Martinez[1,2], Francisco Alarcon[1], Diego Rogel[1], Juan Luis Aragones[2], and Chantal Valeriani[1,†]
[1]Departamento de Estructura de la Materia, Física Térmica y Electrónica , Facultad de Ciencias Físicas, Universidad Complutense de Madrid, 28040 Madrid, Spain
[2]IFIMAC, Facultad de Ciencias, Universidad Autónoma de Madrid, Ciudad Universitaria de Cantoblanco, 28049 Madrid, Spain

Active matter is a branch of condensed matter physics which studies systems that are intrinsically out of equilibrium, because every component of them is out of equilibrium. Physical examples are entities which propel themselves by taking their energy from the environment, such as living particles.

In this context, we are going to focus on differences existing between trapping particles which show collective motion and run-and-tumble ones.

Run-and-tumble particles mimic the motion of a wide variety of microorganism (as *E. coli*), consisting in straight runs interrupted by tumbles (reorientations of the direction of motion) [1]. We model them by using simple rules of uniformly distributed random tumbles at regular time steps, and constant particle speed during straught runs.

Flocking particles are modeled using the well-known Vicsek model [4, 5, 6, 7], where we consider both the metric and the topological choice of neighbors: in the metric model neighbors are chosen within a fixed cutoff radius R [4, 5, 6], while in the topological one we take the Voronoi neighbors of a particle [7], thus a screening of the interactions is taken into account.

Sorting of run-and-tumble particles by asymmetric obstacles (a wall of funnels) has already been described [2] and experimentally tested using *E.coli* [3]. When the persistence length of particles is large enough, active particles concentrate at the small opening side of the wall.

When using an open geometry, consisting in bands with periodic boundary conditions, formed by parallel funnel walls each having its wide opening side opposed with its neighbor's one, the same trapping effect for run-and-tumble particles is observed (see left panel of Fig. 1). When replacing run-and-tumble particles by flocking particles described by the Vicsek model [4, 5, 6], we observe that, surprisingly, particles are trapped differently: first, they concentrate at the wide opening side of the funnels (contrary to run-and-tumble), and second, the entire flock is trapped (right panel of Fig. 1).The reason for this difference is the trapping mechanism, as presented in bottom row of Fig. 1.

In this particular geometry, the difference between using metric or topological Vicsek model is very small.

We have also designed circular traps for flocking particles, where we observe an important difference between trapping of metric and topologic particles (see Fig. 2). In this case, the lower tendency to cluster of the topologic model becomes evident.

† E-mail: cvaleriani@ucm.es

[1] J. Tailleur and M. E. Cates, Statistical mechanics of interacting run-and-tumble bacteria, Phys. Rev. Lett. **100**, 218103 (2008).

[2] M. B. Wan, C. J. O. Reichhardt, Z. Nussinov, and C. Reichhardt, Rectification of swimming bacteria and self-driven particle systems by arrays of asymmetric barriers, Phys. Rev. Lett. **101**, 018102 (2008).

[3] P. Galajda, J. Keymer, P. Chaikin, and R. Austin, A wall of funnels concentrates swimming bacteria, J. Bacteriol. **189**, 8704-8707 (2007).

[4] T. Vicsek, A. Czirók, E. Ben-Jacob, I. Cohen, and O. Shochet, Novel type of phase transition in a system of self-driven particles, Phys. Rev. Lett. **75**, 1226 (1995).

[5] G. Gregoire and H. Chate, Onset of collective and cohesive motion, Phys. Rev. Lett. **92(2)**, 025702 (2004).

[6] F. Ginelli, The physics of the Vicsek model, Eur. Phys. J.-Spec. Top. **225**, 2099-2117 (2016).

[7] F. Ginelli and H. Chate, Relevance of metric-free interactions in flocking phenomena, Phys. Rev. Lett. **105**, 168103 (2010).

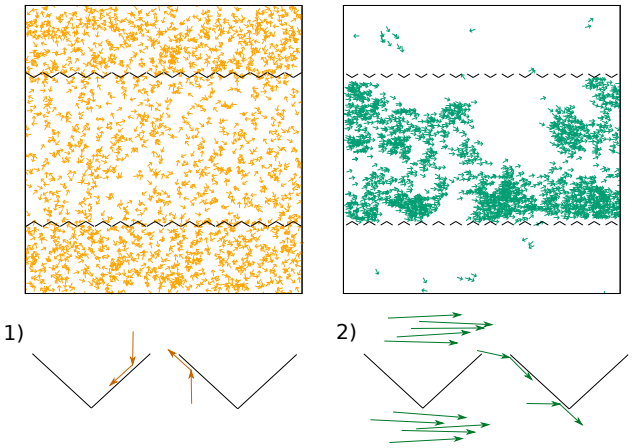

Fig. 1. (Left) Run-and-tumble particles. (Right) Flocking particles in the same geometry. Periodic boundary conditions are used. (Bottom row) Representation of the trapping mechanism: (1) run-and-tumble particles find easier to cross the wall from the wide opening side to the other side, (2) flocking particles, however, first align with the wall and them are pushed to the wide opening side by collisions with walls.

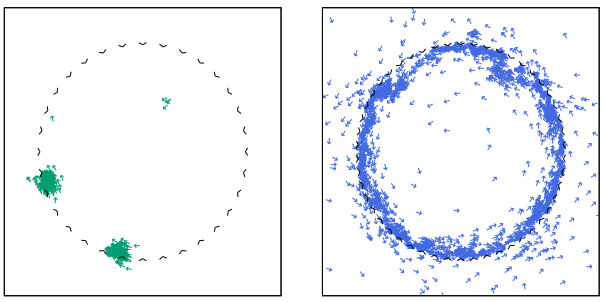

Fig. 2. Circular traps. (Left) Metric Vicsek model. (Right) Topologic one. We see that metric Vicsek model is much more subject to clustering.

Swimming modes of self-assembled magnetic micropropeller

C. Calero[1,3], J. M. García-Torres[1,2,3], F. Sagués[2,3], I. Pagonabarraga[1,4,5], and P. Tierno[1,3,4]
[1]Departament de Física de la Matèria Condensada, Universitat de Barcelona, 08028 Barcelona, Spain
[2]Departament de Ciència de Materials i Química Física, Universitat de Barcelona, 08028 Barcelona, Spain
[3]Institut de Nanociència i Nanotecnologia, Universitat de Barcelona, 08028 Barcelona, Spain
[4]Institute of Complex Systems (UBICS), Universitat de Barcelona, 08028 Barcelona, Spain
[5]CECAM, École Polytechnique Fédérale de Lausanne, Batochime, av. Forel 2, 1015 Lausanne, Switzerland

Controlling the motion of micro and nano propellers is of great interest and the focus of intense research due to their potential applications as efficient drug-delivery vectors, non-invasive microsurgery devices, or chemical biodetectors. A variety of strategies have been devised to design microswimmers and direct their trajectories at low Reynolds numbers, where these systems operate.

Here, we propose the use of self-assembled magnetic aggregates as micropropellers and theoretically investigate the different swimming modes that can be induced by their actuation with time-dependent magnetic fields. In particular, we focus on a hybrid system composed of a ferromagnetic nanorod and a paramagnetic spherical microparticle which self-assemble due to their mutual dipolar attraction. We discuss two different actuation strategies which generate locomotion. We show that the application of in-plane linearly oscillating magnetic fields results in the rotation of the ferromagnetic rod, which governs the motion of the swimmer. We demonstrate that the direction of the rod's rotation (and, thus, of propulsion of the microswimmer) can be selected by balancing gravity, magnetic and hydrodynamic interactions [1] (see Fig. 1).

We also investigate the locomotion of the self-assembled propeller under an in-plane field of constant magnitude which oscillates about a given direction. The basic locomotion mechanism is discussed and leading-order analytical expressions are obtained for the velocity and efficiency of the propeller under small fields, which are tested against computer simulations.

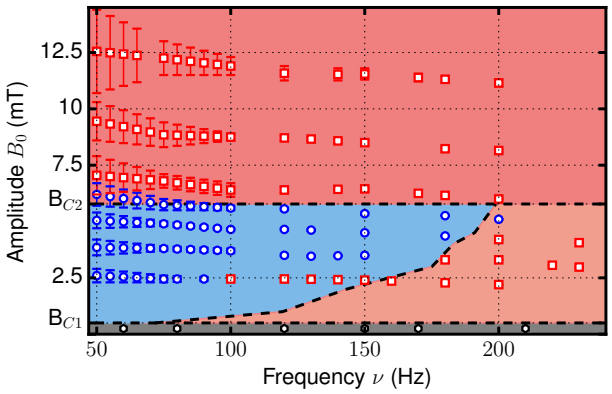

Fig. 1. Diagram of locomotion modes of self-assembled microswimmer as a function of the amplitude and frequency of the external magnetic field. The red (blue) regions indicate values in which the microswimmer is predicted to act as a puller (pusher). Red squares (Blue dots) represent experimental points where the microswimmer acts as a puller (pusher).

[1] J. M. Torres-García, C. Calero, F. Sagués, I. Pagonabarraga, and P. Tierno, Magnetically tunable bidirectional locomotion of a self-assembled nanorod-sphere propeller, Nat. Commun. **9**, 1663 (2018).

Non-Markovian jumping times and evolutionary irreversibility in a computational genotype-phenotype map

Pablo Catalán[1,2], Susanna Manrubia[1,3], and José A. Cuesta[1,2,4,5]
[1]Grupo Interdisciplinar de Sistemas Complejos (GISC), Madrid, Spain
[2]Dept. de Matemáticas, Universidad Carlos III de Madrid, Leganés, Madrid, Spain
[3]Programa de Biología de Sistemas, Centro Nacional de Biotecnología, CSIC, Madrid, Spain
[4]Instituto de Biocomputación y Física de Sistemas Complejos (BIFI), Universidad de Zaragoza, Spain
[5]UC3M-BS Institute of Financial Big Data (IFiBiD), Universidad Carlos III de Madrid, Getafe, Madrid, Spain

Biological evolution is a highly complex dynamical process in which organisms reproduce and mutate through time. The information needed to build organisms (the genotype) is transmitted from parent to offspring, sometimes with mutations. The organism's features (the phenotype) are the target of natural selection, and determine its fitness or reproduction rate. At the level of genotypes, evolutionary dynamics can be modelled as a Markov process. We will assume that natural selection is strong and that mutations are rare, i.e., $\mu N \ll 1$, where μ is the mutation rate and N is the population size. This means mutations arise rarely enough so that they disappear from the population or go to fixation before another new mutation appears. The fixation rate of a new mutation in a haploid asexual population is given by

$$\phi(f,N) = \mu N \frac{f-1}{f^N-1}, \qquad (1)$$

where f is the fitness of the current phenotype relative to that of the mutant. In this scenario, evolution is a random walk in genotype space: when a new mutation appears in the population, it can either become extinct (the random walk stays in the same genotype) or dominate the population (the random walk jumps to a new state), with transition rate $\phi(f,N)$.

The relevant process, however, is evolution at the level of phenotypes, which is what we can measure. Recent work mapping genotypes to phenotypes has determined that many genotypes map to the same phenotype, forming vast neutral networks [1]. Moreover, the number of genotypes that map to a given phenotype is not homogeneous: most phenotypes are rare, but some of them are extremely abundant. Here we show that these properties imply that evolution at the phenotype level is non-Markovian and irreversible.

In order to explore these phenomena, we will make use of toyLIFE, a multilevel computational model inspired by cellular biology [2]. Our toyLIFE genotypes are formed by two binary genes that codify the expression of two proteins in time and space, forming one-dimensional patterns, which will constitute the phenotype. Because of the discrete character of the model, toyLIFE genotypes are equivalent to cellular automata.

In this work, we focus on two particular phenotypes with the same fitness, but with very different abundances: phenotype 1 is codified by 1.652×10^9genotypes, while phenotype 2 is mapped by 3×10^6 genotypes, a difference of three orders of magnitude [Fig. 1 (a)]. A naïve, coarse-grained approach to studying the dynamics between these two phenotypes (disregarding transitions to other phenotypes) is to model this system as a two-state Markov chain. This simple model captures the distribution of transition times from phenotype 2 to phenotype 1, but fails to accurately characterize jumps in the opposite direction. While the two-state Markov chain predicts long, exponential transition times from phenotype 1 to phenotype 2, our results show that two different outcomes can occur, depending on the initial condition

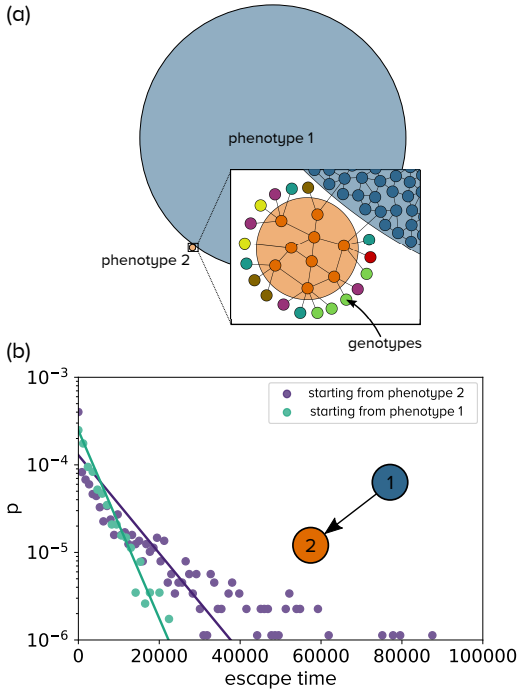

Fig. 1. Phenotypic bias. (a) Phenotype 1 is encoded by more than 10^9 genotypes, while phenotype 2 is three orders of magnitude less abundant. These two phenotypes are connected by mutations. (b) Starting from phenotype 2, the process quickly jumps to phenotype 1 and then takes a non-exponential time to return (blue). Starting from phenotype 1, the process jumps to phenotype 2 faster than the two-state Markov model predicts.

[Fig. 1 (b)]. Starting from phenotype 2, the process quickly jumps to phenotype 1 and then becomes *trapped* there [3], taking a non-exponential time to return. On the other hand, starting from phenotype 1, the population jumps (almost) exponentially to phenotype 2, but faster than predicted by the two-state model. We present a five-state Markov chain that successfully predicts these jump times. This work suggests strategies to model phenotypic evolution, taking into account the underlying structure of genotype space.

[1] J. Aguirre, P. Catalán, J. A. Cuesta, and S. Manrubia, On the networked architecture of genotype spaces and its critical effects on molecular evolution, arXiv:1804.06835.

[2] P. Catalán, A. Wagner, S. Manrubia, and J. A. Cuesta, Adding levels of complexity enhances robustness and evolvability in a multilevel genotype-phenotype map, J. R. Soc. Interface **15**, 20170516 (2018).

[3] S. Manrubia and J. A. Cuesta, Evolution on neutral networks accelerates the ticking rate of the molecular clock, J. R. Soc. Interface **12**, 20141010 (2015).

Magnetic biohybrid vesicles transported by an internal propulsion mechanism

A. Mateos-Maroto, A. Guerrero-Martinez, R. G. Rubio, F. Ortega, and F. Martinez-Pedrero
Departamento de Química-Física I, Universidad Complutense de Madrid, av. Complutense s/n, 28040 Madrid, Spain

Some biological microorganisms can crawl or swim due to coordinated motions of their cytoskeleton or the flagella located inside their bodies, which push the cells forward through intracellular forces [1]. To date, there is no demonstration of a biomimetic self-propelled swimmer operating at a low Reynolds number due to internal movements within an enclosing membrane.

Here, we report lipid vesicles and other more complex self-assembled biohybrid structures able to propel due to the advection flows generated by the actuated rotation of the superparamagnetic particles they contain [2]. The proposed swimming and release strategies, based on near infrared laser pulse-triggered destabilization of the phospholipid membranes, open new possibilities for the on-command transport of minute quantities of drugs, fluids or nano-objects. The lipid membranes protect the confined substances from the outside environment during transportation, thus enabling to work in physiological conditions.

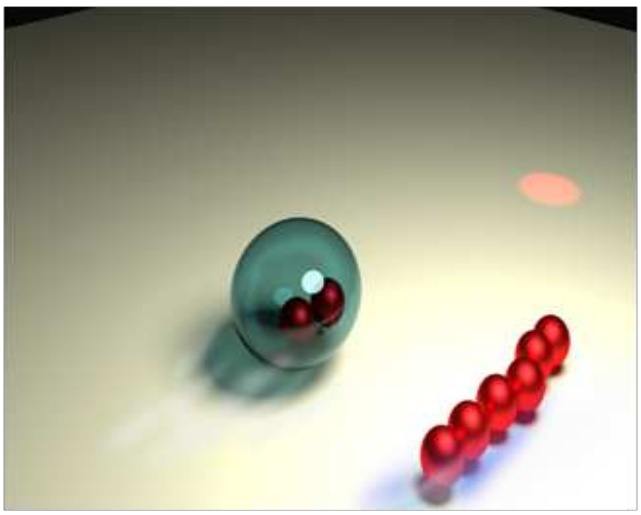

Fig. 1. The sketch shows the motion of one linear aggregate of free particles and two particles encapsulated within a giant vesicle in the presence of a circularly polarized rotating field.

[1] E. Lauga and T. R. Powers, The hydrodynamics of swimming microorganisms, Rep. Prog. Phys. **72**, 096601 (2009).

[2] F. Martinez-Pedrero, A. Ortiz-Ambriz, I. Pagonabarraga, and P. Tierno, Colloidal microworms propelling via a cooperative hydrodynamic conveyor belt, Phys. Rev. Lett. **115**, 138301 (2015).

Cognitive resource allocation determines the organization of personal networks

Ignacio Tamarit[1,2], José A. Cuesta[1,2,3,4], Robin I. M. Dunbar[5,6], and Angel Sánchez[1,2,3,4]

[1]Grupo Interdisciplinar de Sistemas Complejos, Depto. de Matemáticas, Univ. Carlos III de Madrid, 28911 Leganés, Madrid, Spain
[2]Unidad Mixta Interdisciplinar de Comportamiento y Unidad Social (UMICSS), UC3M-UV-UZ, 28911 Leganés, Madrid, Spain
[3]Institute for Biocomputation and Physics of Complex Systems (BIFI), University of Zaragoza, 50018 Zaragoza, Spain
[4]Institute UC3M-BS of Financial Big Data, Universidad Carlos III de Madrid, 28903 Getafe, Spain
[5]Department of Experimental Psychology, University of Oxford, New Richards Building, Old Road Campus, Oxford OX3 7LG, UK
[6]Department of Computer Science, Aalto University, FI-00076 AALTO, Finland

Some of the most robust findings about human social networks are concerned with the size and structure of the individuals' personal networks. These studies suggest that, among humans, an individual typically deals with about 150 relationships including kin and friends. These relationships are further organized into a set of hierarchically inclusive layers (*circles*) of increasing size with decreasing emotional intensity whose sizes follow a characteristic sequence with a scaling ratio close to 3 [1]: 5, 15, 50, 150. Although the overall size of the networks has been connected to our cognitive capacity [2], the layered structure and the consistent scaling ratio are experimental evidences for which no theoretical explanation has been given. By means of the maximum entropy principle [3], we show that the existence of a cost to relationships (in terms of time and/or cognitive investment) and heterogeneity in the relationships (in terms of their benefits and/or emotional content) naturally yield this outcome. Furthermore, we show that the fraction of links in circle k is, under certain conditions, given by

$$\chi_k = \frac{1 - e^{k\mu}}{1 - e^{r\mu}}, \tag{1}$$

where r is the total number of circles and μ is the only parameter of the model.

The model not only accounts for the layered structure previously mentioned, but also predicts the existence of a new kind of regime. If $\mu > 0$, then the relationships are hierarchically distributed as it has been widely reported in the literature, with an approximately constant scaling ratio given by $x \approx e^{\mu}$ —we will call this the *standard* regime. However, if $\mu < 0$, then the individuals tend to have a large number of *close* relationships and little acquaintances —we call this the *inverse* regime. According to the model, the latter should be prompted when the number of available relationships for an individual is particularly small, or, more precisely, when the ratio between available resources and possible relationships is large. Importantly, this second type of structure had not been hitherto reported.

We analyze the standard regime using data from a group of 84 students from a major Middle Eastern university [4]. The results are summarized in Fig. 1 (a) and (b). Most individuals ($\sim 98\%$) have a value of $\mu > 0$, meaning that their circles show the standard structure, as expected. In order to test our prediction about the inverse regime, we focus on four different communities of immigrants whose sociological features suggest that they form independent, small social environments within their places of residence [5, 6]. Figure 1 (c) and (d) shows our results for one of these communities. Remarkably, 96% of its networks lie within the inverse regime with $\mu < 0$, confirming our hypothesis —the results are similar for the remaining three communities.

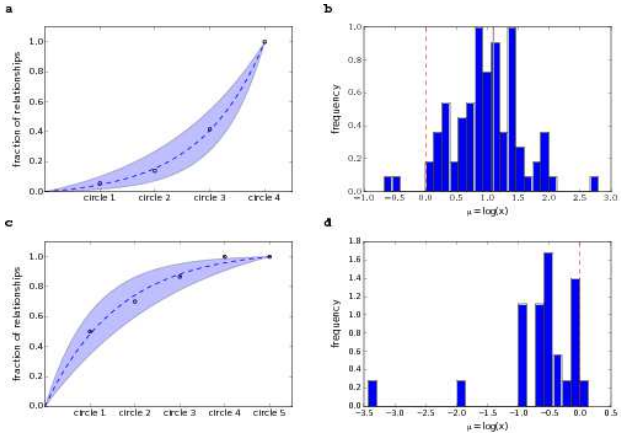

Fig. 1. Summary of the results of the data analysis. Upper panels summarize our results for the community of students, whereas lower panels summarize those for one of the communities of immigrants. Left panels show representative fittings for individuals in both communities. Solid dots represent experimental data, blue dashed lines represent the graph of the fitted model, and shaded regions show the 95% confidence interval for the parameter estimate. Right panels show the distribution of the parameter estimates (μ) for both communities. The red dashed lines mark the change of regime (i.e., $\mu = 0$). (a) Representative fitting for an individual in the community of students –standard regime. (b) Distribution of the parameter estimates for the community of students. The gray, solid line indicates the typically observed scaling ratio $x = 3$ ($\mu = 1.099$). (c) Representative fitting for an individual in one community of immigrants – inverse regime. (d) Distribution of the parameter estimates for one community of immigrants.

[1] W.-X. Zhou, D. Sornette, R. A. Hill, and R. I. Dunbar, Proc. R. Soc. B **272**, 439 (2005).

[2] J. Powell, P. A. Lewis, N. Roberts, M. García-Fiñana, and R. I. Dunbar, Proc. R. Soc. B **279**, 2157 (2012).

[3] E. T. Jaynes, *Probability Theory: The Logic of Science* (Cambridge University Press, 2003).

[4] A. Almaatouq, L. Radaelli, A. Pentland, and E. Shmueli, PLoS ONE **11**, e0151588 (2016).

[5] S. G. Mestres, J. L. Molina, S. Hoeksma, and M. Lubbers, Southeast. Eur. **36**, 208 (2012).

[6] J. L. Molina, S. Petermann, and A. Herz, Field Methods **27**, 223 (2015).

Protein design under competition for amino acids availability

Francesca Nerattini[1], Luca Tubiana[2], Chiara Cardelli[2], Valentino Bianco[2], Christoph Dellago[2], and Ivan Coluzza[3]
[1]Faculty of Physics & VDSP member, University of Vienna, Sensengasse 8/9, 1090 Vienna, Austria
[2]Faculty of Physics, University of Vienna, Sensengasse 8/9, 1090 Vienna, Austria
[3]CIC biomaGUNE, po. Miramon 182, 20014 San Sebastian, Spain

Understanding the origin of the 20 letter alphabet of proteins is a long-lasting biophysical problem. In particular, studies focused extensively on the effect of a reduced alphabet size on the folding properties [1, 2, 3]. However, the natural alphabet is a compromise between versatility and optimisation of the available resources.

Here, for the first time, we include the additional impact of the relative availability of the amino acids. We present a computational protein design scheme that involves the competition for resources between a protein and a potential interaction partner that, additionally, gives us the chance to investigate the effect of the reduced alphabet on protein-protein interactions. We identify the optimal reduced set of letters for the design of the protein, and we observe that even alphabets reduced down to 4 letters allow for single protein folding. However, it is only with 6 letters that we achieve optimal folding, thus recovering experimental observations.

Additionally, we notice that the binding between the protein and a potential interaction partner could not be avoided with the investigated reduced alphabets. Therefore, we suggest that aggregation could have been a driving force for the evolution of the large protein alphabet.

[1] K. W. Plaxco, D. S. Riddle, V. Grantcharova, and D. Baker, Simplified proteins: minimalist solutions to the 'protein folding problem', Curr. Opin. Struct. Biol. **8**, 80-85 (1998).

[2] Z. Sun, R. Lonsdale, X.-D. Kong, J.-H. Xu, J. Zhou, and M. T. Reetz, Reshaping an enzyme binding pocket for enhanced and inverted stereoselectivity: Use of smallest amino acid alphabets in directed evolution, Angew. Chem. Int. Ed. **54**, 12410-12415 (2015).

[3] H. S. Chan, Folding alphabets, Nat. Struct. Mol. Biol. **6**, 994-996 (1999).

Linear and non-linear instabilities for patterning embryonic tissues

Juan Camilo Luna-Escalante[1,†], Pau Formosa-Jordan[1,‡], Nicolas Daudet[2], and Marta Ibañes[1,3]
[1]Department of Física de la Matèria Condensada, Physics, University of Barcelona, Spain
[2]UCL Ear Institute, University College London, London, United Kingdom
[3]Universitat de Barcelona Institute of Complex Systems (UBICS), Barcelona, Spain

During the development of animal embryos, regular patterns of gene activation arise within tissues which subsequently direct the differentiation of cells into distinct cell types. These patterns can arise from self-organization dynamics that involve cell-to-cell communication.

We focus herein in one type of short-range spatial communication that enables periodic pattern formation. This communication arises between adjacent cells and is mediated by the Notch signaling pathway. Notch is a receptor at the cell membrane that directs a signal to the cell nucleus after binding to other proteins (Notch ligands) in adjacent cell membranes. It is well known from theoretical grounds that a linear instability can drive periodic patterning through this type of communication [1]. As we have previously shown, this scenario is consistent with patterning of sensory organs in the inner ear of vertebrates [2, 3]. Herein we address an additional aspect of this process. Empirical evidences show that during sensory organ development, cells can have a dual behavior being mostly sensitive to the spatial communication but occasionally insensitive to it [4, 5].

Through a dynamical mathematical model of cell-to-cell interactions that can reproduce these empirical evidences, we propose that whereas patterning is mediated by a linear instability, the occasional insensitivity arises from a non-linear instability. Based on this, our model drives specific predictions, some of which we address experimentally. Taken together, our results provide a novel framework to understand both sensitivity and insensitivity based on linear and non-linear instabilities.

† Current address: Department of Developmental and Stem Cell Biology, Institut Pasteur, and Laboratoire de Physique Statistique de l'ENS, Paris, France.

‡ Current address: Sainsbury Laboratory, University of Cambridge, Cambridge, United Kingdom.

[1] J. R. Collier, N. A. Monk, P. K. Maini, and J. H. Lewis, Pattern formation by lateral inhibition with feedback: a mathematical model of delta-notch intercellular signalling, J. Theor. Biol. **183**, 429 (1996).

[2] J. Petrovic, P. Formosa-Jordan, J. C. Luna-Escalante, G. Abelló, M. Ibañes, J. Neves, and F. Giraldez, Ligand-dependent Notch signaling strength orchestrates lateral induction and lateral inhibition in the developing inner ear, Development **141**, 2313 (2014).

[3] J. C. Luna-Escalante, P. Formosa-Jordan, and M. Ibañes, Redundancy and cooperation in Notch intercellular signaling, Development (in press).

[4] R. Goodyear and G. Richardson, Pattern formation in the basilar papilla: evidence for cell rearrangement, J. Neurosci. **17**, 6289 (1997).

[5] E. Chrysostomou, J. .E. Gale, and N. Daudet, Delta-like 1 an lateral inhibition during hair cell formation in the chicken inner ear: evidence against cis-inhibition, Development **139**, 3764 (2012).

Nitrogen-fixing cyanobacteria are tuned for evolvability

Victoria Doldán-Martelli, Katherine Gonzales-Moreno, Daniel Bravo-Candel,
Javier Muñoz-García, and Saúl Ares
Grupo Interdisciplinar de Sistemas Complejos, Departamento de Matemáticas, Universidad Carlos III de Madrid, Leganés, Spain

Cyanobacteria produce a significant fraction of the oxygen on the environment and, together with archaea, they fix atmospheric nitrogen used by all other organisms. One of the first forms of multicellular organisms on Earth are filamentous cyanobacteria, which constitute a paradigmatic model organism of the transition between unicellular and multicellular living forms. The genus *Anabaena* forms colonies with cells arranged in one-dimensional filaments; under nitrogen-limiting conditions some cells can differentiate into a nitrogen-fixing heterocysts, forming regular patterns to effectively provide nitrogen for the colony.

By combining genetic, metabolic and morphological features, a mathematical model was recently proposed to understand the regulation of heterocyst differentiation in *Anabaena PCC 7120* [1]. The model quantitatively reproduced the appearance and dynamics of this pattern, allowing to explore the impact of different factors like fixed-nitrogen diffusion, cell division, or stochasticity on pattern formation.

In this contribution we analyze a simplified version of the previous model, using the minimal gene regulatory mechanisms for heterocyst pattern formation at early stages (Fig. 1). Early pattern formation involves mechanisms of local autoactivation and long-range inhibition, governed by the genes *hetR*, and *patS*, respectively.

The analysis of our model (see Fig. 2) for two-cell filament shows that the wild type genotype is poised very close to a critical point in the parameter space, a so-called codimension 2 bifurcation. The proximity of the wild type genotype to the critical point is also supported by stochastic simulations with 50 cell-filaments using the same simplified model.

This result suggests that small variations in the genotype would be enough to produce big qualitative changes in phenotypes, since the wild type lies close to all the different kinds of phenotypes available to the system.

Furthermore, the proximity to the critical point suggests that the regulatory machinery of heterocyst differentiation has optimized evolvability, in the sense that small changes in the genotype, that can be produced in different ways by small mutations, are enough to adapt the system to permanent changes in environmental conditions.

[1] J. Muñoz-García and Saúl Ares, Proc. Natl. Acad. Sci. U.S.A **113**, 6218-6223 (2016).

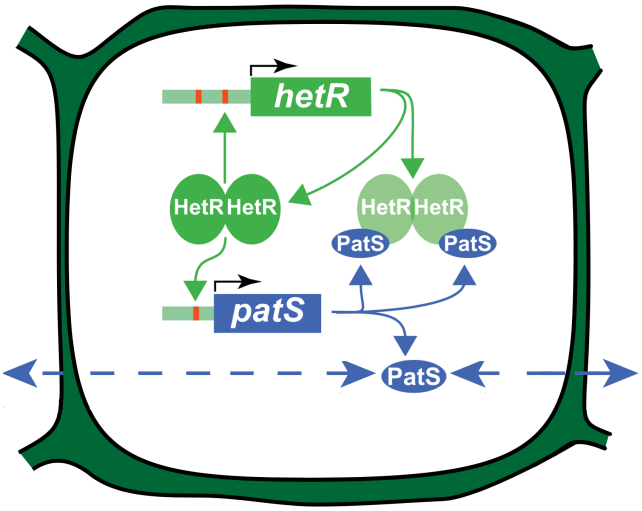

Fig. 1. Minimal model of the genetic network involved in heterocyst pattern formation at early stages. This network includes mechanisms of local autoactivation via HetR dimers and long-range inhibition governed by PatS, that is able to bind and inhibit HetR dimers and also to diffuse between cells (blue dashed arrows).

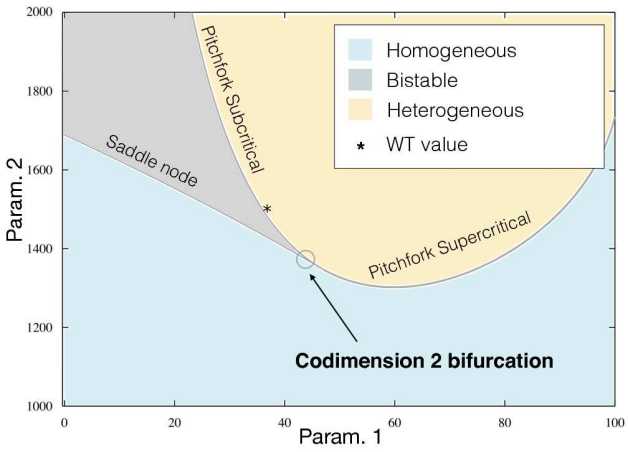

Fig. 2. Two-dimensional bifurcation diagram for two different parameters. The curves for the three types of bifurcations divide the parameter space into different phenotypes of our two-cell system: *heterogeneous* in yellow, *bistable* in grey and *homogeneous* in blue. The wild-type value for the pair of parameters is represented as an asterisk.

Influence of recurrent mobility patterns on the spread of vector-borne diseases

David Soriano-Paños[1,2], Sandro Meloni[2], Juddy Heliana Arias-Castro[3], and Jesús Gómez-Gardeñes[1,2]
[1]Departamento de Física de la Materia Condensada, Universidad de Zaragoza, 50009 Zaragoza, Spain
[2]Instituto de Biocomputación y Física de Sistemas Complejos (BIFI), Universidad de Zaragoza, 50018 Zaragoza, Spain
[2]Departamento de Matemáticas, Universidad del Valle, 25360 Cali, Colombia

Contagious diseases cause more than millions of deaths all over the world according to the World Health Organization [1]. There exists a great variety of contagious diseases depending on the mechanism that drives the epidemic spreading. In this talk, we are going to focus on vector-borne diseases, which are indirectly transmitted among humans via the intermediation of some external agents, denoted as vectors, like mosquitoes, sand-flies, ticks, etc.

The impact of these vector-borne diseases, especially in tropical areas, has raised the necessity of making models capable of predicting their incidence as well as their spatio-temporal propagation patterns. In this sense, the most paradigmatic model is the Ross-Macdonald model [2, 3], in which vectors as well humans can adopt two dynamical states: susceptible of contracting the disease or infected by them. The Ross-Macdonald model has been widely studied by following mean field theories and some important analytical results have been obtained such as estimations of the boundaries between the epidemic phase and the disease free one.

However, these results correspond to closed systems in which agents as well as vectors are assumed not to move. In light of the crucial role that human mobility has played on the spread of many diseases, we want to extend the Ross-Macdonald model to account for recurrent human mobility patterns. Based on the equations previously developed for directly transmitted diseases between humans [4], we will propose a new formalism to assess the effects of human mobility on the spread of vector-borne diseases. To check the validity of the proposed model, we will compare its theoretical predictions with results from Monte Carlo simulations. Figure. 1 shows this comparison by using a SF metapopulation as the underlying mobility network.

Once we have checked the validity of our equations, we will be able to deduce an estimation of the epidemic threshold which will shed light on the effects of mobility on the onset of epidemics. In addition to the differences concerning the contagion mechanisms, the consequences of contracting vector-borne diseases are severe and usually prevent the infected agents from moving in a normal way. For this purpose, we will introduce a restriction in the mobility of infected agents. This way, we will study the influence of the interplay between the mobility of both infected and susceptible agents on the epidemic threshold. Interestingly, we will

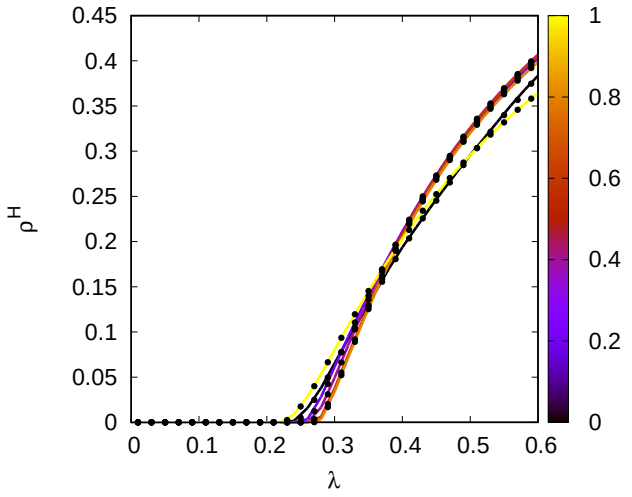

Fig. 1. Total fraction of infected people ρ^h in the stationary state as a function of the infectivity λ between humans and mosquitoes and the mobility, here denoted with the color scale.

reveal that the restriction of mobility of infected agents will be very determinant since it will dramatically change the dependence of the epidemic threshold on the mobility of the susceptible agents.

Finally, we will study the applicability of our model to predict the most affected geographical areas by the outbreak of vector-borne diseases. Thus, we will show that our model is able to capture them for the case of Dengue outbreaks in the city of Cali, Colombia.

[1] WHO Fact sheet N°38 (2014).

[2] R. Ross, *The Prevention of Malaria* (John Murray, London, 1911).

[3] D. L. Smith, K. E. Battle, S. I. Hay, C. M. Barker, T. W. Scott, and F. E. McKenzie, PLoS Pathog. **8**, e1002588 (2012).

[4] J. Gómez-Gardeñes, D. Soriano-Paños, and A. Arenas, Nat. Phys. **14**, 391 (2018).

Modelling the DNA G-quadruplex unfolding

A. Fiasconaro[1], A. E. Bergues-Pupo[2], I. Gutierrez[3], J. R. Arias-Gonzalez[3,4], and F. Falo[1,5]
[1]Departamento de Física de la Materia Condensada, Universidad de Zaragoza, Zaragoza, Spain
[2]Max Planck Institute of Colloids and Interfaces, Department of Theory & Bio-Systems, Science Park Potsdam-Golm, Potsdam, Germany
[3]Instituto Madrileño de Estudios Avanzados en Nanociencia, Cantoblanco, Madrid, Spain
[4]CNB-CSIC-IMDEA Nanociencia Associated Unit "Unidad de Nanobiotecnología", Cantoblanco, Madrid, Spain
[5]Instituto de Biocomputación y Física de Sistemas Complejos (BIFI), Universidad de Zaragoza, Zaragoza, Spain

The G-quadruplexes (G4) are non-canonical secondary DNA and RNA structures composed of four guanine basis bonded each other in quartets forming planes eventually piled in two, three or four layers. They are present both in vivo and in vitro cultures, and have important role in telomere end-protection, chromosome stability, aging control. Their folding patterns and structures are also found in eukaryotic promoter regions of oncogenes, making them increasingly recognized among chemists and biologists due to their potential applications in Nanomedicine as therapeutic targets in cancer treatments.

In the last years, single-molecule techniques have attracted much attention between the scientific community and a number of groups have extensively used them to analyze the mechano-chemical behavior of DNA and RNA chains. Optical and magnetic tweezers, as well as Atomic Force Microscopies, are employed to characterize not only the mechanical stability and unfolding dynamics of G-quadruplexes, but also to unveil structural intermediates not accessible to ensemble-average techniques due to their relatively low occurrence.

The stability of the G-quadruplex structure is related, among the others, to the specific G-quadruplex conformation, and the presence of a cation between each of the G4 planes. Although an increasing number experiments have been conducted with the purpose to finely analyze rupture profiles in single force-extension curves, the theoretical predictions remain difficult, due essentially to the long computational time required by atomistic simulations, which, moreover, use parameter values –specifically the velocity at which one extreme of the quadruplex is pulled to induce the rupture– orders of magnitude far away from the experimental values.

With the aim to bridge the gap between experiment and theoretical expectations, we build a mesoscopic physical model of the G-quadruplex structure with a reduced number of degrees of freedom and a few effective potentials that permits to study the mechanical unfolding in a wider interval of time scales than those allowed in all-atom simulations, in particular under different pulling velocities. The subsequent analysis on the light of the most recent stochastic theories for rupture force –as those of Bell-Evans-Richie, Evans-Hummer-Szabo, and Friddle-Noy-DeYoreo– permit the estimations of the potential barriers and positions that characterize the energy landscape of the unfolding process.

In this communication the model will be presented together with its validation against the results of an unfolding experiment on RNA G-quadruplex pulled by an optical tweezer.

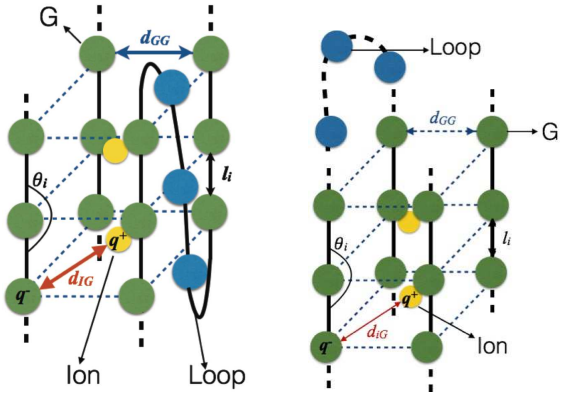

Fig. 1. Mesoscopic model for the G-quadruplex. Scheme of a parallel G4 assembly where each nucleotide is represented by a single bead. The G-tetrad plane are twisted between each other (not represented). (Left) Parallel configuration. (Right) Anti-parallel configuration.

[1] S. Burge, G. N. Parkinson, P. Hazel, A. K. Todd, and S. Neidle, Quadruplex DNA: sequence, topology and structure, Nucleic Acids Res. **34**, 5402 (2006).

[2] E. Y. Lam, D. Beraldi, D. Tannahill, and S. Balasubramanian, G-quadruplex structures are stable and detectable in human genomic DNA, Nat. Commun. **4**, 1796 (2013).

[3] R. Hänsel-Hertsch, M. Di Antonio, and S. Balasubramanian, DNA G-quadruplexes in the human genome: detection, functions and therapeutic potential, Nat. Rev. Mol. Cell Biol. **18**, 279 (2017).

[4] M. de Messieres, J. C. Chang, B. Brawn-Cinani, and A. La Porta, Single-molecule study of G-quadruplex disruption using dynamic force spectroscopy, Phys. Rev. Lett. **109**, 058101 (2012).

[5] M. Garavís, R. Bocanegra, E. Herrero-Galán, C. González, A. Villasante, and J. R. Arias-Gonzalez, Mechanical unfolding of long human telomeric RNA (TERRA), Chem. Commun. **49**, 6397 (2013).

[6] A. E. Bergues-Pupo, J. R. Arias-Gonzalez, M. C. Morón, A. Fiasconaro, and F. Falo, Role of the central cations in the mechanical unfolding of DNA and RNA G-quadruplexes, Nucleic Acids Res. **43**, 7638 (2015).

[7] A. E. Bergues-Pupo, I. Gutierrez, J. R. Arias-Gonzalez, F. Falo, and A. Fiasconaro, Mesoscopic model for DNA G-quadruplex unfolding, Sci. Rep. **7**, 11756 (2017).

Solvent hydrodynamics alter the collective diffusion of quasi two-dimensional systems: From trapped colloids to membrane lipids

Rafael Delgado-Buscalioni[1,2]
[1]Department of Theoretical Condensed Matter Physics, Universidad Autónoma de Madrid, Spain
[2]Condensed Matter Institute (IFIMAC), Madrid, Spain

In many instances, molecules and colloidal particles move confined to a two-dimensional (2D) manifold which is embedded in a 3D solvent. The confined domain could be a perfectly flat plane, like colloids moving in a fluid-fluid interface or trapped by acoustic or optical forces, it could be a fluctuating plane, like in membrane lipids (also spherical vesicles), or maybe just softly confined, like colloids near a charged wall, etc. These dynamics are usually called quasi two-dimensional (q2D) and the situation can be even extended to 1D (kinesines walking along microtubules).

The hydrodynamic interaction with the solvent makes these q2D dynamics particularly surprising. For instance, if we follow a single Brownian q2D particle it would be hard to notice any change with respect the 3D (bulk) diffusion. However, looking at a collection of them (a stain) yields a radically different view. Unlike standard Brownian dynamics, in q2D their displacements become highly correlated and the collective diffusion coefficient D_c (of a stain of wavelength λ) increases without bound with the wavelength! (in particular, like $D_c \sim \lambda$).

This anomalous behavior has been theoretically predicted and experimentally measured (see Ref. [1]). We have recently shown that the same effect is observed in softly confined colloids, provided λ is larger than the confinement width [2]. This enhancement of coherent motions arises from the hydrodynamic propagation of the confinement forces, which act on the particles in normal-to-plane direction. These normal forces are immediately transmitted to the plane via the Oseen solvent hydrodynamics and create a mutual drag which is long-ranged and repulsive, like a "electrostatic" force between the particles [1, 3] (see Fig. 1).

This q2D effect also radically changes the non-equilibrium spectra of density fluctuations so it modifies the way two species mix in the plane [3]. Even more surprisingly, using MD (Martini) and CG dynamics with hydrodynamics, we found that q2D dynamics also rule the short-time collective motion of lipids in membranes [4]. Most probably this q2D dynamics will be also relevant for membrane proteins. Interestingly, the time-lag dependent mutual-mobility indicates a cross-over from q2D to the intrinsic membrane (2D) collective dynamics, where the Saffmann dynamics takes over at long times. However, lipid displacements correlations persist over quite long times!

[1] J. Bleibel, A. Domínnguez, F. Gunther, J. Harting, and M. Oettel, Soft Matter **10**, 2945 (2014).

[2] S. Panzuela, R. P. Peláez, and R. Delgado-Buscalioni, Phys. Rev. E **95**, 012602 (2017).

[3] R. P. Peláez, F. B. Usabiaga, S. Panzuela, Q. Xiao, R. Delgado-Buscalioni and A. Donev, J. Stat. Mech. **2018**, 063207 (2018).

[4] S. Panzuela and R. Delgado-Buscalioni, Phys. Rev. Lett. (in press) [arXiv:1803.03961].

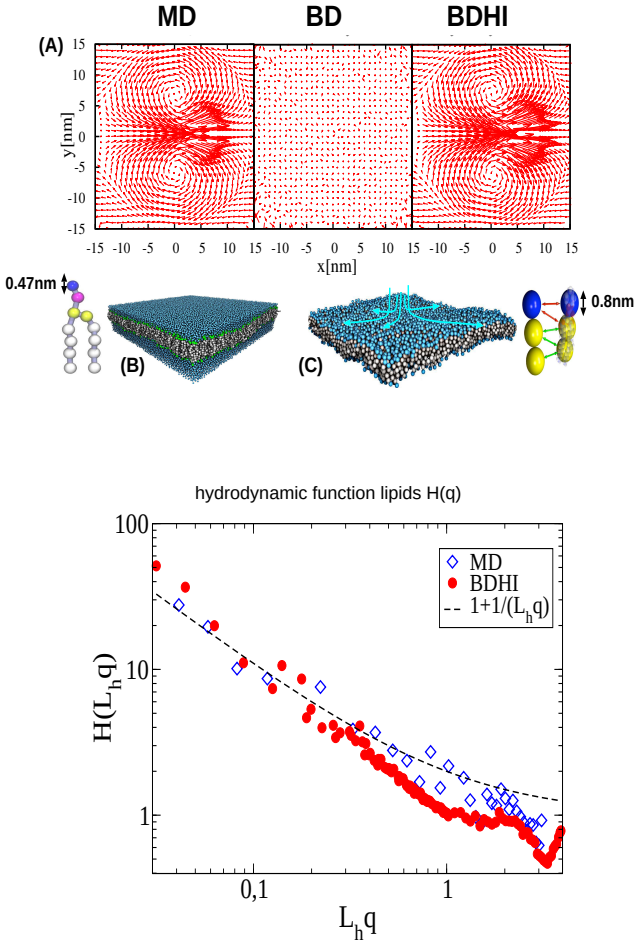

Fig. 1. (Top) Velocity field obtained from the relative displacement of lipids in the membrane. Results from molecular dynamics (Martini model) with explicit water (MD); Brownian dynamics without hydrodynamics (BD) and Immersed boundary method in the Stokes regime (i.e., with implicit solvent hydrodynamics, BDHI). In BD and BDHI, we use the Deserno membrane model. (Bottom) Comparison of the hydrodynamic function $H(q)$ (proportional to the collective diffusion coefficient) for MD and BDHI. The dashed line comes from the theory of q2D.

Mechano-chemical waves in viscoelastic models of cell cytoplasm: Applications to cell locomotion

Francesc Font and Sergio Alonso
Department of Physics, Universitat Politècnica de Catalunya, Barcelona, Spain

The cytoskeleton of the single living cells is a prominent example of a complex active viscoelastic material wherein stresses induce flows along the organism as a result of the action of molecular motors. Experiments with different types of cells have revealed a rich variety of mechano-chemical patterns including standing, traveling and rotating waves that arise from instabilities of spatially homogeneous states. We investigate simple models where an active stress induced by molecular motors is coupled to a model describing the passive viscoelastic properties of the cellular material [1].

Our focus is on the analysis of the conditions that cause destabilization of spatially homogeneous states and the related onset of mechano-chemical waves and patterns. We carry out linear stability analyses and numerical simulations in one spatial dimension for different models [2]. In general, sufficiently strong activity leads to waves and patterns. Specifically, two models for viscoelastic fluids (Maxwell and Jeffrey model) and two models for viscoelastic solids (Kelvin-Voigt and Standard model) are investigated, see differences among both responses in Fig. 1. The primary instability is stationary for all active fluids considered, whereas all active solids have an oscillatory primary instability. All instabilities found are of long-wavelength nature reflecting the conservations of some biochemical concentrations in the models studied [2].

A even more realistic approximation is to assume the cytoplasm as a porous media where a viscoelastic solid formed by the actin network is immersed in the viscous cytosol, formed by water and small molecules [3]. We have applied the concept of active poroviscoelastic cytoplasm [1] to the study of the thickness and chemical oscillations in micro-droplets of *Physarum polycephalum* [4]. The oscillations of such micro-droplets is related with the polarization of the cell and produces the self-organization of the resulting cell and the final motion [5].

The self-organization process inside of the cell is also observed in amoebae motion of neutrophils and other cells like *Dictyostelium discoideum*. We couple the internal polarization processes responsible for the locomotion of such cells and the viscoelastic properties of their cytoplasm for the evaluation of the modifications in the motion properties of the cells. We integrate numerically the resulting equations to characterize the dependence of the velocity on the viscoelastic parameters.

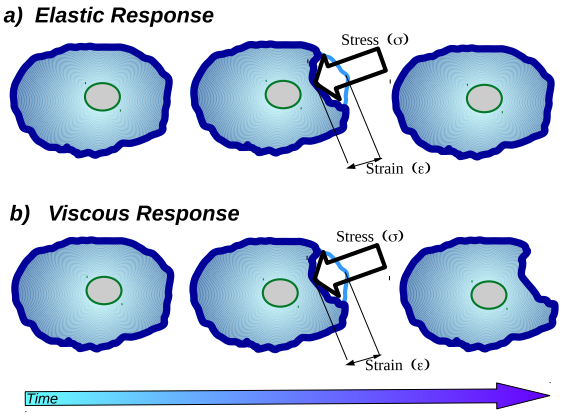

Fig. 1. Scheme of the characteristic responses of an elastic (a) and a viscous (b) cell to an externally applied stress in the limit of solid (cell recovers initial configuration), and fluid (cell interior flows and remains deformed) cytoplasm, respectively.

[1] M. Radszuweit, S. Alonso, H. Engel, and M. Bär, Intracellular mechanochemical waves in an active poroelastic model, Phys. Rev. Lett. **110**, 138102 (2013).

[2] S. Alonso, M. Radszuweit, H. Engel, and M. Bär, Mechanochemical pattern formation in simple models of active viscoelastic fluids and solids, J. Phys D **50**, 434004 (2017).

[3] E. Moeendarbary, L. Valon, M. Fritzsche, A. R. Harris, D. A. Moulding, A. J. Thrasher, E. Stride, L. Mahadevan, and G. T. Charras, The cytoplasm of living cells behaves as a poroelastic material, Nat. Mater. **12**, pages 253-261 (2013).

[4] S. Alonso, U. Strachauer, M. Radszuweit, M. Bär, and M. J. B. Hauser, Oscillations and uniaxial mechanochemical waves in a model of an active poroelastic medium: Application to deformation patterns in protoplasmic droplets of *Physarum polycephalum*, Physica D **318**, 58-69 (2016).

[5] B. Rodiek, S. Takagi, T. Ueda, and M. J. B. Hauser, Patterns of cell thickness oscillations during directional migration of *Physarum polycephalum*, Eur. Biophys. J. **44**, 349-358 (2015).

Contribution of water to protein folding and strategies for protein design

Giancarlo Franzese[1,2]
[1]Secció de Física Estadística i Interdisciplinària, Departament de Física de la Matèria Condensada, Facultat de Física, Universitat de Barcelona, Martí i Franquès 1, 08028 Barcelona, Spain
[2]Institute of Nanoscience and Nanotechnology (IN2UB), 08028 Barcelona, Spain

The mechanisms of cold and pressure denaturation of proteins are matter of debate and are commonly understood as due to water-mediated interactions. Here, we study several cases of proteins, with a unique native state or intrinsically disordered, by means of a coarse-grain protein model in explicit solvent. We show, using Monte Carlo simulations, that taking into account how water at the protein interface changes its hydrogen bond properties and its density fluctuations [1, 2, 3, 4] is enough to predict protein stability regions with elliptic shapes in the temperature-pressure plane, consistent with previous theories.

Our results [5, 6] clearly identify the different mechanisms with which water participates to denaturation and allow us to develop an advanced computational design protocol for protein engineering [7]. In particular, we apply our design analysis to understand why proteins that are functional at ambient conditions do not necessarily work at extreme conditions of temperature T and pressure P, and why there are limits of T and P above which no protein has a stable functional state. We show that the hydropathy profile of proteins is a consequence of evolutionary pressure exerted by water [7]. This result can lead the way for engineering working proteins and drugs at extreme conditions and is potentially relevant in protein self-assembly [8].

The authors acknowledge funding from the Spanish MINECO Grant No. FIS2015-66879-C2-2-P, and the ICREA Foundation.

[1] G. Franzese, V. Bianco, and S. Iskrov, Water at interface with proteins, Food Biophys. **6**, 186 (2011).

[2] V. Bianco, S. Iskrov, and G. Franzese, Understanding the role of hydrogen bonds in water dynamics and protein stability, J. Biol. Phys. **38**, 27 (2012).

[3] G. Franzese and V. Bianco, Water at biological and inorganic interfaces, Food Biophys. **8**, 153 (2013).

[4] V. Bianco and G. Franzese, Critical behavior of a water monolayer under hydrophobic confinement, Sci. Rep. **4**, 4440 (2014).

[5] V. Bianco and G. Franzese, Contribution of water to pressure and cold denaturation of proteins, Phys. Rev. Lett. **115**, 108101 (2015).

[6] V. Bianco, N. Pagès-Gelabert, I. Coluzza, and G. Franzese, How the stability of a folded protein depends on interfacial water properties and residue-residue interactions, J. Mol. Liq. **45**, 129 (2017).

[7] V. Bianco, G. Franzese, C. Dellago, and I. Coluzza, Role of water in the selection of stable proteins at ambient and extreme thermodynamic conditions, Phys. Rev. X **7**, 021047 (2017).

[8] O. Vilanova, V. Bianco, and G. Franzese, Multi-scale approach for self-assembly and protein folding, in *Design of Self-Assembling Materials*, edited by I. Coluzza (Springer International Publishing, 2017), pp. 107-128.

Critical phenomena and their microscopic origin in the current fluctuations of driven diffusive systems

Carlos Pérez Espigares
Departamento de Electromagnetismo y Física de la Materia, Universidad de Granada, 18071 Granada, Spain

The discovery of dynamical phase transitions (DPTs) in the fluctuations of non-equilibrium systems has attracted much attention in recent years. In contrast with standard critical phenomena, which occur at the configurational level when varying a control parameter such as the temperature, DPTs appear in trajectory space when conditioning the system to sustain an unlikely value of dynamical observables such as the time-integrated current. DPTs thus manifest as a change in the trajectories in order to enhance the probability of such large fluctuations, making them far more probable than anticipated due to the emergence of ordered structures such as travelling waves, condensates or hyperuniform states.

Particularly interesting is that driven diffusive systems may undergo DPTs in order to sustain atypical values of the current. This leads in some cases to intriguing symmetry-breaking phenomena at the level of trajectories which increase the probability of such rare events. In this talk we will shed light on both the macroscopic properties and the microscopic origin of such spontaneous symmetry breaking in a paradigmatic diffusive model, the so-called weakly asymmetric exclusion process. By defining a collective order parameter and making use of large deviation theory we will uncover, for any boundary driving, the full dynamical phase diagram. We will additionally show that the optimal profiles in the symmetry-broken phase correspond to the extreme metastable states stemming from the gapless region of the generator of the dynamics. We will finally provide the first direct observation of this phenomenon through extensive numerical simulations generating rare trajectories by means of population dynamics techniques.

These results thus represent a step forward in the connection of current fluctuations in driven diffusive systems with metastability and standard critical phenomena.

Flow properties of particle mixtures in micro and nano-channels coated with responsive-polymer brushes

Joan J. Cerdà[1], Pedro Sánchez[2], Sofia Kantovich[2,3], and Tomàs Sintes[4]
[1]Departament de Física UIB i Institut d'Aplicacions Computacionals de Codi Comunitari (IAC3), Campus UIB, 07122 Palma de Mallorca, Spain
[2]Faculty of Physics, Universität Wien, Boltzmanngasse 5, 1090 Wien, Austria
[3]Ural Federal University, Lenin av. 51, 620000, Ekaterinburg, Russia
[4]IFISC (UIB-CSIC), Campus UIB, 07122 Palma de Mallorca, Spain

Responsive polymer brushes are key actors in many biological structures (like glycocalix) and have found application in many technological applications ranging from medicine to nanotechnology (e.g., nanoactuators). In this work we explore the capacity of some of those polymeric structures to control the flow properties of a polydisperse mixture of particles flowing through micro and nanochannels coated with those responsive structures.

Our results shed light on the complexity of those flows and in the case of magnetic controllable structures [1, 2, 3, 4, 5] we observe that it is possible to induce a lateral separation of the different types of particles and in addition to enhance the differences in the velocity of particles due to their different size (see, e.g., Fig. 1). These features lead us to conclude that these kind of systems could be used in the design of new types of chromatographic columns with enhanced properties when compared with current column models.

J. J. Cerdà, P.S., and S.K. thank the finantial support of the Spanish Ministry of Economy and Competitiveness (MINECO/AEI/FEDER,UE) through the project *Proyecto de I+D (excelencia) DPI2017-86610-P*.

[1] J. J. Cerdà, P. A. Sánchez, C. Holmb, and T. Sintes, Soft Matter **9**, 7185-7195 (2013).

[2] J. J. Cerdà, P. A. Sánchez, D. Lüsebrink, S. Kantorovichbd, and T. Sintes, Phys. Chem. Chem. Phys. **18**, 12616-12625 (2016).

[3] D. Lüsebrink *et al.*, J.Chem. Phys. (under review).

[4] P. A. Sánchez, E. S. Pyanzina, E. V. Novak, J. J. Cerdà, T. Sintes, and S. S. Kantorovich, Faraday Discuss. **186**, 241-263 (2016).

[5] P. A. Sánchez, E. S. Pyanzina, E. V. Novak, J. J. Cerdà, T. Sintes, and S. S. Kantorovich, Macromolecules **48**, 7658-7669 (2015).

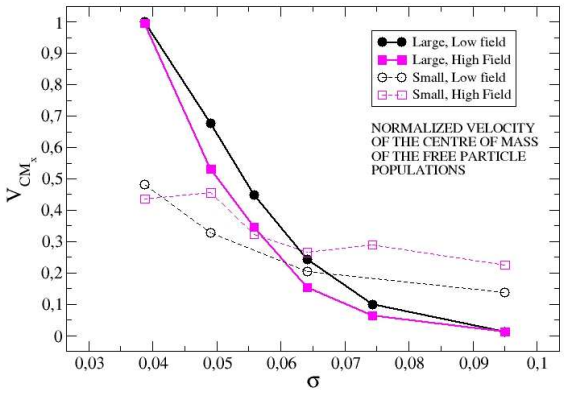

Fig. 1. Normalized velocity of the centre of mass for a bidisperse size distribution mixture of particles (diameter ratio 1:2) as a function of the grafting density of polymers in a magnetic tunable polymeric brush.

Ordering and defects in vibrated monolayers of granular rods

Ariel Díaz-De Armas[1], Martín Maza Cuello[2], Yuri Martínez-Ratón[1], and Enrique Velasco[2]
[1]Departamento de Matemáticas, Universidad Carlos III de Madrid, av. Universidad 30, E-28911 Leganés, Madrid, Spain
[2]Departamento de Física Teórica de la Materia Condensada, Universidad Autónoma de Madrid, E-28049 Madrid, Spain

The appearance of liquid-crystalline structures in 2D fluids of hard anisotropic particles provides a great opportunity for experimentation, aimed towards the study and understanding of liquid-crystal phases and phase transitions. The stability of these structures has been shown to be completely determined by entropy [1, 2]. Particles such as hard rectangles (HR) can be found on a completely unordered state referred to as the **I**sotropic phase, but also a **N**ematic phase where the main particle axis orientates on average along a common director. Unique to HR fluids is the **T**etratic phase where particles align along 2 different directors perpendicular to each other. Other oriented phases such as the **S**mectic phase, formed by layers perpendicular to the particles main axis, are also present. Monolayers of vertically shaken granular rods have been found to present similar liquid-crystal textures as stationary states [3, 4, 5]

Our work presents experiments conducted on a monolayer of granular cylindrical rods whose 2D projections are HR. The particles are vibrated in the vertical direction and they are not allowed to overlap, becoming in practice a 2D system. They are confined to a circular cavity (see Fig. 1 for the sketch of our experimental setup). Among the main lines of our study is that of understanding not only the effect of the shape of the cavity (circular vs. square) on the overall system behaviour but also the changes in the stable spatial patterns induced by the presence of a central obstacle of varying size.

By means of image analysis we are able to calculate local order parameters $Q_n(\mathbf{r})$ for each phase, defined from the angular distribution function of the local particle orientations $h(\phi, \mathbf{r})$, in the frame of the **N** director, as

$$Q_n(\mathbf{r}) = \int_0^{2\pi} d\phi \; h(\phi, \mathbf{r}) \cos(n\phi), \qquad (n = 2, 4), \qquad (1)$$

where ϕ is the angle between particle axis and the **N** director, $\mathbf{r}$ is the spatial coordinate and $Q_2(\mathbf{r})$ and $Q_4(\mathbf{r})$ correspond to the **N** and **T** local order parameters, respectively. At bulk the **T** phase has $Q_2 = 0$ while $Q_4 \neq 0$ due to the symmetry $h(\phi) = h(\phi + \frac{\pi}{2})$ while the **N** phase has both order parameters different from zero because of the symmetry $h(\phi) = h(\phi + \pi)$.

We have found the appearance of four punctual defects in the orientations of the nematic director following the **T** ordering. These defects have a total topological charge of 4 and are approximately located in the corners of a square as the system attempts to solve the frustration induced by the circular cavity. The introduction of the central obstacle has shown to favour the formation of **S** domains, which also present a high value of $Q_2(\mathbf{r})$, separated by blade-like interfaces (Fig. 2) and also pull the defects towards the middle,

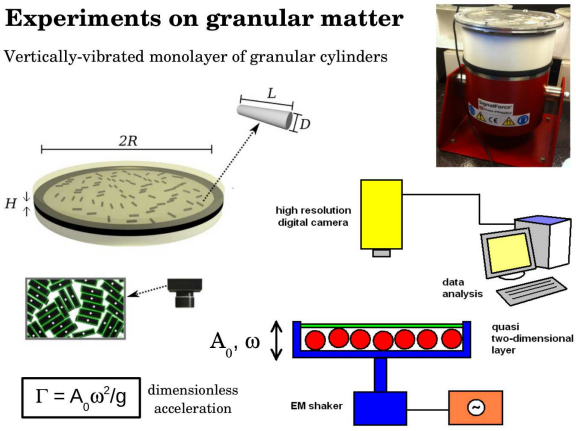

Fig. 1. Experiment concept and setup.

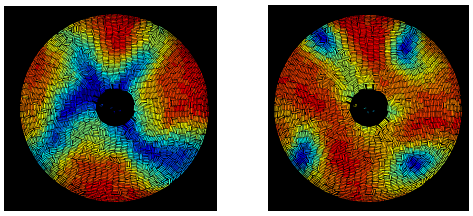

Fig. 2. Images of colored particles according to the values of the local order parameters (going from blue to red as Q_n goes from low to high values). Q_2 and Q_4 are shown left and right, respectively.

sometimes connecting the inner and outer walls through a line. We have also observed that the obstacle induces strong unidirectional rotation once a particular configuration stabilizes.

We have developed ways to track the evolution of defects and studied the impact of clustering in the stability of different phases.

[1] M. A. Bates and D. Frenkel, J. Chem. Phys. **122**, 10034 (2000).

[2] Y. Martínez-Ratón, E. Velasco, and L. Mederos, J. Chem. Phys. **122**, 064903 (2005).

[3] V. Narayan, N. Menon, and S. Ramaswamy, J. Stat. Mech. **2006**, P01005 (2006).

[4] T. Müller, D. de las Heras, I. Rehberg, and K. Huang, Phys. Rev. E **91**, 062207 (2015).

[5] M. González-Pinto, F. Borondo, Y. Martínez-Ratón, and E. Velasco, Soft Matter, **13**, 2571 (2017).

Trasgos: Analysis of the atmospheric properties with a high resolution cosmic ray detector

Irma Riádigos, Damián García-Castro, Diego González-Díaz,
J. A. Garzón-Heydt, and Vicente Pérez-Muñuzuri
TRAGALDABAS Collaboration, Faculty of Physics, Universidad de Santiago de Compostela,
15782 Santiago de Compostela, Spain

Cosmic rays constantly reach the Earth and collide with the nuclei of atmospheric atoms creating billions of secondary particles. The measurement of such particles reaching the surface may provide very valuable information about the properties of the atmosphere.

A strong correlation exists between different variables of the atmosphere and the arrival of the secondary particles called muons. For several years, studies of the influence of temperature have been performed for muons of different energies and angles of incidence [1, 2, 3]. However, modern cosmic ray detectors are mostly committed to the study of solar activity and other astrophysical phenomena, and therefore their intention is to remove those effects using simple techniques, or to use them to coarsely assess the instrument response. Our work is concerned with a deeper comprehension of such atmospheric effects.

For this purpose, a medium-size tRPC detector (1.2×1.5 m^2) of high resolution ($\sigma_{x,y} \sim 3$ cm, $\sigma_t \sim 300$ ps, $\sigma_\theta \sim 2.5°$) of the TRASGO family, called TRAGALDABAS, was installed in the Physics Department of the University of Santiago de Compostela (Spain). Timing resistive plate chambers (or tRCPs) are prime detectors when aimed at large area coverage with ultimate time-of-flight resolution. Due to its granularity and versatile trigger, this instrument is able to select high and low multiplicity events, by individually identifying and reconstructing each of its constituent tracks. In addition, ECMWF reanalysis datasets provide the temperature profiles up to several kilometers, as required for our research.

Current techniques take into account the temperature effect by using an approximation of the integral method for muons, which requires, on the one hand, having the temperature profiles above the detector and, on the other hand, the theoretical distribution of temperature coefficients [4]. However, in our case we have to deal with multiplicities instead of energies and the presence of the soft component in our data as well. Therefore, we need to study the dependence of our data grouped by multiplicities with the several parts of the atmosphere [5]. However, the variations of temperature of the different atmospheric layers are strongly correlated and as a consequence, the study of this dependence turns out to be quite complicated. We perform some statistical methods for analyzing multicollinearity.

Supposing that each multiplicity gives us information about the temperature of different parts of the atmosphere, we could develop an inverse method which allow us to obtain the temperature at different heights using the measured variations in our multiplicity rates.

[1] M. Ambrosio, R. Antolini, G. Auriemma, R. Baker, A. Baldini, G. C. Barish, G. Battistoni, R. Belloti, C. Bemporad *et al.*, Seasonal variations in the underground muon intensity as seen by MACRO, Astropart. Phys. **7** 109-124 (1997).

[2] S. Osprey, J. Barnett, J. Smith, P. Adamson, C. Andreopoulos, R. Armstrong, D. J. Auty, D. S. Ayres, B. Baller *et al.*, Sudden stratospheric warmings seen in MINOS deep underground muon data, Geophys. Res. Lett. **36**, L05809 (2009).

[3] S. Tilav, P. Desiati, T. Kuwabara, D. Rocco, F. Rothmaier, M. Simons, H. Wissing *et al.*, Atmospheric variations as observed by IceCube, arXiv:1001.0776.

[4] A. N. Dmitrieva, R. P. Kokoulin, A. A. Petrukhin, and D. A. Timashkov, Corrections for temperature effect for ground-based muon hodoscopes, Astropart. Phys. **34**, 401-411 (2011).

[5] J. A. Garzón *et al.*, TRAGALDABAS. First results on cosmic ray studies and their relation with te solar activity, the Earth's magnetic field and the atmospheric properties, XXV ECRS 2016 Proceedings, arXiv:1701.07277.

Comunicaciones póster

Poster Communications

Effective Gaussian diffusion of optically trapped spheres along time-scales

Pablo Domínguez-García[1], László Forró[2], and Sylvia Jeney[2]
[1]Dep. Física Interdisciplinar, Universidad Nacional de Educación a Distancia (UNED), po. Senda del Rey 9, 28040 Madrid, Spain
[2]Laboratory of Physics of Complex Matter, Ecole Polytechnique Fédérale de Lausanne (EPFL), 1015 Lausanne, Switzerland

It is widely accepted that the random displacements of a Brownian particle follow a Gaussian distribution. The probability distribution $P(r,t)$ of the displacements of the particle is named as *propagator* or *van Hove autocorrelation function* [1]. Mathematically it is expressed through

$$P(r,t) = \frac{1}{[4\pi D_{\rm G}(\tau)\, t]^{d/2}} \exp\left(-\frac{\Delta r^2}{4D_{\rm G}(\tau)\, t}\right), \quad (1)$$

where $\Delta r = r(t+\tau) - r(t)$ is the displacement, τ is the lapse time between jumps, d is the system dimension. In Eq. (1), we define an *effective* Gaussian diffusion coefficient $D_{\rm G}(\tau)$, which depends on the time-lapse η of each displacement, but does not depend of the *absolute* time t. However, deviations from the Gaussian behavior should be expected to observed when the particle moves in complex fluids [2], or in a lower time-scale where the hydrodynamical effects are relevant [3, 4].

In this work, we study experimentally, through optical spectroscopy and optical trapping [5], the Brownian motion over six orders of magnitude in the time-scale, with a minimum time-step of 0.5 μs, of optically trapped melamine resin micro-sized spheres immersed in Newtonian and viscoelastic fluids. We obtain the Gaussian profiles of the displacements Δr for every fluid, taking into account that the effective diffusion coefficient depends of the time-lapse τ. The observations are in agreement with the Gaussian behaviour defined by Eq. (1), but $D_{\rm G}(\tau)$ behaves differently depending on the time scale. For Newtonian fluids, we observe that $D_{\rm G}(\tau) \simeq D_0$ in the diffusive regime, where D_0 is the usual Stokes-Einstein diffusion coefficient, $D_0 = k_{\rm B}T/6\pi\eta a$. Deviations from that constant value are observed at higher time-scales where the external optical forces are predominant, and also at lower time-scales, in the *transdiffusive* or pre-ballistic regime. While the former behavior can be explained through the solution of the Fokker-Plank equation under a harmonic potential [6, 7], the latter is probably related to a more complex and generalized solution of the Fokker-Plank equation which includes ballistic and transdiffusive regimes [8].

[1] F. Höfling and T. Franosch, Rep. Prog. Phys. **76**, 046602 (2013).

[2] M. Atakhorrami, G. H. Koenderink, C. F. Schmidt, and F. C. acKintosh, Phys. Rev. Lett. **95**, 208302 (2005).

[3] B. Wang, S. M. Anthony, S. C. Bae, and S. Granick, Proc. Natl. Acad. Sci. USA. **106**, 15160-15164 (2009).

[4] B. Wang, J. Kuo, S. C. Bae, and S. Granick, Nature Materials **11**, 481-485 (2012).

[5] T. Franosch, M. Grimm, M. Belushkin, F. M. Mor, G. Foffi, L. Forró, and S. Jeney, Nature **478**, 85-88 (2011).

[6] H. H. Risken, *The Fokker-Planck Equation: Methods of Solution and Applications* (Springer-Verlag, 1984).

[7] M. Pancorbo, M. A. Rubio, P. Domínguez-García, Procedia Comp. Sci. **108**, 166-174 (2017).

[8] M. A. Malkov, Phys. Rev. D. **95**, 023007 (2017).

Dynamics and synchronization of complex networks with coupling delays and fluctuating topology

Otti D'Huys[1], Javier Rodríguez-Laguna[2], Manuel Jiménez[2], Elka Korutcheva[2,3], and Wolfgang Kinzel[4]
[1]Department of Mathematics, Aston University, B4 7ET Birmingham, United Kingdom
[2]Departamento de Física Fundamental, UNED, Spain
[3]G. Nadjakov Inst. Solid State Physics, Bulgarian Academy of Sciences, 1784, Sofia, Bulgaria
[4]Institut für theoretische Physik, Universität Würzburg, Am Hubland, 97072 Würzburg, Germany

The presence of delay in the interaction systems is an important problem in many real-life systems such as communication networks, neural systems or social networks. Of special interest is the study of networks with changing topology that might elucidate some important behaviors in different systems such as continuous changing neural networks due to the synaptic plasticity or real social networks. Other aspect of importance is the study of static hierarchically organized delay-coupled networks in order to understand how the hierarchy affect the functioning of these systems. In the present communication we study the generic properties of directed delay-coupled networks, which topology changes with time and make comments on the role of the hierarchical organization regarding synchronization properties.

In a previous publication [1] we numerically studied synchronization properties of delay-coupled networks with a time-varying topology. We considered an interaction network of coupled chaotic maps with a single coupling delay T_d, with a topology fluctuating among an ensemble of Small-World networks, with a characteristic time-scale T_n. We found that random network switching may enhance the stability of synchronized states, depending on the interplay between the time-scale of the delayed interactions T_d and that of the network fluctuations T_n.

In this communication we consider an interaction network of coupled chaotic Bernoulli maps in a fluctuating topology directed small-world network with delay, where the third timescale is the internal time scale of the nodes T_in. When the network fluctuations are faster than the coupling delay and the internal time scale ($T_\mathrm{n} \ll T_\mathrm{in}, T_\mathrm{d}$) the synchronized state can be stabilized by the fluctuations. As the network time scale T_n increases, the synchronized state becomes unstable when $T_\mathrm{n} \sim T_\mathrm{d}$. Synchronization is more probable as the network time scale increases further. However, in the slow network regime ($T_\mathrm{n} \gg T_\mathrm{d} \gg T_\mathrm{in}$) the long-term dynamics is desynchronized whenever the probability of reaching a non-synchronizing network is finite. In the intermediate regime the system shows a sensitive dependence on the ratio of time scales, and specific topologies, reproduced as well by numerical simulations.

These results have been complemented with analytical results in the linearized limit, where by using the Master Stability Function [2] on a network of alternating topology [3], we expressed the effective adjacency matrix in terms of the three time scales. We showed that when the network fluctuations are much faster than the internal time scale and the coupling delay ($T_\mathrm{n} \ll T_\mathrm{in}, T_\mathrm{d}$), the effective network topology is the arithmetic mean, while in the opposite case ($T_\mathrm{in} \ll T_\mathrm{n} = T_\mathrm{d}$), the effective topology is the geometric mean over the different topologies.

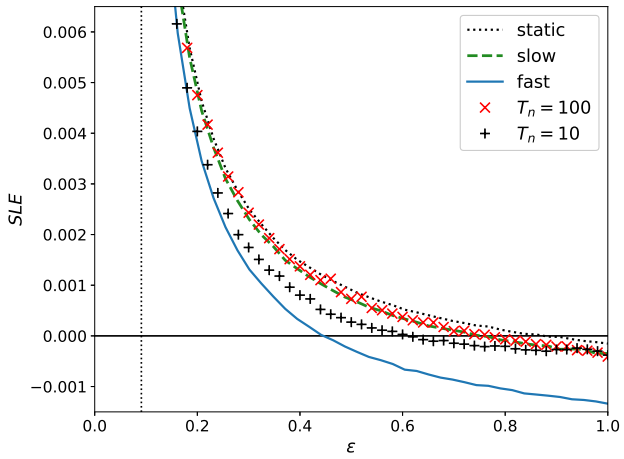

Fig. 1. Numerical synchronization Lyapunov exponent corresponding to the evolution of a time-varying delay-coupled Bernouilli network with $N = 40$ units and time-delay $\tau = 100$, see [3] for details. The solid blue and dashed green lines correspond to the fast and slow effective networks, respectively, obtained as the arithmetic and geometric ensemble mean matrices. We also plot the average SLE of the static case.

Future extensions of the research might be the study of other network ensembles, such as random Erdös-Rényi graphs, scale-free networks or even more complicated graphs of multiplex type with further application to real world problems concerning transport and energy issues or problems of supply networks in the general context of "smart cities".

[1] M. Jiménez Martín, J. Rodríguez-Laguna, O. D'Huys, J. de la Rubia, and E. Korutcheva, Phys. Rev. E **95**, 052210 (2017).

[2] L. M. Pecora and T. L. Carroll, Phys. Rev. Lett. **80**, 2109 (1998).

[3] O. D'Huys, J. Rodríguez-Laguna, M. Jiménez Martín, E. Korutcheva, and W. Kinzel, arXiv:1805.03004.

Non-local hydrodynamic model for flow in slit nanopores

Diego Camargo-Trillos[1], J. A. de la Torre[2], Pep Español[2], and Farid Chejne-Janna[3]
[1]Facultad de Ingeniería y Arquitectura, Universidad Pontificia Bolivariana, Montería, Colombia
[2]Departamento de Física Fundamental, Universidad Nacional de Educación a Distancia, Madrid, Spain
[3]Facultad de Minas, Universidad Nacional de Colombia, Medellín, Colombia

There is a large interest in the understanding of the behaviour of fluids at nanoscales. At these short length scales, the fluid starts displaying features which are absent at the large scales where ordinary Navier-Stokes equations with the no slip boundary condition apply. The density field, for example, displays characteristic layering of the molecules near the walls. In many situations, the fluid slips against the walls. In order to address these problems we have recently formulated in Ref. [1] the equations of hydrodynamics near solid walls starting from first principles. The theory generalizes to non-equilibrium situations the successful Density Functional Theory of classical *simple* fluids [2]. In this hydrodynamic theory the effect of the walls is not through boundary conditions but rather through irreversible forces acting on the fluid and confined near a layer of molecular dimensions near the wall. These forces contain friction transport coefficients given in terms of Green-Kubo formulae [3].

In the present work we study by means of molecular dynamics (MD) simulations the predictions of the theory in planar shear flows. Space is binned and momentum of the fluid, forces due to the walls, and stress of the fluid are defined in terms of finite element basis functions [4, 5] and measured. From these, the Green-Kubo formulae are computed from equilibrium MD simulations. These transport coefficients which are non-local in space, are input of the discrete hydrodynamic equations and allow to predict the flow field in a decay situation from a given initial flow condition. We consider both plug flow and Couette flow that suddenly is left unforced and decay towards equilibrium. The predictions of the theory and the simulations are in a reasonable but not perfect agreement. We attribute the discrepancies to the fact that the Green-Kubo expressions suffer strongly from the plateau problem. This suggest that non-Markovian effects may play a role in this problem.

[1] D. Camargo, J. A. de la Torre, D. Duque-Zumajo, P. Español, R. Delgado-Buscalioni, F. Chejne, J. Chem. Phys, **148**, 064107 (2018).

[2] J. P. Hansen and I. McDonald, *Theory of Simple Liquids* (Academic Press, London, 1986).

[3] L. Bocquet and J. L. Barrat, Phys. Rev. E **49**, 3079 (1994).

[4] P. Español and I. Zúñiga, J. Chem. Phys. **131**, 164106 (2009).

[5] J. A. de la Torre and P. Español, J. Chem. Phys. **135**, 114103 (2011).

Nanoscale hydrodynamics in periodic and confined planar geometries

Diego Duque-Zumajo, J. A. de la Torre, and Pep Español
Universidad Nacional de Educación a Distancia, Madrid, Spain

The behavior of a fluid at large scales is governed by the well-known Navier-Stokes equations of hydrodynamics. At the nanoscale these equations are no longer appropriate because the fluid starts to behave in a non-local way in both space and time, leading to Generalized Hydrodynamics [1, 2, 3, 4]. Correlation functions of hydrodynamic variables are defined in reciprocal space and measured in molecular dynamics (MD) simulations, thus providing a wealth of information about the behavior of fluids at small scales [5, 6, 7].

In this work, we address the problem of hydrodynamics at small scales of a fluid in periodic and confined planar geometries. While Generalized Hydrodynamics usually assumes rotational and translational invariance, in confined systems these symmetries are lost. For this reason, we work in real space and define the hydrodynamic variables in terms of slabs [8, 9]. We choose as relevant variable the transverse momentum after checking through MD simulations that the coupling between this component and the rest of hydrodynamic variables (density, rest of momentum components and energy) is negligible.

Mori projector technique is used to construct an exact linear equation for the correlation function of the transverse momentum, which contains a memory kernel. A clear separation of time scales is invoked in such a way that an approximate Markovian differential equation is obtained. The distinctive feature of the Markovian approximation in Mori theory is to predict a (matrix) exponential decay of the correlation. We show that this prediction is satisfied in our simulations *after* a time of molecular size has elapsed. We also show that after this time, a local approximation seems to be sufficient for describing the decay of the momentum correlation.

This methodology is followed in both unconfined and confined fluids, allowing us to discuss the effects of solid walls on the fluid.

[1] R. D. Mountain, Adv. Mol. Relax. Process. **9**, 225 (1975).

[2] J. P. Boon and S. Yip, *Molecular Hydrodynamics* (McGraw-Hill, New York, 1980).

[3] J. P. Hansen and I. McDonald, *Theory of Simple Liquids* (Academic Press, London, 1986).

[4] W. E. Alley and B. J. Alder, Phys. Rev. A *27*, 3158 (1982).

[5] C. H. Chung and S. Yip, Phys. Rev. **182**, 323 (1969).

[6] I. de Schepper, E. Cohen, C. Bruin, J. van Rijs, W. Montfrooij, and L. de Graaf, Phys. Rev. A **38**, 271 (1988).

[7] R. E. Khayat and B. C. Eu, Phys. Rev. A **39**, 728 (1989).

[8] P. Español and I. Zuñiga, J. Chem. Phys. **131**, 164106 (2009).

[9] J. A. de la Torre and P. Español, J. Chem. Phys **135**, 114103 (2011).

Transición de vidrio a cristal en esferas duras mediante avalanchas de partículas

P. Montero de Hijes[1], P. Rosales-Pelaez[1], P. N. Pusey[2], E. Sanz[1] y Chantal Valeriani[3]
[1]Departamento de Química Física I, Facultad de Ciencias Químicas, Universidad Complutense de Madrid, 28040 Madrid, Spain
[2]SUPA, School of Physics and Astronomy, University of Edinburgh, Edinburgh EH9 3FD, United Kingdom
[3]Departamento de Estructura de la Materia, Física Térmica y Electrónica, Facultad de Ciencias Físicas, Universidad Complutense de Madrid, 28040 Madrid, Spain

Un vidrio es un sólido amorfo fuera del equilibrio termodinámico, formado cuando un líquido se subenfría lo suficiente sin que cristalice en el proceso. En este estado no hay difusión y el movimiento de las partículas se limita a distancias que no superan el propio diámetro de éstas. Dada la inestabilidad termodinámica que presenta, un vidrio tratará, no sin dificultades, de minimizar su energía mediante un proceso de cristalización (devitrificación). El sistema más adecuado para estudiar los fundamentos de la devitrificación son las esferas duras.

Es sabido que los vidrios de esferas duras cristalizan mediante avalanchas de partículas [1] y hay indicios de que regiones de bajo orden cristalino o pseudo-cristalino y de baja densidad [2] pueden jugar un papel importante. También se ha avanzado en aspectos técnicos de la simulación de vidrios de esferas duras [3, 4] lo que nos permite acceder a más información relevante en un menor tiempo de computación.

Sin embargo, ni las avalanchas han sido caracterizadas más allá de su cooperatividad, ni su origen esta bien definido. Recientemente, hemos observado cómo algunas configuraciones vítreas son mucho más propensas a la cristalización que otras, lo que evidencia un origen estructural. Para comprender qué hace a una configuración propensa a cristalizar se estudia qué fenómenos locales pueden alargar la esperanza de vida de un vidrio o de lo contrario, acortarla. También se busca qué características comparten las configuraciones propensas y en cuáles se diferencian de las no propensas a la cristalización. Entre estas posibles características a estudiar encontramos la rigidez local, la distribución de fuerzas o la actividad local.

Destapando estas incógnitas, podemos entender la devitrificación y aprender a preservar los vidrios por más tiempo, lo que sería de utilidad en muchos ámbitos tecnológicos.

[1] E. Sanz, C. Valeriani, E. Zaccarelli, W. C. K. Poon, M. E. Cates, and P. N. Pusey, Avalanches mediate crystallization in a hard-sphere glass, Proc. Natl. Acad. Sci. USA **111**, 75-80 (2014).

[2] T. Yanagishima, J. Russo, and H. Tanaka, Common mechanism of thermodynamic and mechanical origin for ageing and crystallization of glasses, Nat. Commun. **8**, 15954 (2017).

[3] P. Montero de Hijes, P. Rosales-Pelaez, C. Valeriani, P. N. Pusey, and E. Sanz, Brownian *versus* Newtonian devitrification of hard-sphere glasses, Phys. Rev. E **96**, 020602(R) (2017).

[4] P. Rosales-Pelaez, P. Montero de Hijes, E. Sanz, and C. Valeriani, Avalanche mediated devitrification in a glass of pseudo hard-spheres, J. Stat. Mech. **2016**, 094005 (2016).

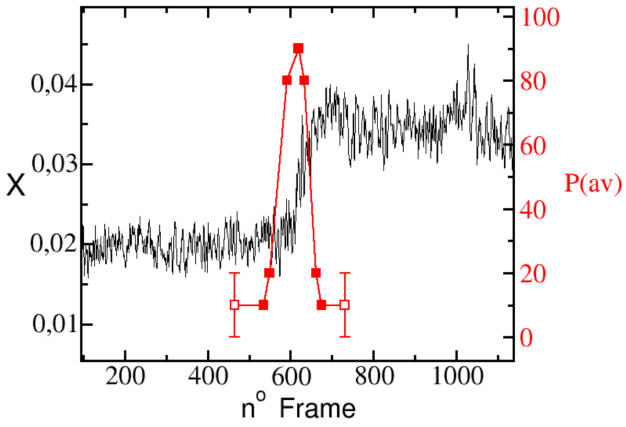

Fig. 1. Cristalinidad del sistema (X, en negro, escala izquierda) y propensidad de avalancha (P(av), en rojo, escala derecha) frente a las correspondientes configuraciones ($\propto t$). Podemos observar un incremento en la cristalinidad que coincide con zonas de mayor propensidad de avalancha lo que sugiere una ruptura de estabilidad mecánica.

Tunable dynamics of flexible magnetic filaments in flow

Daniel Lüsebrink[1], Joan J. Cerdà[2], Pedro A. Sánchez[3], Sofia S. Kantorovich[3], and Tomás Sintes[1]
[1]Instituto de Física Interdisciplinar y Sistemas Complejos (IFISC), UIB-CSIC, Spain
[2]Departamento de Física, Universitat de les Illes Balears, Spain
[3]Faculty of Physics, Universität Wien, Austria

The formation of chain-like structures made of ferromagnetic colloids has been predicted more than four decades ago. Since the pioneering work of Tabata *et al.* [1], and due to advances in experimental techniques, it is possible to synthesize chains of magnetic colloids with different properties. The formation of these chains has important implications in the behaviour of magnetic fluids.

In this poster we present an extensive numerical study in which it is shown how the dynamic properties of flexible magnetic filaments in flow can be controlled with an applied external magnetic field. We found that in the presence of a shear flow the tumbling motion observed at zero field is strongly inhibited when the external magnetic field is applied. The field is able to stabilise the filament with a well defined degree of alignment that depends on the balance between hydrodynamic and magnetic torques. In addition, in the case of a Poiseuille flow, it has been found that the initial position has a long lasting influence on the behaviour of the magnetic filament when the external field is applied [2].

[1] O. Tabata, H. Kojima, T. Kasatani, Y. Isono, and R. Yoshida, Chemo-mechanical actuator using self-oscillating gel for artificial cilia, in *The Sixteenth Annual International Conference on Micro Electro Mechanical Systems, Kyoto, Japan, January 19-23, 2003* (IEEE, New York, 2003), pp. 12-15.

[2] D. Lüsebrink, J. J. Cerdà, P. A. Sánchez, S. S. Kantorovich, and T. Sintes, J. Chem. Phys. **145**, 234902 (2016).

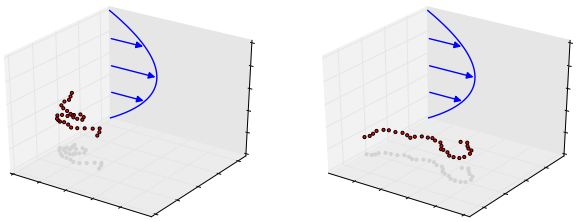

Fig. 1. Two snapshots of the characteristic conformations of a filament subjected to a Poiseuille fluid flow. Tumbling motion observed at zero field $h = 0$.

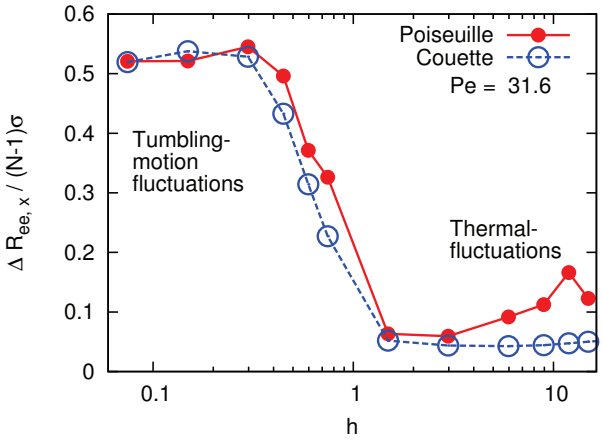

Fig. 2. Fluctuations of the end-to-end distance R_{ee} normalised by the chain contour length $(N-1)\sigma$ of a magnetic filament placed in flow (Couette and Poiseuille with a Peclet number Pe $= 31.6$) as a function of strength of the external magnetic field h.

Statistical theory of phenotype abundance distributions: A test through exact enumeration of genotype spaces

Juan Antonio García-Martín[1,2,3], Pablo Catalán[1,4], Susanna Manrubia[1,2], and José A. Cuesta[1,4,5,6]
[1]Grupo Interdisciplinar de Sistemas Complejos (GISC), Madrid, Spain
[2]Programa de Biología de Sistemas, Centro Nacional de Biotecnología, CSIC, Madrid, Spain
[3]Bioinformatics for Genomics and Proteomics, Centro Nacional de Biotecnología, CSIC, Madrid, Spain
[4]Departamento de Matemáticas, Universidad Carlos III de Madrid, Leganés, Madrid, Spain
[5]Instituto de Biocomputación y Física de Sistemas Complejos (BIFI), Universidad de Zaragoza, Spain
[6]UC3M-BS Institute of Financial Big Data (IFiBiD), Universidad Carlos III de Madrid, Getafe, Madrid, Spain

The evolutionary dynamics of molecular populations are strongly dependent on the structure of genotype spaces. The map between genotype and phenotype determines how easily genotype spaces can be navigated and the accessibility of evolutionary innovations. In particular, the size of neutral networks corresponding to specific phenotypes and its statistical counterpart, the distribution of phenotype abundance, have been studied through multiple computationally tractable genotype-phenotype maps. In this work, we test a theory that predicts the abundance of a phenotype and the corresponding asymptotic distribution (given the compositional variability of its genotypes) through the exact enumeration of several GP maps. Our theory predicts with high accuracy phenotype abundance, and our results show that, in navigable genotype spaces —characterised by the presence of large neutral networks—, phenotype abundance converges to a log-normal distribution.

It has been suggested that the abundance S_{est} of a phenotype can be estimated as follows [1]. If, for a given phenotype, a variable v_i could measure the average number of different letters of the alphabet that show up at site i of its sequences, then

$$S_{\text{est}} = v_1 v_2 \cdots v_L \tag{1}$$

if the genotype is a chain of length L. Suppose an alphabet of k letters, choose a phenotype and count in how many of its genotypes, $m_{\alpha,i}$, letter α shows up at site i. A suitable definition of the *versatility* of site i is

$$v_i = \frac{1}{M_i}\sum_{\alpha=1}^{k} m_{\alpha,i}, \quad M_i \equiv \max\{m_{1,i},\ldots,m_{k,i}\}. \tag{2}$$

In order to evaluate the goodness of this definition, we have tested it for different GP maps regarding how well it predicts the abundance of a specific phenotype component and its relationship with the distribution of phenotype abundances. First, we have folded all RNA sequences of length $L = 16$ and classified them according to their secondary structures (a proxy for their phenotype). Second, we have analysed a variant of this model, made of RNA sequences containing only two complementary bases, in this case G and C. Third, we have analysed the HP model for lattice proteins, where a protein is represented by a self-avoiding chain of hydrophobic (H) or polar (P) beads on a lattice, in its compact and non-compact versions. Finally, we have also analysed tOYLIFE, a multilevel model of a simplified cellular biology [2] in which binary sequences are first mapped to HP-like proteins that interact between themselves, with the genome, and with metabolites. The phenotype is defined by the set of metabolites that a given sequence is able to catabolise. Figure 1 compares the abundance of phenotypes in exact enumerations of genotype spaces with the prediction of Eqs. (1) and (2). A description of all variants of the former GP maps studied and a full discussion of the results can be found in [3].

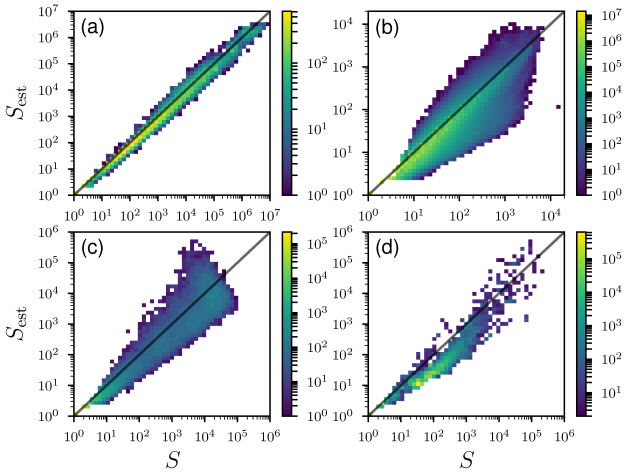

Fig. 1. Log-log-log histograms of the estimated abundance [S_{est} calculated as in Eq. (1)], *versus* actual abundance (S) of the connected components of different GP maps: (a) four-letter RNA of length $L = 16$, (b) two-letter GC-RNA of length $L = 30$, (c) compact HP model 5×6 with $U(HH) = -1$, and (d) tOYLIFE for two genes.

The vastness of genotype spaces prevents a complete characterisation based in computational approaches. Astronomically large numbers are involved in calculations with sequences of length well below that typically found in biochemical processes. An understanding of the structure of realistic GP maps demands further theoretical developments that can be extrapolated to arbitrarily long sequences. The definition of useful quantities such as versatility allows for reliable estimations of the abundance of phenotypes and for the derivation of the expected distribution. Our results yield that distribution in RNA of any length, as well as an estimation of the number of genotypes folding into an arbitrary (typical) structure. Similar derivations should be possible for other GP maps endowed with consistent definitions of phenotype.

[1] S. Manrubia and J. A. Cuesta, Distribution of genotype network sizes in sequence-to-structure genotype-phenotype maps, J. R. Soc. Interface **14**, 20160976 (2017).

[2] C. F. Arias, P. Catalán, S. Manrubia, and J. A. Cuesta, tOYLIFE: a computational framework to study the multi-level organization of the genotype-phenotype map, Sci. Rep. **4**, 7549 (2014).

[3] J. A. García-Martín, P. Catalán, S. Manrubia, and J. A. Cuesta, Statistical theory of phenotype abundance distributions: a test through exact enumeration of genotype spaces, Europhys. Lett. (submitted).

Fusion and fission control the heterogeneity of endosome maturation

Mario Castro[1,2], Grant D. Lythe[2], and Carmen Molina-París[2]
[1]Grupo Interdisciplinar de Sistemas Complejos (GISC) and DNL, Universidad Pontificia Comillas, Madrid, Spain
[2]Department of Applied Mathematics, School of Mathematics, University of Leeds, Leeds, United Kingdom

The fate of many intracellular processes relies on the evolution of an intricate network of endosomes that transport cargo after endocytosis to their final destinations. Recent experimental techniques have provided valuable information about organelle maturation and its specific role in, for instance, the ability of a virus to escape the endosome and release its genetic material in the cytoplasm. Endosome dynamics and function depend on different GTPases (called Rabs) that decorate its membrane. While these molecules have been studied experimentally and even modeled mathematically in the past, there are still many open questions related to their individual dynamics and singularity. In Fig. 2 we depict the interrelationship between different activation states of Rab5 and Rab7 in an endosome.

In this work, we present a mathematical framework, based on the classical theory of drop coagulation and fragmentation to model endosomes with certain levels of Rab5 and Rab7 (in their active form). Let us define $c(x_5, x_7, t)$ as the number of endosomes at a given time t with a given concentration of activated Rab5 and Rab7 (technically, [Rab5:GTP] and [Rab7:GTP], respectively), denoted by x_5, x_7, respectively, at the endosome membrane. That number follows an integro-partial differential equation that is intractable analytically.

Our model allows us to derive simple equations for the mean and standard deviations of the concentrations of Rab5/Rab7 as well as the number of endosomes and fit them to experiments of Dengue virus escape.

$$\dot{N} = S_0 + (K^{(0)}_{\rm FIS} - \mu_0 - \tfrac{1}{2}K^{(5)}_{\rm FUS}R_5 + \tfrac{1}{2}K^{(7)}_{\rm FUS}R_7)N - \tfrac{1}{2}K^{(0)}_{\rm FUS}N^2 \quad (1a)$$

$$\dot{R}_5 = v_{50}N - (v_{55} + \mu_0)R_5 - v_{57}R_7 \quad (1b)$$

$$\dot{R}_7 = v_{70}N + v_{75}R_5 - (v_{77} + \mu_0)R_7 \quad (1c)$$

In Fig. 1 we show the comparison of the theory *vs.* the experimental data for Dengue virus in Ref. [1]. We also make a connection between Rab levels and the endosome pH, thus suggesting a mechanism to account for the experimental variability in the escape times of many viruses.

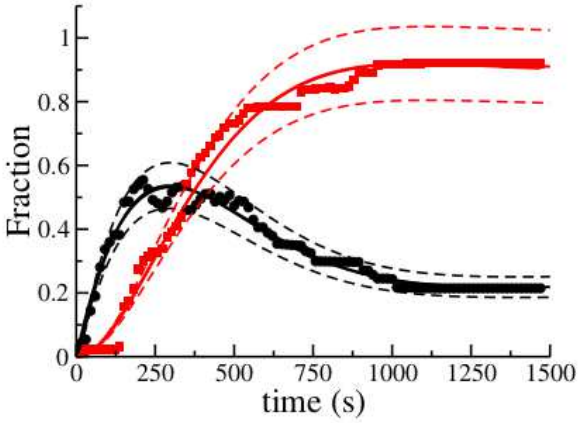

Fig. 1.

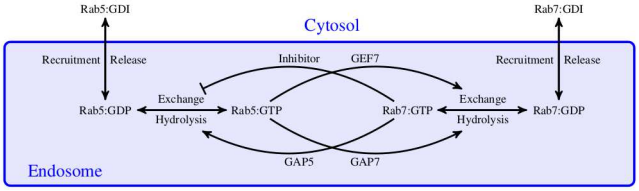

Fig. 2.

Finally, we discuss our approach in the context of other mathematical models that can be derived from our theory and are based on ordinary differential equations for the mean concentrations of Rabs at the cell level.

[1] H. M. van der Schaar, M. J. Rust, C. Chen, H. van der Ende-Metselaar, J. Wilschut, X. Zhuang, J. M. Smit, Dissecting the cell entry pathway of dengue virus by single-particle tracking in living cells, PLoS Pathog. **4**, e1000244 (2008).

El efecto de un obstáculo en la evacuación de personas

A. Garcimartín[1], D. Maza [1], J. M. Pastor [2], D. Parisi [3,4], C. Martín-Gómez[5] e I. Zuriguel[1]
[1]Dpto. de Física y Mat. Apl., Fac. de Ciencias, Universidad de Navarra, 31080 Pamplona, España
[2]Focke Meler Gluing Solutions S.A., Pol. Los Agustinos, calle G nave D-43, 31160 Orkoien, Navarra, España
[3]Instituto Tecnológico de Buenos Aires, CONICET, Lavardén 315, 1437 C. A. de Buenos Aires, Argentina
[4]Comisión Nacional de Investigaciones Científicas y Técnicas (CONICET), Argentina
[5]Dpto. de Construcción, Instalaciones y Estructuras, ETS Arquitectura, Universidad de Navarra, 31080 Pamplona, España

Se pensaba que colocar un obstáculo delante de la salida mejoraría el flujo de personas por una puerta en caso de emergencia. Este efecto, aunque resulte sorprendente, se justifica porque el obstáculo podría reducir la presión en el estrechamiento. Se comprobó experimentalmente que esto es así en un flujo de medios granulares a través de un agujero [1] e incluso en el paso de animales por una puerta [2].

Para ver si el beneficio se obtiene también en el caso de las personas, llevamos a cabo un centenar de evacuaciones en tres días diferentes, los dos primeros con sendos grupos de estudiantes de la Universidad de Navarra y el tercero con soldados del regimiento América 66. Las evacuaciones se realizaron en distintas condiciones: alta competitividad (se permitía empujar, pero sin llegar a lo de Sergio Ramos), baja competitividad (sin contacto físico intencionado), con y sin obstáculo, y éste colocado a diferentes distancias de la puerta. A los participantes se les entrega un gorro rojo, y la salida se filma con una cámara en posición cenital. Una vez identificadas las posiciones de los gorros en cada fotograma, se obtuvo la trayectoria de cada persona mediante la técnica de *particle tracking*. A partir de las trayectorias es fácil calcular las velocidades (Fig. 1).

Como era de esperar, a mayor competitividad, menor caudal. Este efecto, llamado *"Faster-Is-Slower"*, ya se había observado anteriormente [3]. Por lo que respecta al obstáculo delante de la puerta, hemos concluido que no mejora la evacuación, ni en cuanto al tiempo total invertido, ni en cuanto a la disminución de los atascos que se producen. Esto se ha comprobado para los tres grupos citados, y para diferentes colocaciones del obstáculo.

Sin embargo, es posible que el obstáculo sí que tenga un efecto beneficioso: el de reducir los peligrosos movimientos colectivos en forma de bandazos que se producen en situaciones de elevada competitividad (fig. 1). Los hemos caracterizado mediante diferentes cantidades promedio, y calculando la correlación espacial de las velocidades.

[1] I. Zuriguel, A. Janda, A. Garcimartín, C. Lozano, R. Arévalo, and D. Maza, Silo clogging reduction by the presence of an obstacle, Phys. Rev. Lett. **107**, 278001 (2011).

[2] I. Zuriguel, J. Olivares, J. M. Pastor, C. Martín-Gómez, L. M. Ferrer, J. J. Ramos, and A. Garcimartín, Effect of obstacle position in the flow of sheep through a narrow door, Phys. Rev. E **94**, 032302 (2016).

[3] A. Garcimartín, J. M. Pastor, C. Martín-Gómez, D. Parisi, and I. Zuriguel, Pedestrian collective motion in competitive room evacuation, Sci. Rep. **7**, 10792 (2017).

Fig. 1. Instantáneas de evacuaciones en situación de alta competitividad. Las fotografías se tomaron con una cámara cenital situada a 8 metros de altura. La puerta está en la parte superior. Los gorros rojos fueron identificados por procesamiento de imágenes, y las velocidades (*flechas amarillas*) fueron calculadas de las trayectorias obtenidas al procesar el vídeo. En la fotografía superior se aprecia un movimiento colectivo transversal. En la fotografía inferior se muestra un instante de una evacuación con un obstáculo (un depósito cilíndrico, de 1 m de diámetro, relleno con una tonelada de agua) que atenúa esos vaivenes transversales.

Active colloid at a fluid interface

Alvaro Domínguez
Física Teórica, Facultad de Física, Universidad de Sevilla, Spain

The last years have witnessed the growing interest on active colloids, i.e., of colloids made of particles that exhibit chemical activity: this activity induces gradients in the ambient fluid and thus drives a self-induced colloidal dynamics. This kind of systems have attracted attention both as a paradigm of nonequilibrium physics and for its potential applications.

Some recent theoretical work has focused on the case of a monolayer of active colloidal particles at a fluid interface [1, 2, 3]. A new phenomenology arises which is exclusive to the combination "activity + interface", because the interface is also responsive to chemical gradients: the spatial variations of the surface tension induce Marangoni flows in the ambient fluids that manifest themselves as an effective interaction between the colloidal particles and between these and the interface (see Fig. 1).

The most relevant prediction is the existence of "pseudoequilibrium" particle distributions in the monolayer [4]: in these states, the colloidal particles remain at rest although there exist an ambient flow in the embedding fluids. At the mean–field level, the effective interaction due to the Marangoni flow is analogous to two-dimensional Newtonian gravity, and the corresponding "pseudoequilibrium" states describe the coexistence of thermodynamic phases of the monolayer in a layered structure much like in a planet (see Fig. 2). These states, involving many particles, would represent the experimental signature of the Marangoni flows induced by the activity, which are otherwise too weak to be directly observable at the single–particle level [4].

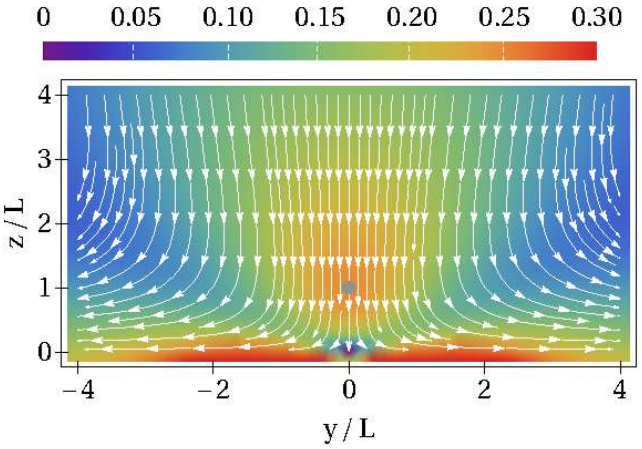

Fig. 1. Marangoni flow induced by the activity of a particle located at the position of the grey dot. The fluid interface is located at the plane $z = 0$. The color scale encodes the magnitude of the flow.

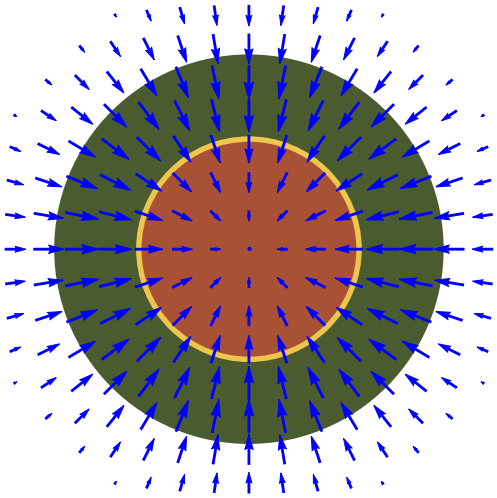

Fig. 2. The predicted structure of a cluster in the monolayer which is confined by its own Marangoni flow (blue arrows), and which exhibits a layered structure of different phases: crystal (brown), hexatic (yellow), and liquid (green). These phases correspond to a mutual interparticle repulsive force decaying like $1/r^4$ with separation r, and have been observed for colloids of ionizable particles [5] or of paramagnetic particles in an external magnetic field [6].

[1] H. Masoud and M. Shelley, Phys. Rev. Lett. **112**, 128304 (2014).

[2] A. Domínguez, P. Malgaretti, M. N. Popescu, and S. Dietrich, Phys. Rev. Lett. **116**, 078301 (2016).

[3] A. Domínguez, P. Malgaretti, M. N. Popescu, and S. Dietrich, Soft Matter **12**, 8398-8406 (2016).

[4] A. Domínguez and M. N. Popescu, arXiv:1804.01451.

[5] C. P. Kelleher, R. E. Guerra, A. D. Hollingsworth, and P. M. Chaikin, Phys. Rev. E **95**, 022602 (2017).

[6] K. Zahn, R. Lenke, and G. Maret, Phys. Rev. Lett. **82**, 2721-2724 (1999).

Experimental results on a granular gas driven by an air-generated stochastic force

Miguel Ángel López Castaño[1], Alvaro Rodríguez-Rivas[1], and Francisco Vega Reyes[1,2]
[1]Universidad de Extremadura, av. Elvas, 06071 Badajoz, Spain
[2]Instituto de Computación Científica Avanzada de Extremadura (ICCAEx), av. Investigación, 06006 Badajoz, Spain

There are many ways to fluidize a granular system, all of which involve injecting energy to it; this can be achieved by many different means, such as through a boundary or by mechanical agitation. But, a less studied method is by interaction of the particles with a gas flow intense enough to initiate movement.

This setup is much inspired on previous works by A. R. Abate, D. J. Durian *et al.* [1, 2, 3]. Contrary to previous works, in our setup there is no potential that causes the particles to recursively return to the system's central zone.

In this experimental work, we analyze the dynamics of a system of granular particles that are excited by means of a vertical air flow (see Fig. 1). The air current is produced by a fan, and carefully homogenized by means of an intermediate layer of polyurethane foam. Uniformity of the air flow is assured by hot-wire anemometer measurements.

More specifically, we investigate the statistical properties of the turbulent air forcing on the granular particles. Spheres are confined within a two-dimensional region so the average 2D occupied area fraction in the system not greater than $\phi \approx 0.01$. Therefore, the system can be regarded as an air-fluidized *granular gas*. The diameter of our particles (ping-pong balls) is $\sigma \approx 4$ cm.

The particles are moving on a metallic mesh and driven by a *uniform air flow* coming from below [1]. The air stream produces a turbulent wake near the ball's surface so that a stochastic force is generated. The intent of the experiment is to approach as much as possible this stochastic force to a white noise [4, 5].

The exact horizontal position and velocity of each particle are measured by a high speed digital camera (under our experimental conditions, the balls never lift up away from the grid). Our camera model is a Phantom VEO 410L, which is capable of recording 5200 fps at maximum resolution (1280×800 pixels).

Detection and tracking of the spheres is performed by a computer vision algorithm. OpenCV's implementation of the *Hough Transform* is applied to the image allowing us to detect borders and find the coordinates and radius of the balls. Thus, we are able to analyze the statistical and hydrodynamic properties of the system.

In a series of measurements, we analyze the experimental value of the coefficient of normal restitution. Additionally, we try to qualitatively deduce the roughness degree of our particles and compare this with previous results from kinetic theory for smooth hard particles [5].

This work is motivated by recent theoretical results that predict a peculiar behavior of the temperature time evolution in granular fluids under the action of a white noise thermostat [6]. By producing sudden changes in the fan's intensity we expect to produce temperature transients where memory effects may show up.

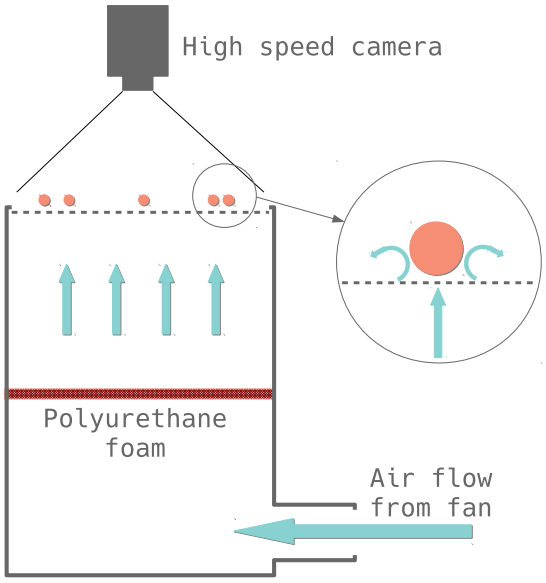

Fig. 1. Experimental setup sketch.

This work has been supported by the Spanish *Ministerio de Economía y Competitividad* Grants No. FIS2016-76359-P (M.A.L.C., A.R.R and F.V.R.) and by the *Junta de Extremadura* Grant No. IB16087 (with partial support from the ERDF).

[1] R. P. Ojha, P. A. Lemieux, P. K. Dixon, A. J. Liu, and D. J. Durian, Statistical mechanics of a gas-fluidized particle, Nature **427**, 521-523 (2004).

[2] M. E. Beverland, L. J. Daniels, and D. J. Durian, Air-fluidized balls in a background of smaller beads, J. Stat. Mech. **2011**, P03027 (2011).

[3] A. R. Abate and D. J. Durian, Partition of energy for air-fluidized grains, Phys. Rev. E, **72**, 1-7 (2005).

[4] N. G. Van Kampen, *Stochastic Processes in Physics and Chemistry* (North Holland, Elsevier, 2003), 3rd. edition.

[5] J. M. Montanero and A. Santos, Computer simulation of uniformly heated granular fluids, Granul. Matter **2**, 53-64 (2000).

[6] A. Lasanta, F. Vega-Reyes, A. Prados, and A. Santos, When the hotter cools more quickly: Mpemba effect in granular fluids, Phys. Rev. Lett. **119**, 1-6 (2017).

Envejecimiento en el desatasco de un silo granular vibrado

B. V. Guerrero[1], L. A. Pugnaloni[2], C. Lozano[3], I. Zuriguel[1] y A. Garcimartín[1]
[1]Dpto. de Física y Matemática Aplicada, Facultad de Ciencias, Universidad de Navarra, 31080 Pamplona, España
[2]Dpto. de Ingeniería Mecánica, Facultad Regional La Plata, Universidad Tecnológica Nacional, CONICET, av. 60 Esq. 124, 1900 La Plata, Argentina
[3]Fachbereich Physik, Universität Konstanz, Konstanz D-78457, Alemania

Cuerpos discretos fluyendo por una abertura estrecha pueden llegar a formar arcos que obstruyen la salida. El surgimiento de arcos hace que el flujo sea intermitente, bloqueándolo permanentemente cuando la energía cinética del sistema ha sido disipada. Un ejemplo representativo de este tipo de flujo es el que ocurre durante la descarga de granos de un silo [1]. Las colisiones y la fricción entre granos pueden disipar la energía permitiendo alcanzar un estado de equilibrio mecánico, del que sólo se puede salir por la acción de algún agente externo.

La vibración externa es idónea para evitar la formación de atascos y para reanudar el flujo una vez atascado. La estabilidad de un arco ante una vibración externa constante está caracterizada por el tiempo requerido para su ruptura [2] y está parcialmente vinculada a su configuración inicial. Sin embargo, para arcos que tardan en romperse, no queda claro cómo la vibración afecta a su dinámica y a su estabilidad. En esta contribución, se presentarán los resultados más recientes, (en parte ya publicados en la ref. [3]), obtenidos a partir del estudio experimental de la dinámica de arcos estables sometidos a vibración constante de baja intensidad. Para esta investigación, empleamos un silo bidimensional, lleno con esferas monodispersas. Desde el instante en que ocurre el atasco hasta su posterior ruptura, el silo es vibrado sinusoidalmente a una intensidad constante (de aceleración máxima de 0.6 veces la de la gravedad). Se registraron las posiciones de los granos en las vecindades de la salida, identificando aquellos que forman parte del arco. Estudiamos su morfología en términos del ángulo ϕ formado para cada bola del arco y sus dos vecinas respectivas.

En particular, encontramos que la desviación estándar $\sigma(t)$ de todos los ángulos ϕ para un instante t dado, describe apropiadamente el desatascamiento. La vibración favorece que el arco tienda a evolucionar hacia configuraciones cada vez más inestables siguiendo una dinámica intermitente, en donde grandes reordenamientos súbitos son alternados por periodos en los que hay apenas hay cambios. La fig. 1 muestra la autocorrelación de σ a dos tiempos $C(t_w, \tau)$, siendo t_w el tiempo de espera para medir correlación y τ el retardo temporal. La función $C(t_w, \tau)$ muestra que a medida que aumenta t_w el sistema relaja más lentamente y que los efectos de memoria son mayores. Este comportamiento evidencia que la ruptura de arcos es un fenómeno con envejecimiento, en concordancia con el rompimiento de ergodicidad esperado [4]. Los efectos de envejecimiento han sido confirmados calculando el desplazamiento cuadrático medio (promediado sobre ensemble) de σ, el cual presenta un crecimiento subdifusivo que decrece a medida que aumenta t_w.

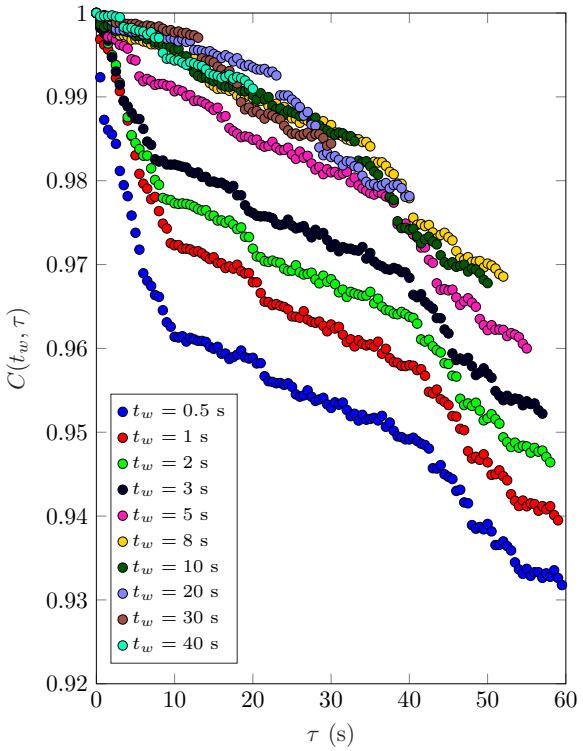

Fig. 1. Funcion de autocorrelación $C(t_w, \tau)$ como función del retardo temporal τ, para varios tiempos de espera t_w.

[1] K. To, P. Y. Lai, and H. K. Pak, Jamming of granular flow in a two-dimensional hopper, Phys. Rev. Lett. **86**, 71 (2001).

[2] C. Lozano, I. Zuriguel, and A. Garcimartín, Stability of clogging arches in a silo submitted to vertical vibrations, Phys. Rev. E, **91**, 062203 (2015).

[3] B. V. Guerrero, L. A. Pugnaloni, C. Lozano, I. Zuriguel, and A. Garcimartín, Slow relaxation dynamics of clogs in a vibrated granular silo, Phys. Rev. E **97**, 042904 (2018).

[4] C. Merrigan, S. K. Birwa, S. Tewari, and B. Chakraborty, Ergodicity breaking dynamics of arch collapse, Phys. Rev. E **97**, 040901 (2018).

Hexbugs: experimentos de comportamiento colectivo con partículas autopropulsadas baratas

I. Zuriguel[1], G. A. Patterson[2,3], D. Parisi[2,3], L. A. Pugnaloni[2] y A. Garcimartín[1]
[1]Dpto. de Física y Mat. Apl., Fac. de Ciencias, Universidad de Navarra, 31080 Pamplona, España
[2]Instituto Tecnológico de Buenos Aires, CONICET, Lavardén 315, 1437 C. A. de Buenos Aires, Argentina
[3]Comisión Nacional de Investigaciones Científicas y Técnicas (CONICET), Argentina

El uso de partículas autopropulsadas artificiales como ejemplo simple y controlable de materia activa está adquiriendo gran relevancia en los últimos años [1]. Aunque por su importancia biológica la mayoría de los estudios se han centrado en partículas autopropulsadas microscópicas inmersas en un fluido, también es cierto que en esta escala se disparan tanto las dificultades experimentales como la complejidad de los problemas. Así pues, la utilización de materia activa compuesta por partículas macroscópicas que interactúan simplemente por contactos físicos, emerge como una solución interesante a la hora de reducir el número de variables implicadas en los distintos problemas.

En relación al modo en que las partículas macroscópicas se pueden propulsar, podemos diferenciar entre dos tipos de situaciones dependiendo de si la excitación es externa o interna. En el primer caso por ejemplo, partículas anisótropas sobre una base vibrada verticalmente pueden desplazarse [2] o rotar [3, 4] dependiendo de su diseño, el cual puede ser fácilmente modificado gracias al desarrollo de la impresión 3D. Para el caso de la excitación interna, sin embargo, diseñar partículas apropiadas es más costoso si se quieren obtener en gran número. Es en este punto donde puede resultar enormemente útil la utilización de *Hexbugs*, partículas autopropulsadas que fueron ideadas como un juguete [fig. 1 (a)].

En este póster presentaremos un estudio del comportamiento de *Hexbugs* al pasar por un estrechamiento [5] y lo relacionaremos con el caso de descarga de silos vibrados y evacuación de personas por puertas angostas. En concreto, se mostrará que el flujo es intermitente con una estadística, tanto en el caso de los tiempos de flujo como en el de los de atasco, idéntica a los ejemplos anteriormente mencionados. Además, la naturaleza de las partículas utilizadas posibilita mantener su número constante en el interior del recinto, facilitando la exploración de este parámetro que resulta clave en el tipo de dinámica que se desarrolla.

[1] C. Bechinger, R. di eonardo, H. Löwen, C. Reichhardt, G. Volpe, and G. Volpe, Active particles in complex and crowded environments, Rev. Mod. Phys **88**, 045006 (2016).

[2] J. Deseigne, O. Dauchot, and H. Chaté, Collective motion of vibrated polar disks, Phys. Rev. Lett. **105**, 098001 (2010).

[3] E. Altshuler, J. M. Pastor, A. Garcimartín, I. Zuriguel, and D. Maza, Vibrot, a simple device for the conversion of vibration into rotation mediated by friction: Preliminary evaluation, PLoS ONE **8**, e67838 (2013).

[4] C. Scholz and T. Pöschel, Velocity distribution of a homogeneously driven two-dimensional granular gas, Phys. Rev. Lett. **118**, 198003 (2017).

[5] G. A. Patterson, P. I. Fierens, F. S. Jimka, P. G. König, A. Garcimartín, I. Zuriguel, L. A. Pugnaloni, and D. R. Parisi, Clogging transition of vibration-driven vehicles passing through constrictions, Phys. Rev. Lett. **119**, 248301 (2017).

[6] A. Deblais, T. Barois, T. Guerin, P.-H. Delville, R. Vaudaine, J.-S. Lintuvuori, J.-F. Boudet, J.-C. Baret, and H. Kellay, Boundaries control collective dynamics of inertial self-propelled robots, Phys. Rev. Lett. **120**, 188002 (2018).

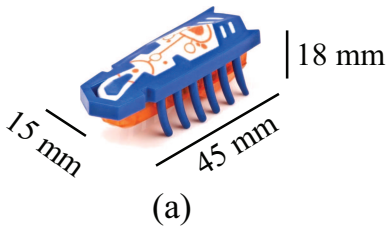

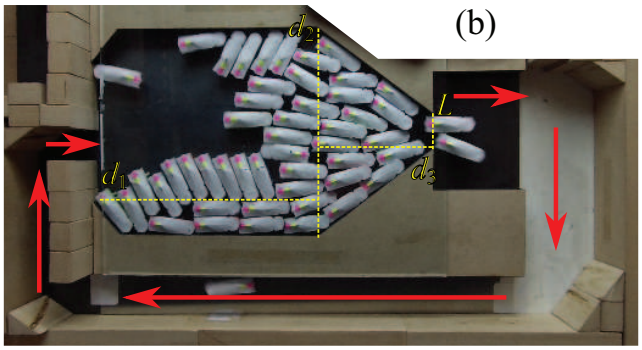

Fig. 1. (a) Fotografía de un *Hexbug* con sus dimensiones. (b) Fotografía de la celda por la que se hacen circular estas partículas autopropulsadas para estudiar la formación de atascos. Las paredes condicionan enormemente el movimiento de los *Hexbugs* [6], así que, jugando con la geometría del circuito se puede conseguir que la circulación se dé en la dirección que indican las líneas rojas.

Uniform phases in fluids of hard isosceles triangles

Yuri Martínez-Ratón[1], Ariel Díaz-De Armas[1], and Enrique Velasco[2]
[1]Departamento de Matemáticas, Universidad Carlos III de Madrid, av. Universidad 30, E-28911 Leganés, Madrid, Spain
[2]Departamento de Física Teórica de la Materia Condensada, Universidad Autónoma de Madrid, E-28049 Madrid, Spain

Two dimensional fluids of hard anisotropic particles are paradigms of systems where liquid-crystal phases can be stabilized solely by entropy [1, 2, 3]. Hard-rod particles such as hard rectangles, discorectangles or ellipses, exhibit the completely disordered isotropic (I) phase, but also a nematic (N) phase at higher densities where particle axes point, on average, along a common director. In two dimensions the N phase does not possess true long-range orientational order, and the N-I transition is usually continuous via a Kosterlitz-Thouless disclination unbinding mechanism. The N phase is stable for high enough aspect ratios and its stability region (in the density-aspect ratio phase diagram) is bounded below by the I phase, and above by other liquid-crystal nonuniform phases such as the smectic or completely ordered crystal phases. At low aspect ratios the I phase can exhibit a direct transition to a plastic crystal or to a more complex crystalline phase in which particle shapes, orientations and lattice structures are coupled in a complex fashion.

In the present work we formulate the scaled particle theory for a general mixture of hard isosceles triangles and calculate different phase diagrams for the one-component fluid and for certain binary mixtures [4]. The fluid of hard triangles exhibits a complex phase behavior: (i) the presence of a triatic (TR) phase with sixfold symmetry, (ii) the I-N transition is of first order for certain ranges of aspect ratios, and (iii) the one-component system exhibits N-N transitions ending in critical points. We found the TR phase to be stable not only for equilateral triangles but also for triangles of similar aspect ratios.

We focused the study of binary mixtures on the case of symmetric mixtures: equal particle areas with aspect ratios κ_i symmetric with respect to the equilateral one $\kappa_1\kappa_2 = 3$. For these mixtures we found, aside from first-order I-N and N-N transitions (the latter ending in a critical point): (i) a region of TR phase stability even for mixtures made of particles that do not form this phase at the one-component limit, and (ii) the presence of a Landau point at which two TR-N first-order transitions and a N-N demixing transition coalesce. This phase behavior is analogous to that of a symmetric three-dimensional mixture of rods and plates. In Fig. 1

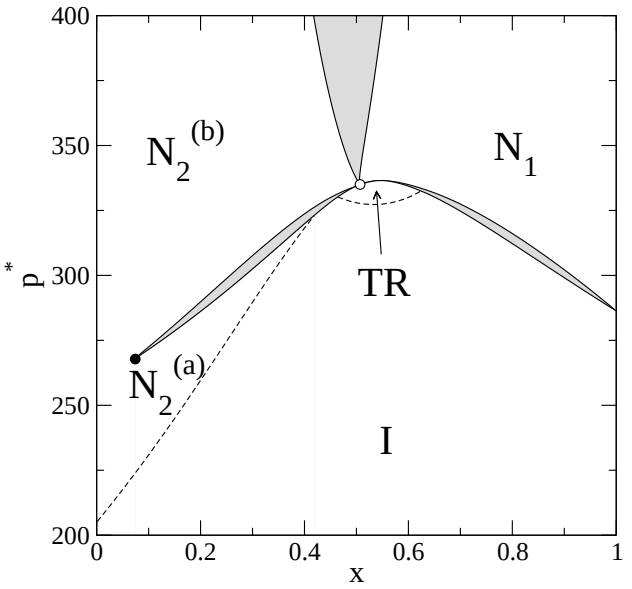

Fig. 1. Phase diagram of a symmetric binary mixture of hard isosceles triangles (see the text for the mixture description).

we show the phase diagram (reduced pressure $p^* = \beta p a_1$ *vs.* composition $x \equiv x_1$) of a symmetric ($\kappa_1\kappa_2 = 3$) binary mixture with $\kappa_1 = 2.52$, equal particle areas $a_1 = a_2$ and the ratio between the bases of triangles is fixed to $b_2/b_1 = 1.453$.

[1] M. A. Bates and D. Frenkel, J. Chem. Phys. **122**, 10034 (2000).

[2] Y. Martínez-Ratón, E. Velasco, and L. Mederos, J. Chem. Phys. **122**, 064903 (2005).

[3] R. Wittmann, C. E. Sitta, F. Smallenburg, and H. Löwen, J. Chem. Phys. **147**, 134908 (2017).

[4] Y. Martínez-Ratón, A. Díaz-De Armas, and E. Velasco, Phys. Rev. E **97**, 052703 (2008).

Out-of-equilibrium dynamics of the Heisenberg model with quenched random anisotropy disorder

A. Astillero[1] and J. J. Ruiz-Lorenzo[2,3]

[1]Dep. de Tecnología de los Computadores y las Comunicaciones and ICCAEx, Universidad de Extremadura, 06800 Mérida, Spain

[2]Dep. Física and Instituto de Computación Científica de Extremadura (ICCAEx), Universidad de Extremadura, 06071 Badajoz, Spain

[3]Instituto de Biocomputación y Física de los Sistemas Complejos (BIFI), Universidad de Zaragoza, 50018 Zaragoza, Spain

We have studied the out-of-equilibrium behavior of the Random Anisotropy Model (RAM), with Hamiltonian [1]

$$\mathcal{H} = -\sum_{\langle \mathbf{r},\mathbf{r}'\rangle} \mathbf{S_r}\cdot\mathbf{S_{r'}} - D\sum_{\mathbf{r}}(\hat{\mathbf{x}}_\mathbf{r}\cdot\mathbf{S_r})^\mathbf{2}\,, \qquad (1)$$

$\mathbf{S_r}$ being classical Heisenberg spins living in a three-dimensional lattice, D is the strength of the anisotropy and $\hat{\mathbf{x}}_\mathbf{r}$ are unit vectors pointing to the direction of the random (quenched) local anisotropy axis. In this work we will consider two probability distributions for the random anisotropy: 1) isotropic distribution and 2) uniformly distributed only on the six axes of the underlying cubic lattice.

Using the techniques of Refs. [2, 3] we have computed the critical exponents (η, z and ν) of this model for the two choices of the random anisotropy. To do that we have extensively run on GPUs. Finally, we compare our results [4] with those obtained in equilibrium numerical simulations [5].

[1] R. Harris, M. Plischke, and M. J. Zuckermann, Phys. Rev. Lett. **31**, 160 (1973).

[2] G. Parisi, F. Ricci-Tersenghi, and J. J. Ruiz-Lorenzo, Phys. Rev. E **60**, 5198 (1999).

[3] M. Lulli, G. Parisi, and A. Pelissetto, Phys. Rev. E **93**, 032126 (2016).

[4] A. Astillero and J. J. Ruiz-Lorenzo, (in preparation).

[5] M. Dudka, Y. Holovach, and J. J. Ruiz-Lorenzo, (in preparation).

Dynamical behavior of the cylindrical wall boundary layer in a co-rotating split-cylinder flow

Jesús O. Rodríguez-García and Javier Burguete
Departamento de Física y Matemática Aplicada, Universidad de Navarra, c. Irunlarrea 1, 31008 Pamplona, Spain

Rotating and turbulent systems are present in many natural and industrial processes. In geophysical flows, rotation is present in many scales creating different instabilities. This kind of behavior is observed in industrial flows too like in liquid mixing processes. The importance of this kind of phenomena has provoked much research to better understand the different processes involved in turbulence and rotation.

To have a better knowledge of these systems, different experiments have been carried out in our group using a von Kármán flow driven by propellers [1, 2, 3] finding very rich phenomena. Now, we have developed a new experimental device motivated by different numerical simulations [4, 5, 6] to continue analyzing rotating flows.

The new experimental setup is a horizontal split-cylinder in which each half is moved independently by two shafts (see Fig. 1). All the split-cylinder set is enclosed in an aluminum cell fulfilled by the working fluid (water for this work). Shafts are moved by two servomotors which allow a co-rotation or counter-rotation regimen which different velocities in each half. The radius R of the cylinder is fixed but the internal length of the halves L can be changed using different bases, so the aspect ratio of the cylinder $\Gamma = 2L/R$, can be modified. In this work Γ is fixed and equal to 2.

Using this setup we can study the different regimes of the flow created inside the split-cylinder and the symmetry-breaking that should appear according to [4] and [5]. To measure the experimental velocity field of the flow an LDV system has been used with silver coated hollow glass spheres as tracers.

First results have been obtained in co-rotation using a differential velocity between halves. We set a main rotation velocity in both sides Ω, and we add or subtract a differential velocity ω, depending on the side, achieving an asymmetric rotation. Assuming that ν is the kinematic viscosity of our working fluid, the flow developed inside the split-cylinder is characterized by two dimensionless parameters, the Reynolds Re and the Rossby Ro numbers defined as

$$\mathrm{Re} = \frac{\Omega R^2}{\nu}, \tag{1a}$$

$$\mathrm{Ro} = \frac{\omega}{\Omega}. \tag{1b}$$

The basic state (BS) described in [5] has been found experimentally. A complex behavior of the cylindrical wall boundary layer is also found with dependence on the Re and the Ro. In addition, the flow presents different azimuthal instabilities depending on the experimental parameters.

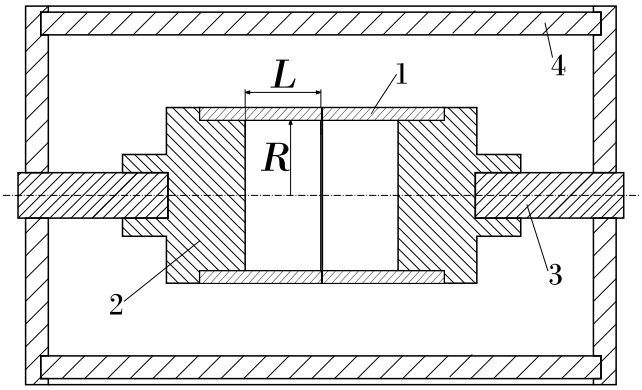

Fig. 1. Cross section of the experimental setup: 1, methacrylate semi-cylinders; 2, aluminum bases; 3, shafts; 4, external cell.

[1] A. de la Torre, J. Burguete, Slow dynamics in a turbulent von Kármán swirling flow, Phys. Rev. Lett. **99**, 054101 (2007).

[2] M. López-Caballero, J. Burguete, Inverse cascades sustained by the transfer rate of angular momentum in a 3D turbulent flow, Phys. Rev. Lett. **110**, 124501 (2013).

[3] O. Liot, J. Burguete, Bifurcation induced by the aspect ratio in a turbulent von Kármán swirling flow, Phys. Rev. E **9**, 013101 (2017).

[4] P. Gutierrez-Castillo, J. M. Lopez, Instabilities of the sidewall boundary layer in a rapidly rotating split cylinder, Eur. J. Mech. B **52**, 76-84 (2015).

[5] J. M. Lopez, P. Gutierrez-Castillo, Three-dimensional instabilities and inertial waves in a rapidly rotating split-cylinder flow, J. Fluid Mech. **800**, 666-687 (2016).

[6] P. Gutierrez-Castillo, J. M. Lopez, Nonlinear mode interactions in a counter-rotating split-cylinder flow, J. Fluid Mech. **816**, 719-745 (2017).

Instabilities triggered in different conducting fluid geometries due to slowly time-dependent magnetic fields

Iván Cortés-Domínguez and Javier Burguete
Departamento de Física y Matemática Aplicada, Universidad de Navarra, c. Irunlarrea 1, E-31008 Pamplona, Spain

The existence of non-linearities in fluid dynamics is a challenge for the scientific community because is the source of the complex behavior that appears in many physical processes. These processes cover different scales from extended natural systems (e.g., atmospheric phenomena, ocean flows, stellar flows) to many other applied systems (e.g., aerodynamics, navigation, medicine, microfluidics). There are many factors that affect the fluid dynamics, being two of them the geometry and the boundary conditions. These boundaries can be very different, from solid physical walls to interfaces where the boundaries are defined by the liquid densities, chemical barriers or magnetic fields. In despite of the diversity of the different physical processes, generic behaviors can be found in those problems with different forcing systems and confinements [1].

In this work we are interested in the study of one of these forcing mechanisms, the non-linearities produced by oscillating magnetic fields in conducting fluids. The critical parameter in this problem is called the interaction parameter N, that basically represents the ratio between the electromagnetic forces on the fluid (Lorentz force), compared to inertia.

In a previos work Burguete and Miranda [2] observed symmetry breaking patterns for very small values of the bifurcation parameter N. They forced an InGaSn droplet with an oscillating magnetic field with non-zero mean. They characterized the presence of non-axisymmetric patterns close to the threshold. Based on this experimental approach, we have previously characterized the existence of patterns for small values of the bifurcation parameter N in an InGaSn droplet using a zero-mean time oscillating magnetic field [3].

In these experiments the vertical time-dependent magnetic field produces an oscillating radial Lorentz force that periodically expands and contracts the fluid drop. An axisymmetric pattern is created that can destabilize for specific regions of the parameter space. In some cases various patterns can coexist for the same experimental parameters and we could observe cycles and other complex dynamics. In order to clarify the mechanisms involved in the pattern formation, the temporal evolution was split into harmonic and sub-harmonic of the Lorentz forces frequencies. There are two different mechanisms that trigger the instabilities associated with each set of modes: surfaces waves generated by the beating of the droplet, that correspond to harmonics of the forcing mechanism frequency; and oscillations for subharmonics frequencies that obey a first order Mathieu-Hill equation.

The main objective of this work [4] is the influence of different geometries on the bifurcation induced by oscillating magnetic fields in a conducting fluid. Depending on the geometry different surface patterns that break the symmetries have been observed. First, an InGaSn drop of fluid where the system breaks the azimuthal and radial symmetries depending on the volume. Second, we extend the study to an InGaSn annular configuration where the presence of patterns open the door to discuss the possibility to extend these results to other configurations as biological systems, where the conducting fluid is an electrolyte. This configuration has an added interest, as it has been proposed that vertigoes triggered on patients in an MRI test could be generated by the interaction of the magnetic field with the electrolyte present in the inner ear.

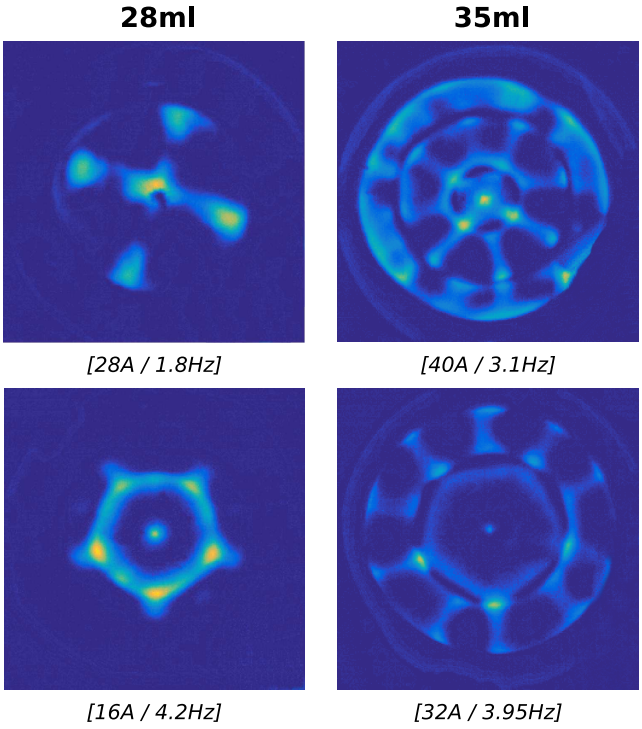

Fig. 1. Snapshots of the surface of the beating liquid metal drop for two sizes and frequencies. Different azimuthal and radial wavenumbers were observed.

[1] I. Cortés-Domínguez, J. Burguete, and H. L. Mancini, Phil. Trans. R. Soc. A **373**, 20150113 (2015).

[2] J. Burguete and M. A. Miranda, Magnetohydrodynamics **48**, 69-75 (2012).

[3] I. Cortés-Domínguez and J. Burguete, Phys. Rev. E **96**, 013103 (2017).

[4] I. Cortés-Domínguez and J. Burguete, Chaos (in press).

An equation for biased diffusion in uniformly growing domains

F. Le Vot[1], S. B. Yuste[1], and E. Abad[2]
[1]Departamento de Física, Facultad de Ciencias, Universidad de Extremadura, E-06071 Badajoz, Spain
[2]Departamento de Física Aplicada, Centro Universitario de Mérida, Universidad de Extremadura, E-06800 Mérida, Spain

Anomalous diffusion models are a very useful tool to describe key features of biological systems where non-Fickian transport is at play. In this context, there are numerous examples where systematic forces influence the particle spreading. The effect of such forces can be accounted for by introducing a bias term in the corresponding transport equation. A typical example is the action of a chemotactic gradient sensed by a collection of bacteria.

While the effect of drift terms on anomalous diffusion processes is well studied in the case of static domains, in a wide variety of biological systems the dissemination of the particles takes place while the medium itself grows at a non-negligible rate. Examples include proliferative tissue growth and the formation of pigmentation patterns in growing organisms. Considering the problem of biased anomalous transport in growing domains is thus of great practical importance.

In the above context, we shall consider the celebrated Continuous-Time Random-Walk model (CTRW), which is well characterized in the case of a one-dimensional static domain [1]. In this model, particles perform instantaneous jumps interrupted by waiting times which follow the probability density function (PDF) $\varphi(t)$. In its simplest version, the single-jump displacement is considered to be uncoupled from the waiting-time PDF and given by the PDF $\lambda^*(y)$. When λ^* has a finite variance Σ^2, the system displays subdiffusion when the Laplace transformed waiting-time PDF behaves as $\tilde{\varphi}(s) \sim 1 - \tau^\alpha s^\alpha$ for $s \to 0$, where $0 < \alpha < 1$. The case $\alpha = 1$ gives rise to normal diffusion.

But, what happens if the medium expands? In this case, the purely diffusive motion is influenced by an additional drift arising from the stretching of physical space. Recent works [2, 3] show that this problem is amenable to analytical treatment by switching to so-called comoving coordinates x. The latter are defined as the projections of the physical points y on the initial domain. In the case of a uniform expansion, the relation between both sets of coordinates is straightforward, i.e., $y = a(t)x$. In comoving space, displacements are thus shortened by the inverse scale factor $1/a(t)$, implying that $\lambda^*(y)$ must be replaced by $\lambda(x,t) = a(t)\lambda^*(a(t)x)$.

The introduction of an external force field, $F^*(y,t)$, results in an asymmetric jump-length distribution. In the simplest case, there is a linear dependence between the force and the jump asymmetry [1]. In comoving coordinates, this force is expressed as $F(x,t) = F^*(a(t)x,t)$. In the long-time limit, the above CTRW scheme leads to the following fractional diffusion equation

$$\frac{\partial W(x,t)}{\partial t} = \frac{K_\alpha}{a^2(t)} \frac{\partial^2}{\partial x^2} {}_0D_t^{1-\alpha} W(x,t) - \frac{1}{\xi_\alpha a(t)} \frac{\partial}{\partial x} \left[F(x,t) {}_0D_t^{1-\alpha} W(x,t) \right], \quad (1)$$

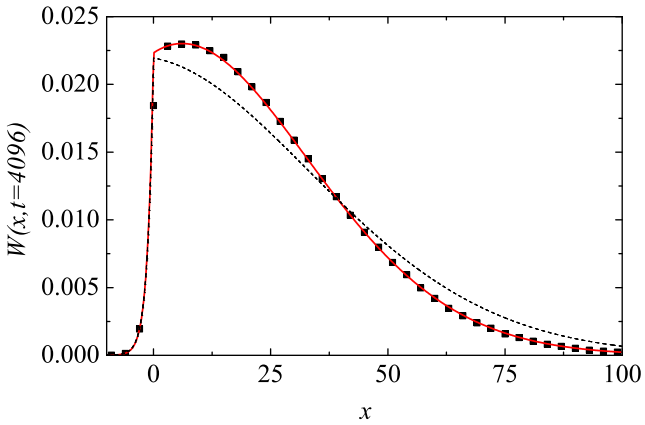

Fig. 1. Comoving propagator at time $t = 4096$ for subdiffusive particles with $\alpha = 1/2$ and $K_\alpha = 1/2$ drifted by a constant force $F_0 = \xi_\alpha/\sqrt{2\pi}$ and an exponential expansion $a(t) = \exp(Ht)$ with $H = 10^{-4}$. The solid line draws a numerical integration of Eq. (1) using the Crank-Nicolson method [4] with time and spatial discretization of $1/10$ units. The squares are the simulation results after 10^6 runs. The dashed line plots the same curve for $H = 0$. It has been obtained by means of the subordination technique [1].

where $K_\alpha = \Sigma^2/(2\tau^\alpha)$ is the diffusivity and ξ_α denotes the generalized friction constant. The operator ${}_0D_t^{1-\alpha} f(t)$ is defined as the inverse Laplace transform of $s^{1-\alpha}\tilde{f}(s)$.

The free boundary solution of Eq. (1) for Brownian particles subjected to a constant force F_0 and to the initial condition $W(x,0) = \delta(x)$ is a shifted Gaussian with time-dependent first moment $F_0 \int_0^t du\ a^{-1}(u)/\xi_1$ and variance $2K_1 \int_0^t du\ a^{-2}(u)$ [2]. However, the numerical integration of Eq. (1) reveals that the propagator is non-symmetric for subdiffusive CTRWs and it may not be represented by a suitable coordinate rescaling of its counterpart for the static case (see Fig. 1). Numerical simulations based on the Monte-Carlo algorithm confirm this finding.

[1] R. Metzler and J. Klafter, The random walk's guide to anomalous diffusion: A fractional dynamics approach, Phys. Rep. **339**, 1 (2000).

[2] S. B. Yuste, E. Abad, and C. Escudero, Diffusion in an expanding medium: Fokker-Planck equation, Green's function and first-passage properties, Phys. Rev. E **94**, 032118 (2016).

[3] F. Le Vot, S. B. Yuste, and E. Abad, Continuous-time random-walk model for anomalous diffusion in expanding media, Phys. Rev. E **96**, 032117 (2017).

[4] S. B. Yuste, Weighted average finite difference methods for fractional diffusion equations, J. Comput. Phys. **216**, 264 (2006).

Hydrodynamic fluctuations in quasi-two dimensional diffusion

Raúl P. Peláez[1], F. Balboa Usabiaga[2,3], S. Panzuela[1], Q. Xiao[2], R. Delgado-Buscalioni[1], and A. Donev[2]
[1]Departamento de Física Teórica de la Materia Condensada, Universidad Autónoma de Madrid, Madrid, Spain
[2]Courant Institute of Mathematical Sciences, New York University, New York, NY, USA
[3]Center for Computational Biology, Flatiron Institute, Simons Foundation, New York, NY, USA

We study the diffusion of colloids on a fluid-fluid interface using particle simulations and fluctuating hydrodynamics. Diffusion of colloidal particles confined to a surface is a key transport mechanism in many technological and biological systems. For example, it is known that the transverse diffusion of proteins embedded in lipid bilayers controls their biological function [1]. In man-made colloidal suspensions, colloidal particles can be confined to diffuse in a plane by walls [2] or electrostatic forces [3]. While much is understood about complex fluid-fluid interfaces, fundamental questions regarding the diffusive transport at interfaces remain unanswered, and while the diffusion of colloids and polymers on a fluid-fluid interface has been studied theoretically since the 1970s [4], *collective diffusion* in a monolayer of colloidal particles confined to a fluid-fluid interface has only recently been explored in some detail [5].

We developed an efficient algorithm for Brownian dynamics with hydrodynamic interactions, suitable for modeling diffusion of spherical colloids of hydrodynamic radius a confined to a two-dimensional plane. We used this algorithm to perform large-scale particle simulations and studied collective diffusion on fluid-fluid interfaces (Quasi2D) and in two-dimensional liquids (True2D). We also perform a new type of numerical experiment by coloring (labeling) a subset of the particles and studying the total and color density fluctuations as necessary to model experiments based on fluorescent techniques.

The nonzero compressibility of the three dimensional flow at the fluid-fluid interface leads to a nonzero divergence of the mobility matrix. Under the action of hydrodynamic fluctuations in the fluid, this compressibility acts like a pairwise repulsive potential of order $k_{\mathrm{B}}T(a/r)$, and changes the nature of diffusion dramatically (see Fig. 1).

The thermal origin of this repulsion demonstrates that density functional theories that do not account for thermal fluctuations are incomplete even for ideal systems. We found that the effective particle-particle repulsion leads to a nontrivial reduction of the long-time self-diffusion coefficient as the packing density increases, even for an ideal gas of non-interacting particles (Fig. 2).

[1] F. L. H. Brown, Continuum simulations of biomembrane dynamics and the importance of hydrodynamic effects, Q. Rev. Biophys. **44**, 391-432 (2011).

[2] B. Lin, B. Cui, X. Xu, R. Zangi, H. Diamant, and S. A. Rice, Divergence of the long-wavelength collective diffusion coefficient in quasi-one-and quasi-two-dimensional colloidal suspensions, Phys. Rev. E **89**, 022303 (2014).

[3] C. P. Kelleher, A. Wang, G. I. Guerrero-García, A. D. Hollingsworth, R. E. Guerra, B. J. Krishnatreya, D. G. Grier, V. N. Manoharan, and P. M. Chaikin, Charged hydrophobic colloids at an oil-aqueous phase interface, Phys. Rev. E **92**, 062306 (2015).

[4] R. B. Jones, B. U. Felderhof, and J. M. Deutch, Diffusion of polymers along a fluid-fluid interface, Macromolecules **8**, 680-684 (1975).

[5] J. Bleibel, A. Domínguez, F. Günther, J. Harting, and M. Oettel, Hydrodynamic interactions induce anomalous diffusion under partial confinement, Soft matter **10**, 2945-2948 (2014).

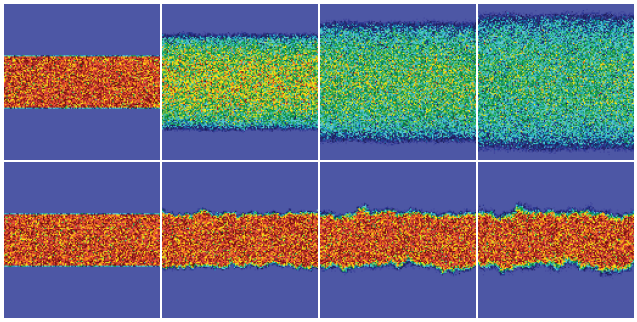

Fig. 1. Diffusion of a density perturbation initially localized in the middle third of the domain. We show snapshots at several points of equal relative time for BD-q2D (top row) and BD-t2D (bottom row). The images show the number density computed by counting the number of particles in each cell of a 128x128 grid; the color bar goes from 0 (blue) to 0.4 (red).

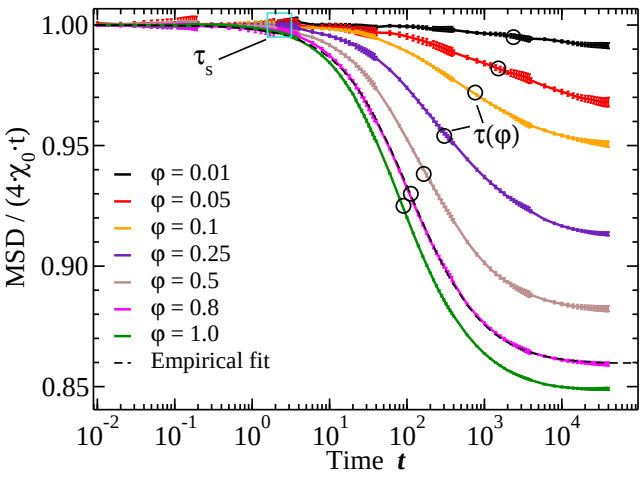

Fig. 2. Mean square displacement of a tagged particle in Quasi2D for different packing densities φ (see legend). Black circles denote the cross-over time $\tau(\varphi)$, and the beginning of the subdiffusive regime τ_s is indicated with a cyan square. χ_0 is the short-time self-diffusion.

Structure *versus* dynamics in neuronal complex networks

Sergio Faci-Lázaro[1], Jordi Soriano[2], and Jesús Gómez-Gardeñes[1,3]
[1]Departamento de Física de la Materia Condensada, University of Zaragoza, Zaragoza E-50009, Spain
[2]Departament d'ECM, Universitat de Barcelona, av. Diagonal 645, 08028 Barcelona, Spain
[3]GOTHAM Lab, Institute for Biocomputation and Physics of Complex Systems (BIFI), University of Zaragoza, Zaragoza 50009, Spain

According to Graph Theory, complex networks can be defined as a set of nodes (or vertices), $V = \{1, 2, \cdots, N\}$, and a set of edges (or links), L, that describe the connections between nodes [1]. In our case, the nodes will be the neurons of our culture; whereas the links will be their synaptic connections. These networks are represented with a matrix, called the adjacency matrix, A, which, in the simplest instance, will be binary. If the *i*-th element is connected to the *j*-th, then $A_{ij} = 1$; otherwise, $A_{ij} = 0$.

The networks are created in a way that emulates the growth of a biological culture of neurons over a surface. A generalization of the method put forward by Orlandi *et al.* [2] will be used, where a connection between neurons will happen only if two conditions are met. First, the axon of a given neuron intersects the dendritic tree of any other neuron. And second, those neurons that fulfill the first condition will connect with probability α, which is independent of the overlapping length between the axon and the dendritic tree that is intersected. Thus, obtaining neurons such as the one presented in Fig. 1 and networks as in Fig. 2.

To describe the dynamics we will use the Izhikevich model [3],

$$\tau_c \dot{v} = k(v - v_r)(v - v_t) - u + I + \eta, \tag{1a}$$

$$\tau_a \dot{u} = b(v - v_r) - u, \tag{1b}$$

which depicts the neuron through two variables: the membrane potential v, and the inhibitory current u. It also introduces the influence of synaptic currents through the term I in Eq. (1a).

Now that both the structural and dynamical models have been explained, in order to characterize our cultures we carry out a series of structural and dynamical measurements. This way we will try to describe the percolation transition and the transition to synchronization when varying the connection probability α, as well as the resistance to failures of our cultures.

To study de percolation transition we measure the average connectivity and the size of the giant component of our cultures. We see that both of these measurements grow rapidly till they saturate. However, the size of the giant component grows significantly faster than de average connectivity. This means that, as α increases, the skeleton of network will be completely formed before it has made all possible connections.

To describe the transition to synchronization, three parameters will be used. A microscopic parameter, designed to account for the pairs of neurons that are synchronized; a macroscopic parameter to show when most of the neurons of our culture are synchronized; and the size of the neuronal avalanches, as defined by Beggs and Plenz in [4]. The results we got from these measurements show that there exists a microscopic synchronization regime in absence of macroscopic synchronization. This behavior has also been observed in Kuramoto oscillators [5].

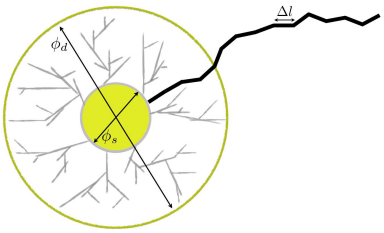

Fig. 1. Model of a neuron: ϕ_s is the diameter of the soma, ϕ_d is the diameter of the dendritic tree, and the axon is built concatenating segments of length Δl.

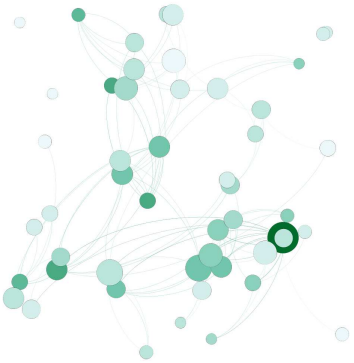

Fig. 2. Example of a network obtained from a culture with 50 neurons, a density of 10 neurons mm^{-2}, and $\alpha = 0.75$.

Finally, to test the resistance of our cultures to failures, we counted the number of avalanches that took place after we had removed the neurons that initiated most of them and compared it to the number of avalanches that happened before removing any neurons. Here, we found out that so long as we do not remove all the neurons that initiate the avalanches, the culture will remain just as active .

[1] M. Newman, *Networks: An Introduction* (Oxford University Press, Oxford, 2010).

[2] J. Orlandi, J. Soriano, E. Alvarez-Lacalle, S. Teller, and J. Casademunt, Noise focusing and the emergence of coherent activity in neuronal cultures, Nat. Phys. **9**, 582 (2013).

[3] E. M. Izhikevich, Simple model of spiking neurons, IEEE Trans. Neural Netw. **14**, 1569 (2003).

[4] J. M. Beggs and D. Plenz, Neuronal avalanches in neocortical circuits, J. Neurosci. **23**, 11167 (2003).

[5] J. Gómez-Gardeñes, Y. Moreno, and A. Arenas, Paths to synchronization on complex networks, Phys. Rev. Lett. **98**, 034101 (2007).

Dynamics of the erythrocyte flickering with a stochastic phase field model

A. F. Gallén[1] and A. Hernández-Machado[1,2,3]
[1]Física de la Matèria Condensada, Universitat de Barcelona, Spain
[2]Centre de Recerca Matemàtica, Edifici C, Campus de Bellaterra, 08193 Bellaterra, Barcelona, Spain
[3] Barcelona Graduate School of Mathematics (BGSMath), Barcelona, Spain

Erythrocyte flickering is the common name given to the fluctuations that suffer the membrane of the red blood cell mainly due to the thermal bath and its soft behaviour. Nowadays it still keeps being researched due to its simple structure but complex geometry and by its apparent active nature in theoretical and experimental works [1, 2, 3].

In this work the fluctuations of the red blood cell membrane are studied by simulations based on a stochastic phase field model. This work is based on existing phase field models for cellular membranes, where the bending energy reigns, this time including a thermal-driven noise that cause the fluctuations. The results are compared with experimental data for several simulated geometries of the membrane. An auto-correlation function for the phase field order parameter is derived. Then the correlation function for both, the phase field and the membrane displacement, is computed obtaining a behaviour for the simulations similar to the experimental data.

Then, by Fourier analysis the power spectral density is computed for the fluctuations, obtaining an algebraic dependence for the wave-vector q that corresponds to non-local fluctuations coupling the membrane with the surrounding fluid.

[1] H. Turlier, D. A. Fedosov, B. Audoly, T. Auth, N. S. Gov, C. Sykes, J.-F. Joanny, G. Gompper, and T. Betz, Equilibrium physics breakdown reveals the active nature of red blood cell flickering, Nat. Phys. **12**, 513-519 (2016).

[2] A. A. Evans, B. Bhaduri, G. Popescu, and A. J.. Levine, Geometric localization of thermal fluctuations in red blood cells, Proc. Natl. Acad. Sci. USA, **114**, 2865-2870 (2017).

[3] R. Rodríguez-García, I. López-Montero, M. Mell, G. Egea, N. S. Gov, and F. Monroy, Direct cytoskeleton forces cause membrane softening in red blood cells, Biophys. J. **108**, 2794-2806 (2015).

Structural and transport properties of confined water in nano geometries

Alberto Zaragoza[1,3], Miguel Ángel González[2], Ana Laura Benavides[1], and Chantal Valeriani[3]
[1]División de Ciencias e Ingenierías, Universidad de Guanajuato, Lomas del Campestre, 37150 León, Mexico
[2]Facultad de Ciencias Químicas, Universidad Complutense de Madrid, av. Complutense s/n, 28040 Madrid, Spain
[3]Facultad de Ciencias Físicas, Universidad Complutense de Madrid, av. Complutense s/n, 28040 Madrid, Spain

Water is undoubtedly the most relevant molecule for living organisms both at a macroscopic scale —the human body consists of 65-70 % of water and a tree of 20-70 %— and at a microscopic scale —a human cell consists of 70-80 % of water and a plant one of 60-70 %. At the latter scale, the features of confined water, that differ with respect of bulk water, play a vital role and understanding them could be of interest in the development of nanomaterials such as nanochannels. In particular, under confinement, water has a different behaviour than in bulk showing a different phase diagram [1] that is still under study. It is important to study water at nanoscale to understand biological/industrial processes such us ions exchange in cells or water desalination [5, 6], respectively.

Computer simulations based on molecular dynamics have shown to be a reliable and powerful tool to study the features, from a molecular approach, of nanoconfined water. At these small scales, experimentalists may find issues to measure some properties or even to work at some conditions of temperature. That is the reason why molecular simulation is a very useful technique to find out how confinement changes the water properties.

In the last decade, works focused on understanding transport properties of confined water have not shown conclusive results [7, 8, 9, 10]. Our goal is to set up numerical simulations that could be considered as a benchmark for future works of confined water.

In this work, by means of molecular dynamics simulations, we study TIP4P/2005 [4] water confined inside nanomaterials (both hydrophobic and super-hydrophobic) such as two parallel sheets and single wall carbon nanotubes (SWCNTs) with a wide diameter range. Structural an dynamical properties, such as diffusion, density, viscosity and the number of formed/broken hydrogen bonds were computed and analysed at several temperatures taking into account the finite size corrections proposed by theoretical studies [3, 2].

Our preliminary results shown that key factors such as hydrogen bonds or viscosity allow water to diffuse faster when confined down to a "limit" diameter ($\approx$ 2 nm). If water is confined under this "limit" size, it trends to adopt chain-like structures that make its dynamic slows-down.

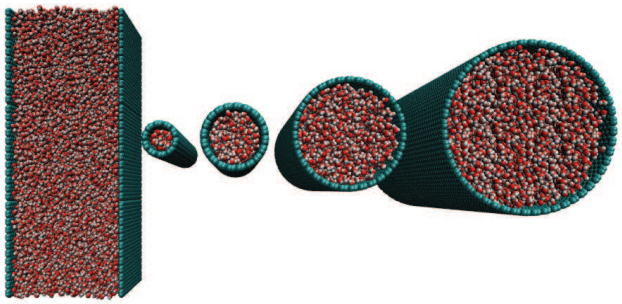

Fig. 1. From left to right: Two parallel graphene sheets having confined water inside, four SWCNTs confining water and with diameter from 1.3 to 7 nm. Carbon atoms are represented by cyan spheres and thewater molecules by red (oxygen) and white (hydrogen) spheres.

[1] D. Takaiwa, I. Hatano, K. Koga, and H. Tanaka, Proc. Natl. Acad. Sci. USA **105**, 39-43 (2008).

[2] S. Tazi, A. Boţan, M. Salanne, V. Marry, P. Turq, and B. Rotenberg, J. Phys.-Condens. Matter **24**, 284117 (2012).

[3] M. Vögele and Gerhard Hummer, J. Phys. Chem. B **120**, 8722-8732 (2016).

[4] J. L. F. Abascal and C. Vega, J. Chem. Phys. **123**, 234505 (2005).

[5] B. Corry, J. Phys. Chem. B **112**, 1427-1434 (2008).

[6] R. Das, M. E. Ali, S. B. Abd Hamid, S. Ramakrishna, and Z. Z. Chowdhury, Desalination **336**, 97-109 (2014).

[7] M. H. Köhler, J. R. Bordin, L. B. da Silva, and M. C. Barbosa, Phys. Chem. Chem. Phys. **19**, 12921-12927 (2017)

[8] M. H. Köhler, J. R. Bordin, L. B. da Silva, and M. C. Barbosa, Physica A **490**, 331-337 (2018).

[9] J. Martí, C. Calero, and G. Franzese, Entropy **19**, 135 (2017).

[10] X. Liu, X. Pan, S. Zhang, X. Han, and X. Bao Langmuir **30**, 8036-8045 (2014).

Bipartite network characterization of fluid flows and its relation with the classical Lyapunov exponent

Rebeca de la Fuente, Cristóbal López, and Emilio Hernández-García
IFISC, CSIC-UIB, Campus Universitat Illes Balears, 07122 Palma de Mallorca, Spain

Mixing and dispersion between different regions of a fluid domain have been characterized during the last decades by the Lagrangian description of motion and dynamical systems theory. A classical measure quantifying dispersion is the Lyapunov exponent, which gives the stretching rate of infinitesimal material line under the evolution of the flow. From the flow-map approach (the flow map is the function that maps initial to final conditions under time evolution during a time τ) we compute the Finite Time Lyapunov Exponent (FTLE) as

$$\lambda(x_0, t_0, \tau) = \frac{1}{2\tau} \log(\Lambda_{\text{max}}), \tag{1}$$

where Λ_{max} is the maximum eigenvalue of the Cauchy-Green strain tensor constructed from the Jacobian matrix of the flow map.

On the other hand, we can also characterize mixing and dispersion between regions from network-theory tools. In Ref. [1] a formalism was developed in which the fluid domain is coarse-grained and a discrete version of the Perron-Frobenious operator, giving a quantification of the amount of fluid going from one fluid box to another one, is used to define link strengths between these fluid boxes, thus defining a temporal, weighted and directed flow network.

Here we develop the above formalism to characterize transport between two layers in a three-dimensional fluid flow (a possible application is the quantification of transport between surface and bottom of the ocean). For our purpose, we construct the flow map for the three dimensional incompressible Arnold-Beltrami-Childress flow model whose velocity field is defined as

$$\dot{x} = A \sin z + C \cos y, \tag{2a}$$
$$\dot{y} = B \sin x + A \cos z, \tag{2b}$$
$$\dot{z} = C \sin y + B \cos x. \tag{2c}$$

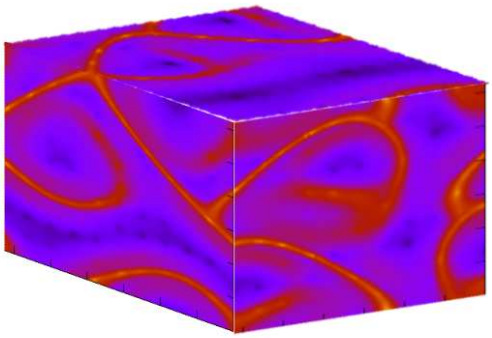

Fig. 1. FTLE of the three dimensional ABC flow with periodic boundary conditions for the integration time $\tau = 3$, and $A = \sqrt{3}$, $B = \sqrt{2}$, $C = 1$

We construct a bipartite network with links describing the amount of fluid transported between fluid boxes located at two horizontal layers embedded into the fluid domain. We then characterize this bipartite network, find similarities between the Lyapunov exponent and network properties (see the three-dimensional FTLE field for this flow in Fig. 1), and extract coherent structures generalizing the ideas in Refs. [1, 2].

[1] E. Ser-Giacomi, V. Rossi, C. López, E. Hernández-García, Flow networks: A characterization of geophysical fluid transport, Chaos **25**, 036404 (2015).

[2] E. Ser-Giacomi, V. Rodríguez-Méndez, C. López, E. Hernández-García, Lagrangian Flow Network approach to an open flow model, Eur. Phys. J.-Spec. Top. **226**. 2057-2068 (2017).

Critical dynamics of reaction-diffusion fronts

B. G. Barreales[1,2], J. J. Meléndez[1,2], R. Cuerno[3], and J. J. Ruiz-Lorenzo[1,2]
[1]Departamento de Física, Universidad de Extremadura, 06071 Badajoz, Spain
[2]Instituto de Computación Científica Avanzada de Extremadura (ICCAEx), Universidad de Extremadura, 06071 Badajoz, Spain
[3]Departamento de Matemáticas and Grupo Interdisciplinar de Sistemas Complejos (GISC), Universidad Carlos III de Madrid, 28911 Leganés, Spain

We have studied the dynamical critical behavior of the reversible process

$$A + A \longleftrightarrow A, \tag{1}$$

whose macroscopic dynamics is described by the Fisher equation [1, 2, 3],

$$\partial_t \rho = D\nabla^2 \rho + k_1 \rho - k_2 \rho^2, \tag{2}$$

where $\rho(\mathbf{r}, t)$ is the local concentration field.

We have revisited this discrete model in two dimensions, performing extensive numerical simulations of the time evolution of the interface separating the stable and unstable phases. In particular, we have measured the critical exponents which characterize the spatio-temporal fluctuations of such front for different lattice sizes. These exponents are in very good agreement with those computed in Ref. [4], and are determined by the Kardar-Parisi-Zhang (KPZ) universality class for one-dimensional interfaces.

Furthermore, we have studied the statistics of rescaled front fluctuations, which had remained thus far unexplored in the literature and allows for a further stringent test of KPZ universality [5, 6].

[1] R. A. Fisher, Ann. Eugen. **7**, 355 (1936).

[2] A. N. Kolmogorov, I. Petrovsky, and N. Piscounov, Mosc. Univ. Bull. Math. A **1**, 1 (1937).

[3] W. van Saarloos, Phys. Rep. **386**, 29 (2003).

[4] E. Moro, Phys. Rev. Lett. **87**, 238303 (2001).

[5] M. Kardar, G. Parisi, and Y-C. Zhang, Phys. Rev. Lett. **56**, 889 (1986).

[6] T. Halpin-Healy and K. A. Takeuchi, J. Stat. Phys. **160**, 794 (2015).

A simple model for clonal-growth plants

Daniel Ruiz-Reynés, Francesca Schönsberg, Emilio Hernández-García, and Damià Gomila
IFISC, CSIC-UIB, Campus Universitat Illes Balears, 07122 Palma de Mallorca, Spain

Vegetation patterns have been widely studied in arid ecosystems [1, 2]. These patterns cover regions of kilometers being an impressive example of self-organization. Water scarcity is usually the limiting factor which drives the ecosystem to form these spatial patterns. However, beyond the case of terrestial ecosystems it have been shown that submarine patterns can also appear in clonal plants such as *P. Oceanica* [3], obviously being the responsible mechanism completely different.

Clonal plants form meadows which cover large extensions under the sea. These meadows provide suitable environmental conditions to support a huge biodiversity, creating one of the most important ecosystems in the world. Thus, the present degradation of these habitats becomes an important issue to overcome. From this perspective, a spatial pattern of vegetation can have a dramatic influence on the functionality of the ecosystem. The characterization of these spatial structures and their dynamics is a crucial point for the preservation of these habitats.

The growth of clonal plant meadows is well described by the Advection-Branching-Death (ABD) model [3]. However, the computational cost is high and the analytical results limited, not being the most suitable model to understand generic features of the dynamics of patterns. The reason of this inconvenience is the fact that clonal growth has to be described taking into account the densities of plants growing in all directions. This introduces in the model, which is initially defined on two-dimensional space, the growth angle as an extra variable. However, the dynamics of the patterns is not critically influenced by the direction of growth. This fact allow us to reduce the problem to two spatial dimensions, being the resultant simplified equation much more tractable than the complete model.

Furthermore, the terms which we obtain from the derivation are the result of the intrinsic mechanisms of growth on the ABD model, giving qualitative insight in the understanding of clonal growth. In addition, the derivation establish a relation between the parameters of both models, providing a simple tool that can give quantitative results and that can be compared with the ABD model and real data.

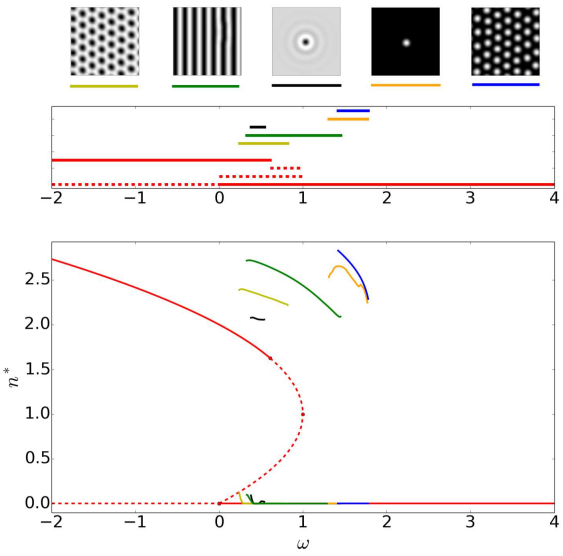

Fig. 1. Bifurcation diagram showing the homogeneous solutions and patterns for the simplified model. The stable (unstable) homogeneous solution is plotted in red (dashed red). The stable part of the five branches associated to each pattern is shown where the maximum and minimum of the density are plotted. From left to right negative hexagons (light green), stripes (green), negative soliton (black), positive soliton (orange), positive hexagons (blue). In the upper plot it is depicted the region of existence only in the control parameter ω, to simplify visualization.

[1] J. Von Hardenberg, E. Meron, M. Shachak, and Y. Zarmi, Phys. Rev. Lett. **87**, 198101 (2001).

[2] M. Rietkerk and J. Van de Koppel, Trends Ecol. Evol. **23**, 169-175 (2008).

[3] D. Ruiz-Reynés, D. Gomila, T. Sintes, E. Hernández-García, N. Marbà, and C. M. Duarte, Sci. Adv. **3**, e1603262 (2017).

Optofluidic control of the diffusion of nanoscale dumbbells

N. Alcázar Cano[1], M. Meléndez[1], R. Delgado-Buscalioni[1], and J. J. Sáenz[2]
[1]Departament of Theoretical Condensed Matter Physics, Universidad Autónoma de Madrid, 28049 Madrid, Spain
[2]Donostia International Physics Center (DIPC), 20018 Donostia, Spain

Optofluidic techniques provide a way to control the transport properties of nanoscale objects and have been applied to the guiding and sorting of particles in microfluidic flows [1, 2, 3, 4]. Numerical experiments have shown that we can tune the diffussivity of a dilute suspension of gold nanoparticles in water by placing them in the intersection of two perpendicular laser beams with a wavelength close to the plasmon resonance in water ($\lambda \approx 395$ nm). In particular, a phase difference of $\pi/2$ enhances the diffusion of a single nanoparticle by a factor proportional to the power density of the laser [5] due to the pattern formed by the standing waves in the electrical field, which form a checkerboard of vortices that propell the nanoparticles towards saddle nodes in the field. Because of thermal fluctuations, the particles leave the saddle nodes, randomly choosing one of two opposite directions and travelling to the next node [Fig. 1 (a)].

Interestingly, we can alter the dynamic behaviour completely just by attaching two nanoparticles by means of a polymer strand, as at the bottom of Fig. 1. We have developed numerical algorithms that take into account the interaction with the incident lasers, the thermal fluctuations and hydrodynamic interactions and have observed that, depending on the laser intensity and the length of the chain, the dumbbells will rotate [Fig. 1 (b)], become trapped in a fixed direction [Fig. 1 (c)] or experience enhanced diffusion. In some cases, the mean square displacement of the chain becomes as large as that of a single nanoparticle, but with an anomalous displacement distribution, in the sense that the motion is still Brownian, but the step size does not follow Gaussian statistics (Fig. 2).

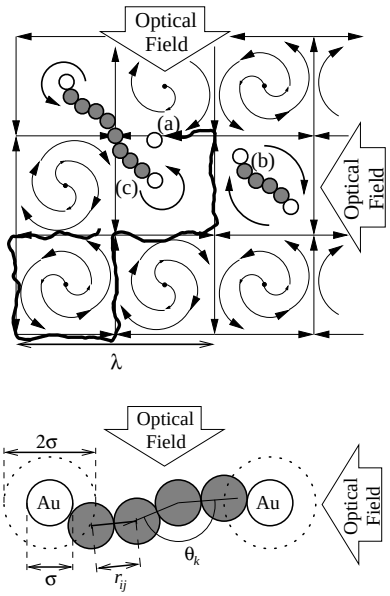

Fig. 1. (Top) Simplified representation of the forces in an optical vortex lattice. A single gold particle (a) experiences enhanced diffusion. Short dumbbells follow similar trajectories. In some cases, we can easily trap the dumbbells (b) and (c) using one or two vortices. (Bottom) The dumbbell is made with two gold particles attached by means of a FENE bead-spring chain (which limits the interparticle separation $r_{ij} < 3r$, where r is the radius of a bead) that interact with an optical force field. WCA interactions with diameter σ model excluded volume effects. An extra coat of transparent material (dotted lines) was included in some of the simulations. Angular springs between consecutive links oppose bending and tend to restore the angles to $\theta_k = \pi$ rad.

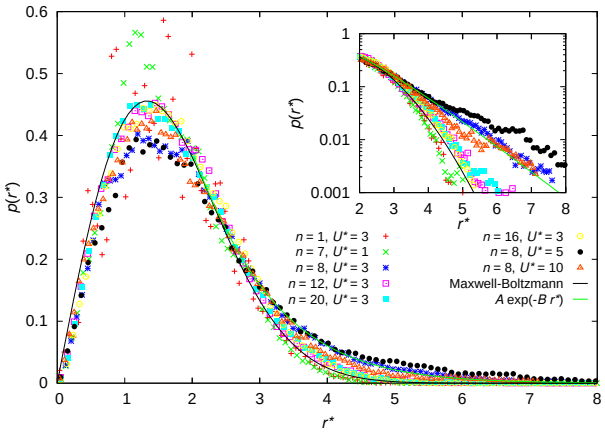

Fig. 2. Probability density function for the displacement of diffusing dumbbells. The horizontal axis represents a scaled step $r^* = r_{\Delta t}/\sqrt{(U^*/n)\Delta t}$, with $\Delta t = 100\sqrt{m\sigma^2/(k_BT)}$. The inset shows the distribution tails on a semi-logarithmic scale. The number of beads n includes the gold nanoparticles. U^* means $U/(k_BT)$, with U standing for the laser energy.

[1] M. P. MacDonald, G. C. Spalding, and K. Dholakia, Nature **426**, 421-424 (2003).

[2] K. Xiao and D. G. Grier, Phys. Rev. E **82**, 051407 (2010).

[3] I. Zapata, R. Delgado-Buscalioni, and J. J. Sáenz, Phys. Rev. E **93**, 062130 (2016).

[4] R. Delgado-Buscalioni, M. Meléndez, J. Luis-Hita, M. I. Marqués, and J. J. Sáenz, arXiv:1709.04424.

[5] S. Albaladejo, M. I. Marqués, F. Scheffold, and J. J. Sáenz, Nano Lett. **9**, 3527-3531 (2009).

[6] B. Wang, M. Anthony, S. C. Bae, and S. Granick, Proc. Natl. Acad. Sci. USA **106**, 15160-15164 (2009).

Inhomogeneities and caustics in passive particle sedimentation in incompressible flows

Cristóbal López, Gabor Drotos, Pedro Monroy, and Emilio Hernández-García
IFISC, CSIC-UIB, Campus Universitat Illes Balears, 07122 Palma de Mallorca, Spain

Sedimentation of small particles in complex flows is an outstanding problem in science and technology. In particular, the sinking of biogenic particles from the marine surface to the bottom is a fundamental process of the biological carbon pump, playing a key role in the global carbon cycle. A complete understanding of this problem is still lacking. It has been recently shown that despite fluid incompressibility, sedimented particles, moving as passive tracers in the ocean, show density inhomogeneities when accumulated on some bottom surface.

Here, we analytically derive the relation between the geometry of the flow and the emerging distribution for an initially homogeneous sheet of tracers. From a physical point of view, we identify the two processes that generate inhomogeneities to be the stretching within the sheet, and the projection of the deformed sheet onto the target surface. We point out that an extreme form of inhomogeneity, caustics, can develop for sheets. We exemplify our geometrical results with simulations of tracer advection in a simple kinematic flow, study the generic dependence on the various parameters involved, and illustrate that the basic mechanisms work similarly if the initial (homogeneous) distribution occupies a more general region of finite extension rather than a sheet.

In Fig. 1 we show the positions of particles (projected onto a vertical plane) at different times in a realistic ROMS (Regional Ocean Model) simulation of the Benguela zone. The numerical experiment consisted in releasing 6000 particles from initial conditions randomly chosen in a square with sides of 1/6 deg, centered at $10.0°\mathrm{E}$ $29.12°\mathrm{S}$ and 100 m depth. The particles' trajectories $\mathbf{r}(t)$ were calculated from

$$d\mathbf{r}/dt = \mathbf{v}_{\mathrm{ROMS}} - W\mathbf{k}, \qquad (1)$$

where $\mathbf{v}_{\mathrm{ROMS}}$ is the velocity from the ROMS model, and

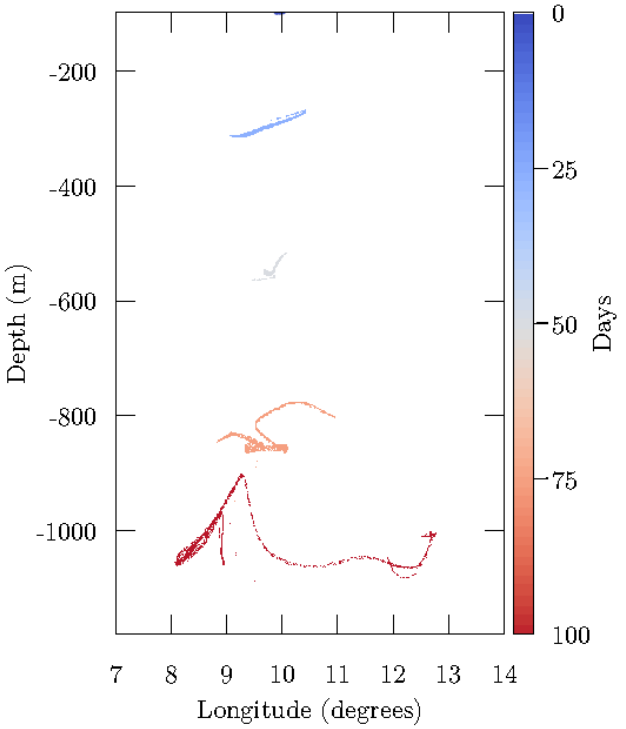

Fig. 1. The positions of particles at different times as they sink in a realistic oceanic flow.

$W = 10$ m/day corresponds to the sinking velocity, pointing in the vertical direction given by the unit vector $\mathbf{k}$.

[1] G. Drotos, P. Monroy, E. Hernández-García, C. López, Inhomogeneities and caustics in passive particle sedimentation in incompressible flows, arXiv:1801.10116.

Influencia de coloides pasivos en suspensiones de coloides activos

D. Rogel-Rodríguez[1,2], R. Martínez[1,2,3], F. Alarcón[1,2] y C. Valeriani[1,2]
[1]Departamento de Estructura de la Materia, Física Térmica y Electrónica, Facultad de Ciencias Físicas, Universidad Complutense de Madrid, 28040 Madrid, Spain
[2]Grupo Interdisciplinar de Sistemas Complejos (GISC), 28040 Madrid, Spain
[3]IFIMAC, Facultad de Ciencias, Univelsidad Autónoma de Madrid, Ciudad Universitaria de Cantoblanco, 28049 Madrid, Spain

Los sistemas de coloides activos están inherentemente fuera del equilibrio, lo cual muchas veces da lugar a comportamientos emergentes interesantes, como lo son la separación de fases inducida por motilidad (MIPS) en sistemas sin ninguna interacción atractiva o de alineamiento. Añadir coloides pasivos a un sistema activo abre la puerta a una infinidad de aplicaciones, en la que destacan el autoensamblaje a la carta y las mediciones micro-reológicas [1]. En este trabajo se ha investigado mediante simulaciones computacionales el comportamiento de las fases de sistemas bidimensionales de mezclas de partículas brownianas esféricas activas y pasivas.

Se ha empleado dinámica browniana para simular sistemas de $N = N_\mathrm{a} + N_\mathrm{p}$ coloides circulares, donde N_a es el número de partículas activas y N_p el número de partículas pasivas, en una caja de longitud L con condiciones periódicas de contorno, con entre 90000 y 180000 coloides en total. Ambos tipos de partículas tienen diámetro $\sigma = 1$ y están sometidas a movimiento browniano, teniendo las activas una fuerza de propulsión de magnitud $|F_\mathrm{a}|$ en la dirección de su vector orientación $\vec{n}$. Las ecuaciones de movimiento para la posición de la partícla i-ésima, $\vec{r}_i$, y para su correspondiente $\vec{n}_i$ pueden escribirse como

$$\dot{\vec{r}}_i = \frac{D}{k_\mathrm{B}T}\left(-\sum_{j\neq i}\nabla V(r_{ij}) + |F_\mathrm{a}|\,\vec{n}_i\right) + \sqrt{2D}\,\vec{\xi}_i,$$
$$\dot{\vec{n}}_i = \sqrt{2D_\mathrm{r}}\,\vec{\xi}_i \times \vec{n}_i,$$

donde $V(r_{ij})$ es el potencial de interacción a pares entre cualquier par de partículas pasivas o activas, k_B es la constante de Boltzmann, T es la temperatura, y las componentes de $\vec{\xi}_i$ representan procesos estocásticos de ruido blanco y media nula. La relación entre el coeficiente de difusión translacional D y el rotacional D_r es la dada por las ecuaciones de Stokes-Einstein, $D_\mathrm{r} = 3D/\sigma^2$. Las partículas pasivas obedecen a las mismas ecuaciones, con $|F_\mathrm{a}| = 0$. Como potencial de interacción se ha empleado el potencial puramente repulsivo de Weeks-Chandler-Andersen (WCA) [3].

Se ha estudiado la MIPS de sistemas con diferentes fracciones de partículas pasivas N_p/N, para distintos números de Péclet y densidades en área ϕ, definidas como $\mathrm{Pe} = 3v/(\sigma D_\mathrm{r})$ y $\phi = \pi N\sigma^2/(4L^2)$ respectivamente, donde $v = |F_\mathrm{a}|D/k_\mathrm{B}T$ es la velocidad de autopropulsión. Los diagramas de fases obtenidos para cada fracción N_p/N se muestran en la fig. 1, donde se observa que, pese a que la presencia de partículas pasivas en el sistema activo dificulta la MIPS, ésta puede darse incluso cuando el 70% de los coloides son pasivos. Cuando los coloides pasivos son el 80% o más, no se ha observado MIPS a ningún ϕ en el rango de números de Péclet evaluados (hasta $\mathrm{Pe} = 250$).

Por otro lado, se ha observado que en sistemas con mezclas de coloides activos y pasivos, la MIPS es muy dinámica, y se produce mediante la formación espontánea de frentes activos que encierran núcleos pasivos y favorecen su cristalización. Ejemplos de estas configuraciones se muestran en la fig. 2. Esto es relevante de cara a diseñar dispositivos experimentales para el ensamblado direccionado mediante el empleo de partículas activas.

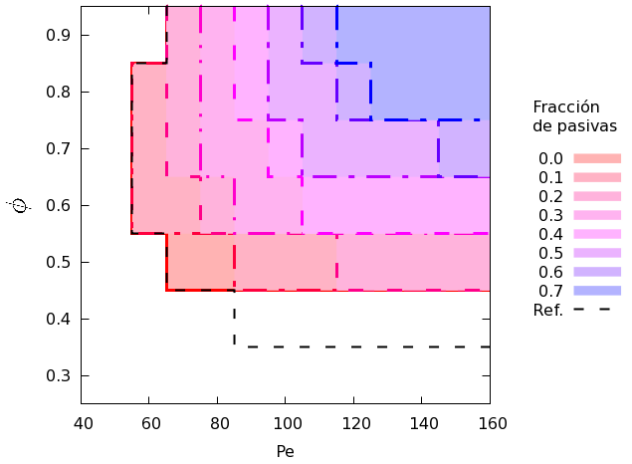

Fig. 1. Diagrama de fases de sistemas de mezclas de coloides activos y pasivos en función de la densidad en área ϕ y el número de Péclet para diferentes fracciones N_p/N de componentes pasivos. La línea negra punteada corresponde a la ref. [2], donde $|F_\mathrm{a}| = \mathrm{cte}$ y Pe cambia con D_r.

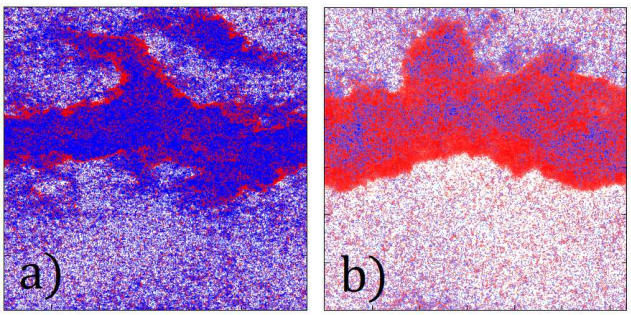

Fig. 2. Fotos de dos simulaciones de mezclas en la fase separada (en rojo, coloides activos y en azul los pasivos): (a) $N_\mathrm{p}/N = 0.6$, $\phi = 0.8$, $\mathrm{Pe} = 190$, (b) $N_\mathrm{p}/N = 0.3$, $\phi = 0.7$, $\mathrm{Pe} = 170$.

[1] A. Wysocki, R. G. Winkler, and G. Gompper, New J. Phys. **18**, 123030 (2016).

[2] J. Stenhammar, D. Marenduzzo, R. J. Allen, and M. E. Cates, Soft Matter **10**, 1489-1499 (2014).

[3] J. D. Weeks, D. Chandler, and H. C. Andersen, J. Chem. Phys. **54**, 5237-5247 (1971).

Biofilm formation dynamics under different growth conditions

L. Dinis[1], F. Alarcón[1], M. Pica Ciamarra[2], A. Canales[3], I. López-Montero[4,†], B. Orgaz[5,†], and C. Valeriani[1,†]
[1]GISC and Departamento de Estructura de la Materia, Física Térmica y Electrónica, Universidad Complutense de Madrid, Spain
[2]Division of Physics and Applied Physics, Nanyang Technological University, Singapore
[3]Departamento de Química Orgánica, Universidad Complutense de Madrid, Spain
[4]Departamento de Química Física, Universidad Complutense de Madrid, Spain
[5]Sección Departamental de Farmacia, Farmacia Galénica y Tecnología Alimentaria, Facultad de Veterinaria, Universidad Complutense de Madrid, Spain

Biofilms are communities of microorganisms which segregate an extracellular polymeric matrix. They are of primary interest due to their relevance in health and food industry but impact also other domains [1]. About half or even more of the microbial infections in humans are caused by bacteria growing as a biofilm. In food industry, biofilms tend to form on production plants and equipment. They also pose sanitation and management problems and extra costs in fish farms, boats, water treatment, etc. Bacteria in biofilms are known to better resist disinfectants, cleaning procedures and even antibiotic attack.

Our current research is aimed at determining the physical and chemical characteristics that contribute to mechanical properties and stability of *Pseudomonas fluorescens* biofilms from experiments in rheology and NMR. To asses the influence of environment, biofilm growth has been carried out in different conditions of agitation and nutrient availability. In this contribution, we present a population dynamics model coupled to nutrient dynamics that can satisfactorily reproduce and explain some of the aspects of bacterial growth in the experiments.

A set of experiments were carried out in vertically disposed coupons half immersed in growth media. Samples at different stages (4, 12, 24, 48, 72, and 96 h) have been extracted to perform cell counting, providing evolution of logarithmic CFU cm^{-2} (CFU, colony forming units) data. Different media have been used for different batches, TSB (rich medium), TSB at half its usual concentration, TSB supplemented with glucose and PMS7Ca (minimal medium). Container shaking has a dramatic effect in biofilm growth and morphology. Figure 1 shows (normalized) cell counts in CFU in TSB stirred and static experiments.

The number of bacteria in the biofilm follows a growth, saturation and decay pattern. We interpret these results as follows. In the initial stages growth is exponential as anticipated as expected. Culture medium is not replaced during the experiment. As a result a saturation in population occurs. As nutrients become scarce an competition intensifies, cells either die or leave the biofilm. This can be directly translated into a population dynamics model where *carrying capacity* is dependent on nutrient concentration and with a rate of feeding proportional to cell number. For suitable parameters the model can reproduce the same behavior (see Fig. 1, blue continuous line). One can expect that static conditions may impact the value of the parameters, and in fact the model can also reproduce the behavior for static conditions by changing some parameter values (see Fig. 1, blue dashed line).

Finally, the system is being analysed also from a different

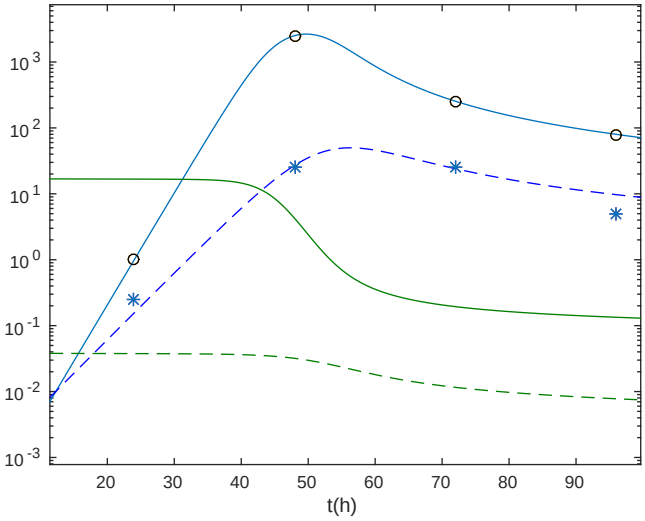

Fig. 1. Circles are the experimental CFU normalized to value at 24 h, blue stars represent experimental data in static conditions. Blue continuous and dashed lines are the solution of the model for population in stirring and static conditions, respectively. Green continuous and dashed lines are nutrient concentration for stirred and static conditions, also from model results in arbitrary units.

scale and degree of detail by performing mesoscopic dissipative particle dynamics (DPD) simulations of bacterial growth, interaction and extracellular matrix secretion. Bacteria are modeled as rods, where each bacterium is formed by a finite size chain of Brownian particles. They reproduce according to the input reproduction parameter. The extracellular matrix can be modeled either explicitly, as chains of Brownian monomers which generate according to a input production rate of bacteria, or implicitly, as an effective depletion force among bacteria. Both cases have interesting effects in the growth of the modeled biofilm. We expect the population dynamics model to provide valuable information and insight to tune and interpret simulation results. Simulations are a valuable tool to understand rheology of biofilms, which is relevant to asses their stability under external mechanical stress.

---

† These authors are Principal Investigators in the staBiofilm collaboration.

[1] M. Ghannoum and G. A. O'Toole (Eds.), *Microbial Biofilms* (American Society of Microbiology Press, 2004).

Inhomogeneous cooling state of a strongly confined granular gas at low density

J. Javier Brey, M. I. García de Soria, and P. Maynar
Física Teórica, Universidad de Sevilla, Sevilla, Spain

The inhomogeneous cooling state describing the hydrodynamic behaviour of a freely evolving granular gas strongly confined between to parallel plates is studied, using a Boltzmann kinetic equation derived recently [1]. By extending the idea of the homogenous cooling state, we propose a scaling distribution in which all the time dependence occurs through the granular temperature of the system, while there is a dependence on the distance to the confining walls both through the density and the temperature.

It is obtained that the velocity distribution is not isotropic, and has different temperature parameters associated to the motion perpendicular and parallel to the confining plates, although their cooling rates are the same. The cooling rate and the temperature are calculated by means of a Gaussian approximation. The theoretical predictions are compared with molecular dynamics simulation results and a good agreement is found.

[1] J. J. Brey, P. Maynar, and M. I. García de Soria, Kinetic equation and nonequilibrium entropy for a quasi-two-dimensional gas, Phys. Rev. E **94**, 040103(R) (2016).

Numerical simulation of the effect of liposomes on a quartz crystal microbalance

M. Meléndez, R. P. Peláez, A. Vázquez-Quesada, and R. Delgado-Buscalioni
Department of Theoretical Condensed Matter Physics, Universidad Autónoma de Madrid, Spain

With the advance of nanotecnology in life-science, the measurement of small quantities of mass has become an important issue on some applications. Quartz crystal microbalance (QCM) is a very popular device to do such a task, due to its high sensibility (10^{-16} kg) and to the simple physical concepts involved in those systems [1]. The base of the QCM is a small disk-shaped piezoelectric quartz crystal resonator which oscillation at high frequencies (of the order of Mhz) can be controlled by the application of an electrical voltage. When the QCM is in contact with bio-fluids, changes in the attached mass to the resonator can be determined through changes on the dissipation and frequency of the crystal.

In this work, we will focus in the case of liposomes attached with DNA molecules to the resonator. Such kind of systems are currently being tested to diagnose cancer in blood. This is done through binding events with tumoral cells: a target protein is attached on the DNA chain anchor to the resonator in order to bind mutant cells; the increase of mass is then detected by the QCM and can be used as a biomaker for cancer allowing its early detection and/or its monitorization [2]. Although the binding mechanism is quite simple, its effect in experiments is understood only qualitatively through very simple mathematical models which can only be applied to very simple situations. For a more quantitative knowledge is necessary to study the system from a more fundamental point of view.

To understand better this problem we have performed mesoscopic simulations with different numerical methods, such as Finite Volume with Immersed Boundary method [3], Langevin dynamics or Dissipative Particle Dynamics (DPD). The scheme of the simplified model used to address this problem is depicted at Fig. 1. The liposomes (represented by a sphere in the figure) are modeled as small spheres linked by Hookean springs. The DNA anchor of the liposome on the QCM is given by another Hookean spring, or by a semiflexible chain. The crystal is modeled as an oscillating wall and its hydrodynamic dissipation is calculated from the velocity gradient on the wall position.

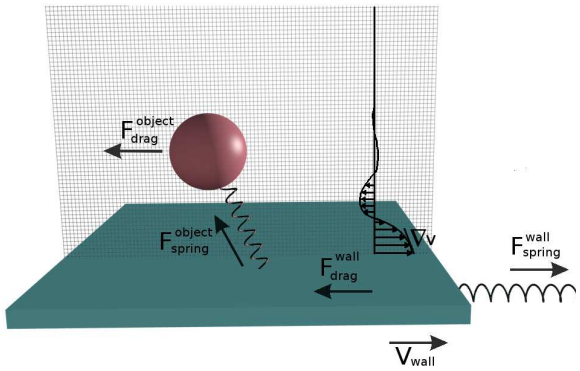

Fig. 1. Scheme of the model.

Resolution studies and comparison with analytical solutions will be shown to check the accuracy of the code. Results about the influence of different features, such as hydrodynamic effects, mass, concentration, radius, length of anchor or rigidity of the liposomes will be also presented.

This work is part of an ongoing FET-OPEN project *Capturing non-Amplified Tumor Circulating DNAwith Ultrasound Hydrodynamics (CATCH-U-DNA)*, whose objective is to increase the mass sensitivity of the QCM setup using dissipative structures, so as to be able to detect minute bulk concentrations (femto to attomolar) of mutant DNA in the sample.

[1] C. Steinem and A. Janshoff (Eds.), *Piezoelectric Sensors, Vol. 5* (Springer Science & Business Media, 2007).

[2] Y. Uludag and I. E. Tothill, Cancer biomarker detection in serum samples using surface plasmon resonance and quartz crystal microbalance sensors with nanoparticle signal amplification, Anal. Chem. **84** 5898-5904 (2012).

[3] A. Vázquez-Quesada, F. Balboa-Usabiaga, and R. Delgado-Buscalioni, A multiblob approach to colloidal hydrodynamics with inherent lubrication, J. Chem. Phys. **141**, 204102 (2014).

Subdiffusion of non-interacting tracers in permanent gels of varying fractral structure

N. Alcázar Cano and R. Delgado-Buscalioni
Department of Theoretical Condensed Matter Physics, Universidad Autónoma de Madrid, 28049 Madrid, Spain

Porous materials are widely used in a large number of technological applications some of them of daily use. Despite the efforts made over few decades, the mass transport through this kind of materials is not fully understood. In particular, the subdiffusion regime still represents a theoretical challenge. We study the subdiffusion of non-interacting nanoparticles in three-dimensional porous media using Brownian Dynamics. The mean-squared displacement of a particle in this kind of environment presents a power-law time dependence $\langle r^2 \rangle \propto t^{\alpha}$, where α is the subdiffusive exponent. The diffusive exponent is strongly dependent on tracer diameter σ [1]. As shown in Fig. 1, α goes to zero as the diffusing particle is larger than some critical value σ_c.

On the other hand, in the gel, the structure of the voids available for the particle to diffuse critically determines its dynamics. The probability of finding an accessible site p in the percolating void-space of a gel is given by two contributions: the probability of being in the largest percolating void-cluster and that of being in an isolated cluster. Mobile particles diffuse through the percolating cluster while trapped tracers remain in the cages of these isolated spaces (this means that $\alpha_{\text{trap}} \simeq 0$). Of course p decreases with σ (the relation being different for random obstacles and connected traps).

For a critical void fraction p_c the percolated void disappears and the diffusion coefficient vanishes [3]. We propose the expression for the subdiffusive exponent

$$\alpha = \alpha_{\text{mob}}(p)\,[1 - p_{\text{trap}}(p)]\,, \qquad (1)$$

which takes into account that, in a fixed gel, a particle is either trapped or mobile ($1 = p_{\text{mob}} + p_{\text{trap}}$). Here α_{mob} is the subdiffusive exponent of mobile tracers.

We also propose a simple argument which yields $\alpha_{\text{mob}} = 1 + a \ln p$, being a a parameter which is seen to slightly depends on the gel structure ($a = 0.20 \pm 0.04$). This estimate of α is compared with our results for several types of gels and also with experimental and numerical works in the literature. We find a fairly good agreement: Figure 2 shows results for α in two of our gels (a random cubic mesh and polymer gels) and a silica gel studied in Ref. [2]. Solid lines are the fits obtained using Eq. (1). Notably, the probability of getting trapped $p_{\text{trap}}(p)$ depends on the gel structure. In polymer gels $p_{\text{trap}} \sim (p/p_c)^{-\gamma}$, while in cubic and silica gels $p_{\text{trap}} \sim \exp[-(p/p_c)]$. Our ansatz also reproduces the subdiffusion observed in actin fibers and random obstacles (Lorentz model).

[1] I. Y. Wong, M. L. Gardel, D. R. Reichman, E. R. Weeks, M. T. Valentine, A. R. Bausch, and D. A. Weitz, Phys. Rev. Lett. **92**, 178101 (2004).

[2] D. Hlushkou, A. Svidrytski, and T. Ulrich, J. Phys. Chem. C **121**, 8416-8426 (2017).

[3] S. Babu, J. C. Gimel, and T. Nicolai, J. Phys. Chem. B **112**, 743-748 (2008).

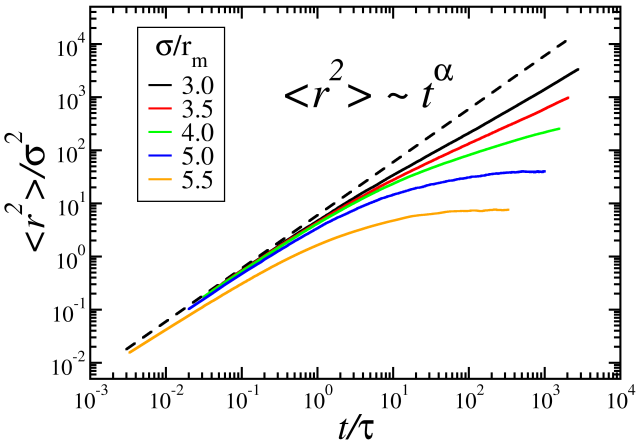

Fig. 1. Mean-square displacement for various particle effective diameter σ in a cubic gel as a function of scale time t/τ, where τ is the time which a free particle spends on travelling the square of its size. The dashed line represents the dymanics of a free particle, which is purely diffusive $\langle r^2 \rangle \sim t$.

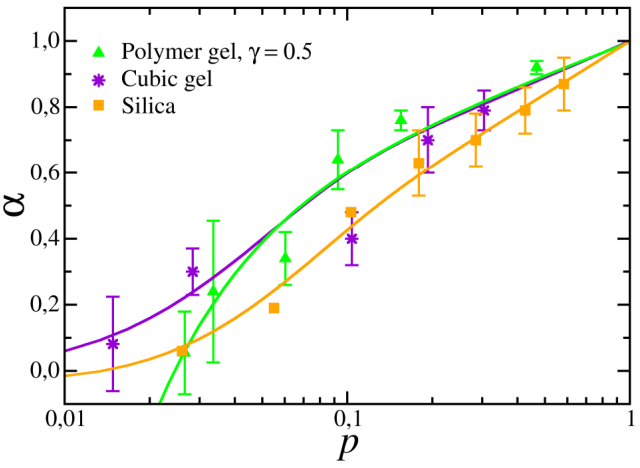

Fig. 2. Subdiffusive exponent α as a function of the accessible volume fraction p for three different systems. α for polymer and cubic gels are the results of our simulations, while silica's results are taking for [2]. Solid lines represent the trend proposed in Eq. (1).

El modelo interfacial no local revisado

José Manuel Romero-Enrique[1], Alessio Squarcini[2,3], Andrew O. Parry[4] y Paul M. Goldbart[5]

[1]Departamento de Física Atómica, Molecular y Nuclear, Área de Física Teórica, Universidad de Sevilla, av. Reina Mercedes s/n, 41012 Sevilla, España

[2]Max-Planck-Institut für Intelligente Systeme, Heisenbergstr. 3, D-70569 Stuttgart, Germany

[3]Institut für Theoretische Physik, Universität Stuttgart, Pfaffenwaldring 57, D-70569 Stuttgart, Germany

[4]Department of Mathematics, Imperial College London, London SW7 2AZ, United Kingdom

[5]School of Physics, Georgia Institute of Technology, 837 State Street, Atlanta, Georgia 30332, USA

En esta presentación se describirá una derivación rigurosa del modelo de hamiltoniano interfacial no-local para fuerzas intermoleculares de corto alcance que ha sido propuesto por algunos de los autores [1, 2, 3, 4, 5, 6, 7, 8]. Nuestro punto de partida es un Hamiltoniano microscópico de Landau-Ginzburg-Wilson con un potencial de doble parábola, a partir del cual derivamos un modelo mesoscópico interfacial usando un método integral, que desarrollamos en términos asociados a los distintos órdenes en la curvatura de las interfases involucradas [9].

Se muestran los resultados para tres situaciones: una fase fluida en contacto con una pared no plana, una interfase libre líquido-vapor y una capa de mojado entre una fase vapor y una pared no plana. En los dos primeros casos, nuestro método identifica la forma correcta de las correcciones de curvatura a la energía libre y, en el casos de la interfase líquido-vapor libre, permite relacionar dichas correcciones con la autointeracción interfacial que ha sido conjeturada previamente en la literatura [8].

Cuando la interfase está en presencia de un sustrato, nuestro método también identifica correcciones en la curvatura para el funcional no-local asociado al potencial efectivo interfacial entre la interfase y la pared. Además, se propone una nueva formulación diagramática para dicho funcional que, en ciertas circunstancias, mejora el desarrollo original introducido en las refs. [1, 2].

[1] A. O. Parry, J. M. Romero-Enrique, and A. Lazarides, Phys. Rev. Lett. **93**, 086104 (2004).

[2] A. O. Parry, C. Rascón, N. R. Bernardino, and J. M. Romero-Enrique, J. Phys.-Condes. Matter **18**, 6433 (2006).

[3] A. O. Parry, C. Rascón, N. R. Bernardino, and J. M. Romero-Enrique, J. Phys.-Condens. Matter **19**, 416105 (2007).

[4] A. O. Parry, C. Rascón, N. R. Bernardino, and J. M. Romero-Enrique, Phys. Rev. Lett. **100**, 136105 (2008).

[5] A. O. Parry, J. M. Romero-Enrique, N. R. Bernardino, and C. Rascón, J. Phys.-Condens. Matter **20**, 505102 (2008).

[6] A. O. Parry, C. Rascón, N. R. Bernardino, and J. M. Romero-Enrique, J. Phys.-Condens. Matter **20**, 494234 (2008).

[7] N. R. Bernardino, A. O. Parry, C. Rascón, and J. M. Romero-Enrique, J. Phys.-Condens. Matter **21**, 465105 (2009).

[8] A. O. Parry, and C. Ráscon, J. Phys.-Condens. Matter **23**, 015004 (2011).

[9] J. M. Romero-Enrique, A. Squarcini, A. O. Parry, and P. M. Goldbart, Phys. Rev. E (in press).

Modelling of *patA* and *hetF* gene function in *Anabaena* heterocyst formation

Pau Casanova, Saúl Ares, and Javier Muñoz-García
Departamento de Matemáticas and Grupo Interdisciplinar de Sistemas Complejos (GISC), Universidad Carlos III de Madrid, 28911 Leganés, Spain

Differentiated cell types can form patterns in filamentous cyanobacteria. Specifically the genus *Anabaena* has received special interest because under nitrogen-limiting conditions some of the vegetative cells differentiate into a nitrogen-fixing form called heterocyst [1]. These heterocysts cannot undergo cell division or have photosynthetic activity, but share fixed nitrogen products with the whole filament. In order to efficiently distribute the fixed nitrogen, heterocysts are arranged forming quasiregular patterns in the filament.

Recent experimental work [2, 3, 4, 5, 6, 7] has advanced on the understanding of the interactions and genetic mechanisms underlying this pattern-forming process. However, the role of many of the genes involved is still unknown. Two of these genes are *patA*, which has an enigmatic mutant phenotype in which heterocysts are only formed at the extremes of the filament, and *hetF*, whose mutant does not form heterocysts under nitrogen deprivation. In this work we investigate their function and provide a model (Figures 1 and 2), based on previous results [8], that explains how *patA* and *hetF* interact with other genes and affect heterocyst pattern formation and maintenance.

Numerical simulations based on this new model reproduce the phenotypes of all simple and multiple mutant conditions and allow to obtain a more complete knowledge of this paradigmatic example of biological pattern formation.

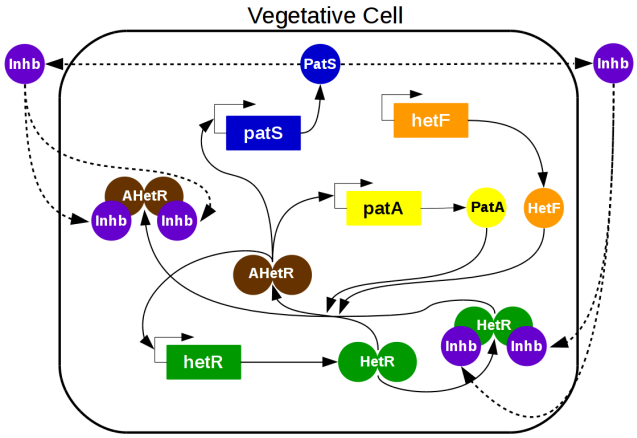

Fig. 1. Vegetative Cell Modelization: While *hetF* (orange) has only a low basal expression, *patA* (yellow) and *patS* (blue) have a regulated expression that depends on the active form AHetR (brown) of the transcription factor HetR (green), which also activates its own expression. At the protein level: The HetR dimer needs to be activated by PatA or HetF to become AHetR. PatS becomes an inhibitor of the transcription factor (purple) by protein transformation during cell to cell transport. The inhibitor thus produced is a small molecule that can diffuse along the filament.

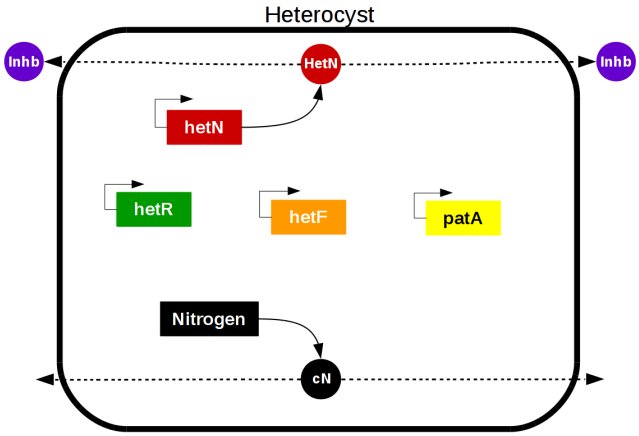

Fig. 2. Heterocyst Cell Modelization: *hetN* (red) is expressed in heterocysts and becomes an inhibitor of the transcription factor (purple), similar at the PatS product, by protein transformation during cell to cell transport. The fixed nitrogen products (black) produced by the heterocyst can also diffuse to act as a inhibitor of AHetR.

[1] A. Herrero, J. Stavans, and E. Flores, FEMS Microbiol. Rev. **40**, 831-854 (2016).

[2] W. J. Buikema and R. Haselkorn, Proc. Natl. Acad. Sci. USA **98**, 2729-2734 (2001).

[3] F. Wong and J. Meeks, J. Bacteriol. **183**, 2654-2661 (2001).

[4] C. C. Orozco, D. D. Risser, and S. M. Callahan, J. Bacteriol. **188**, 1808-1816 (2006).

[5] D. D. Risser and S. M. Callahan, J. Bacteriol. **190**, 7645-7654 (2008).

[6] S. S. Young-Robbins, D. D. Risser, J. R. Moran, R. Haselkorn, and S. M. Callahan, J. Bacteriol. **192**, 4732-4740 (2010).

[7] S. Hou, F. Zhou, S. Peng, H. Gao, and X. Xu, Sci. Bull. **60**, 192-201 (2015).

[8] J. Muñoz-García and S. Ares, Proc. Natl. Acad. Sci. USA **113**, 6218-6223 (2016).

A network approach to airports mobility

Mattia Mazzoli, Riccardo Gallotti, Pere Colet, and Jose J. Ramasco
Instituto de Física Interdisciplinar y Sistemas Complejos (IFISC), CSIC-UIB, Campus UIB, 07122 Palma de Mallorca, Spain

Mobility patterns in public spaces like airports, supermarkets or hospitals, are a topic of main interest to understand how to organize social spaces for economic, health protection and hygienic purposes.

We study a large dataset of anonymized GPS trajectories describing movements inside the London airports by means of temporal and multi-layer networks metrics. Two different behaviors inside airports are found, namely, workers and travelers, showing distinct patterns. We analyze the contact network of all the users in the airport database at different spatial and temporal scales and find a significative assortativity/homophily in the way contacts happen inside the airport between workers and travelers.

Travelers spend more time in contact with other travelers in very crowded spaces as shops, security controls, duty free zones, gates. Conversely, they spend less time with workers. On the other hand, workers spend more time in specific and limited working places with other colleagues for the most of the time and less time on average in contact with travelers at gates or security controls.

We then have to differentiate between arriving, departing and connecting travelers, in order to check if different behaviors may appear. Hence we proceed to associate the four user types to four separated network layers. Each node is an anonymized user and each link represents the presence of two users in the same spatial (10 m^2) and temporal (15 min) discrete space. The resulting networks represent the spatio-temporal coincidences. This allows to infer the main characteristics to be taken into account when modelling epidemic spreading. We randomly subsample the contact network with an increasing number of people, in order to find the critical threshold for a giant component to appear (percolation).

The results are shown in Fig. 1 (left column) for the interactions taking place between 10:00 to 11:00 AM. We have also found that when all the users are present, the system is found above the percolation threshold all day long, even by night as shown in Fig. 1 (right column). With almost one hundredth of the total users we already manage to see a giant component arise, which means an epidemic would be able to spread in the airport. We note that our methodology can be further refined by, within a category, classifying users in communities according to their interaction pattern.

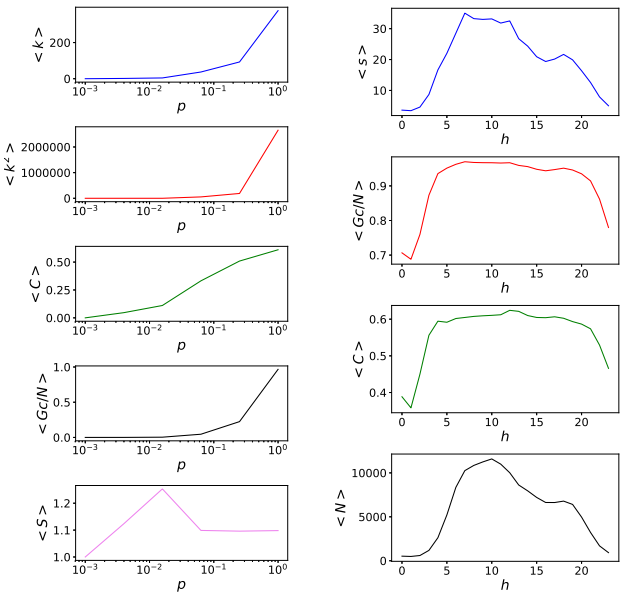

Fig. 1. Characterization of the interaction network. Panels display the mean $\langle k \rangle$ and the second moment $\langle k^2 \rangle$ of the degree distribution, the mean clustering coefficient $\langle C \rangle$, the mean of the giant component relative size $\langle G_c/N \rangle$, the mean size of the components excluding the giant one $\langle S \rangle$ and the number of agents interacting averaged over one hour $\langle N \rangle$.

This study illustrates the opportunity of using the tools of network science for the analysis of spatial trajectories, deepening our knowledge on how humans interact in public spaces. Possible applications include the study of epidemics spreading, opening the doors to the development of models reproducing the observed network features and the behaviors of the different user types and hence to the improvement of epidemics preventions models and policies.

[1] M. Mazzoli, R. Gallotti, P. Colet, and J.J. Ramasco, A network approach to airports mobility, (to appear soon).

Granular suspended bridges as the cause of clogging in vertical narrow pipes

D. López Rodríguez, D. Maza, and I. Zuriguel
Departamento de Física y Matemática Aplicada, Facultad de Ciencias, Universidad de Navarra, Pamplona, Spain

The packing of mono-disperse spheres in a narrow cylinder produces a set of structures as the ratio between the cylinder diameter to the sphere diameter is varied [1]. These structures determine the force distribution between particle to particle and particle to wall. Thus, the packing and the material properties affect the movement of material through a cylindrical channel.

A frequent situation with this type of transportation is clogging. The system clogs due to the development of hanging arches that are able to support the weight of the material above them. The study of this kind of phenomenon can be interesting to other situations, e.g., the blood flow through veins and arteries, the transport of rocks by pipes in mining and the pedestrian flow in narrow corridors.

The experimental study of clogging in verticals pipes has been scarcely studied. The first experimental approach was introduced by Janda [3] where the grannular material was composed by platy particles. Nevertheless, the behavior of spheres has not been yet analyzed experimentally, although some numerical simulations have been performed [4, 5].

In this work we introduce an experimental setup consisting on a long narrow cylinder full of spherical beads which are extracted at a constant rate by means of a conveyor belt placed at bottom (Fig. 1). The granular material is formed by plastic beads of 5 to 8 mm. The cylinder, made of transparent methacrylate has a length of 2000 mm and its placed vertically. The inner diameter is varied between 10-26 mm which implies an aspect ratio between pipe and particle diameters of 2-4. The time between two consecutive clogs, typically named avalanche duration, is registered. The avalanche duration can be converted to avalanche mass by considering the flow rate and later, analyzed to get the avalanche distribution. Also, we register the locations of arches that clog the pipe with a camera. These locations allow us to calculate the probability that a clog occurs at different positions.

We analyze the dependence of clogging on the aspect ratio, the avalanche distribution between clogs and the spatial clog's distribution along the pipe. We also observe an interesting phenomenon, which is the spontaneous formation of helical patterns. Recent findings have shown that these helical patterns lead to clogging reduction [4].

[1] A. Mughal, H. K. Chan, D. Weaire, and S. Hutzler, Phys. Rev. E **85**, 051305 (2012).

[2] M. J. Beus, W. G. Pariseau, B. M. Stewart, and S. R. Iverson, Design of ore passes, in *Underground Mining Methods: Engineering Fundamentals and International Case Studies*, edited by W. A. Hustrulid and R. C. Bullock (Society for Mining and exploration Inc., 2001), pp. 627-634.

[3] A. Janda, I. Zuriguel, A. Garcimartín, and D. Maza, Granul. Matter **17**, 545-551 (2015).

[4] F. Verbücheln, E. Parteli, and T. Pöschel, Soft Matter **11**, 4295-4305 (2015).

[5] J. Hadjigeorgiou and J. F. Lessard, Int. J. Rock Mech. Min. Sci. **44**, 820-834 (2007).

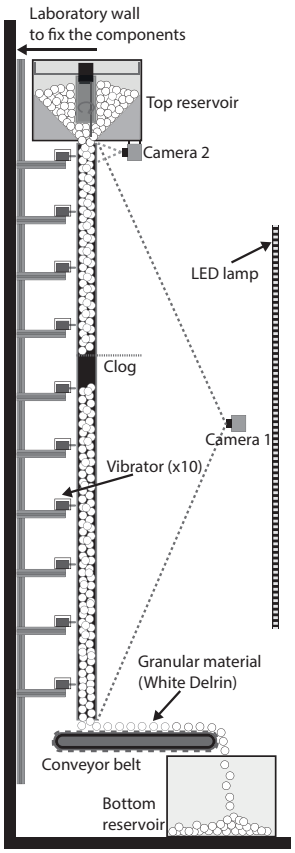

Fig. 1. Experimental setup. In the image from top to bottom: a reservoir from which the cylinder is filled, a camera (Camera 2) used to determine when a clog occurs, a long and narrow cylinder, 10 vibrators controlled independently used to break the clogs, a camera (Camera 1) that takes photos of the entire pipe, a conveyor belt that extracts the granular material; a LED lamp and a bottom reservoir.

Randomly coupled identical nonlinear chemical oscillators presenting Turing instability

David García-Selfa, Mariamo Mussa, and Alberto P. Muñuzuri
Grupo de Física No Lineal, Facultad de Física, Universidad de Santiago de Compostela, 15782 Santiago de Compostela, Spain

Synchronization of nonlinear chemical oscillators constitutes a recent step forward in analyzing the classical problem of synchronization of oscillators. In fact, these chemical oscillators have demonstrated the capability to exhibit multiple configurations ranging from full synchronization and mobbing state till chimera states. The motivations of this type of study in Nature are numerous.

On the other hand, Turing instability is a very powerful mechanism that introduces differentiation in a very natural way and has been pointed out as the mechanism responsible for differentiation in multiple processes in Nature.

In this contribution we present results aiming to obtain a Turing instability in the context of network-organized chemical oscillators. This phenomenon produces the set of identical oscillators to spontaneously differentiate as it is observed in natural systems. This is introduced in a very simple way even in the absence of oscillations.

We consider a large population of interacting Belousov-Zabotinsky (BZ) oscillators included into a reacting environment. Chemical oscillators are modeled as beads loaded with a catalyst and embedded in catalyst-free BZ solution [1, 2]. Thus, beads and surrounding solution are represented as the network nodes and these nodes are interacting diffusively via the network edges through collisions [3]. The node representing the surrounding solution –the environment– is connected to all the beads and the beads are randomly connected between them. The effect of cross-diffusion is considered in our numerical results and resulted to be of crucial importance in the mechanism described [4, 5].

[1] M. R. Tinsley, S. Nkomo, and K. Showalter, Chimera and phase-cluster states in populations of coupled chemical oscillators, Nat. Phys. **8**, 662 (2012).

[2] G. Ghoshal, A. P. Muñuzuri, and J. Pérez-Mercader, Emergence of a super-synchronized mobbing state in a large population of coupled chemical oscillators, Sci. Rep. **6**, 19186 (2016).

[3] H. Nakao and A. S. Mikhailov, Turing patterns in network-organized activator-inhibitor systems, Nat. Phys. **6**, 544 (2010).

[4] V. K. Vanag and I. R. Epstein, Cross-diffusion and pattern formation in reaction-diffusion systems, Phys. Chem. Chem. Phys. **11**, 897 (2009).

[5] M. Mussa, D. García-Selfa, and A. P. Muñuzuri, Non-localized Turing instability in a random network of chemicals oscillators, (in preparation).

Topological defects in vibrated monolayers of granular rods

E. Velasco[1], Y. Martínez-Ratón[2], D. de las Heras[3], J. Renner[3], M. González-Pinto[1], and F. Borondo[4]
[1]Departamento de Física Teórica de la Materia Condensada, Universidad Autónoma de Madrid, Spain
[2]Departamento de Matemáticas, Escuela Politécnica Superior, Universidad Carlos III de Madrid, Spain
[3]Institute of Physics, Universidad de Bayreuth, Germany
[4]Departamento de Química, Universidad Autónoma de Madrid, Spain

We analyse liquid-crystalline ordering in vertically vibrated, quasi-two-dimensional monolayers of rods lying on a horizontal circular cavity, which project on the plate as rectangles. As a result of inelastic collisions involving rods and the cavity walls, energy is transferred to the horizontal plane and the monolayer exhibits some characteristics typical of thermally excited equilibrium systems. In particular, after an initial transient regime, low aspect (length-to-breadth) ratio particles, at high packing fractions, frequently form globally tetratic arrangements with C_4 symmetry [1]. This symmetry, which is incompatible with the circular geometry of the cavity, is restored by the creation of four point defects with a total topological charge of $+4$. The defects show a slow dynamics which we investigate [2].

First, we compare the behaviour of the granular monolayer with equilibrium Monte Carlo simulations of an equivalent system of hard rectangles. As expected, the equilibrium system also exhibits tetratic configurations with four point defects in a square arrangement (Fig. 1). In both systems defects stay close to the surface, which points to the existence of repulsive effective interactions between the defects, mediated by the tetratic medium.

To study the nature of these interactions, we also measure the interdefect distance distribution in the experiment (Fig. 2), and compare it with a simple model where four point particles with logarithmic repulsive interactions are simulated in the cavity using Brownian dynamics. From this comparison we extract a stiffness coefficient for the tetratic medium, which turns out to be of the same order as corresponding elastic constants of tetratic phases in equilibrium systems, thus establishing clear similarities between the elastic properties of this steady-state, dissipative vibrated system, and the corresponding system in thermal equilibrium.

We also point out the differences found between the two systems, which can be ascribed to the nonequilibrium nature of fluctuations in the excited granular monolayer. On the one hand, local excitations of regions with smectic order between defects in the experiment, not present in the equilibrium simulations, tend to make interactions between nearest defects stiffer and renormalise the elastic constant. These regions cause anisotropic defect interactions. Also, particle orientations near the cavity wall are different, which affects the preferred distance between the wall and the defects.

Finally, nonequilibrium simulations of rods regarded as active particles are presented. These simulations show that activity, together with excluded-volume interactions and frustration due to the confining geometry all compete to give a complex behaviour which captures some features of the real experiment on granular rods.

[1] M. González-Pinto, F. Borondo, Y. Martínez-Ratón, and E. Velasco, Clustering in vibrated monolayers of granular rods, Soft Matter **13**, 2571 (2017).

[2] Defects in vertically vibrated monolayers of cylinders, M. González-Pinto, J. Renner, D. de las Heras, A. Díaz de Armas, Y. Martínez-Ratón, and E. Velasco, (to be published).

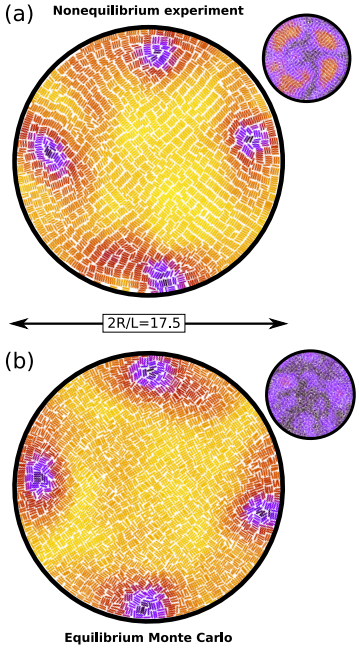

Fig. 1. Colour map of tetratic order parameter (big images) for particular configurations. Upper panel: experiment. Lower panel: Monte Carlo simulation. Particles are mostly arranged in a global tetratic configuration except in four defected regions where the tetratic order parameter is depressed. Colour maps for the uniaxial nematic order parameters are also shown (small images). Smectic regions are not excited in the MC simulations, but they frequently appear in the experiment.

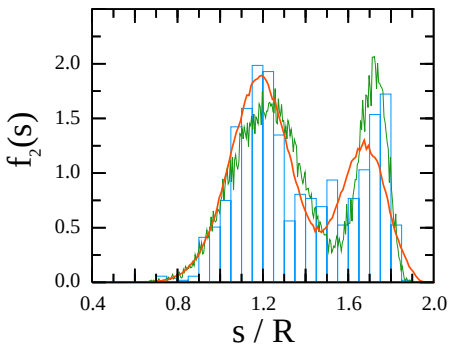

Fig. 2. Defect distance distribution in the experiment (histogram), the MC simulation (red curve) and the Langevin simulation (green noisy curve).

Separación de las contribuciones geométrica y dinámica en el atasco en silos

Diego Gella, Diego Maza e Iker Zuriguel
Departamento de Física y Matemática Aplicada, Facultad de Ciencias, Universidad de Navarra, Pamplona, Spain

Cuando se descarga un silo lleno de material granular a través de un orificio el flujo puede ser interrumpido a causa a la formación de estructuras estables como arcos o bóvedas. La probabilidad de que se produzca este fenómeno es independiente del tiempo [1], por lo que las distribuciones de avalanchas (cantidad de material descargado entre dos atascos) son exponenciales. Por otro lado, la fuerte dependencia de la probabilidad de atasco con el tamaño de agujero se ha explicado de diferentes formas a lo largo de los años. Algunos autores lo hacen introduciendo un agujero crítico a partir del cual no se producen atascos [2, 3] mientras que otros proponen dependencias exponenciales elevadas a la dimensión del problema [3, 4] basándose en argumentos geométricos. Sin embargo, la posible relación de estos sucesos con rasgos cinemáticos o dinámicos del sistema ha pasado casi desapercibida para la comunidad. Para tratar de estudiar experimentalmente esta influencia hemos utilizado una cinta transportadora de velocidad variable para extraer el material de forma controlada.

El equipo experimental consiste en un silo cuasibidimensional lleno de esferas de acero inoxidable de diámetro $d_\mathrm{p} = 4$ cm dispuestas en una sola capa. Para controlar la velocidad de salida se ha colocado la cinta transportadora bajo el orificio a una distancia h del fondo del silo. En primer lugar, se ha llevado a cabo un estudio de la relación de algunas magnitudes cinemáticas (velocidad, flujo, fracción de volumen) en el agujero con la velocidad de la cinta a partir del procesamiento de vídeos tomados con una cámara rápida. Para medir la probabilidad de atasco, el silo se ha complementado con un vibrador, una cámara, un panel led y una balanza. Estos aparatos sincronizados adecuadamente nos permiten medir de forma automatizada las distribuciones de avalanchas entre dos atascos, a partir de las cuales es posible calcular la probabilidad de atasco $1 - p$.

Se han realizado experimentos para tres tamaños de agujero D diferentes abarcando todo el rango de velocidades que nos permite la cinta transportadora. La figura 1 muestra $1 - p$ en función de la velocidad v media de las partículas al pasar por el agujero. La influencia de la cinemática es notable, pues al reducir al máximo la velocidad la probabilidad de atasco incrementa en casi dos órdenes de magnitud para el caso de $D = 17$ mm. Además, vemos que para el límite de velocidades bajas se obtienen valores finitos de probabilidad de atasco que dependen de D. Basándonos en el modelo de Thomas y Durian [4] pero introduciendo una dependencia lineal con la velocidad proponemos la siguiente ecuación

$$1 - p = (a + bv)^{-(D/d_\mathrm{p})^2}. \qquad (1)$$

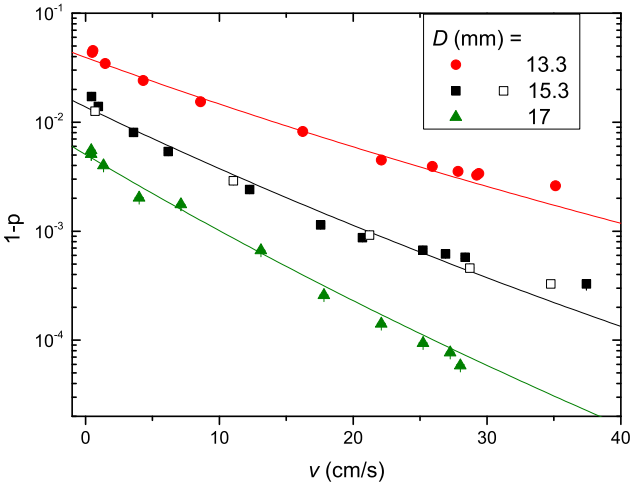

Fig. 1. Probabilidad de atasco $1 - p$ en función de la velocidad media de las partículas al pasar por el orificio para las aperturas indicadas en la leyenda. Los experimentos se han llevado a cabo fijando la cinta a una distancia h de 3.25 mm (puntos rellenos) y 4.5 mm (puntos huecos) a la parte inferior del silo.

Esta expresión incluye dos parámetros: a, que determina la probabilidad de atasco cuando la cinemática es llevada al mínimo, y b, que determina la dependencia de $1 - p$ con v. En nuestro caso, la expresión predice bastante bien los datos experimentales usando los valores de $a = 1.33$ y $b = 0.0128$ (cm/s)$^{-1}$. Además, la generalización de esta ecuación ha sido validada para distintas posiciones de la cinta y para experimentos de descarga en caída libre, es decir, quitando la cinta.

[1] I. Zuriguel, L. A. Pugnaloni, A. Garcimartín, and D. Maza, Phys. Rev. E **68** 030301(R) (2003).

[2] I. Zuriguel, A. Garcimartín, D. Maza, L. A. Pugnaloni, and J. M. Pastor, Phys. Rev E **71**, 051303 (2005).

[3] K. To, Phys. Rev. E **71**, 060301(R) (2005).

[4] C. C. Thomas, and D. J. Durian, Phys. Rev. E **87**, 052201 (2013).

Prediction of atherosclerosis risk from a numerical and experimental investigation of blood flow in vessel branches

A. Otero-Cacho[1], M. Aymerich[1], M. T. Flores-Arias[1], M. Abal[2,3], E. Álvarez[2,3], P. Taboada[1], A. P. Muñuzuri[1], and V. P. Muñuzuri[1]

[1]Faculty of Physics, Universidade de Santiago de Compostela, Santiago de Compostela 15782, Spain
[2]Health Research Institute of Santiago de Compostela (IDIS), Fundación IDIS – SERGAS, Santiago de Compostela 15706, Spain
[3]Centro de Investigación Biomédica en Red – Enfermedades Cardiovasculares (CIBERCV), 28029 Madrid, Spain

Cardiovascular disease is the leading cause of dead. A very large portion of it is attributed to atherosclerosis-related problems. Understanding hemodynamics in blood circulation is, thus, crucial in order to unveil the mechanisms underlying the formation of atherosclerotic plaques.

We performed an exhaustive investigation in a simplified model aiming to characterize those regions in vessel bifurcations that are more likely to develop such lesions. Our investigation is based on numerical simulations (via CFD) and on in-vitro experiments realized in an ad-hoc designed polydimethylsiloxane (PDMS) channel [1]. The results obtained demonstrate that low velocity regions and low shear stress zones are located in the outer walls of bifurcations. In fact, we found that there is a critical range of bifurcation angles that is more likely to vascular disease than the others in correspondence with some previous experimental evidence. The effect of the inflow velocity on this critical range is also analyzed [2].

Furthermore, we carried out numerical simulations aiming to understand nano-and-microparticles behavior in blood flows through a blood vessel stenosis. Different shapes and sizes were analyzed [3].

---

[1] M. Aymerich, E. Álvarez, C. Bao-Varela, I. Moscoso, J. R. González-Juanatey, and M. T. Flores-Arias, Laser technique for the fabrication of blood vessels-like models for preclinical studies of pathologies under flow conditions, Biofabrication **9**, 025033 (2017).

[2] A. Otero-Cacho, M. Aymerich, M. T. Flores-Arias, M. Abal, E. Álvarez, V. Pérez-Muñzuri, and A. P. Muñuzuri, Determination of hemodynamic risk for vascular disease in planar artery bifurcations, Sci. Rep. **8**, 2795 (2018).

[3] A. Otero-Cacho, M. Aymerich, M. T. Flores-Arias, M. Abal, E. Álvarez, P. Taboada, A. P. Muñuzuri, and V. P. Muñuzuri, (in preparation)

Lagrangian structures in two-dimensional quantum turbulence

Rebeca de la Fuente[1], Audun Skaugen[2], Luiza Angheluta[2], Emilio Hernández-García[1], and Cristóbal López[1]
[1]IFISC, CSIC-UIB, Campus Universitat de les Illes Balears, E-07122 Palma de Mallorca, Spain
[2]Department of Physics, University of Oslo, P.O. 1048 Blindern, 0316 Oslo, Norway

The advances in the creation and manipulation of Bose-Einstein condensates in trapped ultracold gases has lead to the possibility of studying two-dimensional and three-dimensional flows in such quantum fluids, including the case of quantum turbulence. These gases are superfluids, and share with the well-studied HeII superfluid the lack of viscosity and the presence of quantized vortices. But at difference with it, compressibility effects may be important.

Much effort is devoted to understand the differences and similarities between this quantum turbulence and conventional turbulence. Essentially all studies have addressed Eulerian quantities such as the energy spectrum and the associated cascades. As in classical 2d turbulence, quantum 2d turbulence is strongly dominated by point vortices and their interactions [1, 2].

Here we study 2d quantum turbulence from the Lagrangian point of view, investigating similarities and differences with the classical case. We analyze flows numerically obtained from the Gross-Pitaevskii equation (see an example of condensate density in Fig. 1), and compute Lyapunov exponent fields (which give an idea of the stretching of material lines and also identify barriers to transport, see Fig. 2), finite-size Lyapunov exponent statistics (which characterize particle dispersion under the flow), and Lagrangian versions of the divergence field (identifying compressibility effects).

[1] A. Bradley and B. P. Anderson, Energy spectra of vortex distributions in two-dimensional quantum turbulence, Phys. Rev. X **2**, 041001 (2012).

[2] A. Skaugen and L. Angheluta, Vortex clustering and universal scaling law in two-dimensional quantum turbulence, Phys. Rev. E **93**, 032106 (2016).

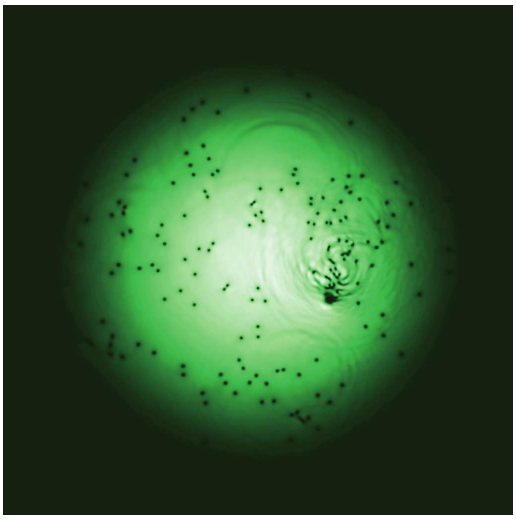

Fig. 1. Density of a trapped condensate stirred by a moving object. Black points are vortex cores.

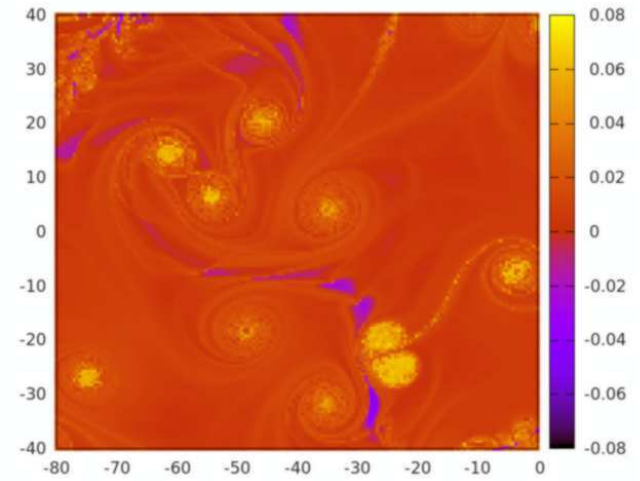

Fig. 2. Backwards finite-time Lyapunov exponent field in a small region of the condensate containing several vortices. Lines along which the strongest stretching occurs are clearly visible.

Stochastic dynamics of spatially extended population with Allee effect

Rodrigo Crespo[1,†] and Francisco J. Cao[1,2]
[1]Departamento de Estructura de la Materia, Física Térmica y Electrónica, Facultad de Ciencias Físicas, Universidad Complutense de Madrid, pl. Ciencias 1, 28040 Madrid, Spain
[2]Instituto Madrileño de Estudios Avanzados en Nanociencia (IMDEA-Nanociencia), c. Faraday 9, 28049 Madrid, Spain

Low population density in some species implies a reduced or negative growth rate. This behavior is known as Allee effect and can lead to local or even global extinctions.

Here, we study the population evolution in the presence of migration, harvesting and environmental stochasticity. We consider a logistic spatially extended model with Allee effect at low densities and density regulation at high densities. Thus, we consider that the growth rate decreases both due to undercrowding and to overcrowding. We characterize the conditions for local and global extinctions induced by stochastic environmental fluctuations.

Our results give insight in the effects of migration and harvesting in species conservation subject to the Allee effect.

† E-mail: rodcresp@ucm.es

[1] N. J. Gotelli, *A Primer of Ecology* (Sinauer Associates, 2008).

[2] R. Lande, S. Engen, and B.-E. Saether, *Stochastic Population Dynamics in Ecology and Conservation* (Oxford University Press, 2003).

[3] J. D. Murray, *Mathematical Biology* (Springer, 2003).

Networks competing between them

Javier M. Buldú[1,2,3], Jaime Iranzo[4], and Jacobo Aguirre[3,5]
[1]Laboratory of Biological Networks, Center for Biomedical Technology, UPM, 28223 Pozuelo de Alarcón, Madrid, Spain
[2]Complex Systems Group, Universidad Rey Juan Carlos, 28933 Móstoles, Madrid, Spain
[3]Grupo Interdisciplinar de Sistemas Complejos (GISC)
[4]National Center for Biotechnology Information, National Library of Medicine, National Institutes of Health, Bethesda, MD, USA
[5]Centro Nacional de Biotecnología, CSIC, c. Darwin 3, 28049 Madrid, Spain

Social, biological, physical and technological systems are composed of a diversity of interacting agents, leading network science, a statistical physics understanding of graph theory, to be a genuine tool for investigating their structure and dynamics [1]. Within the framework of social networks, the topology of the interactions between individuals has been demonstrated to be crucial in, for example, the vanishing of the critical threshold in epidemics [2] or the efficient and fast propagation of innovation [3]. In a similar fashion, the topology of a network itself can be influenced by the dynamical processes occurring in it, giving rise to adaptive mechanisms that rule the evolution of the structure of social networks [4].

The emergence of cooperation, defection or altruism can be investigated by linking game theory to network science. In this way, the intrinsic heterogeneity of social networks, the majority of them showing power-law distributions in the number of connections, has been related in many cases to the emergence of cooperation, contrary to what is observed in homogeneous populations [5]. Furthermore, highly connected individuals have also been shown to be more prone to collaborate than scarcely connected ones [6]. While attention was initially focused on the interplay between nodes' strategies and the structure of the underlying (single) network, more recently, coevolutionary rules have also been related to the emergence of interdependency [7] and multilayer structures [8]. But, what if we are concerned about the interests of a network as a whole instead of its nodes? Does it make sense to consider networks competing or collaborating with other networks? The fruitful recent literature about *networks-of-networks*, or in a more general context about *multilayer networks*, makes these two questions timely and extremely relevant [9]. A diversity of dynamical processes such as percolation [10], diffusion [11] or synchronization [12] have been recently reinterpreted by assuming that real networks unavoidably interact with other networks, a contact that may be beneficial or detrimental to each of the networks belonging to the ensemble.

Here we investigate how $m > 2$ networks compete or cooperate to achieve a relative increase of importance measured as eigenvector centrality, which maximizes their outcome in a variety of dynamical processes [14]. In our competition, networks can vary the way they interact with other networks, evolving in time until they reach a stable situation where all networks refuse to modify their strategy because any change would lead to a worse result. Importantly, an *a priori* optimal connection strategy for a given network may not be reachable due to the actions of the competitor networks, which turns the analysis of the final outcome of the networks into a study of Nash equilibria [13] in a network-of-networks. With this objective in mind, we define a methodology to analyse the competition among networks of any size or topology, demonstrating that several Nash equilibria can coexist, with some of them benefiting the strongest networks and others benefiting the weaker ones. Particularly, we report the existence of a wide regime of the system parameters in which every weak network can induce the rest to cooperate in order to escape from a detrimental Nash equilibrium, taking over the final situation of the whole network-of-networks. Paradoxically, the strong network cannot reverse this phenomenon. This counterintuitive asymmetry that promotes the cooperation among weak networks is independent of the network structure or the competition rules, and it could be applicable to an extensive number of real systems [15].

[1] M. E. J. Newman, *Networks: An Introduction* (Oxford University Press, New York, 2010).

[2] R. Pastor-Satorras and A. Vespignani, Epidemic spreading in scale-free networks, Phys. Rev. Lett. **86**, 3200-3203 (2001).

[3] D. Centola, The spread of behavior in an online social network experiment, Science **329**, 1194-1197 (2010).

[4] T. Gross and B. Blasius, Adaptive coevolutionary networks: a review, J. R. Soc. Interface **5**, 259-271 (2008).

[5] F. C. Santos, M. D. Santos, and J. M. Pacheco, Social diversity promotes the emergence of cooperative behavior, Nature **454**, 213-216 (2008).

[6] L. Dall'Asta, M. Marsili, and P. Pin, Collaboration in social networks, Proc. Natl. Acad. Sci. U.S.A. **109**, 4395-4400 (2012).

[7] Z. Wang, A. Szolnoki, and M. Perc, Self-organization towards optimally interdependent networks by means of coevolution, New J. Phys. **16**, 033041 (2014).

[8] Z. Wang, L. Wang, A. Szolnoki, and M. Perc, Evolutionary games on multilayer networks: a colloquium, Eur. Phys. J. B **88**, 124 (2015).

[9] M. Kivelä, A. Arenas, M. Barthelemy, J. P. Gleeson, Y. Moreno, and M. A. Porter, Multilayer networks, J. Complex Netw. **2**, 203-271 (2014).

[10] S. V. Buldyrev, R. Parshani, G. Paul, H. E. Stanley, and S. Havlin, Catastrophic cascade of failures in interdependent networks, Nature **464**, 1025-1028 (2010).

[11] F. Radichi and A. Arenas, Abrupt transition in the structural formation of interconnected networks, Nat. Phys. **9**, 717-720 (2013).

[12] J. Aguirre, R. Sevilla-Escoboza, R. Gutiérrez, D. Papo, and J. M. Buldú, Synchronization of interconnected networks: the role of connector nodes, Phys. Rev. Lett. **112**, 248701 (2014).

[13] J. Nash, Equilibrium points in n-person games, Proc. Natl. Acad. Sci. U.S.A. **36**, 48-49 (1950).

[14] J. Aguirre, D. Papo, and J. M. Buldú, Successful strategies for competing networks, Nat. Phys. **9**, 230-234 (2013).

[15] J. Iranzo, J. M. Buldú, and J. Aguirre, Competition among networks highlights the power of the weak, Nat. Commun. **7**, 13273 (2016).

Granular gas mixtures of inelastic rough particles: Hard disks and hard spheres

Alberto Megías[1] and Andrés Santos[1,2]
[1]Departamento de Física, Universidad de Extremadura, 06006 Badajoz, Spain
[2]Instituto de Computación Científica Avanzada (ICCAEx), Universidad de Extremadura, 06006 Badajoz, Spain

Granular gas mixtures modeled as systems of inelastic and rough particles, either hard disks on a plane or hard spheres, are considered. Both classes of systems are embedded in a three-dimensional space ($d = 3$) but, while in the hard-sphere (HS) case the translational and angular velocities are vectors with the same dimensionality $d_\mathrm{t} = d_\mathrm{r} = 3$, in the hard-disk (HD) case the translational velocity vectors are planar (i.e., $d_\mathrm{t} = 2$) and the angular velocity vectors are orthogonal to the motion plane (i.e., $d_\mathrm{r} = 1$). This complicates a unified presentation of both classes of systems, in contrast to what happens for smooth, spinless particles, where an unambiguous kinetic-theory treatment of d-dimensional spheres is possible [1].

The kinetic-theory derivation of the energy collisional production rates ξ_{ij}^{tr} and ξ_{ij}^{rot} (where the indices i and j label different components) has been separately carried out for HS [2] and HD [3] multicomponent granular gases. The major aim of this work is to unify those studies by expressing ξ_{ij}^{tr} and ξ_{ij}^{rot} in terms of the dimensionality d_t, after setting $d_\mathrm{r} = 2d_\mathrm{t} - 3$. The HS and HD expressions are recovered by particularizing to $d_\mathrm{t} = 3$ and $d_\mathrm{t} = 2$, respectively. Moreover, in the case of spinless particles with $d = d_\mathrm{t}$, known energy production rates $\xi_{ij}^{\mathrm{tr}} = \xi_{ij}$ of smooth d-dimensional spheres [1] are recovered.

Our results are applied to a comparative analysis of the homogeneous free cooling of HD and HS gases. As an illustration, Fig. 1 shows a density plot of the rotational/translational temperature ratio as a function of the coefficients of normal (α) and tangential (β) restitution. As can be observed, the disparity between both types of temperature is generally more pronounced in the case of disks than in the case of spheres. A similar behavior is exhibited by the rotational/translational nonequipartition in binary mixtures; however, the component/component degree of nonequipartition is stronger in HS gases than in HD gases.

A.M. is grateful to the *Ministerio de Educación, Cultura y Deporte* (Spain) for a *Beca-Colaboración* during the academic year 2017-2018. The research of A.S. has been supported by the *Ministerio de Economía y Competitividad* (Spain) through Grant No. FIS2016-76359-P and by *Junta de Extremadura* (Spain) through Grant No. GR18079, both partially financed by *Fondo Europeo de Desarrollo Regional* funds.

[1] F. Vega Reyes, V. Garzó, and A. Santos, Granular mixtures modeled as elastic hard spheres subject to a drag force, Phys. Rev. E **75**, 061306 (2007).

[2] A. Santos, G. M. Kremer, and V. Garzó, Energy production rates in fluid mixtures of inelastic rough hard spheres, Prog. Theor. Phys. Suppl. **184**, 31-48 (2010).

[3] A. Santos, Interplay between polydispersity, inelasticity, and roughness in the freely cooling regime of hard-disk granular gases, Phys. Rev. E **98**, 012904 (2018).

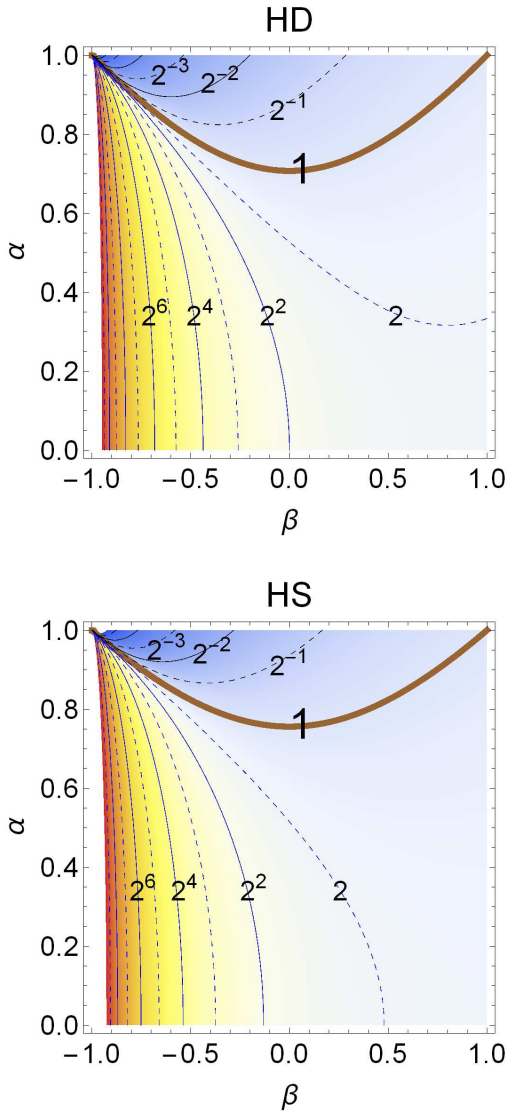

Fig. 1. Density plot of the rotational/translational temperature ratio for HD (top) and HS (bottom) granular gases. The contour lines correspond to the values 1 (thick solid lines), $(2^{-1}, 2^{-2}, \ldots)$, and $(2, 2^2, \ldots)$

Redes de contactos y propagación de esfuerzos en medios granulares

I. Echeverría-Huarte[1], P. M. Pasinetti[2], I. Zuriguel[1], R. C. Hidalgo[1] y D. Maza[1]
[1]Laboratorio de Medios Granulares, Universidad de Navarra, Navarra, España
[2]Dpto de Física, Universidad Nacional de San Luis, INFAP-CONICET, San Luis, Argentina

La propagación de esfuerzos en medios granulares estáticos es un problema complejo que involucra un gran número de grados de libertad. Uno de los ejemplos más evidentes para poner de manifiesto esta complejidad es la propagación de esfuerzos en pilas granulares. Aunque en principio podría asumirse un modelo de propagación difusivo de la carga entre granos, este comportamiento no es capaz de predecir la aparición de un *dip* o mínimo en la carga que soporta la región central de la pila [1]. Este comportamiento se ve magnificado cuando las partículas tiene formas alargadas aunque con curvaturas convexas suaves [2].

En nuestro laboratorio hemos estudiado este efecto considerando una geometría cúbica para las partículas. Esta forma implica añadir nuevos grados de libertad al problema debido a la tendencia de las caras planas de resultar alineadas, además de la dificultad intrínseca que implica la imposibilidad de definir claramente un contacto puntual entre caras planas.

Aunque mediante técnicas experimentales es posible detectar la alineación y posición de las partículas, la magnitud de las fuerzas con que interactúan entre si no es accesible experimentalmente. Así, para comprender qué ocurre con su propagación hasta desarrollar este *dip* en la base, hemos implementado una aproximación mixta, donde a partir de modelos construidos con dinámica de Montecarlo y resultados experimentales, comparamos las propiedades genéricas de ambas redes de contactos a partir de herramientas utilizadas en el análisis de redes complejas.

[1] A. P. F. Atman, P. Brunet, J. Geng, G. Reydellet, P. Claudin, R. P. Behringer, and E. Clément, Eur. Phys. J E **17**, 93 (2005).

[2] I. Zuriguel, T. Mullin, and J. M. Rotter, Phys. Rev. Lett **98**, 028001 (2007).

Engineering of frustration in colloidal artificial ice

Antonio Ortiz-Ambriz[1,3] and Pietro Tierno[1,2,3]
[1]Departament de Física de la Matèria Condensada, Universitat de Barcelona, Barcelona, Spain
[2]Institute of Complex Systems (UBICS), Universitat de Barcelona, Barcelona, Spain
[3]Institut de Nanociéncia i Nanotecnologia, Universitat de Barcelona, Barcelona, Spain

Frustration has become a ubiquitous explanation for long standing problems in soft matter systems, from glassy behaviors [1] to protein folding [2]. It is also present in solid state materials such as water ice [3] or rare earth magnets [4], and it is of technological importance for information storage in traditional magnetic recording devices.

We present an experimental realization of artificial colloidal ice; a mesoscopic system in which we can introduce frustration by design, and on which we can fully control initial conditions [5].

Our system has shown to be a platform to design devices for information storage and magnetronic logic devices, and we have observed both frozen defects such as domain walls and dynamic excitations, present as bound charged quasiparticles with a Coulombic interaction.

We also proved experimentally previous theoretical calculations [6] which predicted how the analogue between artificial spin ice and colloidal ice breaks when the lattice coordination is multiple. This shows how colloidal ice, as a special case of the more general particle ice, holds the promise to deliver rich phenomenology beyond simply replicating the existing plethora of observations in spin ice materials.

[1] C. P. Royall, A. Malins, A. J. Dunleavy, and R. Pinney, Strong geometric frustration in model glassformers, J. Non. Cryst. Solids **407**, 34-43 (2015).

[2] J. D. Bryngelson and P. G. Wolynes, Spin glasses and the statistical mechanics of protein folding, Proc. Natl. Acad. Sci. USA **84**, 7524-7528 (1987).

[3] L. Pauling, The structure and entropy of ice and of other crystals with some randomness of atomic arrangement, J. Am. Chem. Soc. **57**, 2680-2684 (1935).

[4] R. Siddharthan, B. S. Shastry, and A. P. Ramirez, Spin ordering and partial ordering in holmium titanate and related systems, Phys. Rev. B **63**, 184412 (2001).

[5] A. Ortiz-Ambriz and P. Tierno Engineering of frustration in colloidal artificial ices realized on microfeatured grooved lattices, Nat. Commun. **7**, 10575 (2016).

[6] C. Nisoli, Dumping topological charges on neighbors: Ice manifolds for colloids and vortices, New J. Phys. **16**, 113049 (2014).

Secondary control may prevent Braess' paradox in AC power grids

E. B. Tchawou Tchuisseu[1], Damià Gomila[1], Pere Colet[1], Dirk Witthaut[2], Marc Timme[3], and Benjamin Schäfer[3]
[1]Instituto de Física Interdisciplinar y Sistemas Complejos (IFISC), CSIC-UIB, 07122 Palma de Mallorca, Spain
[2]Institute for Theoretical Physics, University of Cologne, 50937 Köln, Germany
[3]Network Dynamics, Max Planck Institute for Dynamics and Self-Organization (MPIDS), 37077 Göttingen, Germany

For a stable operation in electric networks, supply and demand have to match at all times since the grid itself cannot store any energy. To guarantee this match, different mechanisms, like day-ahead and intra-day markets are used. For unexpected mismatches, e.g., random fluctuations [1, 2], disturbances or extreme weather, fast control mechanisms are required. The control in power system is thus realized on different time scales to cope with short-term fluctuations and long-term power imbalance alike. Assuming a sudden shortage of energy or any failure in the system, the first second of the disturbance is mainly uncontrolled, i.e., energy is drawn from the spinning reserve of the generators. Within the next seconds, the primary control sets in to stabilize the frequency and prevents a large drop. To restore the frequency back to its nominal value of 50 Hz or 60 Hz, secondary control is necessary [1].

Due to the continuous increase in demand and the high penetration of renewable energy sources, the future grid topology and control mechanisms have to adapt to cope with this increase and with spatially distributed and fluctuating renewable generation. Grid adaptation includes additional transmission lines and increasing capacity of existing lines. Contrary to expectations, not all added lines are beneficial to the stability of a grid. Indeed, adding some lines may cause the grid to lose its operating state via Braess' paradox [3] (Fig. 1).

Many studies investigate the effect of the fast primary control on frequency quality and power grid stability. However, secondary control is rarely considered. In this work, we propose a simple implementation of secondary control and demonstrate its effectiveness in stabilizing the power grid.

We model each node by the well-known *swing equation* including primary and secondary control [1]. In the limit of instananeous response of the primary control the dynamics of a node can be written as

$$\dot{\theta}_i = \omega_i, \tag{1a}$$

$$\dot{\omega}_i = -\alpha_i\omega_i - \gamma_i\theta_i + P_i - \sum_{j=1}^{n} K_{ij}\sin(\theta_i - \theta_j), \tag{1b}$$

where θ_i and ω_i represent the voltage phase angle and the angular velocity deviation, respectively, α_i is the damping constant, γ_i is the gain of the secondary control, P_i is the effective power fed into the grid or consumed at node i, and K_{ij} determines the capacity of the line (i, j).

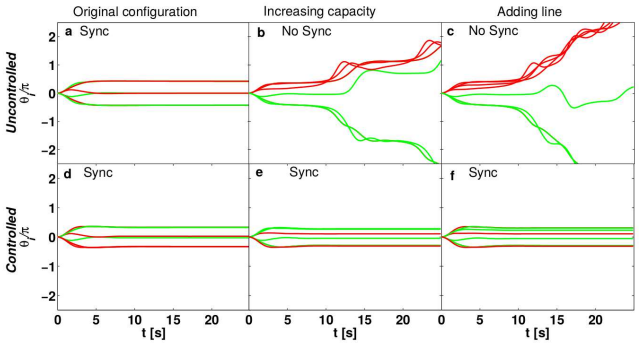

Fig. 1. Secondary control stabilizes a network. Braess' paradox in power grids observed when increasing the capacity of a line or adding an additional line in [3] is prevented.

We find that including secondary control in all nodes prevents Braess paradox in that, increasing the capacity of a line or including a new one carries always a positive effect on the stability of the network. However we have also found that when control is avalable to generator nodes only, as it is typically the case in present power grid configurations, the stability depends strongly on which line capacity is increased, indicating a non trivial interaction between control and topology.

[1] E. B. Tchawou Tchuisseu, D. Brunner, D. Gomila, and P. Colet, Effects of dynamic-demand-control appliances on the power grid frequency, Phys. Rev. E **96**, 022302 (2017).

[2] B. Schäfer, C. Beck, K. Aihara, D. Witthaut, and M. Timme, Non-Gaussian power grid frequency fluctuations characterized by Lévy-stable laws and superstatistics, Nat. Energy **3**, 119 (2018).

[3] D. Witthaut and M. Timme, Braess's paradox in oscillator networks, desynchronization and Power Outage, New J. Phys. **14**, 083036 (2012).

Mechanics of cell constriction during division

Elena Beltrán-Heredia[1,2], Víctor G. Almendro-Vedia[2], Francisco Monroy[2,3], and Francisco J. Cao[1,4]
[1]Departamento de Estructura de la Materia, Física Térmica y Electrónica, Universidad Complutense de Madrid, pl. Ciencias 1, 28040 Madrid, Spain
[2]Departamento de Química Física, Universidad Complutense de Madrid, av. Complutense s/n, 28040 Madrid, Spain
[3]Unit of Translational Biophysics, Instituto de Investigación Sanitaria Hospital Doce de Octubre (imas12), av. Córdoba s/n, 28041 Madrid, Spain
[4]Instituto Madrileño de Estudios Avanzados en Nanociencia (IMDEA Nanociencia), c. Faraday 9, 28049 Madrid, Spain

The cell division cycle is a central process in biology, the essential mechanism whereby cells grow and duplicate. A decisive step of cell division is the symmetric constriction necessary to cleave the mother cell into two identical daughter cells (see Fig. 1). Independently of the details of the constriction engine, the membrane component responds against deformation by minimizing the elastic energy at every constriction state following a pathway still unknown.

In this work, we address a theoretical study of the mechanics of membrane constriction in a simplified model that describes the cell as a homogeneous membrane vesicle in which a given constriction force is applied to create a circumferential furrow positioned at the cell equator.

The shape of the cell is determined by the minimum of its total energy $E_T = E_b + W$, which is leaded by the bending energy of the membrane E_b, and subjected to the geometric constraints of area A and volume V that require a work $W = \Sigma A + \Delta p V$, where Σ is the membrane tension and Δp is the pressure difference between the outer medium and the cell interior ($\Delta p = p_{out} - p_{in}$). The bending energy of the shell is given in terms of its mean curvature H by the Helfrich form

$$E_b = \frac{\kappa}{2}\int (2H - C_0)^2 \mathrm{d}A, \qquad (1)$$

where κ is the bending rigidity of the membrane and C_0 is the spontaneous curvature that represents the tendency of the membrane to bend in the equilibrium state, usually due to the compositional asymmetry between the inner and the outer sides.

By minimizing the total energy along the constriction pathway, we derive analytical approximate formulas for the main properties of the constricted vesicle (or simplified cell). These results are compared with the exact solution obtained from numerical computations, getting a good agreement for all the computed quantities (energy, area, volume, and forces). The initial cell shape (before constriction) is shown to be determined through the quantity [1]

$$\Lambda = (1 - C_0 R_m)^2 + 2\Sigma R_m^2/\kappa + \Delta p R_m^3/\kappa, \qquad (2)$$

where R_m is the polar radius of the spheroid. $\Lambda = 1$ stands for the sphere, while $0 < \Lambda < 1$ gives prolate (rod-like) and $\Lambda > 1$ oblate (disk-like) spheroids; for $\Lambda < 0$ constriction is not possible (see Fig. 2).

The more favorable conditions for division are determined, obtaining that smaller constriction forces are required for low or negative membrane tension and hypotonic media. Our results evidence that stable symmetric constriction requires positive effective spontaneous curvature, while spontaneous constriction requires a spontaneous curvature higher than the characteristic inverse cell size. We also show that the stability and spontaneity of symmetric constriction increases as constriction progresses.

This work contributes to a better quantitative understanding of the mechanical pathway of cellular division and can serve to get insight on other biological processes involving membrane bending, such as exocytosis and endocytosis. In the emergent area of artificial life our predictions could also assist the design of artificial divisomes in self-actuated microsystems. The method is sufficient general and powerful to accommodate easily further complexities present that participate actively to drive cytokinesis in real cells.

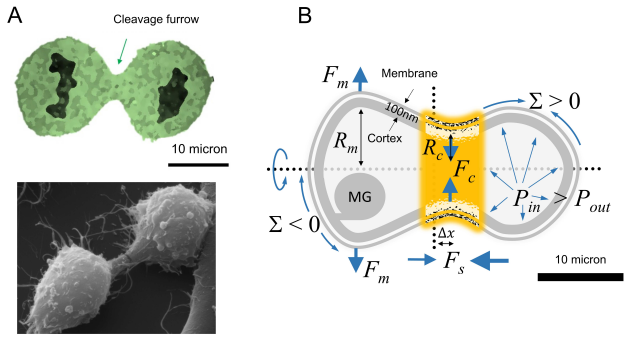

Fig. 1. (a) Real cells undergoing constriction. Upper panel: Formation of the cleavage furrow (from A. Siegel and H. C. Smith, SUNY at Buffalo). Lower panel: Scanning electron micrograph during final stage of constriction (from A. Wilde University of Toronto). (b) Our minimal model cell and its characteristic parameters.

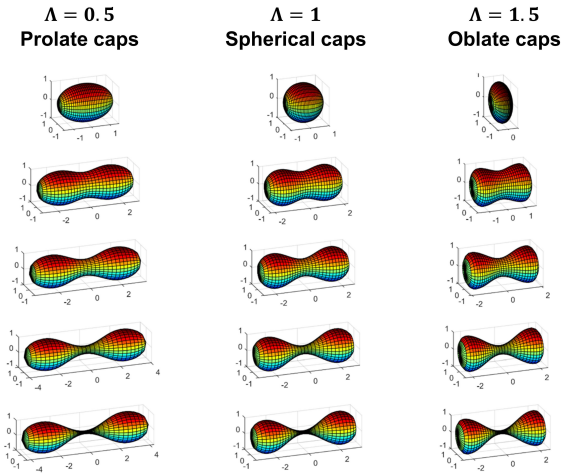

Fig. 2. Minimum energy shapes during division.

[1] E. Beltrán-Heredia, V. G. Almendro-Vedia F. Monroy, and F. J. Cao, Modeling the mechanics of cell division: Influence of spontaneous membrane curvature, surface tension, and osmotic pressure, Front. Physiol. **8**, 312 (2017).

[2] E. Beltrán-Heredia, F. Monroy, and F. J. Cao, Mechanical conditions for stable symmetric cell constriction, (submitted for publication).

Development of a 3D computational model of centripetal calcium wave propagation in atrial cells

Miquel Marchena[1], Enric Alvarez-Lacalle[1], Yohannes Shiferaw[2], and Blas Echebarria[1]
[1]Departament de Física, Universitat Politècnica de Catalunya, 08028 Barcelona, Spain
[2]Department of Physics, California State University, Northridge, CA, USA

Calcium is an important cell messenger, that mediates in many physiological processes. Ca^{2+} takes part, for instance, in oocyte activation at fertilization, axonal growth, gene expression, or excitation-contraction coupling in myocytes, where an increase in the concentration of intracellular calcium initiates the contraction of the cell. Any dysfunction in the handling of Ca^{2+} can thus lead to serious pathologies.

Inside cardiac cells, most intracellular Ca^{2+} is stored in a complex structure called sarcoplasmic reticulum (SR). Ca^{2+} is released from this internal network via the Ryanodine Receptors (RyR, red and black dots in Fig. 1) when a threshold calcium concentration in the cytoplasm is achieved. This happens due to a small influx of calcium through the L-type calcium channels (LCC, blue dots in Fig. 1) during the cardiac action potential. RyRs open and close collectively in clusters forming functional units known as Calcium Release Units (CaRU), which are often confronted to a cluster of LCCs. In each CaRU the number of RyR and LCC is small (of the order of 10-100 of the former and 5-10 of the latter), thus, its dynamics is intrinsically stochastic. CaRUs are distributed inside the cell, resulting in random and discrete Ca^{2+} release events, known as Ca^{2+} sparks. The (seemingly deterministic) global calcium signal appears from the coordination of several tens of thousands of these CaRUs.

Even though the same mechanism triggers the transient elevation of Ca^{2+} in both ventricular and atrial myocytes, there are substantial differences in the intracellular structures. In ventricular cells, the CaRUs arrange along invaginations of the cell membrane, called transversal tubules (t-tubules), that define regions known as z-planes. These regions are repeated every $\sim 1.5\mu$m along the longitudinal direction. The absence of t-tubules in the z-planes of atrial myocytes produces inhomogeneous spatio-temporal calcium patterns when the calcium release occurs. In particular, the excitation starts at the cell membrane and then propagates to the interior. This is a key difference between atrial and ventricular cells. In the latter, the opening of LCC channels along the t-tubules synchronizes the release of calcium from the SR. In the former, synchronization is due to this inward wave.

We have developed a 3D computational model to study inward wave propagation in atrial cells. RyR distribution is shown in Fig. 1 where we have adapted the method in [1] to develop a 3D algorithm to create a CaRU structure. This algorithm performs Monte-Carlo simulations of stochastic self-assembly of RyR clusters using a simple growth model with three probabilities. In particular, our study is focused on the gap between external (cell membrane) and internal spaces. Because of this cleft, in normal conditions, the internal RyRs remain closed during the excitation-contraction (EC) coupling and calcium is only released on the periphery (Fig. 2).

However, during atrial fibrillation (AF) the cell structure

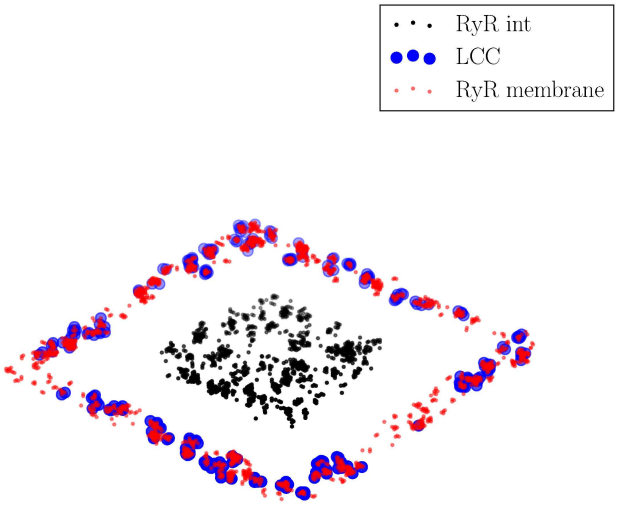

Fig. 1. Spatial distribution of RyRs and LCCs within a z-plane.

Fig. 2. 3D calcium profiles at different times. With this model, we can study calcium firing and diffusion within a z-plane.

changes and this gap could eventually be reduced. With our model, we aim to understand the effects of gap reduction on the centripetal wave propagation. Besides, because of the submicron spatial discretization, the model is well suited to study the effects of changes in the microstructure (position of the RyR clusters, inhomogeneities, etc). Both situations, gap reduction [2] and changes in CaRU distribution [3] promote the internal excitation leading to complex spatio-temporal patterns of intracellular Ca^{2+} signal propagation. With this in mind, our simulations illustrate that subtle changes in cell structure may have non-intuitive effects on Ca^{2+} signal initiation.

[1] D. Baddeley, I. D. Jayasinghe, L. Lam, S. Rossberger, M. B. Cannell, and C. Soeller, Proc. Natl. Acad. Sci. USA **106**, 22275-22280 (2009).

[2] R. Thul, K. Rietdorf, M. D. Bootman, and S. Coombes, Biochim. Biophys. Acta-Mol. Cell Res. **1853**, 2131-2143 (2015).

[3] N. Macquaide, Cardiovasc. Res. **108**, 387-398 (2015).

Linear shear rheology of aging beta-casein films adsorbing at the air/water interface

F. Martinez-Pedrero[1], J. Tajuelo[2], P. Sanchez-Puga[2], F. Ortega[1], M. A. Rubio[2], and R. G. Rubio[1]
[1]Departamento de Química-Física I, Universidad Complutense de Madrid, av. Complutense s/n, 28040 Madrid, Spain
[2]Departamento de Física Fundamental, Universidad Nacional de Educación a Distancia (UNED), 28040 Madrid, Spain

In this work, the viscoelasticity of fragile beta-casein films has been followed using different macro- and microrheological techniques. The modulus of the complex surface viscosity varies with time, allowing for the monitoring of the protein adsorption and annealing. Beta-casein adsorption creates a soft glassy gel at the interface that experiences an aging process.

Macrorheological experiments with multiple probe sizes in addition to microrheological experiments demonstrated the consistency of the surface rheological properties over a broad range of viscosities. Surface pressure measurements were performed to complement the characterization of the processes [1, 2].

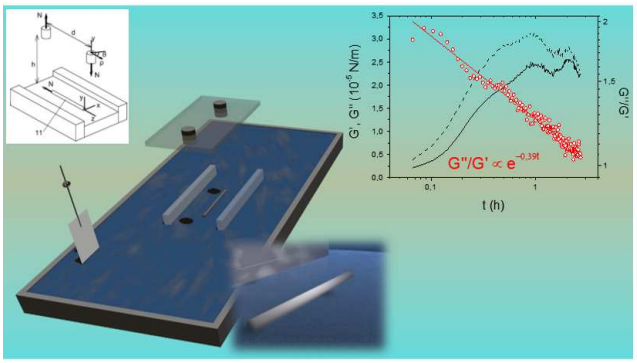

Fig. 1. We have characterized the adsorption of beta-casein by monitoring the change of the dynamic moduli G' and G'', by means of active measurements, in which the forced translational motion of a magnetic microwire at the interface is employed to infer layer rheology

.

[1] F. Martinez-Pedrero, J. Tajuelo, P. Sanchez-Puga, F. Ortega, M. A. Rubio, and R. G. Rubio, Linear shear rheology of aging casein films adsorbing at the air/water interface, J. Colloid Interface Sci. **511**, 12-20 (2018).

[2] J. Tajuelo, J. M. Pastor, and M. A. Rubio, A magnetic rod interfacial shear rheometer driven by a mobile magnetic trap, J. Rheol. **60**, 1095-1113 (2016).

Diffusion-limited coalescence and annihilation on a one-dimensional expanding medium

F. Le Vot[1], C. Escudero[2,3], E. Abad[4], and S. B. Yuste[1]
[1]Departamento de Física, Facultad de Ciencias, Universidad de Extremadura, E-06071 Badajoz, Spain
[2]Departamento de Matemáticas, Universidad Autónoma de Madrid, E-28049 Madrid, Spain
[3]Instituto de Ciencias Matemáticas, CSIC, E-28049 Madrid, Spain
[4]Departamento de Física Aplicada, Centro Universitario de Mérida, Universidad de Extremadura, E-06800 Mérida (Spain)

We consider diffusion-controlled reactions (reactions in which the typical reaction time is short in comparison to the typical time spent by a pair particles before reacting) which take place on a one-dimensional expanding medium. In particular, we consider the irreversible single-species coalescence reaction $A + A \to A$, and the irreversible single-species annihilation reaction $A + A \to \emptyset$.

These reactions have been extensively studied in static media. It is well known that a simple mean-field approach does not work when the mixing of the reactants is impaired by, e.g., the low dimensionality of the medium. A method that is able to cope with this scenario for a one-dimensional medium is the Interparticle Distribution Function (IPDF) method [1]. Here we generalize this method to the case of uniformly expanding media. We discover that the mixing of diffusing particles and the corresponding reaction kinetics are, in some cases, largely modified by the expansion of the medium.

The mathematical complexities induced by the expansion can be reduced to a large extent if one works with comoving coordinates. Let $x = y(0)$ be the coordinate of a fixed point at the initial time $t = 0$. Due to the expansion, this fixed point changes its position, $y(t)$ being its coordinate at time t. If the expansion of the medium is uniform $y(t)$ and x are related by $y(t) = a(t)x$, where $a(t)$ is the scale factor and $a(0) = 1$. The quantity $x = y/a(t)$ is the comoving coordinate associated with the position y at time t.

The interparticle probability density function $p(x,t)$ is defined as the density of probability of finding a gap of size x (in comoving coordinates) between two neighboring particles. Let us define the auxiliary function $q(x,t) = p(x,t)/c(t)$, where $c(t)$ is the number density of particles in comoving space, and let us define the Brownian conformal time $\tau(t)$ as

$$\tau(t) = \int_0^t \frac{ds}{a^2(s)}. \tag{1}$$

It is possible to prove [2] that the auxiliary function $q(x,t)$ satisfies a standard diffusion equation

$$\frac{\partial q}{\partial \tau} = 2D\frac{\partial^2 q}{\partial x^2}, \tag{2}$$

where D is the diffusion constant of the reacting particles. This is a key result because from $q(x,t)$ we can find the survival probability $S(t)$ of a particle, the structure of the system (arrangement of particles), etc. In particular,

$$c(t) = c(0)S(t) = \int_0^\infty q(x,t)dx. \tag{3}$$

In some cases we can get exact solutions from these expressions. For example, for a completely random initial distribution of particles (Poisson distribution) one obtains

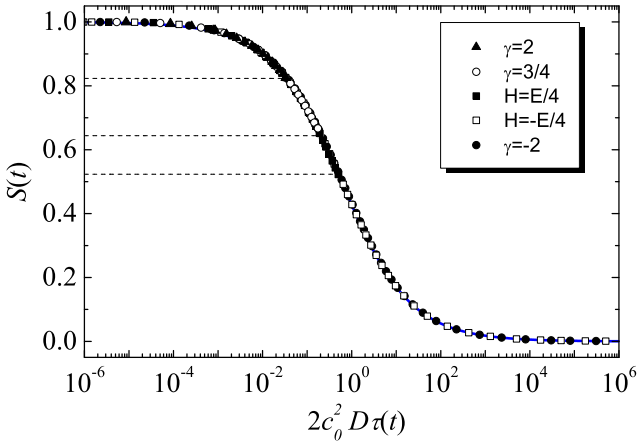

Fig. 1. Survival probability $S(t)$ *vs.* $z^2 = 2c_0^2 D\tau(t)$ for coalescence. The symbols correspond to simulation results for power-law expansions with $t_0 = 1000$ and $\gamma = 2, 3/4, -2$, and exponential expansions with $H = 10^{-4}$ and $H = -10^{-4}$. Dashed lines correspond to the limiting value S_∞ of the survival probability for $\gamma = 2$ ($S_\infty \approx 0.823$), $\gamma = 3/4$ ($S_\infty \approx 0.644$), and $H = 10^{-4}$ ($S_\infty \approx 0.523$). The solid line is the exact solution in Eq. (4).

$$S(t) = e^{z^2}\mathrm{erfc}(z), \tag{4}$$

with $z = c_0\sqrt{2D\tau(t)}$ for coalescence reactions and $z = 2c_0\sqrt{2D\tau(t)}$ for annihilation reactions. In Fig. 1 we compare, for coalescence reactions, $S(t)$ obtained by means of Eq. (4) with simulation results. The agreement is excellent. It is clear that the behaviour of $S(t)$ depends on $\tau(t)$, or equivalently, on the expansion scale factor $a(t)$. It turns out that $\tau(t \to \infty) = \tau_\infty < \infty$ for some (fast) expansions, e.g., a power-law expansion $a(t) = (1 + t/t_0)^\gamma$ with $\gamma > 1/2$ or an exponential expansion $a(t) = \exp(Ht)$ with $H > 0$. In these cases the survival probability of the reacting particles tends to a finite value at long times, $S(t \to \infty) = S_\infty > 0$, in other words, the expansion is so fast that the reactions stop prematurely and the spatial distribution of particles freezes before reaching the fully self-ordered state. This behavior is similar to the freeze-out behaviour displayed by the early universe in the context of cosmology.

[1] D. ben-Avraham and S. Havlin, *Diffusion and Reactions in Fractals and Disordered Systems* (Cambridge University Press, Cambridge, 2005).

[2] F. Le Vot, C. Escudero, E. Abad, and S. B. Yuste, Encounter-controlled coalescence and annihilation on a one-dimensional growing domain, arXiv:1804.03213.

A non-linear model to explain how plants integrate light and temperature to decide how much to grow

Pablo Catalán[1,2], Cristina Nieto[3], Salomé Prat[3], and Saúl Ares[1,2]
[1]Grupo Interdisciplinar de Sistemas Complejos (GISC), Madrid, Spain
[2]Dept. de Matemáticas, Universidad Carlos III de Madrid, Leganés, Madrid, Spain
[3] Centro Nacional de Biotecnología, CSIC, Madrid, Spain

Plants need to assess the environmental cues to decide how much to grow after germination. Buried in the ground, the plant's hypocotyl (its young stem) must grow until it reaches the surface. Once this happens, the hypocotyl stops growing and the plant develops leaves to absorb sunlight. Many signals and mechanisms take part in this process. It is of particular interest to understand how the plants integrates light and temperature signals in this decision-making process.

Recent work with *Arabidopsis thaliana* plants [1] shows that the protein phytochrome B (PHYB) integrates temperature and light signals, and therefore PHYB has been proposed as the main regulator of hypocotyl growth after germination.

Based on new experimental data growing *Arabidopsis* plants under different light and temperature conditions, we propose a non-linear, mechanistic model of hypocotyl growth which includes the effect of proteins early-flowering 3 (ELF3) and constitutively photomorphogenic 1 (COP1) as well as that of PHYB. ELF3 is a transcriptional regulator that is related to *Arabidopsis*'s circadian clock, while COP1 marks other proteins for degradation. Our simulations agree very well with the data (Fig. 1).

Our model suggests that COP1 plays a much more relevant role than that of PHYB in integrating both temperature and light signals for hypocotyl growth in *Arabidopsis* after germination.

[1] J.-H. Jung, M. Domijan, C. Klose, S. Biswas, D. Ezer, M. Gao, A. K. Khattak, M. S. Box, V. Charoensawan, S. Cortijo, M. Kumar, A. Grant, J. C. W. Locke, E. Schäfer, K. E. Jaeger, and P. A. Wigge, Phytochromes function as thermosensors in Arabidopsis, Science **354**, 886-889 (2016).

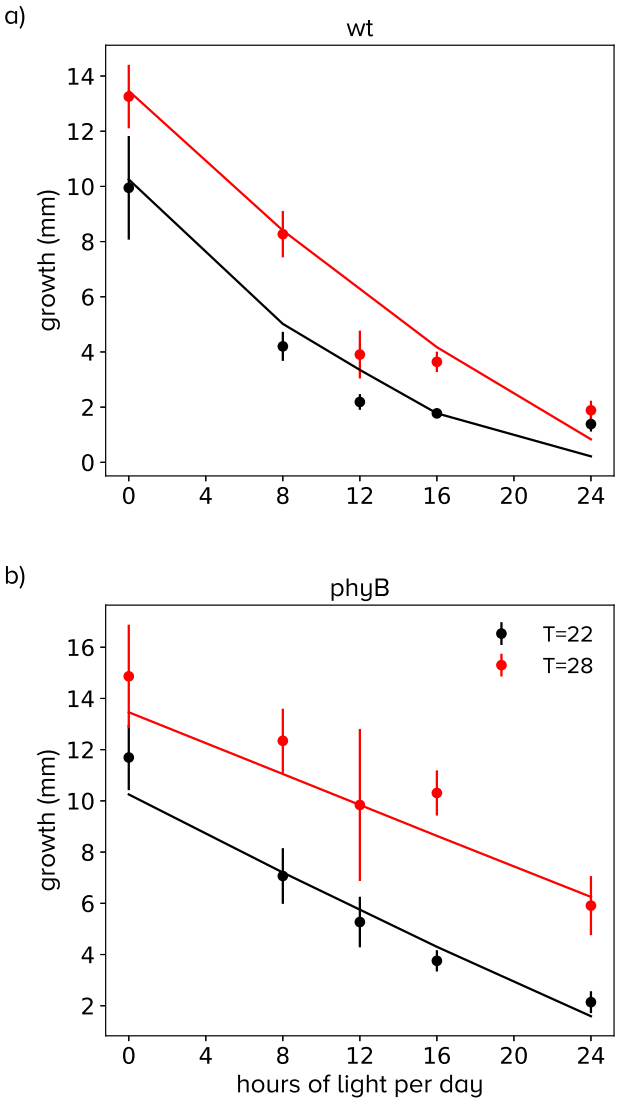

Fig. 1. Hypocotyl growth after 5 days. Plants were grown with red light for 5 days (120 horus), under two temperatures (22°C, black, and 28°C, red) and five daylength conditions (0, 8, 12, 16 and 24 hours of light per 24 hours of experiment). Points show average size of the plant (bars represent one standard deviation), while lines are the prediction of our dynamical model, for the wild type (a) and a mutant that lacks the protein PHYB (b).

Simulación numérica de materia granular descargada a velocidad constante en tubos verticales

Dariel Hernández-Delfin, Iker Zuriguel y Raúl Cruz Hidalgo
Dpto. de Física y Matemática Aplicada, Facultad de Ciencias, Universidad de Navarra, 31080 Pamplona, Spain

El flujo de medios granulares impulsado por la aceleración gravitacional en el interior de tubos verticales es ampliamente usado en la industria (ej: transportes entre contenedores, minas con esquema de echadero y reactores de lecho fluidizado circulante). Se conoce que si las dimensiones radiales de los tubos son solo unas pocas veces más grandes que las dimensiones de las partículas, es probable la aparición de arcos de fuerzas, capaces de detener el flujo [1].

En estos sistemas es bien conocido que los tiempos de avalancha, los cuales son definidos como el intervalo en el que se mantiene el flujo sin la aparición de un atasco, siguen una distribución exponencial. Este tipo de distribución implica que la probabilidad de que ocurra un atasco es constante en el tiempo.

Recientemente se han ejecutado experimentos que involucran esferas monodispersas impulsadas por la aceleración gravitacional dentro de tubos, controlando el flujo mediante una cinta que extrae las esferas desde la parte inferior [2]. Así, se ha comprobado experimentalmente que existen relaciones de aspecto $\phi = D/d$ (siendo D y d los diámetros de los tubos y las partículas respectivamente) para las cuales la probabilidad de aparición de atascos es notablemente mayor.

Estos experimentos tienen limitaciones como no poder implementar determinados valores de ϕ o la imposibilidad de acceder a la micromecánica del sistema, sin la cual llegar a un entendimeinto de la fenomelogía existente se hace muy complicado. Es por esto que los esfuerzos de esta contribución están orientados en desarrollar simulaciones numéricas, con el objetivo de acceder a estos parámetros no accecibles experimentalmente y así esclarecer los aspectos que marcan la ocurrencia de atascos o no para determinados valores de ϕ.

Las simulaciones numéricas han sido desarrolladas utilizando el código para partículas discretas MercuryDPM [3, 4]. El modelo lineal viscoelástico fue escogido tanto para las interacciones entre las propias partículas como para las partículas con las paredes del tubo.

Los resultados preliminares muestran la existencia de dos regiones en el dominio de relaciones de aspecto ϕ, donde es muy probable que ocurran atascos, lo cual concuerda con los resultados experimentales. Además, podemos anticipar que son regiones donde existe un mayor número de contactos por celda elemental para y donde se da el máximo valor de compactación [5]. En nuestra presentación se darán más detalles acerca de la micromecánica que distingue entre los regímenes donde aparecen atascos y los que hay un flujo ininterrumpido.

[1] A. Janda, I. Zuriguel, A. Garcimartín, and D. Maza, Clogging of granular materials in narrow vertical pipes discharged at constant velocity, Granul. Matter **17**, 545-551 (2015).

[2] D. López-Rodríguez, I. Zuriguel, and D. Maza, Clogging of granular material in vertical pipes discharged at constant velocity, EPJ Web Conf. **140**, 03033 (2017).

[3] A. R. Thornton, T. Weinhart, S. Luding, and O. Bokhove, Modeling of particle size segregation: Calibration using the discrete particle method, Int. J. Mod. Phys. C **23**, 1240014 (2012).

[4] T. Weinhart, A. R. Thornton, S. Luding, and O. Bokhove, From discrete particles to continuum fields near a boundary, Granul. Matter **14**, 289-294 (2012).

[5] A. Mughal, H. K. Chan, D. Weaire, and S. Hutzler, Dense packings of spheres in cylinders: Simulations, Phys. Rev. E **85**, 051305 (2012).

Granular convection of horizontally shaked granular layers: Simulation

D. Hernández-Delfin[1], D. Maza[1], K. Asencio[1], R. C. Hidalgo[1], and A. Batista-Leyva[2]
[1]Departamento de Física y Matemática Aplicada, Facultad de Ciencias, Universidad de Navarra, Spain
[2]Instituto Superior de Tecnologías y Ciencias Aplicadas, Universidad de la Habana, Cuba

Granular convection is a controversial topic due to the variety of mechanisms proposed to justify the experimental observations. To bring some light to this problem, we study a setup which shakes a single layer of spherical beads horizontally. We found that global collective movements can be induced if break the symmetry of the applied excitation signal. Nevertheless, advective transport can also be observed even if symmetric perturbations are used. Although the origin of both dynamics seems to be the same, the role of the boundary condition effects and the external forcing can be isolated.

When a sinusoidal signal is applied, four rolls can be distinguished. In order to understand the role of the lateral walls on the resulting patterns, we simulate the experimental conditions but tunning the friction coefficient of the lateral wall.

The present contribution is devoted to a numerical study of the effects of the friction and the asymmetry of the input signal on the resulting dynamic of a spheric particles monolayer in a cylindrical oscillating base. The asymmetrical input signals are piecewise functions with a period T, which are composed of two sinusoidal functions with different periods T_1 and T_2. We carry out numerical simulations using the discrete particle modeling code MercuryDPM [1, 2].

We have found that global collective movements can be observed in a horizontally shaken granular monolayer. When a non-symmetric signal is applied, the symmetry breaking induces a momentum gradient along the excitation direction that produces the displacement of the particles from the less energetic (less dense) zone to the densest (more dissipative) region. This observation is opposed to the mechanism of the natural convection where most energized areas are advected to the *cold* zones. To understand the origin of the observed collective motions, the wall friction must be discussed, as we show simulating a comparable situation but considering frictionless lateral wall.

[1] A. R. Thornton, T. Weinhart, S. Luding, and O. Bokhove, Modeling of particle size segregation: Calibration using the discrete particle method, Int. J. Mod. Phys. C **23**, 1240014 (2012).

[2] T. Weinhart, A. R. Thornton, S. Luding, and O. Bokhove, From discrete particles to continuum fields near a boundary, Granul. Matter **14**, 289-294 (2012).

The NeufDix experiment in the International Space Station: Giant Fluctuations in microgravity

J. M. Ortiz de Zárate[1,†], P. Baaske[2], H. Bataller[3], M. Braibanti[4], M. Carpineti[5], R. Cerbino[6], F. Croccolo[3,7], A. Donev[8], L. García Fernández[3], W. Köhler[9], A. Vailati[5], and Shenghua Xu[10]

[1]Facultad de Física, Universidad Complutense, Madrid, Spain
[2]Nanotemper Technologies GmbH, Munich, Germany
[3]Lab. des Fluides Complexes et leurs Réservoirs - IPRA, UMR5150, CNRS/TOTAL/UNIV PAU & PAYS ADOUR, Anglet, France
[4]ESA-Estec, Noordwijk, The Netherlands
[5]Dip. di Fisica, Università degli Studi di Milano, Milano, Italy
[6]Dip. Biotecnologie Mediche e Medicina Traslazionale, Università degli Studi di Milano, Segrate, Italy
[7]Centre Nationale d'Etudes Spatiales, Paris, France
[8]Courant Institute of Mathematical Sciences, New York University, USA
[9]Physikalisches Institut, Universität Bayreuth, Bayreuth, Germany
[10]Key Laboratory of Microgravity, Institute of Mechanics, Chinese Academy of Sciences, Beijing, China

Mass and thermal diffusion processes in a liquid mixture are accompanied by non-equilibrium fluctuations. The amplitude of these fluctuations at small wave vectors is orders of magnitude larger than that of the equilibrium ones [1, 2]. On Earth gravity quenches non equilibrium fluctuations of long wavelength [3, 4], while in microgravity conditions they are fully developed and span all the available length scales up to the macroscopic size of the system [5, 6]. Available theoretical models, based on linearized fluctuating hydrodynamics, provide an accurate description of the static and dynamic properties of these giant fluctuations under ideal conditions such as small gradients and stationary states [1].

The aim of the Giant Fluctuations space project is to investigate Non-EqUilibrium Fluctuations during DIffusion in In compleX liquids (NEUF-DIX), under conditions that cannot be tackled easily by theoretical models, such as transient diffusion, concentrated samples and large gradients [7]. The focus of the project is on the investigation of the non-equilibrium fluctuations in complex liquids, because of the rich phenomenology that can be attained by tuning the interactions in such systems. Since gravity quenches long-wavelength non-equilibrium fluctuations, in order to fully exploit the scale-free behavior of the fluctuations we envision performing experiments under microgravity conditions. The project has received initial approval by the European Space Agency (ESA) and has already entered its A/B engineering development phase, with the ultimate goal of being flown on-board the International Space Station not earlier than 2020.

The proposed experiment concept considers a fluid cell containing various samples, which are diagnosed by the optical tool "Shadowgraphy", while a temperature gradient is applied onto the fluid cell in the direction of the optical beam. The particular scientific objectives of the project are related to several challenging problems that emerged during the last years, such as:

1. understanding the non-equilibrium fluctuations in a complex ternary mixture including a polymer [8],
2. understanding the non-equilibrium fluctuations in a complex ternary mixture including a polymer close to a glass transition [9, 10],
3. checking the theoretical predictions of Casimir-like forces induced by non-equilibrium fluctuations [11, 12],
4. the investigation of the onset of fluctuations during transient diffusion [13],
5. understanding the non-equilibrium fluctuations in concentrated colloidal suspensions [14], a problem also related with the detection of Casimir forces,
6. understanding the effect of non-equilibrium fluctuations on antibodies.

We envision to parallel these experiments with state of the art multiscale simulations [15, 16], as well as to fully develop the theory required for the understanding of the experimental results.

UCM team gratefully acknowledges funding from *Agencia Estatal de Investigación* under grant No. ESP2017-83544-C3-2-P.

† Corresponding author e-mail: jmortizz@ucm.es

[1] J. M. Ortiz de Zárate and J. V. Sengers, *Hydrodynamic Fluctuations in Fluids and Fluid Mixtures* (Elsevier, Amsterdam 2006).

[2] F. Croccolo, J. M. Ortiz de Zárate, and J. V. Sengers, Eur. Phys. J. E **39**, 125 (2016).

[3] A. Vailati and M. Giglio, Nature **390**, 262 (1997).

[4] F. Croccolo *et al.*, Ann. NY Acad.Sci. **1077**, 365 (2006).

[5] A. Vailati *et al.*, Nat. Commun. **2**, 290 (2011).

[6] F. Croccolo *et al.*, Microgravity Sci. Technol. **28**, 467 (2016).

[7] P. Baaske, H. Bataller, M. Braibanti, M. Carpineti, R. Cerbino, F. Croccolo, A. Donev, W. Köhler, J. M. Ortiz de Zárate, and A. Vailati, Eur. Phys. J. E **39**, 119 (2016).

[8] H. Bataller *et al.*, Eur. Phys. J. E **40**, 35 (2017).

[9] J. Rauch, W. Köhler, Phys. Rev. Lett. **88**, 185901 (2002).

[10] J. Rauch, W. Köhler, J Chem. Phys. **119**, 11977 (2003).

[11] T. R. Kirkpatrick, J. M. Ortiz de Zárate, and J. V. Sengers, Phys. Rev. Lett. **110**, 235902 (2013).

[12] T. R. Kirkpatrick, J. M. Ortiz de Zárate, and J. V. Sengers, Phys. Rev. Lett, **115**, 035901 (2015).

[13] R. Cerbino, Y. Sun, A. Donev, and A. Vailati, Sci. Rep. **5**, 14486 (2015).

[14] F. Giavazzi *et al.*, Eur. Phys. J. E **39**, 103 (2016).

[15] A. Donev and E. Vanden-Eijnden, J. Chem. Phys. **140**, 234115 (2014).

[16] A. Donev *et al.*, Phys. Fluids **27**, 037103 (2015).

Aggregation of discoidal particles due to depletion interaction

C. Calero[1,2] and I. Pagonabarraga[1,3,4]
[1]Departament de Física de la Matèria Condensada, Universitat de Barcelona, 08028 Barcelona, Spain
[2]Institut de Nanociència i Nanotecnologia, Universitat de Barcelona, Barcelona, Spain
[3]Universitat de Barcelona Institute of Complex Systems (UBICS), Universitat de Barcelona, Barcelona, Spain
[4]CECAM, École Polytechnique Fédérale de Lausanne, Batochime, av. Forel 2, 1015 Lausanne, Switzerland

Depletion forces are effective interactions of entropic origin ubiquitous in a large variety of colloidal systems. They arise when big colloidal particles are immersed in a solution of smaller non-adsorbing particles or polymers. To maximize the volume available to the smaller solutes and thus increase the entropy of the system, the aggregation of the larger colloids is favored, generating an effective interaction between them [1, 2].

Depletion interactions are of special relevance in biological systems, where the medium is often crowded with different types of polymers. A case where this interaction might play a crutial role is in the formation of aggregates in blood. Indeed, it has been long known that erythrocytes, with discoidal geometry, aggregate into columnar structures called rouleaux when blood is at rest. The driving force of such aggregation process is still controversial, being the depletion interaction generated by the presence of large concentrations of proteins in blood plasma a possible important effect [3].

In this contribution I propose a simple model to understand the equilibrium aggregation properties of a solution of disc-shaped colloids due to the depletion interaction. Built upon simple arguments borrowed from the theory of self-assembly of micelles, the model is analytically solvable, providing simple expressions to predict the equilibrium distribution of aggregates in terms of the relevant parameters of the problem (concentrations of discs and polymers, size of the discs and length of polymers). To validate the model, I also report the results of molecular dynamics simulations of a system of discs and polymers in contact with a thermal bath interacting solely via steric repulsive interactions; the agreement between both approaches, with no fitting parameters, is excellent (see Fig. 1). Corrections to the model and possible consequences in the formation of aggregates of red blood cells will be discussed.

[1] S. Asakura and F. Oosawa, On interaction between two bodies immersed in a solution of macromolecules, J. Chem. Phys. **22**, 1255 (1954).

[2] B. Götzelmann, R. Evans, and S. Dietrich, Depletion forces in fluids, Phys. Rev. E **57**, 6785 (1998).

[3] O. Baskurt, B. Neu, and H. J. Meiselman, *Red Blood Cell Aggregation* (CRC Press, 2012).

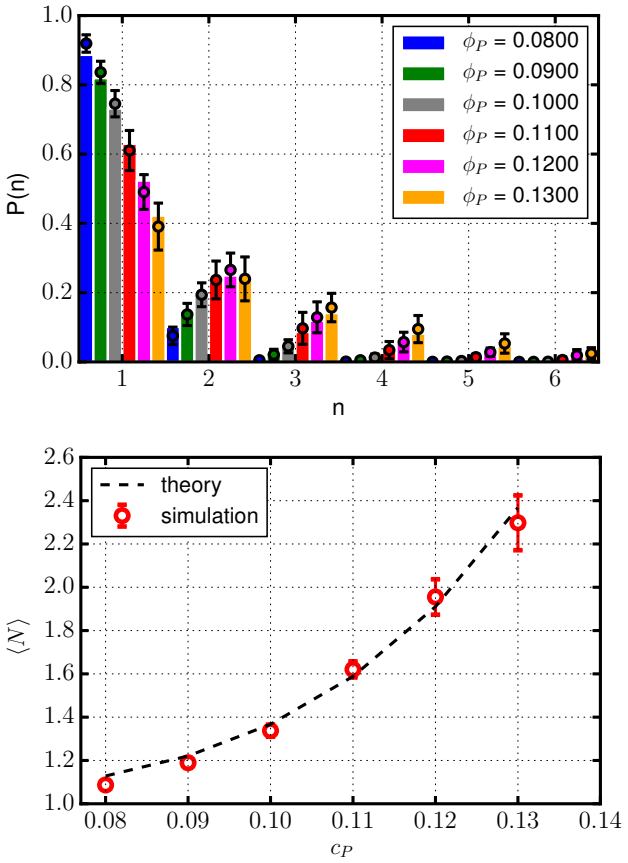

Fig. 1. Comparison between molecular dynamics simulations and analytical model. (Top) Probability of finding an aggregate of size n for different values of polymer concentration as obtained in theory (bars) and simulation (circles). (Bottom) Average number of discs per aggregate as a function of polymer concentration as obtained in theory (dashed line) and with simulations (circles).

Deciphering the effect of nonlinearities induced by protein binding

Josep Mercadal[1,2], Nadja Bosch[3], Isabel Betegón-Putze[3], Ainoa Planas-Riverola[3], Ana I. Caño-Delgado[3], and Marta Ibañes[1,2]

[1]Department of Condensed Matter Physics, Universitat de Barcelona, 08028 Barcelona, Spain
[2]Universitat de Barcelona Institute of Complex Systems, Universitat de Barcelona, 08028 Barcelona, Spain
[3]Department of Molecular Genetics, Centre for Research in Agricultural Genomics (CRAG), CSIC-IRTA-UAB-UB, Campus UAB, Cerdanyola del Vallès, 08193 Barcelona, Spain

Deciphering and understanding the gene regulatory interactions that control biological processes is an active area of research, and one of the fundamental problems in modern biology. Mathematical and computational models have been helpful to investigate the emergent properties of such networks and circuits, as they often display behaviours which are only understood in the context of nonlinear dynamics, such as bistability, oscillations or excitability [1]. Yet, as more data are acquired, new layers of interactions are being included, such as epigenetic regulations and protein-protein interactions. Molecular titration, i.e., the formation of complexes, has been shown to induce ultrasensive responses in gene regulatory networks [2], a key behaviour in the cell's functional repertoire which allows decisive and fast responses when needed. For instance, protein interactions are though to play an important role in the regulation of quiescent states in stem cells of the *Arabidopsis thaliana* root [3].

Herein we study the effect of protein-protein interactions and how these influence the behaviour of gene expression, focusing on two genetic circuits which exhibit the same type of transcriptional response. These circuits involve only two genes, which mutually regulate each other's transcription. One of them involves only transcriptional regulations, while the other includes, beside transcriptional regulation, the formation of protein complexes through pair-wise interactions. The dynamics of the two protein types, x and y, are governed by the following two-dimensional dynamical system

$$\frac{dx}{dt} = g_x(x,y) - \lambda xy - x, \tag{1a}$$

$$\frac{dy}{dt} = g_y(x,y) - \lambda \epsilon xy - y, \tag{1b}$$

where the parameter λ, the rate of complex formation, is set to $\lambda = 0$ in the circuit without protein interactions (circuit B). The functions g_x and g_y encode all the transcriptional interactions, including possible self-activations and self-repressions as well as the cross-regulations between the two genes. We study how the parameters λ and ϵ, the ones quantifying the formation of complexes, affect the behaviour of circuit A with respect to circuit B over several circuit architectures. We also evaluate how the loss of function of proteins (mutant genotypes) alters the system's behaviour in the steady state, both in protein concentrations, measured by x and y, and transcriptional activity, measured by g_x and g_y. We find that different architectures can induce degeneracy in transcriptional responses, that is, generating the same behaviour from distinct interactions, but different behaviour in protein concentrations. This raises the question of how genetic interactions can be inferred only with transcriptional data.

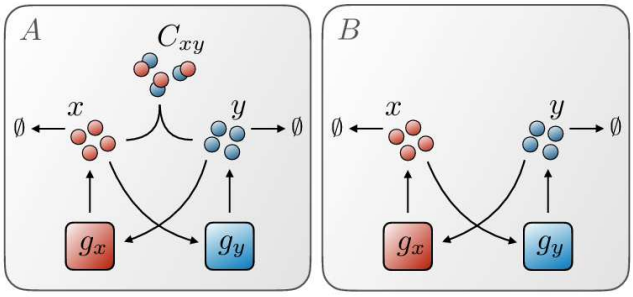

Fig. 1. Regulatory circuits may display the same kind of transcriptional responses eventhough their inherent architecture is different. In circuit A, two genes regulate each other and the product proteins can bind pair-wise to form complexes. In circuit B, no protein binding occurs, so the only relevant interactions are transcriptional. Cross-regulation arrows can indicate both transcriptional activation and repression.

We further study which is the role of stochasticity in our circuits. Both transcription and translation are inherently stochastic processes [5], and as such their dynamics can exhibit behaviours far from expected by their deterministic counterparts. These include, for example, noise induced transitions in bistable and excitable systems, which may play an important role as prime drivers of cellular differentiation.

[1] J. Garcia-Ojalvo, Physical approaches to the dynamics of genetic circuits: A tutorial, Contemp. Phys. **52**, 439-464 (2011).

[2] N. E. Buchler and M. Louis, Molecular titration and ultrasensitivity in regulatory networks, J. Mol. Biol. **384**, 1106-1119 (2008).

[3] J. Vilarrasa-Blasi, M.-P. González-García, D. Frigola, N. Fàbregas-Vallvé, K. G. Alexiou, N. López-Bigas, S. Rivas, A. Jauneau, J. U. Lohmann, P. N. Benfey, M. Ibañes, and A. I. Caño-Delgado, Regulation of plant stem cell quiescence by a brassinosteroid signaling module, Dev. Cell **30**, 36-47 (2014).

[4] P. François and V. Hakim, Core genetic module: The mixed feedback loop, Phys. Rev. E **72**, 031908 (2005).

[5] A. Raj and A. van Oudenaarden, Nature, nurture, or chance: Stochastic gene expression and its consequences, Cell **135**, 216-226 (2008).

First-passage distributions for the one-dimensional Fokker-Planck equation

Oriol Artime, Nagi Khalil, Raúl Toral, and Maxi San Miguel
Instituto de Física Interdisciplinar y Sistemas Complejos (IFISC), CSIC-UIB, Campus UIB, 07122 Palma de Mallorca, Spain

Imagine we know the state of a system, say the position of a diffusive particle, at an arbitrary initial time, and we let the system evolve, under whatever stochastic dynamics. In these conditions, one might inquire into the time needed for the system to reach another particular state or to return to the original state for the first time. The concepts of first-passage (FP) and first-return (FR) times are intuitively related to these scenarios. They provide valuable information of the temporal properties of the system and, in turn, are relatively easy to obtain experimentally or by means of simulations. A consequence of this has been their immediate applicability in a myriad of problems within statistical physics and beyond: spreading of diseases [1], animal or human movement [2], neuron firing dynamics [3], diffusion controlled reactions [4], controlled kinetics [5], or renewal and non-renewal systems [6], ... At an analytical level, many techniques have been developed to compute the FP and FR times, their associated probability density functions and the moments of these distributions [7, 8]. However, general formulations are scarce, since one finds a large variability from one problem to another: the geometry on which the system is embedded, the nature of the boundary conditions, the continuum or discrete character of the dynamics, and, specially, the microscopical rules driving the evolution of the system. In simple cases, though, this is a solved problem. For example, if the dynamics is described by means of a Fokker-Planck equation, one can relate its solution with the FP and FR distributions. Can we infer relevant information about these distributions when the solution is unknown?

We tackle this and related questions along the article in this work [9]. Specifically, we explore the FP and FR time distributions of the large family of models represented by the one dimensional Fokker-Planck equation in bounded domains, with state dependent drift and diffusion terms. We prove analytically that the distributions of all these models may decay as a power law whose exponents can take different values, depending on some conditions involving the diffusion and drift terms as well as the initial and final states. When the diffusion coefficient is positive and the drift term is bounded, like the random walk, both distributions obey a universal law that exhibits a power-law decay of exponent $-3/2$ for low and intermediate times. We also discuss the influence of an absorbing state, characterized by a vanishing diffusion coefficient and/or a diverging drift term. Remarkably, the random walk exponent is still found, as far as the departure and arrival regions are far enough from the absorbing state. Close enough to the absorbing point, though, new universal laws emerge, their particular properties depending on the behavior of the diffusion and drift. We focus on the case of a diffusion term vanishing linearly. In this case, FP and FR distributions show a new *universality class*, characterized by the eventual presence of a power law with exponent -2. As illustration of the predictions of our general theory, we systematically study, both analytically and computationally, different models of increasing complexity. The

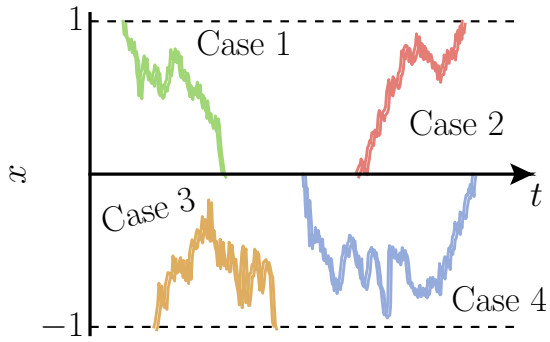

Fig. 1. Types of trajectories that we study. In cases 1 and 2 we compute the first-passage time distribution from the border of the domain to its center, and viceversa. In cases 3 and 4, we compute the first-return time distribution, departing from and arriving to the same border of the domain, and departing from and arriving to the center of the interval.

models can be mapped into a family of two-parameter models which include the random walk, the Ornstein-Uhlenbeck process, the voter model, and two noisy variations of the latter. We use them as representative examples of the different universality classes and the rich behaviour of the temporal properties of the FP and FR distributions.

The impact of the work is twofold. First, it permits to connect under a general lens some independent results that have been separately obtained. Second, it allows an immediate identification between the power law decays and the type of dynamics driving the system. Therefore, our results offer the possibility to unveil the main properties of a process (e.g., presence of absorbing states, nature of the physical boundaries, ...) just by looking at the first-passage and first-return distributions.

[1] A. L. Lloyd and R. M. May, Science **292**, 1316-1317 (2001).

[2] M. C. Gonzalez, C. A. Hidalgo, and A. L. Barabasi, Nature **453**, 779-782 (2008).

[3] H. C. Tuckwell, *Introduction to Theoretical Neurobiology: Vol. 2, Nonlinear and Stochastic Theories* (Cambridge University Press, 2005).

[4] A. Szabo, K. Schulten, and Z. Schulten, J. Chem. Phys. **72**, 4350-4357 (1980).

[5] A. Godec and R. Metzler, Sci. Rep. **6**, 20349 (2016).

[6] K. Ptaszynski, Phys. Rev. E **97**, 012127 (2018).

[7] S. Redner, *A Guide to First-Passage Processes* (Cambridge University Press, 2001).

[8] A. J. Bray, S. N. Majumdar, and G. Schehr, Adv. Phys. **62**, 225-361 (2013).

[9] O. Artime, N. Khalil, R. Toral, and M. S. Miguel, arXiv: 1805.00053.

Flow behavior of particle suspensions in dry granular media scenarios

J. Fonçeca, R. C. Hidalgo, and D. Maza
Laboratorio de Medios Granulares, Depto. de Física y Matemática Aplicada, Universidad de Navarra, Navarra, Spain

Recent works on the flow of dry granular materials have deeply explored and improved the characterization of the flow of particles W through the aperture for spherical particles as a function of both relevant radii: aperture and particles [1, 2]

$$W = \frac{2}{m}\int_0^D \sigma\phi(x)\boldsymbol{V}(x)dx = \frac{4}{\pi d^2}\beta\left(\frac{\upsilon+2}{2\upsilon},\frac{1}{2}\right)\sqrt{g}\,\phi_\infty\left[1-\frac{\alpha_1}{e^{R/\alpha_2}}\right]R^{3/2}, \quad (1)$$

where m is the mass of particles, R is the radius of the particles, σ is the surface density, $\phi(x)$ is the volume fraction, $\boldsymbol{V}(x)$ is the velocity vector, g is the gravity acceleration, d is the hopper diameter, ϕ_∞ is the asymptotic value of the volume fraction, α_1, α_2 and υ are fitting parameters. This equation was found to be valid for two different orders of magnitude, including a region where clogging occurs, for a given set of fitting parameters [2].

Efforts to address the same problem in wet scenarios have been recently performed [3, 4] and they suggest that the Beverloo equation is also valid in an order of magnitude, implying that the fitting parameters in Beverloo equation are able to capture a much wider phenomenology than the one expected for the flow of dry granular materials.

The aim of the present work has been to experimentally study the flow of granular materials through hoppers in a range of different wet scenarios, by varying the setup angle, viscosity of the interstitial fluid and the ratio $r = 2R/d$. Our current experimental setup consists of a quasi-2D and transparent and sealed silo filled with 2 mm diameter beads of stainless steel and a mixture of 99.5% glycerin and pure water. The silo is portable enough such that we are able to keep it fixed in different angles, regarding the normal to the surface, using a mechanical scissor platform. The particles are left to fall under gravity and we record the process with a high resolution camera. Keeping the hopper size fixed, we have observed the linear behavior of the number of particles crossing the hopper regarding the time for different angles (see Fig. 1). The results presented here cannot be only described by using Beverloo equation.

In brief, we expect to further explore the flow behavior when changing variables such as viscosity, diameter ratio r and explore a wider range of angles and its limiting angle as a function of viscosity. To achieve those proposed goals, we are improving our experimental setup to easily adjust the mentioned variables and then record new videos and process the data.

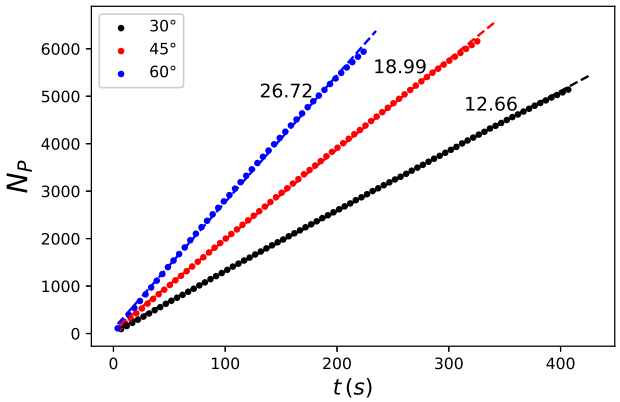

Fig. 1. Number of particles crossing the hopper as a function of time in seconds for different angles. The values shown are the slope of the plotted regressions. The data shown was halted from original data to consider only the steady-state regime.

[1] C. Mankoc, A. Janda, R. Arévalo, J. M. Pastor, I. Zuriguel, A. Garcimartín, and D. Maza, The flow rate of granular materials through an orifice, Granul. Matter **9**, 407-414 (2007).

[2] A. Janda, I. Zuriguel, and D. Maza, Flow rate of particles through apertures obtained from self-similar density and velocity profiles, Phys. Rev. Lett. **108**, 248001 (2012).

[3] T. J. Wilson, C. R. Pfeifer, N. Mesyngier, and D. J. Durian, Granular discharge rate for submerged hoppers, Pap. Phys. **6**, 060009 (2014).

[4] A. M. Cervantes-Álvarez, S. Hidalgo-Caballero, F. Pacheco-Vázquez, The simultaneous discharge of liquid and grains from a silo, arXiv:1801.05747.

Generic model of population dynamics

L. Stucchi[1,2], J. M. Pastor[2], J. García-Algarra[3], and J. Galeano[2]
[1]Departamento Académico de Ingeniería, Universidad del Pacífico, Lima, Perú
[2]Grupo de Sistemas Complejos, Universidad Politécnica de Madrid, 28040 Madrid, Spain
[3]U-Tad – Centro Universitario de Tecnología y Arte Digital, 28290 Las Rozas, Madrid, Spain

Population dynamics has been modelled using differential equations since Malthus, more than two centuries ago. At this moment, there is no unified or general model that encapsulates all biotic interactions, given that the most used models, denominated as Holling's types I, II and III functionals, involves too many variations and ad hoc premises. Here we discuss a different approach in order to model ecological equations, based on the logistic-mutualistic model of García-Algarra *et al.* [1]. We propose that Holling's types functionals reflect only a self-saturation limit and that García-Algarra's model, once generalised, reflects both inter and intraspecific saturation limits. *Any ecological model can be formulated by specific growth rate terms plus the competition terms that limits the population growth*. Even when a complete ecological model surely must involve both limits, population dynamics tend to stay within only one of the regimes.

In this general model one can include in the equation of species i any species interacting with it, even itself. The interaction between individuals of the same species can be beneficial, namely, *cooperation*, or detrimental, as can be *cannibalism* or violent competition. In any case, it is possible to include the effect of the own species in its growth rate, so the general ecological interaction model can be written as

$$\dot{X}_i = X_i \left[\left(r_i + \sum_{j=1}^{n} b_{ij} X_j \right) (1 - \epsilon_i X_i) \right], \qquad (1)$$

where the subscript i runs from 1 to n. Note that the effective growth rate term includes the interaction between individuals of the same species in the summand $j = i$, where the coefficient b_{ii} is positive if it represents *cooperation* or negative if it represents violent competition.

One can go one step further if one considers the intrinsic growth rate r_i as an *interaction* with the environment, in such a way that the parameter r_i can be written as

$$r_i = b_{i0} X_0, \qquad (2)$$

where X_0 can be considered constant. The identification of the intrinsic growth rate r_i as another interaction term allows us to reformulate Eq. (1) as a Verhulst equation with a growth rate given by the addition/subtraction of all the beneficial/detrimental interactions terms, including the environment and the own species. Now in Eq. (1) the sum can be extended from $j = 0$ to $j = n$ and a generic ecological interaction model can be expressed as

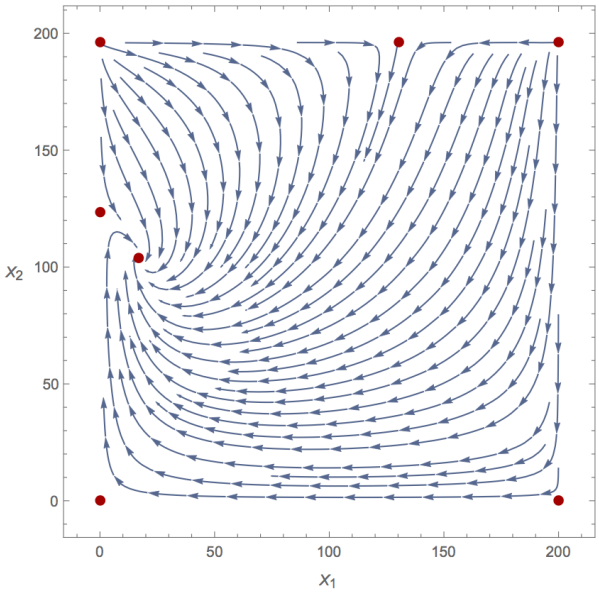

Fig. 1. Space phase with different fixed points in red.

$$\dot{X}_i = \sum_{j=0}^{n} b_{ij} X_j \, (1 - \epsilon_i X_i) \, X_i, \qquad (3)$$

where i runs from $i = 1$ to $i = n$ (as long as X_0 is considered constant), and the term $b_{i0} X_0$ represents the intrinsic growth rate r_i. Note that there are n equations for n interacting species, and the coefficients b_{ij} can be positive, negative or null, for a beneficial, detrimental or negligible interaction, respectively. Now Eq. (3) consists of three independent factors, namely, the Malthusian factor X_i, the effective growth rate $\sum_j b_{ij} X_j$, and the Verhulst or intraspecific-interaction factor $1 - \epsilon_i X_i$. The Verhulst term allows for a particular carrying capacity for each species given by $K_i = 1/\epsilon_i$.

We show a rich dynamical behaviour in our unified model using the lineal stability analysis.

[1] J. García-Algarra, J. Galeano, J. M. Pastor, J. M. Iriondo, and J. J. Ramasco, Rethinking the logistic approach for population dynamics of mutualistic interactions, J. Theor. Biol. **363**, 332-343 (2014).

Cystic fibrosis lung microbiota: Coexistence of prey and predators

R. Vida[1], J. de D. Caballero[2,3], L. García-Regueiro[1], R. del Campo[2,3], and J. Galeano[1]
[1]Grupo de Sistemas Complejos, Universidad Politécnica de Madrid, 28040 Madrid, Spain
[2]Servicio de Microbiología, Hospital Ramón y Cajal, 28034 Madrid, Spain
[3]Instituto Ramón y Cajal de Investigación Sanitaria (IRYCIS), 28034 Madrid, Spain

Cystic fibrosis (CF) is a genetic disorder that affects mostly the lungs. It is caused by the occurrence of mutations in a particular gene. The natural evolution of CF pulmonary disease consists in a progressive decline in lung function caused by a vicious circle of inflammation and tissue destruction that is triggered and maintained by chronic bacterial colonisation of the lower respiratory tract. The main pathogen detected in the CF airway by conventional culture techniques is *Pseudomonas aeruginosa*, which has a major influence on patients survival and their quality of life.

The application of the recent molecular techniques based on massive nucleotide sequencing for the study of the composition of the lung microbiota has allowed us to discover a completely unknown ecosystem.

In the present work was to monitor the lung microbiota composition of 15 CF patients during a year in relation to their clinical data and antibiotic consumption. The fifteen CF-adults contributed with 3-4 induced sputum samples during a follow-up period of a year. Samples were processed for classical microbiology cultures and also submitted to massive sequenciation by bioinformatic analysis to determine the lung microbiota composition. A new computational model based was design to predict the ecological interactions of CF-pathogens and prey-predator bacteria along time. For this model we used as prey bacteria *Pseudomonas, Staphylococcus* and *Haemophilus* whereas the predator species were *Vampirovibrio* and *Bdellovibrio*.

The microbiological cultures of the 56 sputum samples recruited demonstrated chronic lung colonisation by *P. aeruginosa* (11 patients), *S. aureus* (11 patients), *Burkholderia* (1 patient) and *Pandoreae* (1 patient). *P. aeruginosa* and *S. aureus* co-colonisation was observed in the 8 patients with lowest lung function.

Considering all samples, 156 bacterial species were detected, corresponding 90% the classical cultivable CF-pathogens. Unexpectedly, the recognise predators *Vampirovibrio* (17 samples, 12 patients, 0.003%) and *Bdellovibrio* (6 samples, 3 patients, 0.002%) were detected. Computational model results were consistent with the extinction of all populations except one predator and one prey that finally coexist. Finally, introducing a high initial population of predators (0.15% instead 0.03%) all populations disappear.

Thanks to these results, we present an agent based model designed to simulate the Predator-Prey ecological interrelation-ships that could be present in the lung microbiota. For this purpose, and considering the real proportions observed in our sputum samples, the bacteria selected as preys were *P. aeruginosa* and *Staphylococcus*, whereas

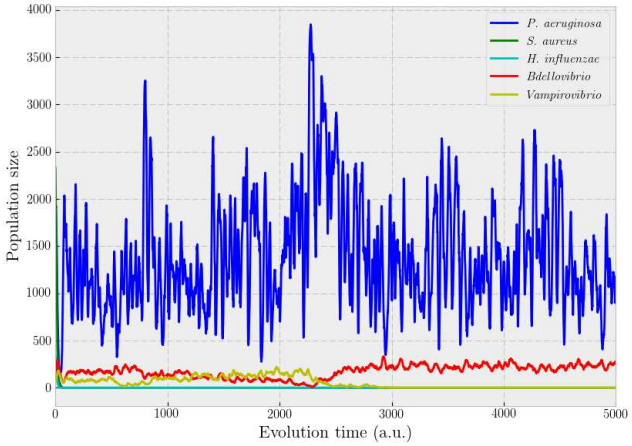

Fig. 1. Temporal evolution of bacterial population size. Initial distribution: 2000 *Pseudomonas*, 2000 *Staphylococcus*, 250 *Haemophilus*, 500 *Bdellovibrio*, and 250 *SPP bacteria*.

Bdellovibrio was considered a predator. Because of uncertainty about the role of *Vampirovibrio*, we decided to introduce as a second putative predator (SPP) [1].

The model analyse the behaviour of the agents, including the spatial distribution and the overall results obtained at the arbitrary time points reproduce the classical oscillatory solution of the Lotka-Volterra equations and were consistent with the extinction of all populations except one predator and one prey, which ultimately coexist in equilibrium. To understand the influence of the initial populations of predators, there were performed a great number of simulations, studying whether populations survive or die by using the survival rate. A threshold appears in the simulations, and it becomes relevant if the objective is changing the final state of equilibrium. The newly designed computational model allows us to hypothesise that inoculation of predators into the lung microbioma could eradicate CF pathogens in early stages of the process.

In conclusion, the presence of predator bacteria was described for first time in the lung microbiota of CF-patients. The computational model could help us to understand the bacterial ecology linked to CF-environment.

[1] J. de D. Caballero, R. Vida, M. Cobo, L. Máiz, L. Suárez, J. Galeano, F. Baquero, R. Cantón, and R. del Campo, Individual patterns of complexity in cystic fibrosis lung microbiota, including predator bacteria, over a 1-year period, mBio **8**, e00959–17 (2017).

Water drops on ice

Luis G. MacDowell[1], David Sibley[2], Pablo Llombart[1,3], Eva G. Noya[3], and A. Archer[2]
[1]Departamento de Química Física, Universidad Complutense de Madrid, 28040 Madrid, Spain
[2]Department of Mathematical Sciences, University of Loughborough, Leicestershire LE11 3TU, Reino Unido
[3]Instituto de Química Física Rocasolano, Consejo Superior de Investigaciones Científicas, 28006 Madrid, Spain

Does water wet ice? As the triple point is approached, the surface disorder grows steadily at the ice-air interface, and a liquid film of *premelted* water is formed. Whether this film attains a finite thickness or diverges at the triple point has remained a controversial issue for a long time. However, recent confocal microscopy experiments confirm early observations of water droplets standing on the surface of ice very close to the triple point, while ice crystal terraces grow and spread below the droplet [2, 3]. Whereas the appearence of an incomplete wetting state of very low energy has been predicted theoretically on the basis of the Lifshitz theory of van der Waals interactions [1], still a great number of open questions remain to be solved.

Indeed, in the experiments by Murata *et al.* [3], the droplets are formed only significantly above saturation, and likewise, disappear reversibly above saturation as the vapor pressure is decreased. Furthermore, a second wetting state seems to appear in this systems at higher saturation, since a thick film appears to emerge below the droplets. More strikingly, the authors observe the formation of distinct droplets well below the vapor-liquid coexistence line. How can we explain this unexpected phenomenology from current knowledge on wetting?

Clearly, one expects here a rather complicated phenomenology, as both vapor condensation, freezing, evaporation and sublimation come into play simultaneously, together with Young-Laplace effects, crystal growth, ice nucleation and terrace spreading. Can this complicated situation be explained from equilibrium thermodynamics at all? What happens on the solid surface right below the wetting film?

In this communication we will pursue previous computer simulations studies [4] and new mesoscopic models to describe and rationalize the puzzling physics of water droplets on ice. The modeling requires to address simultaneously the properties of vapor-liquid and ice-liquid interfaces, as well as the terraced structure of the disordered solid interface. Furthermore, because of the occurrence of premelting on this surface, one needs to take into consideration the interaction of such surfaces via the interface potential, which is dominated in the nanometer scale by retarded interactions. A successful explanation of these experiments thus requires understanding the physics of the problem from the tenth of a nanometer to the micrometer scale. From atomistic simulations of the premelting film and its surface fluctuations to the mesoscopic modeling of spreading droplets.

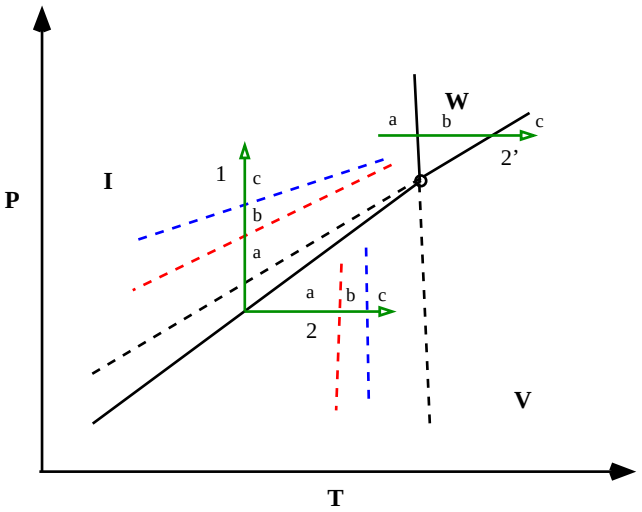

Fig. 1. Wetting phase diagram of water on ice. The phase coexistence lines (black) have to be supplemented with the metastable prolongation of liquid-vapor coexistence in the freezing state. As pressure is increased at constant temperature (path 1), droplets emerge only above the red line; a second change occurs above the blue line when thick films spread from the droplet. Such behavior was reported to occur also at subsaturation along line 2, but likely impurities could shift the triple point making the system to heat above the triple point as in path 2'.

[1] M. Elbaum, S. G. Lipson, and J. G. Dash, J. Cryst. Growth **129**, 491 (1993).

[2] G. Sazaki, S. Zepeda, S. Nakatsubo, M. Yokomine, and Y. Furukawa, Proc. Natl. Acad. Sci. USA **109**, 1052 (2012).

[3] K. Murata, H. Asakawa, K. Nagashima, Y. Furukawa, and G. Sazaki, Proc. Natl. Acad. Sci. USA **113**, E6741 (2016).

[4] J. Benet, P. Llombart, E. Sanz, and L. G. MacDowell, Phys. Rev. Lett. **117**, 096101 (2016).

Morphological transitions of CTAB aggregates

Pablo Llombart[1,†], Eva G. Noya[1], and Luis G. MacDowell[2]
[1]Instituto de Química Física Rocasolano, CSIC, c. Serrano 119, 28006 Madrid, Spain
[2]Departamento de Química-Física, Facultad de Ciencias Químicas, Universidad Complutense de Madrid, 28040 Madrid, Spain

More than 150 years ago, Faraday discovered some peculiar properties of the colloids, in particular gold colloids ("Gold becomes partially transparent not as a result of cracks or holes, but by the brightness of the light through their environment"). Today, thanks to the rise of nanotechnology, numerous synthesis methods of gold colloids have been developed during the last years, and got multitude of applications.

One of the most common synthesis methods is the growth from gold seeds that autocatalyze the reduction of gold ions on the surface of the seed. In this method, the use of some surfactant that prevents gold seeds from being added and controls the morphology of the colloids formed. This is because the surfactant is added around the seeds and controls the flow to the surface of gold salts. Depending on the concentration of surfactant used in the synthesis are able to generate channels of water on the surface of the seed. These channels allow a optimal heat transfer between the water at the same time that allow a reformation of the seeds that like result they generate perfect nanoparticles from an optical point of view, as is the case of the nanorods.

To try to understand the details of this mechanism we performed Molecular Dynamics (MD) simulations for a different number of CTAB molecules present in the aggregates at different concentrations of a widely used surfactant such as CTAB. In our work we have found several morphological transitions for the CTAB in dissolution, ranging from micelles to bilayers or perfectlys developed cylinders.

On the other hand we have seen that the surfactant is added forming micelles on the surface of gold whose internal structure depends on the surface golden atom on which it is adsorbed. MD simulations have helped us to understand this mechanism by providing a microscopic explanation about the growth of gold nanorods and thereby try to optimize the synthesis processes with the the aim of making them more efficient.

---

† E-mail: pablollombart@hotmail.es

Spontaneous NaCl-doped ice: Focus on the mechanisms of ion inclusion

M. M. Conde[1], C. Vega[1], M. Rovere[2], and P. Gallo[2]
[1]Departamento de Química Física, Facultad de Ciencias Químicas, Universidad Complutense de Madrid, 28040 Madrid, Spain
[2]Dipartimento di Matematica e Fisica, Università Roma Tre, via della Vasca Navale 84, 00146 Roma, Italy

Ice-doping processes are of great interest in fields such as atmospheric chemistry, astrophysics and geophysics. In recent years, various studies revealed the existence of subsurface salty oceans and the presence of high-pressure ice polymorphs in the interior of some planetary bodies such as Jupiter's satellites or exoplanets such as Proxima b [1, 2]. These ices, stable over several gigapascals and hundreds of Kelvin, can contain a significant amount of small ions in their structure. The presence of doped ice suggests a plausible explanation for the behaviour and different physical properties observed in the interior of these icy bodies.

Sodium chloride in water is the most common aqueous solution present in nature. The maximum amount of salt dissolved in water at equilibrium is given by solubility. The value of the solubility depends on the salt, the solvent, and the thermodynamic conditions (i.e., temperature and pressure). When it is added to ice, the salt first dissolves in the liquid water layer that is always present on the surface, thereby lowering its freezing point below the ice coexistence temperature. Moreover, when water freezes from aqueous salty solutions, the salt ions are rejected from the solid phase and saturate the liquid phase giving rise to the appearance of the phenomenon known as brine rejection. Pockets of brine form inside the polycrystalline blocks of ice. Below the melting point the rejected brine phase is liquid until the eutectic temperature of the salt. At temperatures below the eutectic point the salt begins to precipitate.

In addition to the brine phase, during the ice growth a small amount of ions can be accommodated in the solid lattice causing ice doping [3, 4]. The ice-doping process raises fundamental questions concerning the mechanisms by which ions are incorporated into the ice structure, and what their positions and effects are once they get there. While the properties of pure ice have been extensively studied, this has not been so for doped ice. Experiments evidenced that the presence of Na^+ and Cl^- ion dopants in the lattice modifies the properties of ice, as the incorporation of ions causes the appearance of extrinsic defects in the lattice that increase the static conductivity of the system and affect the dielectric properties of doped ice. A small amount of doping impurities is sufficient to induce considerable changes in these properties [5].

The detailed mechanisms for the doping processes in ice have not yet been fully explored. It is in fact still not clear where exactly the impurities are located in the lattice, and the location is important because it affects the concentration of defects that cause conduction.

In this work molecular dynamics simulations on microsecond time scale have been performed on an aqueous solution of TIP4P/2005 water and NaCl by using the direct coexistence technique to study the ice growth and the interface ice/liquid water. At different pressures, for temperatures above the eutectic point of the salt and at several concentrations the brine rejection phenomenon and the spontaneous growth of a ice slab doped by the salt are obtained, as found in natural terrestrial and planetary environments. Experiments indicate that Cl^- goes substitutional to ice sites. In line with these evidences we find a new result: the Cl^- ion included in the lattice always substitutes not one but two water molecules leaving the ice structure around not distorted. The Na^+ ion shows lower probability to be included in the ice and it occupies an interstitial site, causing a local distortion of the lattice. No sign of significative ions diffusion is observed in the lattice [6].

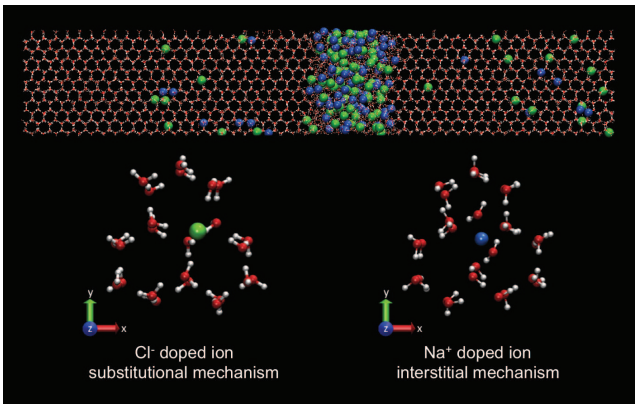

Fig. 1. Final snapshot for the ice/NaCl(aq) system after 2 microsecond (top). Frontal view of a doped ice lattice portion containing a Cl^- ion (bottom left) and a Na^+ ion (bottom right).

[1] E. Pettinelli, B. Cosciotti, F. D. Paolo, S. E. Lauro, E. Mattei, R. Orosei, and G. Vannaroni, Rev. Geophys. **53**, 593 (2015).

[2] L. E. Bove, R. Gaal, Z. Raza, A. A. Ludl, S. Klotz, A. M. Saitta, A. F. Goncharov, and P. Gillet, Proc. Natl. Acad. Sci. USA **112**, 8216 (2015).

[3] G. W. Gross, Adv. Chem. **73**, 27 (1968).

[4] A. W. Cobb and G. W. Gross, J. Electrochem. Soc. **116**, 796 (1969).

[5] V. F. Petrenko and R. W. Whitworth, *Physics of Ice* (Oxford University Press, 1999).

[6] M. M. Conde, M. Rovere, and P. Gallo, Phys. Chem. Chem. Phys. **19**, 9566 (2017).

High-order *vs.* structured interactions in competitive ecosystems

Violeta Calleja-Solanas[1], Sandro Meloni[1,2], and Jesús Gómez-Gardeñes[1,2]
[1]Department of Condensed Matter, University of Zaragoza, Zaragoza, Spain
[2]Institute for Biocomputation and Physics of Complex Systems (BIFI), Zaragoza, Spain

Ecological systems present a remarkably robust biodiversity, for which ecologists have proposed several mechanisms. This emergent property is being explained theoretically in terms of interacting species models on one part, and immigration and speciation models on the other [1]. In fact, simple dynamical models of competitors can produce a stable persistence when high-order interactions are considered, in which the interaction between two species is modulated by one or more other species [2]. Without this assumption, species densities fluctuate through time. The evolution of the density of one of the species is therefore proposed to depend on the outcome of the competition among them [1].

Even if the model does not consider the single effect of every individual of a given species on every individual of the others, it yields convergence to equilibrium. However, this deterministic-approximation approach ignores that single individuals can interact in diverse ways with multiple partners, whose identity can change not only with time but also with location. Here we propose a spatial model, in which each cell of a square lattice is occupied by an individual of a certain species. This representation provides a different context to test whether the structure of the ecosystem and the spatial distribution of individuals may be other candidates for the maintenance of biodiversity. At each time step, a random individual dies and only two neighbours compete to fill the gap, namely, we do not consider high-order interactions. Neighbours are chosen among surrounding cells upon a tuneable radius.

We have observed that the extension of the individual's neighbourhood plays an important stabilizing role. When the neighbourhood comprises neighbours up to a distance radius r of four, the system exhibits coexistence, and fluctuations around the equilibrium densities decrease with radius, Fig. 1. If the neighbourhood radius is larger, we obtain wider amplitude fluctuations similar to those of the dynamical model where no high-order interactions are considered. The method used to choose the neighbourhood can be generalised in terms of the Laplace transform, where the probability of being chosen decrease with the distance from the dead cell. In this new scenario we also find that, when the probability of choosing remote neighbours is negligible, the regime has little fluctuations in densities equilibrium. However, if the system is embedded in a random network, only wide fluctuations appear regardless of neighbourhood's size. Thus inclusion of a regular spatial structure in competitive network models can stabilise dynamics, making species fluctuations decrease and allowing coexistence.

Moreover, our model also allows us to study processes taking place in these systems such as the spatial redistribution of species. Lattice-based models exhibit similar power-law scalings in the geometry of clusters, including communities sizes [3], Fig. 2. In particular, it has been suggested

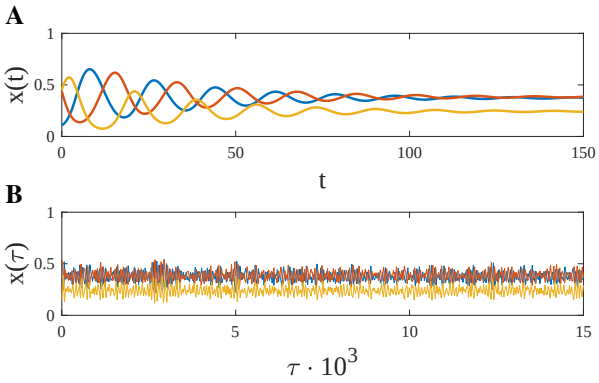

Fig. 1. (a) Reproduction of density evolution for a 3-species ecosystem in [1] with 3-order interactions. (b) Dynamics of our lattice-based model with $r = 3$ in a 100×100 lattice.

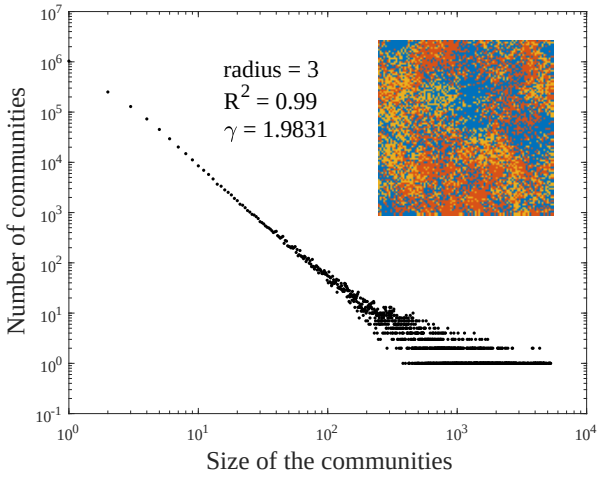

Fig. 2. Power law fit of the stable regime of Fig. 1 (b). Insert is a snapshot of the system at the end of the simulation.

that deviations from power laws are a symptom of instability [4]. Numerical confirmation of these results will be additionally presented, at which different neighbourhood radii will be considered.

[1] S. Allesina, M. J. Michalska-Smith, J. Grilli, and G. Barabás, Nature **548**, 210-213 (2017).

[2] E. Bairey, E. D. Kelsic, and R. Kishony, Nat. Commun. **7**, 12285 (2016).

[3] M. Pascual, M. Roy, F. Guichard, and G. Flierl, Phil. Trans. R. Soc. Lond. B **357**, 657-666 (2002).

[4] S. Kéfi, M. Rietkerk, C. L. Alados, Y. Pueyo, V. P. Papanastasis, A. ElAich, and P. C. de Ruiter, Nature **449**, 213-217 (2007).

Communities and graph similarity in departmental structure of academic collaboration networks

Francisco Bauzá Mingueza, David Iñiguez Dieste, Alfonso Tarancón Lafita, and Jesús Gómez Gardeñes
Institute for Biocomputation and Physics of Complex Systems, Universidad de Zaragoza, 50018 Zaragoza, Spain

Complex networks and graph theory have been widely applied in the study of scientific collaboration networks. In the recent years, many works have obtained results supporting this application, such as the formation of "small worlds" in collaboration networks [1], the correlation between the structure of collaboration networks and the research performance of scholars [2], or the influence of betweeness centrality in the attachment of new researchers to these systems [3].

In this work, we present an study about efficiency and optimization of researchers collaboration through the analysis of the community structure of collaboration networks. To this aim, we have used typical magnitudes and procedures of community detection in complex networks, such as Modularity and Girvan-Newman algorithm, and usual graph similarity indicators, such as Wallace [4] and Rand indexes. With these tools we make a comparison between the departamental and community structure of the scientific collaborations in the University of Zaragoza (Fig. 1).

The collaboration network has been modeled using the researchers co-authorship in published papers. In addition we have used the JCR impact of these papers to assign the weights of the links between two authors, so that those successful collaborations becomes highlighted in the network backbone. Based on this model, we assume that the higher is the modularity of the network the more efficient is the community structure improving the already existing profitable collaborations between researchers. Once the partition corresponding to the maximum modularity has been obtained we compare it with the existing departmental partition to assess their similarity. In addition, we calculate the modular partition that maximizes similarity with the departmental structure and the partition that, having the smallest number of clusters, display a large modularity value.

Our study points out that it is possible to minimize the number of departments in a university while keeping the performance of their researchers based on community detection methods.

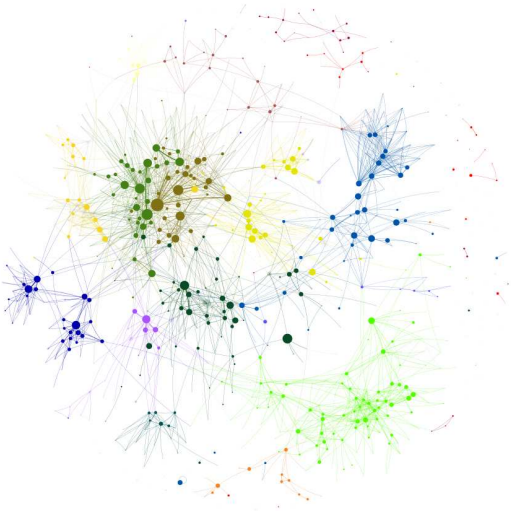

Fig. 1. Collaboration network within the Science area in the University of Zaragoza. Departamental structure appears represented by the colours of nodes.

[1] M. E. J. Newman, The structure of scientific collaboration networks, Proc. Natl. Acad. Sci. USA **98**, 404-409 (2001).

[2] A. Abbasi, L. Hossain, and L. Leydesdorff, Betweenness centrality as a driver of preferential attachment in the evolution of research collaboration networks, J. Informetr. **6**, 403-412 (2012).

[3] A. Abbasi and J. Altmann, On the correlation between research performance and social network analysis measures applied to research collaboration networks, in *44th Hawaii International Conference on System Sciences* (IEEE, 2011).

[4] D. L. Wallace, A method for comparing two hierarchical clusterings: Comment, J. Am. Stat. Assoc. **78**, 569-576 (1983).

Evolución lingüística en Galicia a traves de un modelo reactivo-difusivo

Alberto Pérez Muñuzuri y Mariamo Mussa Juane
Universidade de Santiago de Compostela, rua de Jose María Suárez Nuñez s/n, Santiago de Compostela, Spain

El estudio de fenomenos sociales desde la perspectiva de la física esta en boga. La física nos puede ayudar a comprender como la movilidad humana afecta a la forma en que la informacion se propaga. Y esta movilidad, y por tanto propagacion, está mediada por el tejido social que integra una comunidad concreta.

En nuestro caso, nos centraremos en el fenómeno sociolingüístico de evolución de lenguas en Galicia. Se pretende analizar cómo el gallego y el castellano se propagan a través del territorio y analizar cómo evoluciona la fracción de hablantes de ambas lenguas debido a las interconexiones de las distintas regiones.

Para modelizar la variación temporal de la fracción de hablantes, empleamos un sistema de ecuaciones reactivo-difusivas en el que los hablantes se difunden por la red de interconexión de las regiones gallegas. El ritmo de evolución de la fracción de hablantes de cada región se verá afectado por el grado de conectividad que tenga la región, es decir, por la densidad de tejido social que tenga o el acceso a información diversa. Las zonas mas rurales tendrán conectividades inferiores a las zonas urbanas lo que restringe el acceso que puedan tener a la información.

El rico abanico que va de lo rural a lo urbano, de lo poco conectado a lo muy conectado, da lugar a ritmos de evolución heterogéneos. Este patrón temporal es nuestro objeto a estudiar.

The effect of network topology in electrical power grids

A. Chacoma, D. Gomila, and P. Colet
IFISC, UIB-CSIC, Palma de Mallorca, Spain

The transportation of electricity from power plants to consumers centers is achieved by the transmission and distribution power lines. This electrical wiring shapes the power grid, an interconnected network built to provide electricity to the consumers. The grid is then constituted by nodes (generators/consumers) and the links (the power lines).

Network stable operation requires the nodes to run with the same frequency (50 or 60 Hz) and phase differences lower than a certain tolerance [1, 2]. If the two requirements are achieved the network is said to be synchronized.

In this condition, network theory allows us to make an abstraction of the transmission system to study how the structure of the network affects the electrical signal properties. It is well known that the changes on the network topology in this systems directly affects the natural frequencies of the system [3], and consequently, the network synchronization and the signal quality. Therefore, this study is directly related to give theoretical support to possible technical issues.

We faced this work by using analytical and numerical techniques. First of all, we modeled small power grids with different topologies to study how this differences affect the natural frequencies of the system (see Fig. 2). In a second stage, we performed a similar analysis on the structure of real grids, by modeling the electrical power grid of Balearic Islands (see Fig 1).

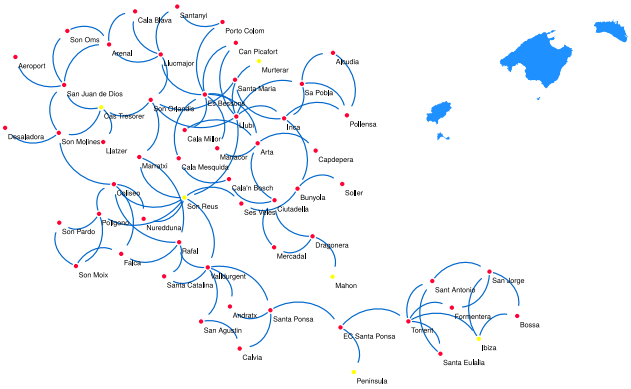

Fig. 1. Representation of the power grid in Balearic Islands, Spain.

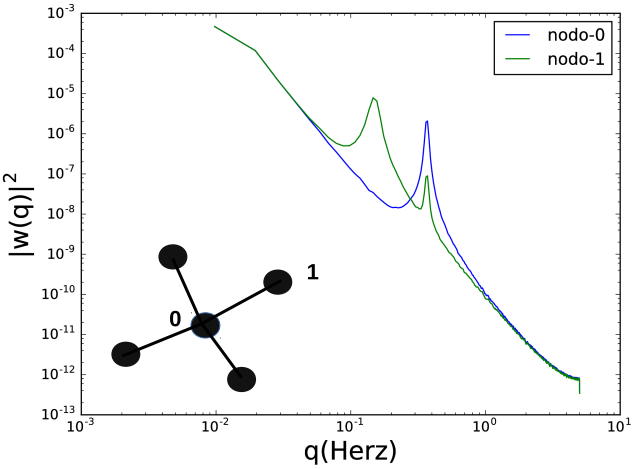

Fig. 2. Frequency signal power spectrum, for two nodes in a power grid with star topology.

[1] F. Dörfler, M. Chertkov, and F. Bullo, Synchronization assessment in power networks and coupled oscillators, Proc. Natl. Acad. Sci. USA **110**, 2005-2010 (2013).

[2] J. W. Simpson-Porco, F. Dörfler, and F. Bullo, Voltage collapse in complex power grids, Nat. Commun. **7**, 10790 (2016).

[3] L. M. Pecora and T. L. Carroll, Master stability functions for synchronized coupled systems, Phys. Rev. Lett. **80**, 2109 (1998).

Gathering tourist indicators by using twitter data analysis

A. Chacoma, J. Ramasco, and A. Tugones,
IFISC, CSIC-UIB, Palma de Mallorca, Spain

Nowadays tourism stand for important revenues in most countries economies [1]. For instance in Spain, the travel industry represents 11% of its GDP, only in the year 2017 it provided 2.3 million jobs position on hotel, restaurant and transport sectors, and is growing [2]. The highly impact that tourism has on the economy clearly demands a deeper understanding of both the industry internal dynamics and the tourists preferences and behavior.

On the other hand, during the latest years, we have witnessed the outstanding growing of both smart-phone technologies and social media (Twitter, Facebook, Instagram, etc.). This disruptive combination has brought on the noteworthy increase of available information about people behavior. The literature shows a plethora of works using this information to study different problems regarding to social life [3], marketing and businesses [4], and tourism as well [5]. The latter is specially interesting because people tend to increase their social network activity when they are traveling [6]. This fact implies that there are a huge among of information available about tourists preferences that can be used to obtain precise tourists indicators in order to enhances the travel companies management, and improve the tourists experiences.

We aim to use data from Twitter to obtain tourism indicators in the Mediterranean coast area. Tourism in this region has steadily grown since the post-war years, when the industry, following the mass production paradigm, started to standardize holiday packages offering relaxing time of sun and sea at a competitive price [7]. In this work, we analyzed the European tourists preferences in the zone (see Fig. 1), the differences between low and hight seasons, which are the most popular places, where the tourist frequently returns, which languages do they use, and the tourist movement around the cities.

[1] D. R. Hall, M. K. Smith, and B. Marciszewska (Eds.), *Tourism in the New Europe: The Challenges and Opportunities of EU Enlargement* (CAB International, 2006).

[2] R. Paci and E. Marrocu, Tourism and regional growth in Europe, Pap. Reg. Sci. **93**, S25-S50 (2014).

[3] P. A. Grabowicz, J. J. Ramasco , E. Moro, J. M. Pujol, and V. M. Eguiluz, Social features of online networks: The strength of intermediary ties in online social media, PLoS ONE **7**, e29358 (2012).

[4] T. L. Tuten and M. R. Solomon, *Social Media Marketing* (Sage, 2017).

[5] A. Bassolas, M. Lenormand, A. Tugores, B. Gonçalves, and J. J. Ramasco, Touristic site attractiveness seen through Twitter, EPJ Data Sci. **5**, 12 (2016).

[6] A. Királ'ová and A. Pavlíčeka, Development of social media strategies in tourism destination, Procedia-Soc. Behav. Sci. **175**, 358-366 (2015).

[7] E. Fayos-Solá, Tourism policy: a midsummer night's dream?, Tourism Manage. **17**, 405-412 (1996).

[8] `http://simap.ted.europa.eu/web/simap/nuts`

[9] `https://www.iso.org`

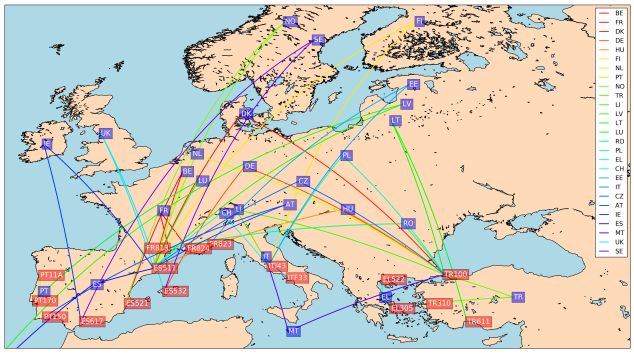

Fig. 1. The map shows the connection between the European Union countries and the places in the Mediterranean area where the tourists from those countries frequently travel. The name of the places is giving by the *NUT* 2 code [8], and for the countries by the standard *ISO* 3166-2 [9].

Stochastic soliton ratchets

Bernardo Sánchez-Rey[1], Jesús Casado-Pascual[2], and Niurka R. Quintero[1]
[1]Departamento de Física Aplicada I, E.S.P., Universidad de Sevilla, c. Virgen de África 7, 41011 Sevilla, Spain
[2]Física Teórica, Universidad de Sevilla, apdo. correos 1065, 41080 Sevilla, Spain

Ratchet-like transport phenomena are identified as the net motion of particles or solitons generated by zero-average forces. Experiments in shaken drops, ferrofluids, optical lattices, and Josephson junctions [1, 2, 3] show the net transport of particles, cold atoms or fluxons under harmonic forces.

Solitons are nonlinear waves, which propagates with a constant velocity defined by the initial conditions. In particular, the so called kinks are exact solutions of the sine-Gordon equation

$$\Phi_{tt} - \Phi_{xx} + \frac{dU}{d\Phi} = 0, \tag{1}$$

where the field $\Phi(x,t)$ depends both on the space x and on the time, and $U(\Phi) = 1 - \cos\Phi$ represents the sine-Gordon potential. This system describe, for instance, the propagation of magnetic flux along the Josephson junctions [3].

The study of the symmetries of the equations fix the necessary conditions that the external forces must break in order to generate net motion of kinks or particles [4, 5, 6], regardless of the initial conditions.

Recently we have suggested a mechanism, in which no net force is necessary to induce net motion of the sine-Gordon kinks [7]. The motion is consequence of the transitions among different states of the potential. In this contribution we show a novel mechanism of soliton ratchets, in which these transitions occur stochastically. The importance of this mechanism is that huge average velocity can be achieved.

[1] X. Noblin, R. Kofman, and F. Celestini, Phys. Rev. Lett. **102**, 194504 (2009).

[2] A. Engel, H. W. Müller, P. Reimann, and A. Jung, Phys. Rev. Lett. **91**, 060602 (2003).

[3] A. V. Ustinov, C. Coqui, A. Kemp, Y. Zolotaryuk, and M. Salerno, Phys. Rev. Lett. **93**, 087001 (2004).

[4] P. Reimann, Phys. Rep. **361**, 57 (2002).

[5] J. A. Cuesta, N. R. Quintero, and R. Álvarez-Nodarse, Phys. Rev. X **3**, 041014 (2013).

[6] J. Casado-Pascual, J. A. Cuesta, N. R. Quintero, and R. Álvarez-Nodarse, Phys. Rev. E **91**, 022905 (2015).

[7] B. Sánchez-Rey, J. Casado-Pascual, and N. R. Quintero, Phys. Rev. E **94**, 012221 (2016).

Reaction-diffusion model for the understanding of tuberculosis dynamics at the scale of a secondary pulmonary lobule

Martí Català, Sergio Alonso, Clara Prats, and Daniel López
Departament de Física, Universitat Politècnica de Catalunya, 08028 Barcelona, Spain

Tuberculosis (TB) is still one of the major humankind threats, being one of the 3 main causes of death by an infectious disease worldwide. TB is a communicable chronic infectious disease caused by *Mycobacterium tuberculosis* (*Mtb*). An infection with *Mtb* often causes no symptoms, remaining controlled as a non-contagious latent tuberculosis infection, but a 10% of infected people will develop the contagious active disease (i.e., a TB) even several years after the infection. An 85% of the TB cases correspond to a pulmonary disease, while the rest are extrapulmonary [1]. Despite the global efforts to fight the disease, its incidence is still stable, being the infectious disease that has killed most people in history. European cities today face a significant challenge to control TB infection and spread. The End TB Strategy by the World Health Organization [2] identifies the Latent Tuberculosis Infection as one of the challenges to overcome in order to accomplish the stated objective.

Mathematical and computational models may be used for making progress on the understanding and control of the latent infection.

We built a reaction diffusion model to reproduce tuberculosis infection in a secondary lobule. This model is formed by 10 elements: b_i (intracellular bacilli, bacilli contained inside macrophages), b_e (extracellular bacilli, bacilli outside macrophages), m_u (uninfected macrophages, macrophages with no bacilli inside), m_i (infected macrophages, macrophages with bacilli inside), m_a (activated macrophages, macrophages that are activated and can kill bacilli), n (neutrophils), T (T-cells), f (fibroblasts), s (inflammatory response signal) and V_nc (necrotic volume, volume occupied by dead cells).

The model consists of 10 partial differential equations that determine the evolution of each element from an initial state. Elements interact with each other and diffuse to the nearest alevoli.

All these elements and reactions are considered to occur inside each alveolus. The size of a secondary pulmonary lobule is around 1 cm^3 and contains around 10^5 alveoli. In our model it was implemented as a $52 \times 52 \times 52$ alevoli grid.

In Fig. 1 the results of the evolution of an initial infected macrophage with one bacillus are shown. During the first lysis cycle extracellular bacilli are more than intracellular ones. When immune response is activated the number of bacilli is reduced and number of uninfected macrophages are dominant. This results and the numbers obtained reproduce biological data [3]. Lesions encapsulation success depended on fibroblast diffusion coefficient. If fibroblast molecules did not diffuse rapidly enough the infection was out of control. Immune system induced a faster control of the lesions, which were smaller and easier to encapsulate. In Fig. 2 the encapsulation process of a lesion in a host where immune system is properly activated. It can be seen that when the lesion reached the septum it is surrounded by fibroblasts.

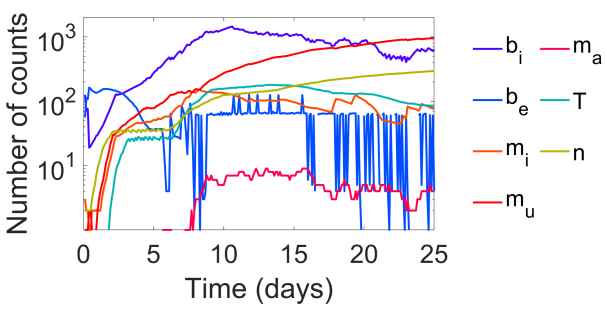

Fig. 1. Number of counts of the different elements of the model at the alveolus where infection starts. The elements are intracellular bacilli b_i, extracellular bacilli b_e, uninfected macrophages m_u, infected macrophages m_i, activated macrophages m_a, neutrophils n, and T-cells T.

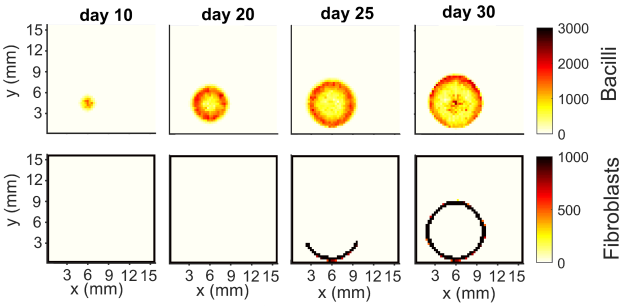

Fig. 2. Number of bacilli and fibroblasts observed in a secondary lobule at different times. Fibroblast encapsulate the lesion when the septum is reached.

[1] World Health Organization, *Global Tuberculosis Report 2017* (World Health Organization, Geneva, 2017).

[2] World Health Organization, *The End TB Strategy* (World Health Organization, Geneva, 2014).

[3] P.-J. Cardona, Patogénesis de la tuberculosis y otras micobacteriosis, Enferm. Infec. Microbiol. Clin. **36**, 38-46 (2018).

Anomalous diffusion in models of fluorescence recovery after photobleaching

S. B. Yuste[1,2], K. Lindenberg[3], A. Baumgaertner[1], and E. Abad[2,4]
[1]Departamento de Física, Facultad de Ciencias, Universidad de Extremadura, E-06071 Badajoz, Spain
[2]Instituto de Computación Científica Avanzada (ICCAEx), Universidad de Extremadura, Spain
[3]Department of Chemistry and Biochemistry, and BioCircuits Institute, University of California San Diego, 9500 Gilman Drive, La Jolla, CA 92093-0340, USA
[4]Departamento de Física Aplicada, Centro Universitario de Mérida, Universidad de Extremadura, E-06800 Mérida, Spain

Anomalous diffusion, in particular subdiffusion, is frequently invoked as a mechanism of motion in dense biological media and may have a significant impact on the kinetics of binding/unbinding events at the cellular level. Here, we extend a previously developed model for FRAP experiments to account for anomalous diffusion [1]. Our particular implementation of subdiffusive transport is based on a continuous time random walk (CTRW) description of the motion of fluorescent particles, as CTRWs lend themselves particularly well to the inclusion of binding/unbinding events. In order to model switching between bound and unbound states of fluorescent subdiffusive particles, we derive a fractional reaction-subdiffusion equation of rather general applicability. Using suitable initial and boundary conditions, this equation is then incorporated in the model describing 2D kinetics of FRAP experiments. We find that this model can be used to obtain excellent fits to experimental data. Moreover, recovery curves corresponding to different radii of the circular bleach spot can be fitted by a single set of parameters. While not enough evidence has been collected to claim with certainty that the underlying transport mechanism in FRAP experiments is one that leads to anomalous diffusion, the compatibility of our results with experimental data fuels the discussion as to whether normal diffusion or some form of anomalous diffusion is the appropriate model and as to whether anomalous diffusion effects are important to fully understand the outcome of FRAP experiments.

In the above context, we also address the problem of diffusion on a comb whose teeth display a varying length [2]. Specifically, the length ℓ of each tooth is drawn from a probability distribution displaying power law behavior at large ℓ, $P(\ell) \sim \ell^{-(1+\alpha)}$, ($\alpha > 0$). We first focus on the computation of the anomalous diffusion coefficient for the subdiffusive motion along the backbone. This quantity is subsequently used as an input to compute concentration recovery curves mimicking fluorescence recovery after photobleaching experiments in comb-like geometries such as spiny dendrites. Our method is based on the mean-field description provided by the well-tested Continuous Time Random Walk approach for the random comb model, and the obtained analytical result for the diffusion coefficient is confirmed by numerical simulations of a random walk with finite steps in time and space along the backbone and the teeth. Finally, we show that recovery curves obtained with the help of the analytical expression for the anomalous diffusion coefficient cannot be fitted perfectly by a model based on scaled Brownian motion, i.e., a standard diffusion equation with a time-dependent diffusion coefficient. However, differences between the exact curves and such fits are small, thereby providing justification for the practical use of models relying on scaled Brownian motion as a fitting procedure for recovery curves arising from particle diffusion in comb-like systems.

[1] S. B. Yuste, E. Abad, and K. Lindenberg, A reaction-subdiffusion model of fluorescence recovery after photobleaching (FRAP), J. Stat. Mech. **2014**, P11014 (2014).

[2] S. B. Yuste, E. Abad, and A. Baumgaertner, Anomalous diffusion and dynamics of fluorescence recovery after photobleaching in the random-comb model, Phys. Rev. E **94**, 012118 (2016).

Exploiting optical chaos for speckle reduction in double pass imaging

Donatus Halpaap[1,2], Jordi Tiana-Alsina[2], Meritxell Vilaseca[1], and Cristina Masoller[2]
[1]Centre for Sensors, Instruments and Systems Development, Universitat Politècnica de Catalunya, Terrassa, Spain
[2]Nonlinear Dynamics, Nonlinear Optics and Lasers Group, Universitat Politècnica de Catalunya, Terrassa, Spain

The Double pass (DP) imaging technique is a diagnostic method used to obtain an overall estimation of the optical quality of an eye, containing information on scattering as well as higher order aberrations [1]. This is achieved by measuring the point spread function of the eye by recording the image of a point source on the retina, i.e., a collimated light beam enters the eye, passes the ocular media, is reflected at the retina, passes through the ocular media again in reverse direction and is recorded after exiting the pupil. DP images are usually suffer from speckle noise, if no action is taken against it. Is this work we study the use of semiconductor optical chaos for speckle reduction in this application.

For this, we first study the use of optical chaos for reducing speckle in a full-field imaging setup. We obtain optical chaos from a semiconductor laser diode by subjecting it to different amounts of optical feedback as well as modulating its pump current, with the aim of reducing the coherence length of the source and thus reducing speckle formation [2]. For example, the speckle contrast C, within the white circle of Fig. 1 is reduced from $C = 0.41$ to $C = 0.30$ simply by subjecting the laser diode to optical feedback, where $C = \sigma_I/\langle I\rangle$, with the mean intensity of the pattern $\langle I\rangle$,and its standard deviation σ_I [3].

Once we have found feedback parameters for best speckle reduction, we will apply the chaotic source in a DP imaging experiment.

[1] J. L. Güell, J. Pujol, M. Arjona, F. Diaz-Douton, and P. Artal, Optical quality analysis system: Instrument for objective clinical evaluation of ocular optical quality, J. Cataract Refract. Surg. **30**, 1598-1599 (2004).

[2] J. Ohtsubo, *Semiconductor Lasers: Stability, Instability and Chaos* (Springer, 2012).

[3] J. W. Goodman, *Speckle Phenomena in Optics: Theory and Applications* (Roberts & Company, 2007).

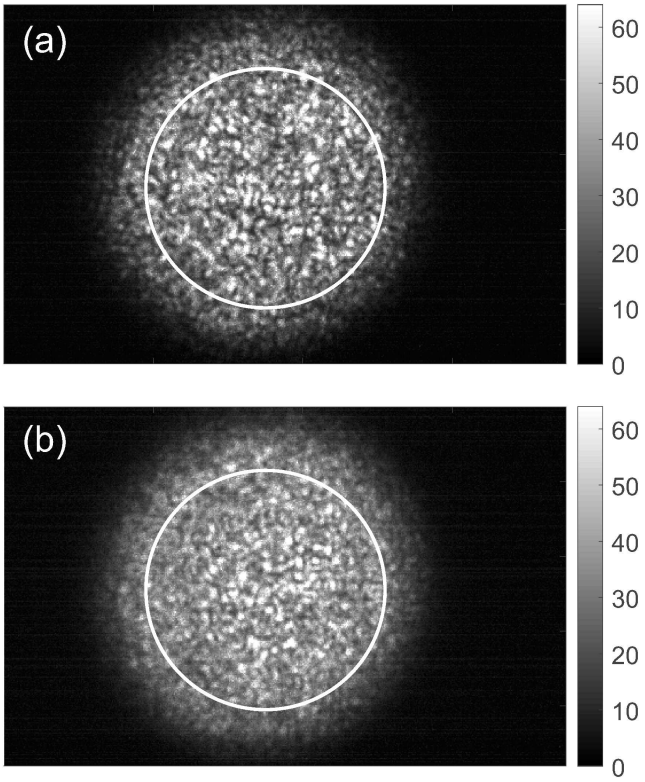

Fig. 1. Speckle patterns with intensity shown in gray-scale (arbitrary units). Source: laser diode. (a) No feedback. (b) With optical feedback.

Optimization of the extraction of pauses in molecular dynamics

Francisco J. Cao[1,2] and Andrés Tejedor Reyes[2]
[1]Instituto Madrileño de Estudios Avanzados en Nanociencia (IMDEA-Nanociencia), c. Faraday 9, 28049 Madrid, Spain
[2]Universidad Complutense de Madrid, pl. Ciencias 1, 28040 Madrid, Spain

Single-molecule experiments to study molecular motors once at a time have been developed in recent years. One of the critical points of the data analysis is the identification, characterization and extraction of the effect of the pause states in the motor dynamics [1]. The theoretical model is well-known, but in practice satisfactory results are dificult to attain. We have developed and optimized an algorithm to separate the pause and displacement contributions to the velocity histograms, in order to determine the displacement rate (see Fig. 1).

We simulate a molecular motor (DNA-Polymerase) moving with a displacement rate k_p (replication rate), entering a pause state with rate k_{a1} and exiting from it with rate k_{1a}. We mimic the experimental limitations by assuming the trajectories have a Gaussian random noise in position and measuring the process at given time intervals mimicking the experimental data sampling.

The algorithm has allowed us to identify the optimal speed histogram obtained with our method. We have measured the displacement rate of the motor quite precisely in spite of the experimental limitations simulated in our work.

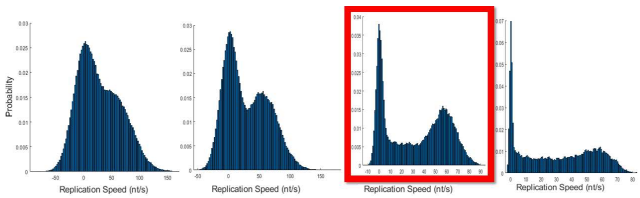

Fig. 1. Replication speed histograms obtained with our algorithm. Histogram for the optimal value indicated with a red box

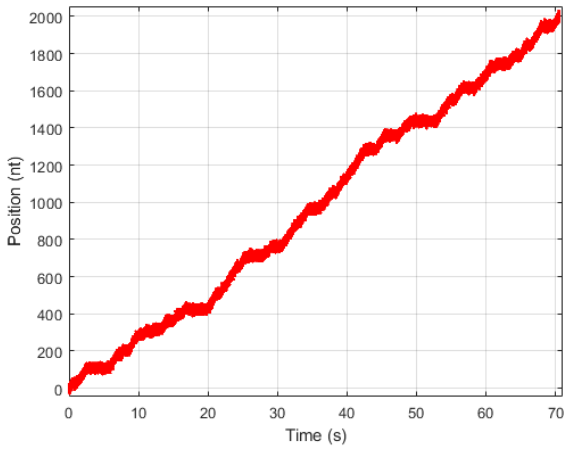

Fig. 2. Synthetic trajectory for DNA-Polymerase during the replication. We include the Gaussian random noise in positions measures.

[1] J. A. Morin, F. J. Cao, J. M. Lázaro, J. R. Arias-González, J. M. Valpuesta, J. L. Carrascosa, M. Salas, and B. Ibarra, Active DNA unwinding dynamics during processive DNA replication, Proc. Natl. Acad. Sci. USA **109**, 8115-8120 (2012).

Exponential-like concentration distribution in modeling the specific consumption rate in substrate-limited microbial growth

F. J. Arranz[1] and J. M. Peinado[2]
[1]Grupo de Sistemas Complejos, Universidad Politécnica de Madrid, av. Puerta de Hierro 2-4, 28040 Madrid, Spain
[2]Departamento de Microbiología III, Universidad Complutense de Madrid, c. José Antonio Nováis 2, 28040 Madrid, Spain

The specific consumption rate of substrate, as well as the associated specific growth rate, is an essential parameter in the mathematical description of substrate-limited microbial growth. In this communication we present a new model of substrate transport [1], based on recent knowledge on the structural biology of transport proteins [2], which correctly describes very accurate experimental results at near-zero substrate concentration values found in the literature [3, 4], where the widespread Michaelis-Menten model fails.

In order to establish the model for the specific consumption rate, the following two assumptions are considered:

1. The local substrate concentration, in the immediate neighbourhood of the corresponding membrane transport protein, fluctuates around the mean concentration (bulk concentration) with high probability for concentration below the mean and with low probability for concentration above the mean.

2. The substrate penetrates cell membrane if and only if the local substrate concentration, in the immediate neighbourhood of the transport protein, reaches or exceeds certain concentration threshold which will be named as *activation concentration*. Then, the substrate penetrates cell membrane at constant rate.

The first assumption concerns the features of substrate solution in the neighbourhood of the corresponding transport protein. As is represented in Fig 1 (a), substrate at bulk concentration C is transported into the cell by the corresponding protein with rate q_t, so that local substrate concentration c in the immediate neighbourhood of the transport protein will decrease. Forced convection in the liquid medium would immediately restore bulk concentration, but the existence of the cell wall prevents forced convection, so that bulk concentration will be restored by means of diffusion. Since substrate diffusion is a very slow process, it seems reasonable that the local concentration is smaller than bulk concentration with high probability, and greater than bulk concentration with low probability. The exponential distribution is the simplest probability distribution with these features among other suitable features

$$\mathcal{P}(c) = \frac{1}{C}\exp\left(-\frac{c}{C}\right). \qquad (1)$$

However, since exponential distribution has its maximum probability density at the perhaps unrealistic value $c = 0$, in Ref. [1] the model was improved by using the more general Weibull distribution, which includes the exponential distribution as a particular case.

The second assumption concerns the features of the mechanism of transport. The latest research on this issue [2] shows the existence of *several binding sites*, which, when activated, would also induce conformational changes. As is well known, in this case the kinetics is described by Hill equation which, for a high number of binding sites, tends rapidly to a smoothed Heaviside step function.

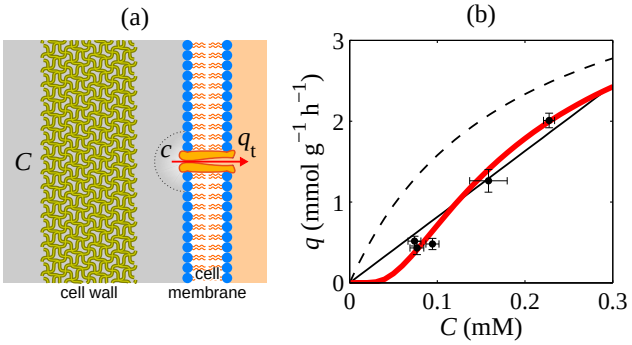

Fig. 1. (a) Schematic representation of the cell interface in the neighbourhood of a transport protein, with consumption rate q_t, showing the concept of local substrate concentration c *versus* bulk concentration C. (b) Experimental values of specific consumption rate q *versus* substrate concentration C for *S. cerevisiae*, taken from Boender *et al.* [4]. The fitted curve corresponding to the proposed model (red line) along with the fitted curve from the Michaelis-Menten based model (black line) are also depicted. Notice that Michaelis-Menten curve degenerates into a straight line. Additionally, the Michaelis-Menten curve corresponding to the fitting parameters from the proposed model, assuming Michaelis constant $K = c_{ac}$, has also been represented (dashed black line).

Thus, considering both assumptions jointly, if the substrate penetrates cell membrane through each transport protein at the constant rate q_t when the local concentration fulfills $c \geq c_{ac}$, and each cell has n transport proteins on average, then the statistically observable value of the specific consumption rate $q(C)$ will be given by

$$\begin{aligned} q(C) &= q_{max} \cdot \int_{c_{ac}}^{\infty} \mathcal{P}_\beta(c)\,\mathrm{d}c \\ &= q_{max} \cdot \exp\left(-\frac{c_{ac}}{C}\right), \end{aligned} \qquad (2)$$

with $q_{max} = nq_t$, resulting in the functional form for the specific consumption rate from the proposed model.

[1] F. J. Arranz and J. M. Peinado, PLoS ONE **12**, e0171717 (2017).

[2] G. Diallinas, Front. Pharmacol. **5**, 207 (2014).

[3] J. A. Diderich, M. Schepper, P. van Hoek, M. A. H. Luttik, J. P. van Dijken, J. T. Pronk, P. Klaassen, H. F. M. Boelens, M. J. Teixeira de Mattos, K. van Dam, and A. L. Kruckeberg, J. Biol. Chem. **274**, 15350-15359 (1999).

[4] L. G. M. Boender, E. A. F. de Hulster, A. J. A. van Maris, P. A. S. Daran-Lapujade, and J. T. Pronk, Appl. Environ. Microbiol. **75**, 5607-5614 (2009).

Model of pedestrian races as a social network

M. Rebollo[1,2,†], Javier Galeano[2,‡], Juan Carlos Losada[1,⋆], and Javier LLuch[3,∗]
[1]Grupo de Tecnología Informática-Inteligencia Artificial, Universitat Politècnica de València, Spain
[2]Grupo de Sistemas Complejos, Universidad Politécnica de Madrid, Spain
[3]Instituto Universitario de Automática e Informática Industrial, Universitat Politècnica de València, Spain

Most of the tools that register and tracks the evolution of a race consider runners as individuals. Participants in a race can upload their records, but their progress is isolated from the rest of the group. In this work, a race is studied as a network, where runners are the nodes, and they are linked when the distance between them is below some range.

The network evolves with time as long as the runners' progress and the neighbors' changes depending on their velocity. A factor that has been observed during races is that the path of a runner is affected by the other runners that are around them. A slow runner can increase its path when he or she is close enough to a faster group. Alternatively, runners can be slowed down by their surroundings. Other effects can affect the path, such as the age [6], or the regularity [3, 5]. Besides popular runners, this effect has been observed in professional athletes [1] or even in other sports [2].

Data from the 200 first classified into different races has been retrieved to analyze this effect. Races of different distances are included: from 5000 m to 10000 m, half marathon, and marathon, and also trails with different distances.

Depending on the distance considered among the runners, the network is divided into some groups. With the minimal distance, as many groups as runners are created. Moreover, this number is reduced when longer distances are considered until one connected component is created. All the races behave similarly, and a common pattern emerges: an exponential relation appears between the considered distances for the links and the number of groups created in the network (Fig. 1). All these functions collapsed (Fig. 2), and the parameter of the exponential distribution follows a power law distribution that depends only on the total distance of the race.

This behavior can be used by the organizers to distribute the medical services, organize roadblocks efficiently, or decide the location for provisioning and volunteers.

† E-mail: mrebollo@upv.es

‡ E-mail: javier.galeano@upm.es

⋆ E-mail: juancarlos.losada@upm.es

∗ E-mail: jlluch@upv.es

[1] S. Aragón, D. Lapresa, J. Arana, M. T. Anguera, and B. Garzón, Tactical behaviour of winning athletes in major championship 1500-m and 5000-m track finals, Eur. J. Sport Sci. **16** 279-286 (2016).

[2] M. Amatria, D. Lapresa, J. Arana, M. T. Anguera, and G. K. Jonsson, Detection and selection of behavioral patterns using theme: A concrete example in grassroots soccer, Sports **5**, 20 (2017).

[3] P. Balducci, M. Clémençon, and C. Hautier, "Relatively" slow and steady wins the race, J. Sport Human Perf. **4**, 1-6 (2016).

[4] M. D. Hoffman, Pacing by winners of a 161-km mountain ultramarathon, Int. J. Sports Physiol. Perform. **9**, 1054-1056 (2014).

[5] H. A. Kerhervé, G. Y. Millet, C. Solomon, The dynamics of speed selection and psycho-physiological load during a mountain ultramarathon, PLoS ONE **10**, e0145482 (2015).

[6] D. S. March, P. M. Vanderburgh, P. J. Titlebaum, M. L. Hoops, Age, sex, and finish time as determinants of pacing in the marathon, J. Strength Cond. Res. **25**, 386-391 (2011).

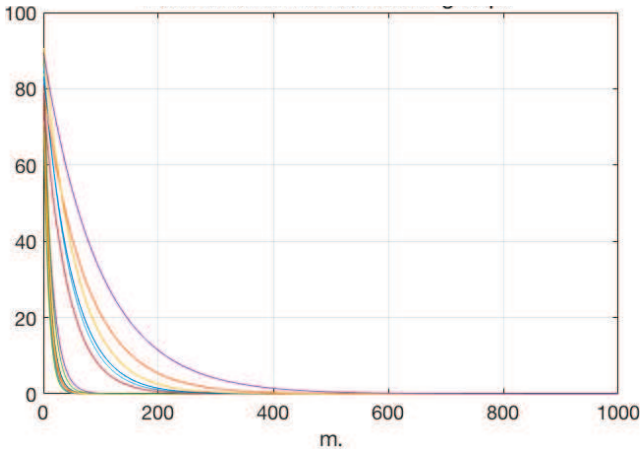

Fig. 1. Size of the groups formed depending on the distance between runners.

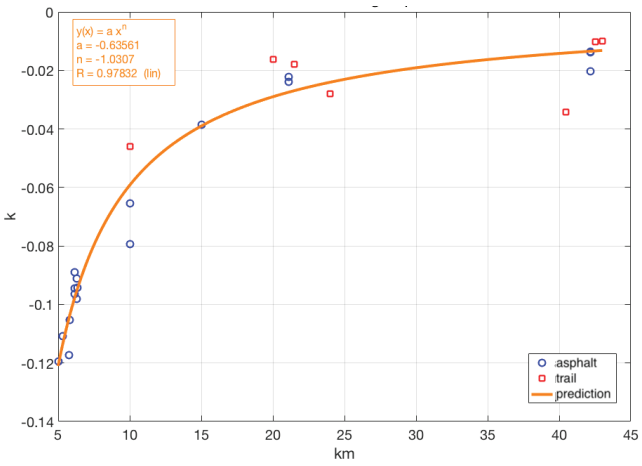

Fig. 2. Relation between groups and distance collapses depending on the length of the race.

Modeling chemotactic response and contact interactions of amoeboid cells

Eduardo Moreno and Sergio Alonso
Physics Department, Universitat Politècnica de Catalunya, av. Dr. Marañón 44-50, 08028 Barcelona, Spain

Individual cells are connected with the environment, they sense the the exterior with their receptors and process the incoming information. They respond first chemically (polarization) and second mechanically (locomotion) moving toward food, enemy or target direction. It is known that without external signal the cell may randomly swing producing random dynamics, while in other way under a chemical gradient the cell produces a persistent motion in gradient's direction [1, 2, 3].

We apply a phase field for the description of the interior (where the polarization processes takes place) and the exterior of the cells (where the biochemical species diffuse) to model the interaction of both environments at the membrane of the cell. The model we use is described in [2] and has the particularity to include a parameter that tunes the balance between the mechanism of polarity formation and intracellular noise. The model is described as follow

$$\tau\frac{\partial\phi}{\partial t} = \gamma\left(\frac{-G^{'}}{\epsilon^2} + \nabla^2\phi\right) - \beta\left[\left(\int\phi dx - A_0\right) + \alpha c\right] \mid \nabla\phi \mid . \tag{1}$$

In other way, inside the cell there is a reaction-diffusion process governed by a biochemical component c according to

$$\frac{\partial c}{\partial t} = k_\alpha c(1-c)(c-\delta) - \rho c + \frac{1}{\phi}\nabla\cdot(\phi D\nabla c) + \xi(\boldsymbol{x},t)\phi(1-\phi). \tag{2}$$

We tune different parameters of the biochemical reaction rates to compare the resulting dynamics of the computer model of the motion of *Dictyostelium discoideum* in absence and presence of a linear chemical gradients of the chemo-attractant cAMP (cyclic adenosine monophosphate) as shown in Figs. 1 (a) and (b), respectively. One of this parameters is k_α, which is responsible of the transition from slow erratic for small values to fast and persistent motion for large values.

Furthermore, we add to the model the contact interaction among cells under confinement and in absence of chemical gradient where we see that the cells follow circular trajectories as observed in many experiments (see Fig. 2).

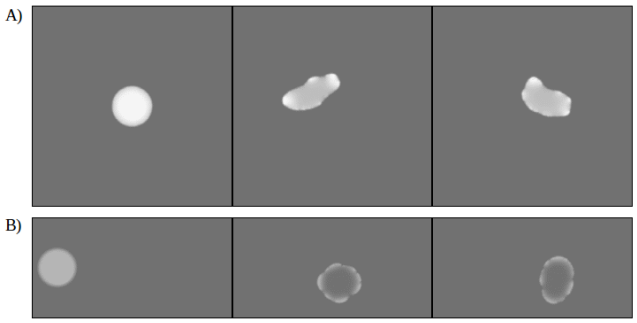

Fig. 1. Screenshots taken every 200 seconds for cell trajectories and parameter $k_\alpha = 2$. (a) Simulation results of a cell in absence of cAMP gradient in a 60×60 μm^2 grid. (b) Simulation results of a cell in presence of cAMP gradient in a 30×60 μm^2 grid.

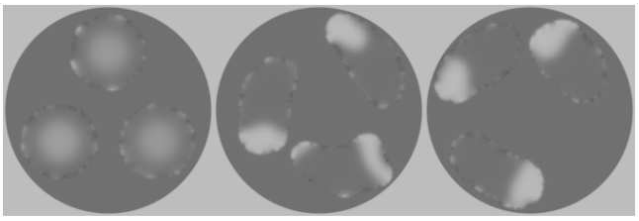

Fig. 2. Simulation Results of three cells under confinement and absence of cAMP in a 33.75×33.75 μm^2 grid. The screenshots were taken every 200 seconds with parameter $k_\alpha = 2$.

[1] L. Song, S. M. Nadkarni, H. U. Bödeker, C. Beta, A. Bae, C. Franck, W.-J. Rappel, W. F. Loomis, and E. Bodenschatz, *Dictyostelium discoideum* chemotaxis: Threshold for directed motion, Eur. J. Cell Biol. **85**, 981-989 (2006).

[2] S. Alonso, M. Strange M, and C. Beta, Modeling random crawling, membrane deformation and intracellular polarity of motile amoeboid motion, (to be published).

[3] G. Amselem, M. Theves, A. Bae, E. Bodenschatz, and C. Beta, A stochastic description of *Dictyostelium* chemotaxis, PLoS ONE **7**, e37213 (2012).

Reducción de entropía por información en *flashing ratchets* retroalimentadas

Daniel Villarrubia Moreno[1] y Francisco J. Cao García[1,2]
[1]Departamento de Estructura de la Materia, Física Térmica y Electrónica, Universidad Complutense de Madrid, pl. Ciencias 1, 28040 Madrid, España
[2]Instituto Madrileño de Estudios Avanzados en Nanociencia (IMDEA Nanociencia), c. Faraday 9, 28049 Madrid, España

Las *ratchets* son sistemas que generan un flujo de partículas en contra de una cierta fuerza externa mediante la rectificación de su movimiento browniano, de manera que puede obtenerse una cierta cantidad de trabajo de ellas. Su funcionamiento se basa en el encendido o apagado de un determinado potencial que obliga a las partículas a desplazarse hasta sus mínimos cuando está encendido, y que las permite difundir libremente cuando está apagado. El encendido y apagado del potencial está determinado por un protocolo que puede ser retroalimentado. En este caso, cada cierto tiempo se mide la posición de las partículas en el sistema, y con la información obtenida se determina qué acción realizar con el potencial. El uso de la información sobre el estado del sistema permite optimizar el protocolo de control y así extraer una cantidad mayor de trabajo.

En el estudio de los motores brownianos, supondremos que las partículas que lo componen siguen una evolución caracterizada por una cadena markoviana, lo que lleva a que su ecuación de evolución es la ecuación de Langevin sobreamortiguada

$$\gamma\dot{x} = -\alpha(t)\partial_x V(x) + F_{\text{ext}}(x) + \xi(t). \qquad (1)$$

La correlación existente entre la medida de la posición de la partícula y la consecuente acción posterior del controlador implica una reducción de la entropía física del sistema entre antes y después de cada medida y actuación del controlador. Esta reducción resulta ser exáctamente la información mutua entre la posición y la acción llevada a cabo.

Generalizando esto para una serie de k medidas consecutivas, y teniendo en cuenta la no markovicidad del historial de acciones del controlador (por venir prefijadas por la posición), se obtiene la tasa de reducción de entropía

$$\Delta H_k(C) = \lim_{k\to\infty} \frac{H(C_k, C_{k-1}, ..., C_1)}{k}. \qquad (2)$$

Este límite no se sabe obtener explícitamente por la no markovicidad de las acciones del controlador; por eso aquí obtenemos numéricamente los primeros *órdenes* del mismo. Se entiende por órdenes los distintos valores crecientes del número de medidas k. Existen unas cotas entre las cuales debe encontrarse el valor de dicho límite: H_{up} y H_{low}.

El análisis de estos resultados muestra que debido a la redundancia de la información, la reducción de entropía es mayor para mayores periodos de control, mientras que la reducción de entropía por unidad de tiempo es mayor para tiempos de control más cortos.

[1] D. V. Moreno, *Reducción de Entropía por Información en* Ratches *Retroalimentadas Espacialmente Contínuas*, trabajo de fin de máster, Universidad Complutense de Madrid, 2017.

[2] J. Jarillo, T. Tangarife, and F. J. Cao, Efficiency at maximum power of a discrete feedback ratchet, Phys. Rev. E **93**, 012142 (2016).

[3] F. J. Cao and M. Feito, Thermodynamics of feedback controlled systems, Phys. Rev. E **79**, 041118 (2009).

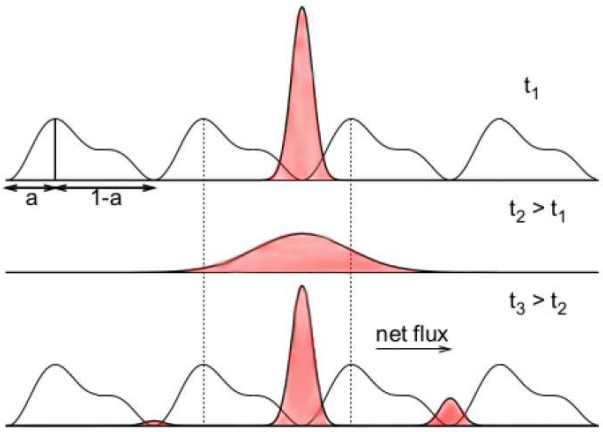

Fig. 1. Evolución de las partículas en el interior de la *ratchet*. Obsérvese cómo la fase del potencial apagado permite sobrepasar el máximo del potencial, lo que es poco probable cuando está encendido. La asimetría del potencial o del protocolo son claves para generar transporte dirigido.

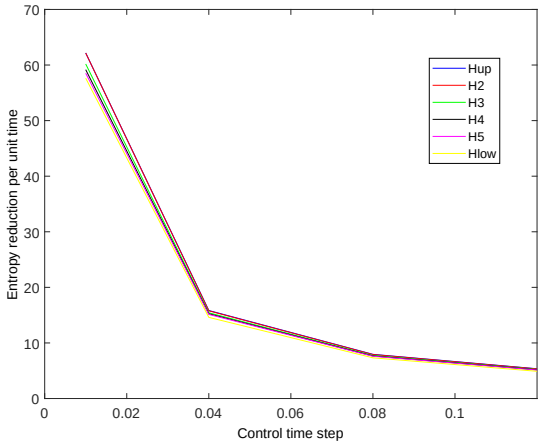

Fig. 2. Reducción de entropía por unidad de tiempo en función del tiempo de control. Las distintas líneas muestran los distintos órdenes calculados, así como las cotas superior e inferior existentes.

Solvent hydrodynamics enhances the collective diffusion of membrane lipids

S. Panzuela† and R. Delgado-Buscalioni
Department of Theoretical Condensed Matter Physics, Autonomous University of Madrid, Spain

Our work unveils a new and generic mechanism for collective lipid diffusion in membranes which is due to the hydrodynamic interaction between the membrane and the embedding solvent. Since 1975, the collective dynamics of membrane lipids have been described by the celebrated Saffman-Delbrück (SD) theory which predicts the slowing down of large flow patterns of lipids due to the solvent's *tangential* friction on the membrane[1]. Following the SD theory, lipid flow patterns smaller than the Saffman length λ_S (about one micron) are thought to be unaffected by the solvent traction, leading to the believe that the lipid hydrodynamics at submicron scale is essentially 2D, with negligible momentum exchange with the solvent.

We show that this conclusion is incorrect and in this respect prove that the SD theory is incomplete. We performed molecular dynamics and coarse-grained models with implicit 3D hydrodynamics and find that the ambient liquid strongly *enhances* the collective diffusion of lipids at all scales, even much smaller than λ_S. Our findings match quantitatively with the theoretical predictions for the anomalous collective diffusion of colloids confined in a 2D plane but embedded in a 3D solvent [2, 3]. While SD theory considers the solvent *tangent traction* on the membrane, we find that the solvent momentum in *normal direction* spreads tangentially over the plane creating long-ranged repulsive hydrodynamic forces between lipids. The resulting collective diffusion becomes anomalous, increasing proportionally to the disturbance wavelength. This phenomena is dominant over at least 100 nanoseconds, gradually decaying at long times, leading to the expected Saffman-Debruck membrane hydrodynamics.

Our results at large wavenumbers are in good agreement with spin echo experiments [4] and confirm the existence of strong localized lipid currents [5], probably related to the described phenomena. The life-span of the present phenomena (submicron scales and hundred of nanoseconds and below) is a new milestone in the understanding of the collective motion of lipids, key for many biological process such as the spontaneous nanopore formation, kinetics of lipid rafts and protein collective motion, to name a few.

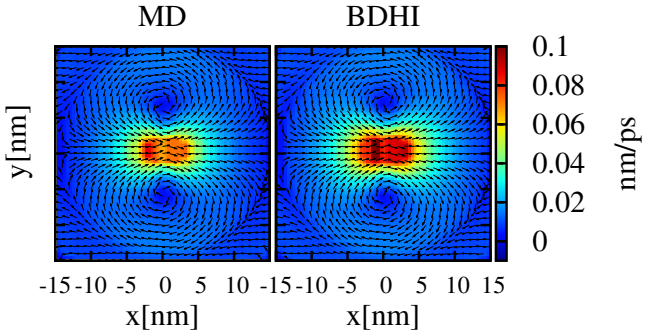

Fig. 1. Averaged velocity field evaluated from lipid displacements with respect to a central tagged lipid. Colour box represent the modulus of the velocity field.

† E-mail: sergio.panzuela@uam.es

[1] P. G. Saffamn and M. Delbrück, Proc. Natl. Acad. Sci. USA **72**, 3111 (1975).

[2] S. Panzuela, R. P. Peláez, and R. Delgado-Buscalioni, Phys. Rev. E **95**, 12602 (2017).

[3] J. Bleibel, A. Domínguez, and M. Oettel, Phys. Rev. E **95**, 032604 (2017).

[4] C. L. Armstrong, L. Toppozini, H. Dies, A. Faraone, M. Nagao, and M. C. Rheinstädter, ISRN Biophysics **2013**, 439758 (2013).

[5] T. Apajalahti, P. Niemelä, P. N. Govindan, M. S. Miettinen, E. Salonen, S.-J. Marrinkd, and I. Vattulainen, Faraday Discuss. **144**, 411 (2010).

Information transmission in random and modular neuronal networks

Cristina Masoller and Maria Masoliver Vila
Universitat Politècnica de Catalunya, Terrassa Campus, rbla. Sant Nebridi s/n, 08022 Terrassa, Spain

Despite intensive research, the mechanisms by which neurons encode information in spike trains remain poorly understood. Recent work has focused on how a FitzHugh-Nagumo neuron encodes a weak (subthreshold) sinusoidal signal, in a noisy environment [1], and on the impact of a second neuron, which does not perceive the signal [2]. By applying a symbolic time-series analysis method to the sequence of inter-spike-intervals (ISIs) [3], preferred and infrequent spike patterns were detected, whose probabilities encode information of both, the amplitude and the frequency of the weak signal.

Here we investigate whether this symbolic information-encoding mechanism is robust when we work with larger neurons ensembles. First we analyze how the signal is transmitted and encoded in a small random network and second in a small modular network (motivated by the modular structure of the brain). We assume that the weak signal is perceived by the neurons in only one of the modules, and the information is transmitted to the other modules in the form of more expressed and less expressed spike patterns. We analyse how the coupling parameters, the network size and its modular structure impact the encoding of weak periodic or aperiodic signals.

[1] J. A. Reinoso, M. C. Torrent, and C. Masoller, Emergence of spike correlations in periodically forced excitable systems, Phys. Rev. E **94**, 032218 (2016).

[2] M. Masoliver and C. Masoller, Subthreshold signal encoding in coupled FitzHugh-Nagumo neurons, Sci. Rep. **8**, 8276 (2018).

[3] C. Bandt and B. Pomper, Permutation entropy: A natural complexity measure for time series, Phys. Rev. Lett. **88**, 174102 (2002).

The influence of network topologies in drug treatments

Victoria Doldán-Martelli[1] and David Gómez Míguez[2]
[1]Grupo Interdisciplinar de Sistemas Complejos, Departamento de Matemáticas, Universidad Carlos III de Madrid, Leganés, Spain
[2]Centro de Biología Molecular Severo Ochoa, Universidad Autónoma de Madrid, Madrid, Spain

An accurate prediction of the outcome of a given drug treatment requires quantitative data of all parameters and concentrations involved as well as a detailed characterization of the network of interactions where the target molecule is embedded. This is especially relevant if nonlinearities and feedback interactions are involved in the signaling pathway.

Here we present a high-throughout *in silico* screening of all potential networks of three nodes to study the effect of the initial conditions of the network in the efficiency of drug treatment.

To characterize the effect of the network topology, we compare the dose-response curves of the same drug treatment starting from two different initial conditions in the activity of the network [see Fig. 1 (right)].

Our analysis reveals that the initial conditions affect the efficiency of the treatment in most network topologies of three nodes. This dependence is translated into modifications in the dose-response curves and changes in the *EC50* as well as in the overall effect of the inhibitor.

Moreover, we found network configurations that show a novel behavior characterized by the inversion of the steady states respect to the initial conditions. In some conditions, this "inverse bistability" of the target node can also result in "inverse hysteresis loops", where the reduction of the efficiency of the treatment also occurs when the concentration of inhibitor is varied gradually. An example of a network topology inducing inverse hysteresis and its corresponding dose-response curve is shown in Fig. 1.

Finally, our study shows that most of the topologies that present this inverse bistability and hysteresis behaviors contain core motifs of four links, composed by a positive feedback and a negative regulation. These results were represented in an atlas (Fig. 2) that correlates topologies by their architecture.

Our results illustrate how the dependence of the drug effect on the initial state of the network may be affecting the reproducibility of drug studies and clinical trials.

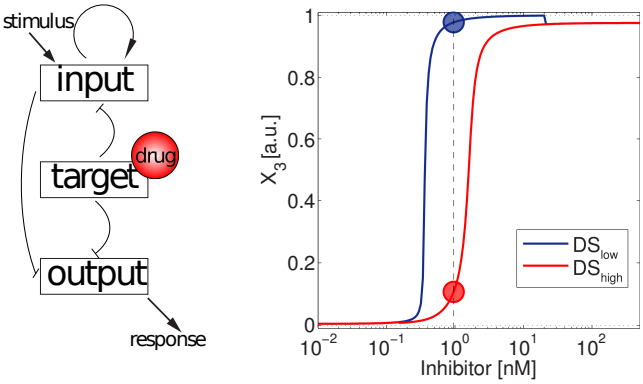

Fig. 1. (Left) Example of a network architecture that induces inverse hysteresis. (Right) Dose-response curves DS_{low} (blue) and DS_{high} (red) for initial conditions IC_{low} and IC_{high}, respectively.

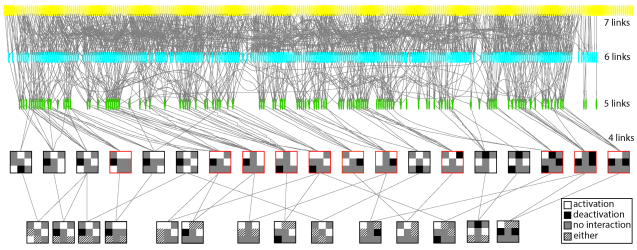

Fig. 2. Atlas for all network topologies that induce "inverse bistability" and "inverse hysteresis loops". Circles represent each of the topologies where our screening has shown inverse bistable response to drug treatment.

Linguistic laws in oral communication

I. G Torre[1], B. Luque[1], L. Lacasa [2], J. Luque[3], and A. Hernández-Fernández[4],
[1]Departamento de Matemática Aplicada, ETSIAE, Universidad Politécnica de Madrid, Spain
[2]School of Mathematical Sciences, Queen Mary University of London, Mile End Road E14NS, London, UK
[3]Telefonica Research, Edificio Telefónica-Diagonal 00, Barcelona, Spain
[4]Complexity and Quantitative Linguistics Lab, Institut de Ciències de l'Educació, Universitat Politècnica de Catalunya, Spain

During the last decades, a great effort has been made to describe and quantify statistical regularities in natural language in written corpus and those patterns, or linguistic laws, have been proposed to be ubiquity and universal. Some of these well-known statistical laws are [1]: Zipf's law (relation between the frequency of appearance of words), Brevity Law (tendency of more frequent elements in communication to be shorter), Heap's Law (vocabulary of a text grows allometrically with the text length), Menzerath-Altmann law (the longer a word, measured in number of syllables, the shorter the syllabic duration) [1][2].

In our previous work we proposed a method that allows to measure those patterns in acoustic signal without needing access to the language corpus underneath. We recovered some linguistic laws of human communication at timescales below the phoneme and another link between complexity and criticality in a biological system was found [2].

In this research we inted to unify both point of view studying linguistic laws in oral communication. We use automated forced alignment techniques for segmenting at word and phonemic level speech signal coming from spontaneus conversation in Spanish. Then, we analyze well-known physical magnitudes of oral communication such as time elapsed in seconds and energy released. Statistical laws are usually explained in terms of efficiency of communication that have been optimized during evolution so it is expected that this process has been developed in oral language and that the laws studied in written corpus emerge from it [3].

In Fig. 1 we show the Brevity Law in terms of duration and energy released instead of the usual way to use letters or syllables. It is shown that there is a tendency of more frequent words to be shorter and also less energetic. Heap's law is represented in Fig. 2 showing that exists a clear regularity in the appearance of new words according to the length of the text measured both in the number of total words (tradicional way) and in elapsed time (seconds). Finally we report Menzerath-Altmann's law (Fig. 3) at two levels: Outer panel shows the relationship between the size of phrases in terms of number of words and the size of words in terms of their mean duration; Inner panel represents the relation between the size of words in terms of number of phonemes and the size of phonemes in terms of their mean duration.

Although there are previous studies in which these scaling laws of linguistics are analyzed in written texts and in oral corpus, as far as we know, this is the first time that these linguistic laws are reported from spontaneous speech using both physical magnitudes (duration and energy) of acoustical communication.

[1] M. D. Esposti, E. G. Altmann, and F. Pachet, *Creativity and Universality in Language* (Springer, 2016).

[2] I. G. Torre, B. Luque, L. Lacasa, J. Luque, and A. Hernández-Fernández, Emergence of linguistic laws in human voice, Sci. Rep. **7**, 43862 (2017).

[3] R. Ferrer-i-Cancho, A. Hernández-Fernández, D. Lusseau, G. Agoramoorthy, M. J. Hsu, and S. Semple, Compression as a universal principle of animal behavior, Cogn. Sci. **37**, 1565-1578 (2013).

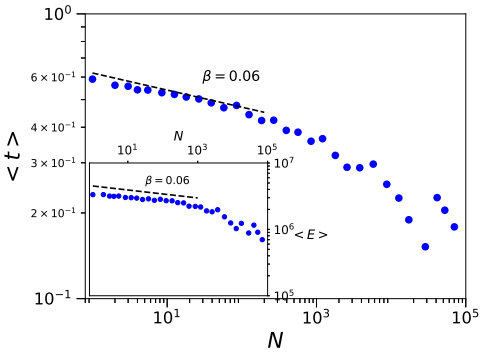

Fig. 1. Zipf's Law of Brevity in oral communication. It is shown mean duration of vocabulary (outer) and mean energy released (inner) depending on the frequency of appearance.

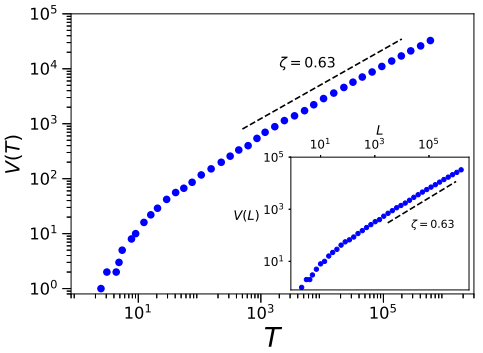

Fig. 2. Heap's law: Number of different words depending on time elapsed T (outer) and on the total words L that have been appeared (inner).

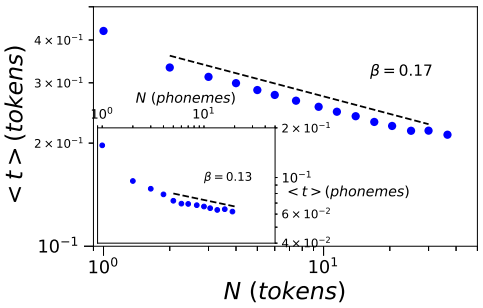

Fig. 3. Menzerath-Altmann's law in oral communication at using two different scales.

On a graph-theoretical structure of real numbers

Jorge Calero[1], Bartolo Luque[1], and Lucas Lacasa[2]
[1]Department of Applied Mathematics and Statistics, EIAE, Technical University of Madrid, pl. Cardenal Cisneros, 28040 Madrid, Spain
[2]School of Mathematical Sciences, Queen Mary University of London, Mile End Road E14NS, London, UK

In this work, we study properties of real numbers through a set of graphs named *Farey graphs*, which we show are in bijection with real numbers in $[0,1]$. The Farey graphs can be navigated by an operator $\mathcal{R}$. This operator induces a dynamics and we make a classification of dynamical attractors (fixed points, periodic or aperiodic orbits and chaos) which has a correspondence in the real numbers. Furthermore, we can define an entropy on Farey graphs, and its maximization connects with the previous dynamical classification.

The Farey sequence of order n is the ordered set of irreducible fractions between $[0,1]$ whose denominators do not exceed n. The Farey sequence $\mathcal{F}_n$ has a representation called *Farey Tree* (see Fig. 1). When $n \to \infty$, the Farey sequences are the real numbers between $[0,1]$.

The set of Farey graphs is constructed recursively using a initial graph (two nodes joined by a link) and an inner operation named concatenation (see Fig. 2). We prove that there exists a bijection between the Farey graphs and Farey fractions, ie, between the interval $[0,1]$. This implies that the Farey graphs have an order and we can represent them in a tree named *Farey Graph Tree*.

The operator $\mathcal{R}$ is a map of the set of Farey graphs into itself removing the nodes with degree $k=2$ and merging its two incident edges into a single edge. $\mathcal{R}$ has an algebraically equivalent operator in real numbers: the operator $T:[0,1]\to[0,1]$

$$T(\omega)=\begin{cases}\frac{\omega}{1-\omega} & \text{if } \omega \le 1/2\\ 1-\frac{1-\omega}{\omega} & \text{if } x>1/2\end{cases}. \qquad (1)$$

The dynamics of this operator induces a classification of real numbers into families:

1. **Fixed Points:** The point $\omega = 0$ is an attractor for all rational initial conditions.
2. **Unstable Periodic Orbits:** The quadratic irrationals belong to a cycle, i.e, they verify:
   $\exists\, m \ge 2 :\ T^{(m)}(\omega)=\omega$ iff ω is quadratic irrational.
3. **Chaos:** All other initials conditions (e.g, non-quadratic algebraic irrational and trascendental numbers).

Finally, we are interested in a particular graph entropy over the degree distribution $P(k)$. We compute this entropy for all graphs with at least 1000 nodes (see Fig. 3). We prove that the most Farey-entropic graph corresponds to the fractional part of the Golden ratio. Other form a periodic orbit and they correspond to the quadratic irrationals.

[1] R. L. Graham, D. E. Knuth, and O. Patashnik, *Concrete Mathematics* (Addison-Wesley, 1989/1994).

[2] B. Luque, F. J. Ballesteros, A. M. Nunez, and A. Robledo, Quasiperiodic graphs: Structural design, scaling and entropic properties, J. Nonlinear Sci. **23**, 335-342 (2013).

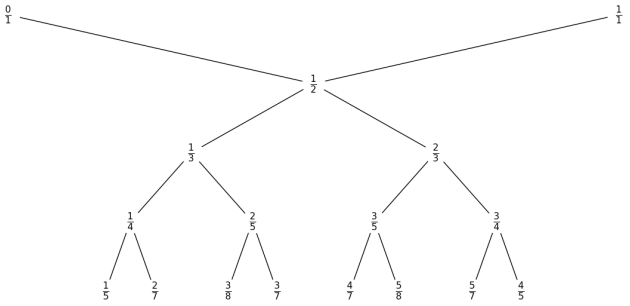

Fig. 1. The first five layers of Farey Tree.

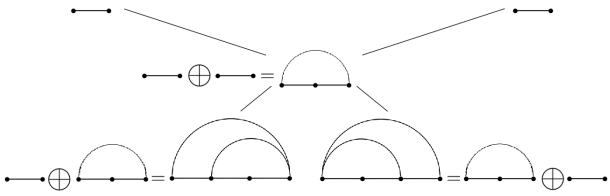

Fig. 2. An illustration of the concatenation operation.

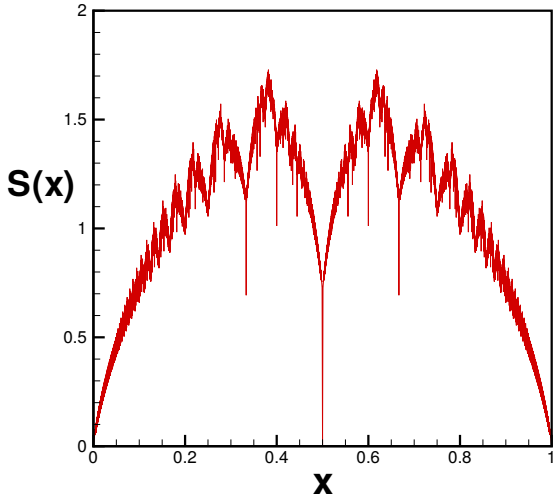

Fig. 3. Number entropy $h(\omega) = -\sum P(k)\log P(k)$ for $G = G_\omega$.

Dynamical phase transitions in dissipative strongly-interacting atomic ensembles

Carlos Pérez-Espigares[1], Juan P. Garrahan[1], Igor Lesanovsky[1], and Ricardo Gutiérrez[1,2]
[1]School of Physics and Astronomy and Centre for the Mathematics and Theoretical Physics of Quantum Non-equilibrium Systems, University of Nottingham, Nottingham NG7 2RD, UK
[2]Complex Systems Group & GISC, Universidad Rey Juan Carlos, 28933 Móstoles, Madrid, Spain

The physics of highly-excited (Rydberg) atoms is governed by blockade interactions that hinder the excitation of atoms in the proximity of a previously excited one. In the limit of strong dephasing, the evolution is given by a classical master equation with configuration-dependent rates for transitions between the ground state and the excited state [1]. Those rates contain a single parameter R, which gives the length of the blockaded region around an excited atom [2]. From this blockade, which is reminiscent of the excluded volume effects of soft condensed matter, a space-time dynamic heterogeneity similar to what is observed in the dynamics of glass-forming systems arises.

We establish theoretically the existence of a glassy dynamical regime in a dissipative Rydberg gas, which originates from a phase coexistence at a first-order phase transition, see Fig. 1. In our analysis, we consider the activity per unit time $k = K/t$, where K counts the number of transitions in a trajectory of duration t, as the order parameter. The transition occurs between an active phase of low density in which dynamical processes take place on short timescales, and an inactive phase in which excited atoms are dense and the dynamics is highly arrested. The control parameter conjugate to k is the field s, which "tilts" the systems towards more (if $s < 0$) or less (if $s > 0$) active dynamics. The inactive space-time regions that appear as the transition is approached from the active side, are "bubbles of inactivity", corresponding to a manifestation in trajectories of fluctuations associated with the dynamical first-order transition (cf., e.g., vapor bubbles in a liquid near liquid-vapor coexistence). The natural dynamics ($s = 0$) lies precisely at the coexistence point between the two phases.

We probe the transition through the numerical diagonalization of the relevant dynamical generator for finite sizes. Furthermore, a mean-field approach gives us analytical insight into the transition, and allows us to explore the relevant phase diagram as function of the blockade length R, and also the decay rate κ of the excited state, which is a parameter of great experimental relevance. For small R, the transition is shown to end at a critical point beyond which a sharp crossover is observed, see Fig. 2. A sufficiently strong decay also smooths out the transition, the critical point corresponding to a value of κ that is experimentally accessible in modern cold atoms experiments.

Not only have we unveiled a dynamical phase transition from which a previously observed complex dynamics stems, but our results will also be useful in the development of protocols for engineering Rydberg interactions with the aim of attaining specific dynamical regimes.

[1] I. Lesanovsky and J. P. Garrahan, Kinetic constraints, hierarchical relaxation, and onset of glassiness in strongly interacting and dissipative Rydberg gases, Phys. Rev. Lett. **111**, 215305 (2013).

[2] R. Gutiérrez, J. P. Garrahan, and I. Lesanovsky, Self-similar nonequilibrium dynamics of a many-body system with power-law interactions, Phys. Rev. E **92**, 062144 (2015).

[3] C. Pérez-Espigares, I. Lesanovsky, J. P. Garrahan, and R. Gutiérrez, Glassy dynamics due to a trajectory phase transition in dissipative Rydberg gases, arXiv:1804.03070.

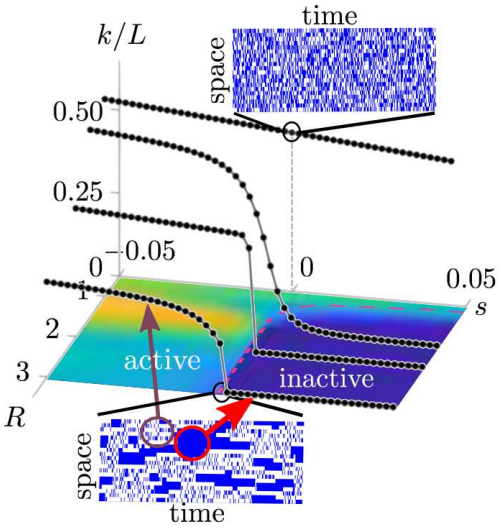

Fig. 1. Dynamical first-order phase transition underlying the dynamics of dissipative Rydberg gases. Activity $k(s)/L$ as a function of the tilting field s and the blockade length R. Representative trajectories for $R = 1$ (upper panel) and $R = 3$ (lower panel) are displayed. Blue and white indicate excited and ground state atoms, respectively.

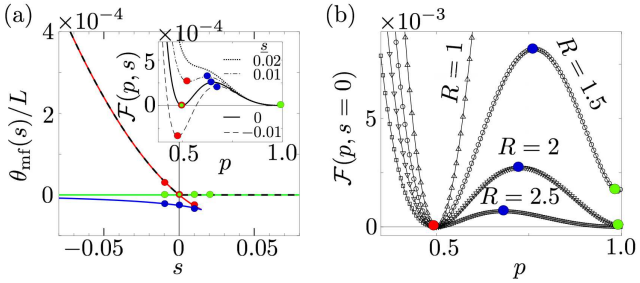

Fig. 2. Mean-field analysis of the dynamical phase transition. (a) Negative variational free energy $-\mathcal{F}(p, s)$ for $R = 3$ evaluated at the stationary points including two maxima (red and green lines) and one minimum (blue line), and normalized SCGF $\theta_{\rm mf}(s)/L$ (dashed black line). Inset: Variational free energy $\mathcal{F}(p, s)$ as a function of p in the neighborhood of $s = 0$. (b) Variational free energy $\mathcal{F}(p, s = 0)$ for values of R around the critical value for a transition at $s = 0$.

Unveiling the chaotic structure in molecular systems using Lagrangian descriptors

F. Revuelta[1,2], R. M. Benito[1], and F. Borondo[2,3]
[1]Grupo de Sistemas Complejos, Escuela Técnica Superior de Ingeniería Agronómica, Alimentaria y de Biosistemas, Universidad Politécnica de Madrid, av. Puerta de Hierro 2-4, 28040 Madrid, Spain
[2]Instituto de Ciencias Matemáticas (ICMAT), Cantoblanco, 28049 Madrid, Spain
[3]Departamento de Química, Universidad Autónoma de Madrid, Cantoblanco, 28049 Madrid, Spain

The phase space structure of a dynamical system determines, among other issues, its regular or chaotic behavior, and then several indicators have been developed in order to correctly detect, characterize, and analyze it. Among them, the illustrative Poincaré surface of section (PSOS) or the more quantitative Lyapunov exponents [1] are worth mentioning.

In this communication, published in [2], we apply the Lagrangian descriptor method [3, 4], defined by the p-norm of a dynamical flow $\dot{\mathbf{z}} = \mathbf{f}(\mathbf{z}, t)$ as

$$M_p(\mathbf{z}_0, t_0, \tau) = \int_{-\tau}^{\tau} dt \sum_{i=1}^{n} |\dot{z}_i|^p, \qquad (1)$$

where $p \leq 1$, and τ is the integration lapse of time to unveil the chaotic structure of the phase space of the LiNC⇌LiCN isomerizing molecular system, using the two degrees-of-freedom (2-dof) Hamiltonian model [5] defined by

$$H = \frac{1}{2\mu_1} P_R^2 + \frac{1}{2}\left(\frac{1}{\mu_1 R^2} + \frac{1}{\mu_2 r_{\text{eq}}^2}\right) P_\theta^2 + V(R, r_{\text{eq}}, \theta), \qquad (2)$$

where R is the distance between the Li and the center of mass of the C-N fragment, r the C-N distance (hold frozen at its equilibrium value r_{eq} in the 2-dof approximation), θ the angle between them. P_R, P_θ (and P_r in the 3-dof version) are the corresponding conjugate momenta and $\mu_{1,2}$ the Li-CN and C-N reduced masses, respectively. The potential energy surface $V(R, r_{\text{eq}}, \theta)$ exhibits two wells, one at $\theta = \pi$ rad corresponding to the most stable isomer with linear configuration Li-NC, and the other at $\theta = 0$ rad for Li-CN. Along the minimum energy path $R_{\text{MEP}}(\theta)$ joining these two wells there is a saddle with triangular configuration that appears at $\theta \simeq 0.28\pi$ rad. We also study the importance of different effects in the definition (1), such as using p-norms instead of the *standard* one, or the magnitude of the integration time lapse.

Some results for the (ψ, P_ψ)-PSOS computed for $\rho = 0$ and $\dot{\rho} > 0$ and $E = 4000$ cm^{-1}, using the following canonical transformation

$$\begin{aligned} \rho &= R - R_{\text{MEP}}(\theta), \quad & P_\rho &= P_R, \\ \psi &= \theta, & P_\psi &= P_\theta + \left(\tfrac{dR_{\text{MEP}}}{d\theta}\right)_{\theta=\psi} P_\rho, \end{aligned} \qquad (3)$$

are shown in the panel (a) of the figure. In it, the existence of two regions of regular motion at the isomers, embedded in a sea of chaos, is apparent. In panel (b) we show the corresponding values of the Lagrangian descriptor for trajectories starting at points in the PSOS. Notice the ability of Lagrangian descriptors to identify the different structures in phase space, such as in the areas of regularity at the isomers and at $\theta \simeq 0.6\pi$ rad, or even more striking of the homoclinic tangle originated at the saddle; this fact is explained since the Lagrangian descriptors present singularities along the invariant manifolds, which render abrupt changes in the colormap in (b).

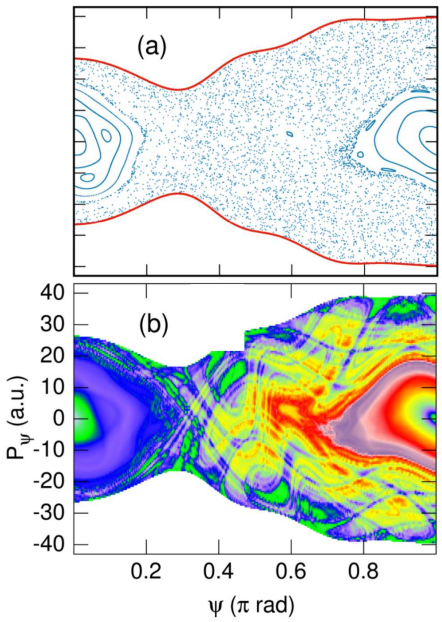

Fig. 1. Composite Poincaré surface of section (a), and Lagrangian descriptors (b) for the 2-dof model ($r = r_{\text{eq}}$, $P_r = 0$ a.u.) of the LiCN/LiNC molecular system. The computations have been performed by setting in Eq. (1) $p = 0.4$ and $\tau = 2 \cdot 10^4$ a.u. for a vibrational energy equal to E = 4000 cm^{-1}.

Finally, we have also applied the Lagrangian descriptors to study a more accurate model of our molecular system that includes the three vibrational dof's, i.e., not freezing r at its equilibrium value in (2, where the popular and useful PSOS method cannot be applied. Results will be presented at the conference.

[1] A. J. Lichtenberg and M. A. Lieberman, *Regular and Chaotic Dynamics* (Springer, New York, Berlin, Heidelberg, 2010).

[2] F. Revuelta, R. M. Benito, and F. Borondo, Lagrangian descriptors and the phase space structures of molecular systems, (in press).

[3] J. A. J. Madrid and A. M. Mancho, Distinguished trajectories in time dependent vector fields, Chaos **19**, 013111 (2009).

[4] C. Lopesino, F. Balibrea-Iniesta, V. J. García-Garrido, S. Wiggins, and A. M. Mancho, A theoretical framework for Lagrangian descriptors, Int. J. Bifurcation Chaos **27**, 1730001 (2017).

[5] F. Revuelta, T. Bartsch, P. L. Garcia-Muller, R. Hernandez, R. M. Benito, and F. Borondo, Transition state theory for solvated reactions beyond recrossing-free dividing surfaces, Phys. Rev. E **93**, 062304 (2016).

Let's cool the world by illuminating it: A thermodynamical model for heat harversters

J. J. Fernández
Departamento de Física Fundamental, Universidad Nacional de Educación a Distancia (UNED), 28040 Madrid, Spain

Emissive energy harversters (EEHs) have been proposed in the last 3 years as a new form to produce clean electricity by converting the energy waste (heat) into electricity [1, 2, 3, 4, 5, 6, 7]. In the first works the researchers presented calculations of EHHs efficiencies obtained using the Detailed Balance Method (DBM) and the first principle of the thermodynamics. According to that calculations EEHs working at temperatures between 500 and 700 K are able to produce output powers of a few tenths of W/m^2 at efficiencies about between the 20 and 30%.

Very recently I have published a work [8] in which an endoreversible model of an EHH is developed. This new model combines the DBM and the endoreversible thermodynamics and allows to calculate EHH efficiencies taking into account the entropy losses happening in the interaction of the EHH and the hot/cold reservoirs assisting the conversion. In this poster I present the most important features of the model and discuss the impossibilities of optimizing the efficiency of EHHs with respect to any of the internal parameters defining its functioning.

[1] S. J. Byrnes, R. Blanchard, and F. Capasso, Harvesting renewable energy from Earth's mid-infrared emissions, Proc. Natl. Acad. Sci. U.S.A **111**, 3927-3932 (2014).

[2] R. Strandberg, Theoretical efficiency limits for thermoradiative conversion, J. Appl. Phys. **117**, 055105 (2015).

[3] R. Strandberg, Heat to electricity conversion by cold carrier emissive energy harversters, J. Appl. Phys. **118**, 215102 (2015).

[4] W.-C. Hsu, J. K. Tong, B. Liao, Y. Huang, S. V. Boriskina, and G. Chen, Entropic and near-field improvements of thermoradiative cells, Sci. Rep. **6**, 34837 (2016).

[5] S. V. Boriskina, J. K. Tong, W.-C. Hsu, B. Liao, Y. Huang, V. Chiloyan, and G. Chen, Heat meets light on the nanoscale, Nanophotonics **5**, 134-160, (2016).

[6] T. Liao, X. Zhang, X. Chen, B. Lin, and J. Chen, Negative illumination thermoradiative solar cell, Optics Lett. **42**, 3236 (2017).

[7] J. J. Fernández, Thermoradiative energy conversion with quasi-Fermi level variations, IEEE Trans. Electron Devices **64**, 250-255 (2017).

[8] J. J. Fernández, Endoreversible model of thermal to radiative energy converters, J. Appl. Phys. **123**, 164501 (2018).

Hydrodynamic quantization in bouncing droplets

J. Montes[1], F. Revuelta[1,2], and F. Borondo[2,3]
[1]Grupo de Sistemas Complejos, Escuela Técnica Superior de Ingeniería Agronómica, Alimentaria y de Biosistemas, Universidad Politécnica de Madrid, av. Puerta de Hierro 2-4, 28040 Madrid, Spain
[2]Instituto de Ciencias Matemáticas (ICMAT), Cantoblanco, 28049 Madrid, Spain
[3]Departamento de Química, Universidad Autónoma de Madrid, Cantoblanco, 28049 Madrid, Spain

Over the past few years, a new set of experiments consisting of a milimetric droplet bouncing on an excited (below Faraday's threshold) liquid surface [1] has shown in a macroscopic system features that were assumed of only purely quantum systems, such as the interference pattern through a double slit [2], tunneling [3], quantization of periodic orbits [4], or orbital level spliting [5].

The fascinating analogies existing between quantum systems and bouncing droplets can be understood through the pilot-wave theory developed by Louis de Broglie [6]: In the hydrodynamic setting, the vibrating surface of the fluid plays the role of the underlying (quantum) pilot-wave, whose shape determines the dynamics of the particle (bouncing droplet).

In this communication [7], we push the analogies between bouncing droplets and quantum systems one step further by demonstrating the existence of some hydrodynamic constant in the limit of high memory, which plays a role similar to that of the Planck constant in quantum mechanics. For that purpose, we analyze the dynamics of a bouncing droplet in the highly chaotic quartic potential [8, 9]

$$V(x,y) = \frac{1}{2}x^2y^2 + \frac{1}{400}(x^4+y^4), \qquad (1)$$

by solving the corresponding equation of motion [1]

$$\kappa\,\ddot{\mathbf{q}}(t) + \dot{\mathbf{q}}(t) = -\nabla V(\mathbf{q}(t)) - \beta\,\nabla\psi(\mathbf{q}(t)), \qquad (2)$$

where $\mathbf{q}(t)$ is the particle position vector at time t, κ is the reduced mass of the particle, β is the memory strength parameter, and $\psi = \int_{-\infty}^{t} J_0(|\mathbf{q}-\mathbf{q}(s)|)\,e^{-(t-s)}\,ds$ is a term, evaluated along the droplet trajectory, accounting for the force exerted by the liquid surface.

Panel (a) of Fig. 1 shows the average height of the liquid surface, i.e., the mean field, as a function of the position x and β. The liquid surface shows a very clear regular pattern at certain values of the memory strength β, with a number of nodes that increases with the value of the parameter, as shown in panels (b)-(d).

The main conclusion of this Communication is that the position of these maxima satisfy a quantization condition similar to that of Bohr-Sommerfeld formulae for the wave functions of quantum mechanics.

[1] J. W. M. Bush, Annu. Rev. Fluid Mech. **47**, 269 (2015).

[2] Y. Couder and E. Fort, Phys. Rev. Lett. **97**, 154101 (2006).

[3] A. Eddi, E. Fort, F. Moisy, and Y. Couder, Phys. Rev. Lett. **102**, 240401 (2009).

[4] E. Fort, A. Eddi, A. Boudaoud, J. Moukhtar, and Y. Couder, Proc. Natl. Acad. Sci. USA **107**, 17515 (2010); A. U. Oza, D. M. Harris, R. R. Rosales, and J. W. M. Bush, J. Fluid Mech. **744**, 4045 (2014); A. U. Oza, O. Wind-Willassen, D. M. Harris, R. R. Rosales, and J. W. M. Bush, Phys. Fluids **26**, 082101 (2014).

[5] S. Perrard, M. Labousse, M. Miskin, E. Fort, and Y. Couder, Nat. Commun. **5**, 3219 (2014); M. Labousse and S. Perrard, Phys. Rev. E **90**, 022913 (2014).

[6] L. de Broglie, Comptes Rendues **177**, 507 (1923); *Une Interprétation Causale et Nonlinéaire de la Mechanique Ondulatoire: La Théorie de la Double Solution* (Gauthiers-Villars, Paris, 1956).

[7] J. Montes, F. Revuelta, and F. Borondo, Hydrodynamic quantization constants in bouncing droplets, (in press).

[8] F. Revuelta, E. Vergini, R. M. Benito, and F. Borondo, Phys. Rev. E **87**, 042921 (2013).

[9] J. Montes, F. Revuelta, and F. Borondo, Indian Acad. Sci. Conf. Ser. **1**, 213 (2017) [Proceedings of the Conference on Perspectives in Nonlinear Dynamics 2016].

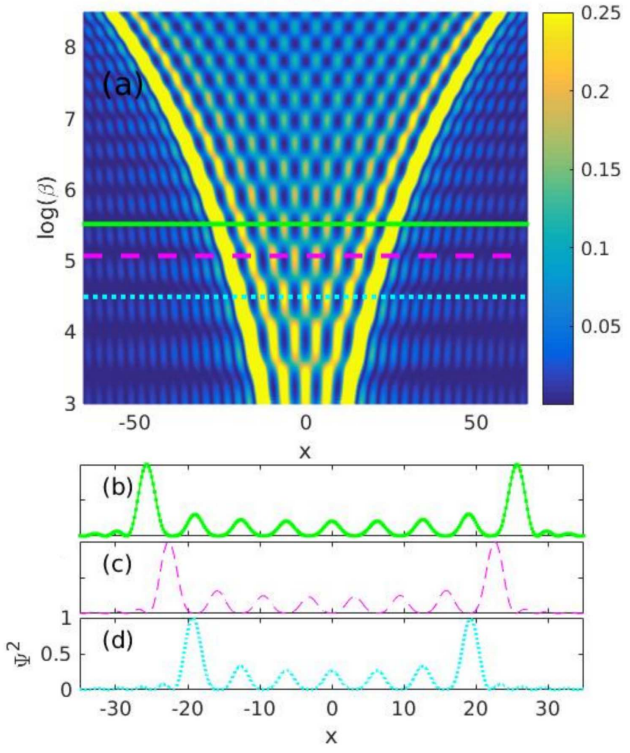

Fig. 1. Time-average for the square of the liquid wave function for a reduced mass $\kappa = 8$. (a) Surface as a function of the memory strength β and the position x. (b)-(d) Sections for a constant memory strength equal to (b) $\beta = 250$, (c) $\beta = 160$, and (d) $\beta = 90$.

A Hilbert approach to investigate climate connectivity

Dario A. Zappalà[1], Marcelo Barreiro[2], and Cristina Masoller[1]
[1]Universitat Politècnica de Catalunya, Departament de Física, 08222 Terrassa, Barcelona, Spain
[2]Universidad de la República, Instituto de Física, Facultad de Ciencias, Iguá 4225, Montevideo, Uruguay

The Hilbert transform (HT) is a well-known method of time series analysis that has been applied to a wide variety of oscillatory signals (physiological, neurological, geophysical, etc.). We have already used it to get, from temperature time series, instantaneous amplitude, phase and frequency [1]. Recently, we used it to find patterns of change in temperature dynamics that arised during the last decades [2]. In the present work we investigate atmospheric data (ERA-Interim reanalysis) at the global scale using the HT. We consider surface air temperature with daily resolution, covering the period 1979–2017.

Firstly, we use the HT to quantify phase synchronisation: we calculate the well-known Kuramoto parameter in three large-scale regions: northern extratropics, southern extratropics and the tropical belt. The result is shown in Fig. 1. We find that the degree of synchronisation in the extra-tropics is high (being higher in the NET than in the SET, likely due to the presence of larger land masses), while the degree of synchronisation in the tropical region is very low.

In a second step, we measure the statistical similarity of time series at different geographical sites by means of cross-correlation coefficient. We use this information to build a climate network and analyse the connectivity of selected regions. In particular, we compare connections computed from temperature anomaly with the ones computed from Hilbert time series (instantaneous amplitude, phase and frequency).

In the extra-tropics, we find that the HT uncovers similar spatial patterns of connectivity as temperature anomalies (the analysis of the connectivity patterns as a function of time lag allows us to interpret them as the effects of Rossby waves). In the tropics, Hilbert amplitude and temperature anomaly uncover similar connectivity maps, while in contrast Hilbert frequency analysis does not reveal any statistically significant connectivity. We interpret these results as due to the fact that, in the extratropics, temperature dynamics are similar due to the strong annual cycle; while in tropical regions the annual cycle is weak and fast temperature variability (captured by large instantaneous frequency variations) is uncorrelated with the activity in the rest of the globe.

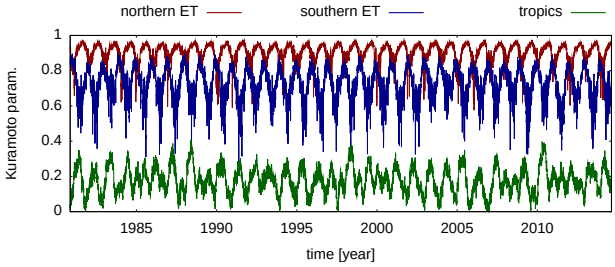

Fig. 1. Evolution of the Kuramoto parameter, calculated separately for three geographical regions: northern extratropics (lat > 30), southern extratropics (lat < -30) and tropics ($-30 \leq$ lat ≤ 30).

[1] D. A. Zappalà, M. Barreiro, and C. Masoller, Global atmospheric dynamics investigated by using Hilbert frequency analysis, Entropy **18**, 408 (2016).

[2] D. A. Zappalà, M. Barreiro, and C. Masoller, Quantifying changes in spatial patterns of surface air temperature dynamics over several decades, Earth Syst. Dynam. **9**, 383-391 (2018).

Synchronization invariance under network structural transformations

Lluís Arola-Fernández[1], Albert Díaz-Guilera[2,3], and Alex Arenas[1]
[1]Departament d'Enginyeria Informàtica i Matemàtiques, Universitat Rovira i Virgili, 43007 Tarragona, Spain
[2]Departament de Física Fonamental, Universitat de Barcelona, Martí i Franquès 1, 08028 Barcelona, Spain
[3]Universitat de Barcelona Institute for Complex Systems (UBICS), Barcelona, Spain

The study of dynamical processes running on top of complex networks has become a central issue in many research fields, ranging from the microscopic realm of genes and neurones to large technological and social systems. However, many times the information we can accede to about the actual topology of interactions is partially incomplete. Moreover, given that the only reflection of the dynamics on networks is usually a certain macroscopic observable, it turns out that many topologies are compatible with the same dynamical output, raising the problem of multi-valuation. Following this perspective, we analyze the relation between function and structure in a novel mapping problem: given a certain network structure and a dynamical process on top of it, we wonder how to transform the network into a different structural connectivity so that the collective behavior of the system remains invariant.

To derive the network transformations, we focused on a paradigmatic example of emergent phenomena, the synchronization of coupled phase oscillators in the Kuramoto Model (KM) [2], which consists of a population of N coupled phase oscillators that evolve in time according to

$$\dot{\theta}_i = \omega_i + K \sum_{j=1}^{N} \lambda_{ij} \sin(\theta_j - \theta_i), \ \forall i \ \in N, \qquad (1)$$

where θ_i is phase of the i-oscillator, ω_i its natural frequency, drawn from a probability distribution $g(\omega)$, λ_{ij} are the elements of the coupling matrix $\mathbf{\Lambda}$ that capture the presence of a connection and its intensity and K is a constant coupling strength that scales all the weights. The collective behavior of the KM is described through the complex order parameter $re^{i\Psi(t)} = \frac{1}{N}\sum_{j=1}^{N} e^{i\theta_j}$, where the modulus r measures the overall degree of synchrony. Here, we assume that r is the only available observable from measurements, and we look for transformations of $\mathbf{\Lambda}$ that keep r invariant, for any value of the control parameter K. In particular, we study the mapping between two structurally different networks (the target $\mathbf{A}$ and candidate $\mathbf{B}$) of N distinguishable oscillators. We aim to find transformations of the weights (the intensity of the connections) in the candidate network, without altering its structure, in a way that the macroscopic response $r(K)$ is identical to the one in the target network.

Inspired by the derivation of statistical mechanics from information theory as a particular case of statistical inference, see [3], we tackle the mapping as an optimization problem for the unknown weights subject to local structural constraints in the system. In particular, we impose an entropy maximization for the weights distribution subject to a detailed balance that constraint, up to a given order m, the input strengths of the nodes (the sum of incoming connections of the m-neighbors) in both networks. We derive analytical expressions for the weights according to different

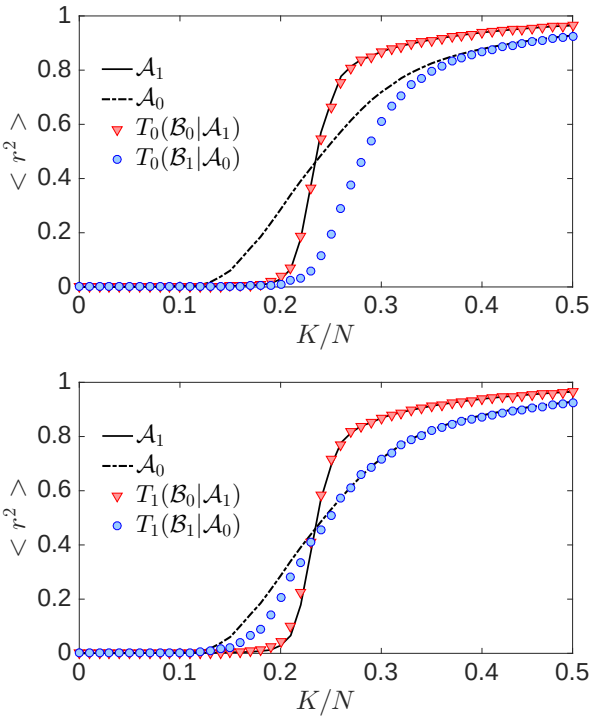

Fig. 1. Synchronization diagrams ($N = 2000$) for target networks A_1 (Erdös-Rényi) and A_0 (power-law), which are unweighted and symmetric, and its respective transformations $T(B_1|A_0)$ and $T(B_0|A_1)$, (top) preserving only zero-order input-strengths and (bottom) preserving also the first-neighbours input-strengths (exploiting more information).

states of available information, and we show that the invariance condition can be achieved even if the mapped networks have very different connectivity patterns or the system is in the non-linear regime. Furthermore, we show that the mapping of homogeneous networks into heterogeneous ones is usually less accurate and requires more -costly- microscopic information than the reverse process, unveiling a symmetry-unbalance phenomenon that emerges from the partial impossibility of preserving the properties of the nodes in the transformation (see Fig.1). The presented formalism can be applied in a wide spectra of existing problems beyond the mapping scenario and provides new analytical insight to tackle real complex scenarios when dealing with uncertainty in the measurements of the underlying connectivity structure.

[1] L. Arola-Fernández, A. Díaz-Guilera, and A. Arenas, Phys. Rev. E **97**, 060301(R) (2018).

[2] A. Arenas, A.Díaz-Guilera, J .Kurths, Y. Moreno, C. Zhou, Phys. Rep. **469**, 93-153 (2008).

[3] E. T. Jaynes, Phys. Rev. **106**, 620-630 (1957).

Seeding approach to bubble nucleation

Pablo Rosales-Peláez[1], Chantal Valeriani[2], and Eduardo Sanz[1]
[1]Departamento de Química-Física, Universidad Complutense de Madrid, Spain
[2]Departamento de Estructura de la Materia, Física Térmica y Electrónica, Universidad Complutense de Madrid, Spain.

Liquid-to-vapor transition plays a very important role in science and technology, as shown by issues such as degassification of steel, jet printers or volcanism. Homogeneous bubble nucleation occurs from a metastable liquid; i.e., a liquid heated over the coexistence temperature (boiling) or stretched below the coexistence pressure (cavitation). To understand this transition the Classical Nucleation Theory (CNT) is typically used although there are some discrepancies, even for Lennard-Jones fluids, in the numerical results of the nucleation rate, that is, the number of critical bubbles formed per unit time and volume [1, 2].

With the goal of understanding this discrepancy, we perform Molecular Dynamics simulations and we use a novel technique called Seeding that we have implemented in liquid-to-solid transition [3]. We embed an artificial bubble of a certain size in the metastable fluid and then estimate the temperature at which this seed is critical. This information combined with CNT gives results for the interfatial free energy and the nucleation rate. This cheap but approximate technique can easily be used in more complex systems like water, where other expensive calculations have already been done [4].

[1] S. L. Meadley and F. A. Escobedo, Thermodynamics and kinetics of bubble nucleation: Simulation methodology, J. Chem. Phys. **137**, 074109 (2012).

[2] Z.-J. Wang, C. Valeriani, and D. Frenkel, Homogeneous bubble nucleation driven by local hot spots: A molecular dynamics study, J. Phys. Chem. B **113**, 3776 (2008).

[3] J. R. Espinosa, C. Vega, C. Valeriani, and E. Sanz, Seeding approach to crystal nucleation, J. Chem. Phys. **144**, 034501 (2016).

[4] G. Menzl, M. A. Gonzalez, P. Geiger, F. Caupin, J. L. Abascal, C. Valeriani, and C. Dellago, Molecular mechanism for cavitation in water under tension, Proc. Natl. Acad. Sci. USA **113**, 13582 (2016).

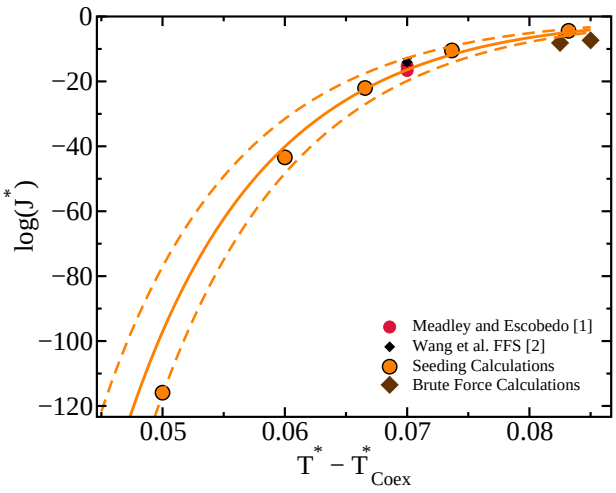

Fig. 1. Nucleation Rate as a function of temperature scaled with the coexistence temperature at constant pressure of $P^* = 0.026$. Seeding calculations are shown in orange: points for data and lines for fit (solid) and error (dashed).

Influence of water models on AQP1

Miguel A. Gonzalez[1], Charlotte I. Lynch[2], José Luis F. Abascal[1],
Mark S. P. Sansom[2], and Chantal Valeriani[3]

[1]Universidad Complutense de Madrid, Facultad de Ciencias Químicas, Departamento de Química Física, 28040 Madrid, Spain
[2]University of Oxford, Structural Bioinformatics and Computational Biochemistry Unit, Department of Biochemistry, Oxford OX1 3QU, United Kingdom
[3]Universidad Complutense de Madrid, Facultad de Ciencias Físicas, Departamento de Física Aplicada, 28040 Madrid, Spain

Membrane proteins are vital for the correct functioning of cells, being responsible for cell-cell communication and both active and passive transport of molecules across the membrane [1]. The latter include protein channels and pores, and constitute a large family whose members have different features depending on the nature of the transported molecules. Aquaporins (AQP) are protein pores enabling the passage of water [2] across the membrane, characterised by high selectivity and rates of permeability. Although they have been widely studied, key aspects of the mechanisms relevant for their function remain unclear. Molecular dynamics (MD) is powerful numerical tool for investigating the features of a membrane protein, simulating a full complex system consisting of the membrane protein, the bilayer lipid membrane, water molecules, and ions. In such a system, water plays a key role in the lipid-protein interaction, given that the lipid membrane structure is governed by hydrophobic-hydrophilic forces (as well as the protein structure). Hence, it is essential to properly describe both the water-protein and water-membrane interactions. However, so far in biological simulations, water models have been selected for their ability to reproduce the behaviour of biological molecules, for example, how lipids assemble into a membrane or the dynamics of a protein [3, 4].

In our work, we propose a different point of view: the choice of the water model might influence the predicted transport properties of aquaporins [5, 6]). We will be focusing on newer water models, such as TIP4P/2005 [7] and OPC [8], known to reproduce and to predict the values of a huge range of thermodynamics properties [3, 4]. We have carried out several simulations for AQP1 in combination with TIP3P [9], TIP4P/2005 and OPC as the water potential. We have calculated the water flux through the channel, the water molecule orientation into the channel and the water dipole moment for the three systems. Our preliminary results for all systems reproduce the molecular mechanism described by Tajkhorshid *et al.* [6]. However, the number of water molecules crossing the channel depends on the water model. The thermodynamic properties of the water potential in bulk are extremely different, thus modifying the protein behaviour.

[1] B. Alberts, A. Johnson, J. Lewis, M. Raff, K. Roberts, and P. Walter, *Molecular Biology of the Cell* (Garland Science, 2002).

[2] D. Kozono, M. Yasui, L. S. King, and P. Agre, J. Clin. Invest. **109**, 1395-1399 (2002).

[3] S. L. Rouse and M. S. P. Sansom, J. Phys. Chem. B **119**, 764-772 (2015).

[4] E. J. Denning and O. Beckstein, Chem. Phys. Lipids **169**, 57-71 (2013).

[5] Y. Fujiyoshi, K. Murata, K. Mitsuoka, T. Hirai, T. Walz, P. Agre, J. B. Heymann, and A. Engel, Nature **407**, 599-605 (2000).

[6] E. Tajkhorshid, P. Nollert, M. Ø. Jensen, L. J. W. Miercke, J. O'Connell, R. M. Stroud, and K. Schulten, Science **296**, 525-530 (2002).

[7] J. L. F. Abascal and C. Vega, J. Chem. Phys. **123**, 234505 (2005).

[8] S. Izadi, R. Anandakrishnan, and A. V. Onufriev, J. Phys. Chem. Lett. **5**, 3863-3871 (2014).

[9] M. W. Mahoney and W. L. Jorgensen, J. Chem. Phys. **112**, 8910-8922 (2000).

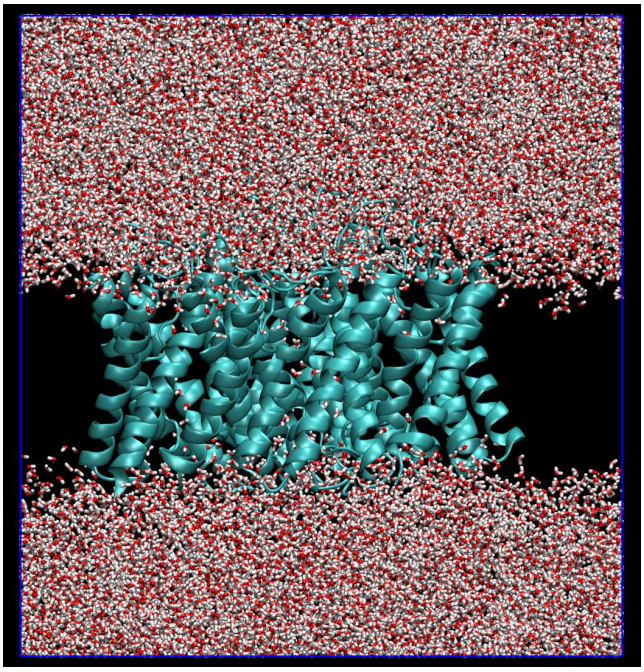

Fig. 1. Snapshot of an AQP1 (in Cyan) embedded into a POPC membrane, lipids from membrane are removed to ease the visualization of the protein).The water is represented by red-white licorice model, red for oxygen and white for hydrogen.

Modelling the out-of-equilibrium dynamics of colloids by Monte Carlo simulations

Daniel Corbett[1], Alejandro Cuetos[2], and Alessandro Patti[1]
[1]School of Chemical Engineering and Analytical Science, The University of Manchester, Manchester, M13 9PL, United Kingdom
[2]Department of Physical, Chemical and Natural Systems, Pablo de Olavide University, 41013 Sevilla, Spain

Colloids have a striking relevance in a wide spectrum of industrial formulations, spanning from personal care products to protective paints. Their behaviour can be easily influenced by extremely weak forces, which disturb their thermodynamic equilibrium and dramatically determine their performance. Motivated by the impact of colloidal dispersions in fundamental science and formulation engineering, we have designed an efficient Dynamic Monte Carlo (DMC) approach to mimic their out-of-equilibrium dynamics.

Our recent theory, which provided a rigorous method to reproduce the Brownian motion of colloids by MC simulations [1, 2], is here generalised to reproduce the Brownian motion of colloidal particles during transitory unsteady states, when their thermodynamic equilibrium is significantly modified [3]. In particular, we have recently proposed a DMC algorithm to investigate the Brownian motion of pure systems [1] and mixtures [2] of colloidal particles in isotropic, nematic and smectic liquid crystal phases. By rescaling the MC time step with the acceptance ratio of particle displacements and rotations, we demonstrated the existence of a unique MC time scale that allows for a direct comparison with BD simulations.

In the present work, we extend our theoretical framework to the case in which an external stimulus perturbs the thermodynamic equilibrium of a colloidal system conmsisting of monodisperse or bidisperse rod-like particles. From a steady-state condition of dynamic equilibrium, where all the observables, including the above mentioned acceptance ratio A, are independent of time t, the system undergoes a transitory unsteady state taking it to a new equilibrium configuration. We apply our DMC simulation technique to simulate the effect of an external field forcing an isotropic phase of rod-like colloidal particles to reorient along a common direction and thus form a nematic liquid crystal. We also study the behaviour of the system once the external field is removed and show that, even when $A = A(t)$, our DMC simulations, which are in excellent quantitative agreement with BD simulations, can be employed to extract reliable dynamical information also from out-of-equilibrium systems.

[1] A. Patti and A. Cuetos, Phys. Rev. E **86**, 011403 (2012).

[2] A. Cuetos and A. Patti, Phys. Rev. E **92**, 022302 (2015).

[3] D. Corbett, A. Cuetos, D. Dennison, and A. Patti, Phys. Chem. Chem. Phys. **20**, 15118 (2018)

The role of ice III in crystal nucleation

J. R. Espinosa[1], Angel Diez[2], C. Vega[1], J. Ramirez[3], C. Valeriani[2], and E. Sanz[1]
[1]Departamento de Química-Física, Universidad Complutense de Madrid, Spain
[2]Departamento de Estructura de la Materia, Física Térmica y Electrónica, Universidad Complutense de Madrid, Spain
[3]Departamento de Ingenieria Química Industrial y Medio Ambiente, Escuela Técnica Superior de Ingenieros Industriales, Universidad Politécnica de Madrid, Spain

In 1975, Kanno, Speedy, and Angell [1], investigated experimentally homogeneous ice nucleation (i.e., in the absence of surfaces and impurities) for pressures up to 2000 bar. By measuring the temperature at which microscopic emulsified water drops freeze when cooled at a rate of a few Kelvin per minute, they established the so-called homogeneous nucleation line (HNL), whose slope is negative and larger than that of the melting line. Thus, they found that whereas water remains liquid for temperatures down to -38 °C at ambient pressure, at high pressures it is possible to have liquid water at temperatures as low as -92 °C. Therefore, applying pressure significantly increases the range of temperatures at which liquid water may exist. This important experimental result is the basis of state-of-the art coolers used for the preservation of biological samples [2, 3]. Despite its importance, the experiment by Kanno *et al.* has long remained unexplained.

The HNL is a line in the pressure-temperature plane where the ice nucleation rate, or the number of growing ice clusters nucleated per unit time and volume, remains constant [4]. Thus, computing the HNL for a given ice polymorph requires obtaining the nucleation rate as function of temperature for different pressures. We suggest the kink in the experimentally measured HNL [2] is due to a change in the nucleation path from ice Ih to ice III.

To test our hypothesis, we perform Molecular Dynamics simulations using a technique called *seeding* [5, 6]. This technique consists in embedding a crystalline cluster of a certain size of the desired stable phase (ice III in this work) in the metastable phase (liquid). The temperature at which this cluster is critical is then obtained and using the Classical Nucleation Theory (CNT) we can obtain both the interfacial free energy and the nucleation rate. Three different cluster sizes are investigated and the HNL of ice III is computed and compared with the one of ice Ih (computed in [4]). We observe that the crossing point of these curves coincides with the kink in the HNL obtained experimentally.

[1] H. Kanno, R. J. Speedy, and C. A. Angell, Supercooling of water to -92 °C, Science, **189**, 880 (1975).

[2] G. J. Morris and E. Acton, Controlled ice nucleation in cryopreservation – A review, Cryobiology **66**, 85 (2013).

[3] D. Studer, High-pressure freezing system, US Patent No. 6 269 649 (2001).

[4] J. R. Espinosa, A. Zaragoza, P. Rosales-Pelaez, C. Navarro, C. Valeriani, C. Vega, and E. Sanz, Interfacial free energy as the key to the pressure-induced deceleration of ice nucleation, Phys. Rev. Lett. **117**, 135702 (2016).

[5] E. Sanz, C. Vega, J. R. Espinosa, R. Caballero-Bernal, J. L. F. Abascal, and C. Valeriani, Homogeneous ice nucleation at moderate supercooling from molecular simulation, J. Am. Chem. Soc. **135**, 15008 (2013).

[6] J. R. Espinosa, C. Vega, C. Valeriani, and E. Sanz, Seeding approach to crystal nucleation, J. Chem. Phys. **144**, 034501 (2016).

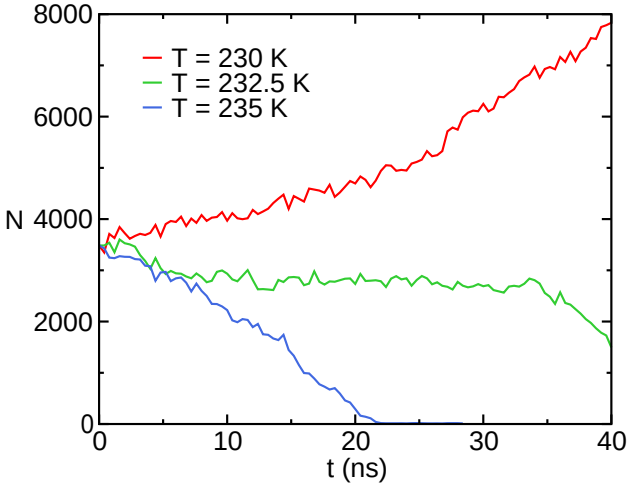

Fig. 1. Evolution of the number of particles of the cluster N as a function of time t for different temperatures and for one cluster size. Lower temperatures make the cluster to grow while high temperatures make the cluster to shrink.

Out-of-equilibrium annealing of travelling colloidal carpets

Helena Massana-Cid[1], Fanlong Meng[2], Daiki Matsunaga[2], Ramin Golestanian[2], and Pietro Tierno[1]
[1]Departament de Física de la Matèria Condensada, Universitat de Barcelona, Barcelona, Spain
[2]Rudolf Peierls Centre for Theoretical Physics, University of Oxford, Oxford OX1 3NP, United Kingdom

Paramagnetic colloids can be assembled into two-dimensional colloidal clusters (carpets) by using an in-plane rotating magnetic field [1]. The applied field induces a finite magnetic torque on the particles, which sets them in rotation at a given angular speed and forces the colloids to assemble into clusters [2, 3, 4]. These structures can be steered in any direction of the plane by adding a perpendicular component to the in-plane rotating field.

We studied the stability and the structures of these carpets for different parameters of the actuating magnetic field and compared the corresponding experimental phase diagram with a theoretical one. The latter was obtained by balancing hydrodynamic with magnetic torque and performing a linear stability analysis. We find that for certain parameters, when the carpet is propelling, the particles in the back can jump on top of the two-dimensional colloidal structure and travel through the carpet's lattice to the opposite side. These particles either fill out existing holes in the carpet or deposit on the other side following the lattice order. This provides a new out-of-equilibrium way to anneal colloidal structures, by transforming initial disordered clusters of particles with defects to perfect crystalline lattices. We study the dynamics of this process. We see that, counter-intuitively, the faster the dynamics of the carpet, the sooner a monocrystal is formed.

[1] F. Martinez-Pedrero and P. Tierno, Phys. Rev. Appl. **3**, 051003 (2015).

[2] J. Černák and G. Helgesen, Phys. Rev. E **78**, 061401 (2008).

[3] J. Yan, S. C. Bae, and S. Granick, Soft Matter **11**, 147 (2015).

[4] J. Schwarz-Linek, C. Valeriani, A. Cacciuto, M. E. Cates, D. Marenduzzo, A. N. Morozov, and W. C. K. Poon, Proc. Natl. Acad. Sci. USA **109**, 4052 (2012).

Epidemic spreading in localized environments with recurrent mobility patterns

Clara Granell[1,2,3] and Peter J. Mucha[3]
[1]Departament de Física de la Matèria Condensada, Universitat de Barcelona, Martí i Franquès 1, E-08028 Barcelona, Spain
[2]Universitat de Barcelona Institute of Complex Systems (UBICS), Universitat de Barcelona, E-08007 Barcelona, Spain
[3]Carolina Center for Interdisciplinary Applied Mathematics, Department of Mathematics, University of North Carolina, Chapel Hill, NC 27599-3250, USA

The spreading of epidemics is very much determined by the structure of the contact network, which may be impacted by the mobility dynamics of the individuals themselves. In confined scenarios where a small, closed population spends most of its time in localized environments and has easily identifiable mobility patterns —such as workplaces, university campuses or schools— it is of critical importance to identify the factors controlling the rate of disease spread. These kinds of scenarios are usually represented using metapopulation models [3]. In such settings, the nodes of the network represent a population, which is occupied by individuals, and the links of the network represent the migration of individuals from one population to another. This scenario is particularly useful in the study of the spreading of epidemics, given that many real-life patterns of interactions happen in structured, localized populations connected by some degree of migration.

The problem of modeling such scenarios relies on finding the appropriate level of abstraction to grasp the main macroscopic features of the epidemic spreading process for individuals across the particular environment. Traditionally, models for epidemic spreading in metapopulations assume that individuals diffuse randomly and that subpopulations with the same number of connections are treated as statistically equivalent. Although useful, this approach does not capture some important real-world features, like the fact that human dynamics are are often dominated by recurrent patterns where individuals have memory of the location they come from and are likely to return to their original location after a short exploration of the network.

In this work we present a discrete-time Markov-chain model for epidemic spreading in structured populations with a recurrent pattern of migrations between the locations in a bipartite network. The aim of this model is to quantify the extent of an SIS-like epidemic in the scenario where each individual spends his time between two locations: their *residence* and *common* locations (where mixing with individuals coming from other residence subpopulations happen). In short, the dynamics are as follows: for each day, agents leave their residence sites with probability p and choose a common location according to the network topology W. Then, both the agents remaining in their residences and the ones that have traveled can get infected by contacting the other agents populating their destination node. After this is done, the individuals return to their residence, and another infection step is performed. Additionally, we introduce a typical mechanism of isolation —such as reducing the mobility of infected individuals— to see if it is able to contain the spreading of the disease.

Our analytical formulation is based on discrete-time Markov-chains [1, 2] and it is able to calculate the fraction of infection at each patch of the metapopulation network. It also allows us to derive analytically the exact expression of the epidemic threshold. We have crosschecked the results of our model with extensive Monte Carlo simulations, with remarkable correspondence.

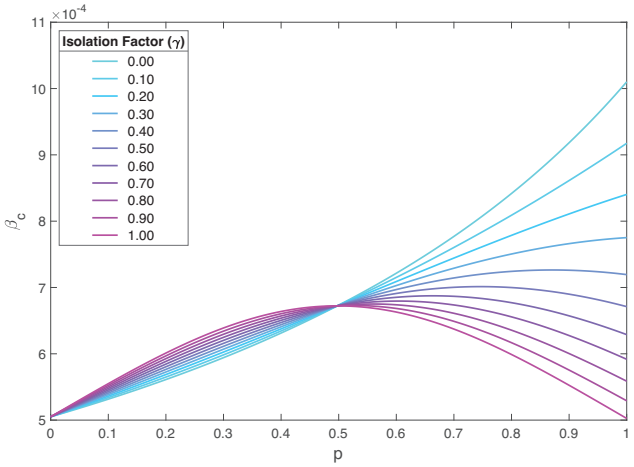

Fig. 1. Epidemic threshold as a function of the mobility parameter p, for different values of the isolation factor γ, where $\gamma = 0$ means that infected individuals cannot travel and $\gamma = 1$ means infected individuals do travel with the same probability than the susceptible ones. For this particular topological configuration, the value of p^* is 0.5, as seen for the curve corresponding to $\gamma = 1$. As the isolation factor γ decreases (more restriction in the mobility of the infected) the optimum mobility p^* is shifted right (the disease is more contained as the mobility increases).

Among our findings, we have observed that the curve of the epidemic threshold as a function of the mobility probability p does not have a monotonic behavior. Instead, there is an optimum value of the mobility (p^*), which makes the epidemic threshold maximum. That value is the value of the mobility probability that causes all subpopulations in the network to be of the same (or most similar) effective size during the daytime infection step. We also explored the effect of isolation, i.e., the reduction of mobility of the infected individuals. We find that as the mobility of the infected individuals is more restricted, the epidemic threshold increases with increasing mobility (see Fig. 1), meaning that if infected individuals are contained in their residences, the lower spreading of the disease will happen when the susceptible individuals travel the most out of their residence.

[1] S. Gomez, A. Arenas, J. Borge-Holthoefer, S. Meloni, and Y. Moreno, EPL **89**, 38009 (2010).

[2] J. Gomez-Gardeñes, D. Soriano-Paños, and A. Arenas, Nat. Phys. **14**, 391-395 (2017).

[3] V. Colizza, R. Pastor-Satorras, and A. Vespignani, Nat. Phys. **3**, 276-282 (2007).

Better than counting: Density profiles from force sampling

Daniel de las Heras and Matthias Schmidt
Theoretische Physik II, Physikalisches Institut, Universität Bayreuth, D-95440 Bayreuth, Germany

The one-body density distribution plays a central role in statistical physics. Accurate measurements of the density profile are very valuable to study, e.g., wetting properties, crystal nucleation, the liquid-vapor interface, and capillary effects, as well as to assess the validity of new density functional theories. Traditionally, the density profile is measured experimentally, or calculated in computer simulations, by literally counting the number of particles in each bin of a predefined spatial grid.

We have developed an alternative method [1] based on a histogram of the local force density. Using the exact force balance equation of an equilibrium system, the density profile can be obtained from the local force density profile via a simple spatial integration. The method eliminates the ideal gas fluctuations, reducing therefore the statistical uncertainty and the computation time as compared to the traditional counting method.

We have tested the method in Monte Carlo, Brownian dynamics, and molecular dynamics. In all cases, obtaining the density profile via the force density profile performs significantly better than just counting the number of particles in a given bin. A representative example is shown in the figure.

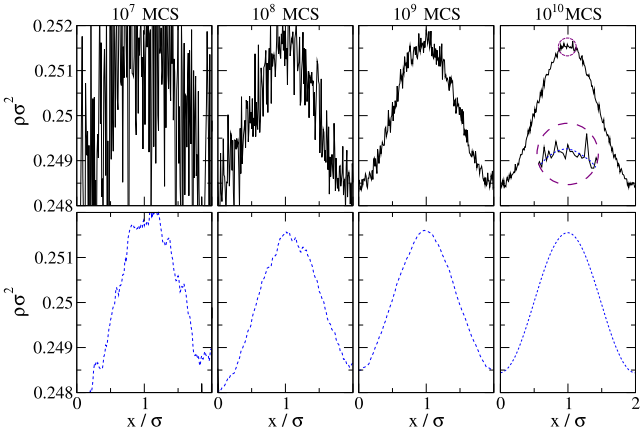

Fig. 1. Density profiles obtained with Monte Carlo simulations for different number of Monte Carlo steps (MCS), as indicated. The profiles have been obtained with the traditional counting method (top profiles) and the force sampling method (bottom profiles). The bin size is $\Delta x/\sigma = 0.01$ with σ the particle length. The profiles correspond to an equilibrium system of Lennard-Jones particles in an external potential.

[1] D. de las Heras and M. Schmidt, Phys. Rev. Lett. **120**, 218001 (2018).

Superadiabatic forces in overdamped Brownian dynamics

D. de las Heras, P. Krinninger, T. Geigenfeind, S. Hermann, T. Eckert, N. Stuhlmüller, and M. Schmidt
Theoretische Physik II, Physikalisches Institut, Universität Bayreuth, D-95440 Bayreuth, Germany

Power functional theory (PFT) [1] is an exact generalization of equilibrium density functional theory to nonequilibrium Brownian dynamics.

In PFT the exact dynamics of overdamped Brownian particles is described by a unique time-dependent power functional that depends on both the one-body density distribution and the one-body current. By construction, the functional attains a minimum with respect to the current at the physical time evolution of the system.

PFT goes beyond the adiabatic approximation implicit in dynamic density functional theory [2] by including superadiabatic forces. The superadiabatic forces are generated via functional differentiation of the excess (over ideal gas) power functional, which plays the analogous role as the excess free energy functional in equilibrium density functional theory.

We present an explicit and simple approximation for the superadiabatic excess power functional based on the local velocity gradient [3]. The resulting superadiabatic forces, obtained via functional differentiation, are in very good agreement with Brownian dynamics simulations, and explain a broad range of phenomena, such as viscous forces, structural forces, lane formation in colloidal systems, shear migration, and motility induced phase separation in active systems.

---

[1] M. Schmidt and J. M. Brader, J. Chem. Phys. **138**, 214101 (2013).

[2] U. M. B. Marconi and P. Tarazona, J. Chem. Phys. **110**, 8032 (1999).

[3] D. de las Heras and M. Schmidt, Phys. Rev. Lett. **120**, 028001 (2018).

Relaxation time of the global order parameter on multiplex networks: The role of interlayer coupling in Kuramoto oscillators

A. Allen-Perkins[1,2], T. A. de Assis[1], J. M. Pastor[2], and R. F. S. Andrade[1]
[1]Instituto de Física, Universidade Federal da Bahia, 40210-210 Salvador, Brazil
[2]Complex System Group, Universidad Politécnica de Madrid, 28040 Madrid, Spain

This work presents a new formalism to study analytically the time scales of the global order parameter and the interlayer synchronization of coupled Kuramoto oscillators on multiplex networks [1].

We consider an undirected multiplex $\mathcal{M}$ with $M = 2$ layers G^α, $1 \leq \alpha \leq M$, where each layer contains N nodes identified by x_n^α, $1 \leq n \leq N$ (see Fig. 1). The oscillator in each node x_n^α of the layer G^α is characterized by its phase θ_n^α, whose dynamics is described by

$$\dot{\theta}_n^\alpha = \Omega_n^\alpha + \lambda^\alpha \sum_{x_m^\alpha \in G^\alpha} w_{nm}^\alpha \sin(\theta_m^\alpha - \theta_n^\alpha) + \lambda^{12} w_{nn}^{12} \sin(\theta_n^\beta - \theta_n^\alpha). \quad (1)$$

Here, Ω_n^α is the natural frequency of the oscillator x_n^α, λ^α and λ^{12} are the coupling strength of the layer α and of the interlayer 12, respectively, w_{nm}^α is the weight of the connection between the nodes x_n^α and x_m^α, and w_{nn}^{12} is the weight of the connection between the nodes x_n^α and x_n^β.

For two-layer multiplexes with an initially high degree of synchronization in each layer (see Fig. 2), the difference between the average phases in each layer, denoted by $\Delta = \psi^1 - \psi^2$, with

$$\psi^\alpha(t) = \mathrm{Arg}\left(\frac{1}{N}\sum_{x_n^\alpha \in G^\alpha} e^{i\theta_n^\alpha(t)}\right), \quad (2)$$

is analyzed from two different perspectives: the spectral analysis and the nonlinear Kuramoto model.

Both viewpoints confirm that the time scales of the global order parameter r, being

$$r(t) = \frac{1}{2N}\left|\sum_{x_n^\alpha \in \mathcal{M}} e^{i\theta_n^\alpha(t)}\right| \approx \left|\cos\left(\frac{\Delta}{2}\right)\right|, \quad (3)$$

and of the interlayer synchronization Δ are inversely proportional to the interlayer coupling strength, λ^{12}. Thus, increasing the interlayer coupling always shortens the transient regimes of both r and Δ

The analytical results show that the convergence of the global order parameter is faster than the interlayer synchronization, and the latter is generally faster than the global synchronization of the multiplex. The formalism also outlines the effects of frequencies on the difference between the average phases of each layer, and it identifies the conditions for an oscillatory behavior. Computer simulations are in fairly good agreement with the analytical findings, and they reveal that the time scale of the global order parameter is half the size of the time scale of the multiplex, if not smaller.

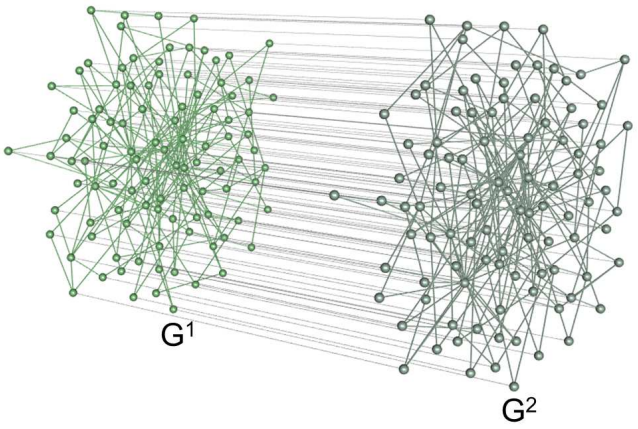

Fig. 1. Example of an undirected multiplex network with two layers, G^1 and G^2. Taken from Ref. [1].

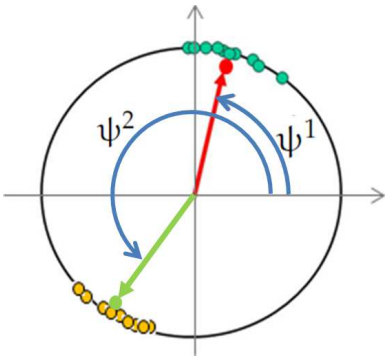

Fig. 2. Example of an undirected multiplex network with two layers and a high degree of synchronization in each layer (turquoise and yellow dots for, respectively, the phases of the oscilators in G^1 and G^2).

[1] A. Allen-Perkins, T. A. de Assis, J. M. Pastor, and R. F. S. Andrade, Relaxation time of the global order parameter on multiplex networks: The role of interlayer coupling in Kuramoto oscillators, Phys. Rev. E **96**, 042312 (2017).

Quantum transport on lattices: A story of bosons, fermions, and spins

Daniel Manzano
Electromagnetism and Condensed Matter Department, University of Granada, Granada, Spain

Quantum transport in lattices is a major field of study nowadays. It has been probed that a lattice compose by harmonic oscillators connected to two thermal baths at different temperatures behaves ballistically in any dimension [1]. On the other hand, if the lattice is composed by spins it is ballistic only in the one dimensional case [2, 3]. In the simplest two-dimensional spin lattice, a ladder, it has been numerically probed the existence of both ballistic and non-ballistic channels [4].

In this contribution I show that both fermionic and bosonic uniform d-dimensional lattices can be reduced to a set of independent one-dimensional chains [5]. This reduction leads to the expression for ballistic energy fluxes in uniform fermionic and bosonic lattices. By the use of the Jordan-Wigner transformation we can extend our analysis to spin lattices, proving the coexistence of both ballistic and non-ballistic subspaces in any dimension and for any system size. We then relate the nature of transport to the number of excitations in the homogeneous spin lattice, indicating that a single excitation always propagates ballistically and that the non-ballistic behaviour of uniform spin lattices is a consequence of the interaction between different excitations.

[1] A. Asadian, D. Manzano, M. Tiersch, and H. J. Briegel, Phys. Rev. E **87**, 012109 (2013).

[2] M. Znidaric, Phys. Rev. E **83**, 011108 (2011).

[3] D. Manzano, M. Tiersch, A. Asadian, and H. J. Briegel, Phys. Rev. E **86**, 061118 (2012).

[4] M. Znidaric, Phys. Rev. Lett. **110**, 070602 (2013).

[5] D. Manzano, C. Wand, and J. Cao, New J. Phys. **18**, 043044 (2016).

Comportamiento reológico de una suspensión coloidal con interacción de largo alcance

P. Malgaretti[1], I. Pagonabarraga[2,3] y R. C. Hidalgo[4],
[1]Max-Planck-Institut für Intelligente Systeme, Heisenbergstr. 3, 70569 Stuttgart, Alemania
[2]Departament de Física de la Materia Condensada, Universitat de Barcelona, España
[3]CECAM, École Polytechnique Fédérale de Lausanne (EPFL), Suiza
[4]Departamento de Física y Matemática Aplicada, Facultad de Ciencias, Universidad de Navarra, 31080 Pamplona, España

En este trabajo estudiamos el comportamiento constitutivo de suspensiones coloidales para concentraciones moderadas y altas. Específicamente, utilizando simulaciones de Lattice Boltzmann, examinamos numéricamente suspensiones que fluyen a través de canales estrechos, y exploramos la influencia de la interacción entre partículas, en la respuesta macroscópica del sistema.

Cuando solo se considera un potencial de interacción de corto alcance, siempre se recupera un comportamiento newtoniano y la viscosidad efectiva del sistema depende principalmente de la concentración de la suspensión. Sin embargo, cuando usamos un potencial de Lennard-Jones, identificamos dos respuestas reológicas dependiendo de la intensidad de la interacción, la fracción de volumen y la caída de presión.

Aprovechando un modelo de reología no local explicamos los resultados numéricos y proponemos relaciones de escalado para identificar las escalas energéticas relevantes involucradas en estos procesos de transporte. Además, encontramos que la distribución espacial de los coloides en capas paralelas a la dirección del flujo, no correlaciona con los cambios en la respuesta macroscópica del sistema. Curiosamente, lo que se correlaciona con los cambios reológicos es la distribución espacial de los coloides dentro de las capas individuales. A saber, las suspensiones caracterizadas por una respuesta newtoniana muestran una estructura cúbica de los coloides dentro de capas individuales, mientras que para las suspensiones con coloides de respuesta no newtoniana se organizan en una estructura hexagonal.

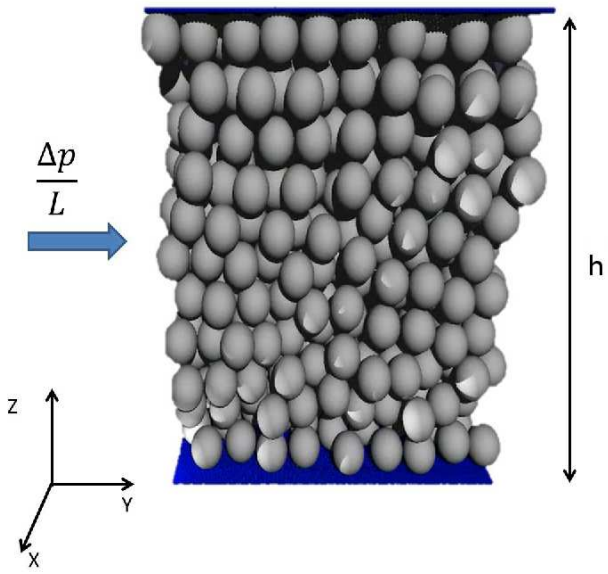

Fig. 1. Ilustración de la suspensión coloidal, que se mueve impulsada por una caída de presión $\Delta p/L$ que actúa en la dirección Y. El sistema está confinado en la dirección Z por paredes sólidas, y condiciones periódicas se imponen en direcciones X y Y.

Emergence of Gaussian statistics as a symmetry far from equilibrium

Enrique Rodríguez-Fernández and Rodolfo Cuerno
Departamento de Matemáticas and Grupo Interdisciplinar de Sistemas Complejos (GISC), Universidad Carlos III de Madrid, av. Universidad 30, 28911 Leganés, Madrid, Spain

Suitable non-equilibrium conditions have been recently shown to allow for *symmetry emergence*, as opposed to *spontaneous symmetry breaking*, in extended systems [1]. A paradigmatic model in statistical physics is the stochastic Burgers equation,

$$\partial_t \phi = \nu \partial_x^2 \phi + \lambda \phi \partial_x \phi + \eta, \quad (1)$$

where η is space-time, white noise. Indeed, Eq. (1) appears in many different contexts [2], see, e.g., Fig. 1. Moreover, Eq. (1) can be generalized to higher dimension, as, e.g., [3]

$$\partial_t \phi = \nu_x \, \partial_x^2 \phi + \nu_y \, \partial_y^2 \phi + \lambda_x \phi \partial_x \phi + \lambda_y \phi \partial_y \phi + \eta, \quad (2)$$

which also generalizes the Hwa-Kardar (HK; $\lambda_y = 0$) equation that describes avalanches in running sandpiles [4]. Furthermore, Burgers equation is strongly related with other important models: The change of variable $\phi = \partial_x h$ transforms the deterministic terms of Eq. (1) into those of the 1D Kardar-Parisi-Zhang (KPZ) equation, another paradigm of contemporary non-equilibrium statistical physics [5].

Both the KPZ and the stochastic Burgers equations exhibit generic scale invariance [6]: The variance W^2 of the field grows up to a saturation value $W_{\rm sat}^2$ at time $t_{\rm sat}$, such that $W_{\rm sat} \sim L^\alpha$ and $t_{\rm sat} \sim L^z$, where L is the lateral size of the system. Universality classes occur, which are characterized by the values of α, z, and by the statistics of fluctuations; for the 1D KPZ equation, the latter is provided by the Tracy-Widom (TW) distribution [5], whose universal, nonzero skewness manifests the lack of up-down symmetry ($h \leftrightarrow -h$) of the system.

The scaling exponents of Eqs. (1)-(2) have been investigated both analytically [4, 7] and numerically [3, 8]. However, the statistics of the field had not been reported in the literature for the Burgers and Hwa-Kardar equations yet. Due to their nonlinearities, Eqs. (1)-(2) also lack up-down symmetry ($\phi \leftrightarrow -\phi$); hence, fluctuations in ϕ are expected to be skewed and non-Gaussian, as in the KPZ case. However, this seems not to be the case.

In this work [9], we revisit the universality class of the Burgers and the (generalized) HK equations, focusing on the statistics of fluctuations. Remarkably, these turn out to be Gaussian, see Fig. 2. We reach this conclusion from numerical simulations and from dynamic renormalization group calculations of the skewness and kurtosis of the field ϕ.

The scaling exponents of Eqs. (1)-(2) are fixed by the hyperscaling ($2\alpha + d = z_d$) and Galilean ($\alpha + z_d = 1$) scaling relations, induced by non-renormalization of noise and nonlinearity, respectively [3, 4, 7]. Actually, both the Gaussian statistics and these exponent values are *exact* for the *linear* (hence, up-down symmetric) equation

$$\partial_t \hat{\phi} = \left(- \sum_{i=1}^{d} |k_i|^{z_d} \right) \hat{\phi} + \hat{\eta}, \quad (3)$$

where hat is space Fourier transform and $\mathbf{k}$ is wave-vector.

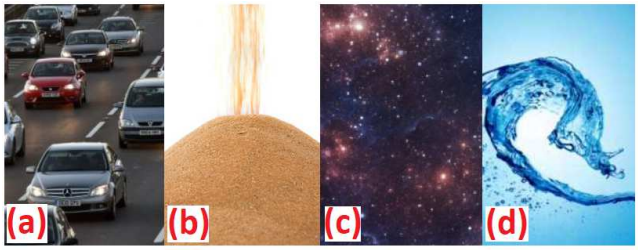

Fig. 1. Systems described by Eqs. (1)-(2) and meaning of ϕ [2, 3, 4]: (a) traffic models (vehicle density), (c) avalanche dynamics (pile height), (b) cosmology (mass density in the early universe), and (d) turbulence (fluid velocity).

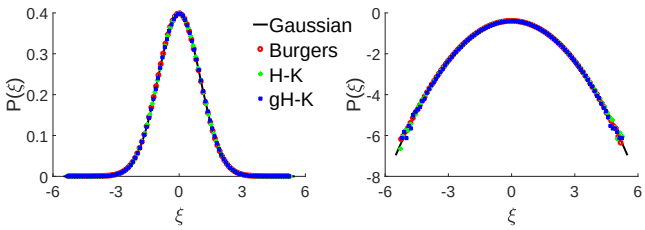

Fig. 2. Normalized fluctuation histogram from numerical simulations of the Burgers and (generalized) Hwa-Kardar equations, Eqs. (1)-(2). Here, $\xi = (\phi - \bar{\phi})/\mathrm{Var}(\phi)$.

Overall, the up-down symmetry, notably absent from Eqs. (1)-(2) themselves, *emerges* at the critical point which governs their large-scale behavior, in the form of up-down-symmetric, Gaussian fluctuations. Indeed, Gaussian statistics can be expected far from equilibrium, even for systems which are closely related with non-Gaussian, KPZ universality.

[1] L. M. Sieberer, S. D. Huber, E. Altman, and S. Diehl, Phys. Rev. Lett. **110**, 195301 (2013).

[2] J. Bec and K. Khanin, Phys. Rep. **447**, 1 (2007).

[3] E. Vivo, M. Nicoli, and R. Cuerno, Phys. Rev. E **89**, 042407 (2014).

[4] T. Hwa and M. Kardar, Phys. Rev. A **45**, 7002 (1992).

[5] T. Halpin-Healy and K. A. Takeuchi, J. Stat. Phys. **160**, 794 (2015).

[6] U. C. Täuber, *Critical Dynamics* (Cambridge University Press, 2014).

[7] D. Forster, D. R. Nelson, and M. J. Stephen, Phys. Rev. A **16**, 732 (1977).

[8] F. Hayot and C. Jayaprakash, Phys. Rev. E **56**, 4259 (1997).

[9] E. Rodríguez-Fernández and R. Cuerno, (in preparation).

Tailoring Janus swimmers by mesoscopic simulations

C. Herrero[1], E. N. Argemí[2,3], S. A. Mallory[4], F. Alarcon[1], A. Cacciuto[5], I. Pagonabarraga[3,6], and C. Valeriani[1]
[1]GISC and Dpto. de Estructura de la Materia, Física Térmica y Electrónica, Univ. Complutense de Madrid, 28040 Madrid, Spain
[2]Departament de Física de la Matèria Condensada, Universitat de Barcelona, 08028 Barcelona, Spain
[3]University of Barcelona Institute of Complex Systems (UBICS), 08028 Barcelona, Spain
[4]Chemical Engineering, California Institute of Technology, Pasadena CA 91125, USA
[5]Chemistry, Columbia University, New York NY 10027, USA
[6]Centre Européeen de Calcul Atomique et Moléculaire (CECAM), Ecole Polytechnique Fédérale de Lausanne, 1015 Lausanne, Switzerland

Active matter is one of the most exciting fields in statistical mechanics and materials engineering. Thanks to the groundbreaking work of synthetic chemists and material scientists, there is now a continually growing library of synthetic microswimmers and active colloids. These active particles are the synthetic analogs of swimming bacteria, but the synthetic variants have the advantage of tuning systematically both the inter-particle interactions and the hydrodynamic signature of the colloids.

Due to their non-equilibrium nature, most cases of active systems develop emergent behaviors such as collective motion, orientational order or *living clusters*. Some of us have already studied living cluster formation [1], where we have focused on the influence of the hydrodynamic interactions and the competition between the swimming velocity and the interaction strength among active particles with an attractive and isotropic potential, more recently, some of us have also studied the effect of a anisotropic potential in the formation of self-assembled states [2] using active amphiphilic dry colloids. Both studies help to understand in a systematic way, how active and hydrodynamic forces can be exploited in conjunction with anisotropic pair interactions to design macroscopic assemblies with desired structural properties.

Our current research focus on study systematically active amphiphilic swimmers, where in one hand, we have carried out Lattice Boltzmann simulations to model explicitly the swimmers hydrodynamics and on the other hand, we have carried out Brownian dynamics simulations to study systems where temperature plays a role but hydrodynamics interactions are absent.

To model swimmers we have used squirmer model, while the direct interaction between a pair of squirmers has been model in general by a pair-wise potential that depends on the the center-center distance and their attractive patch orientation

$$V(\vec{r}_{ij}, \hat{p}_i, \hat{p}_j) = V_{\text{rep}}(\vec{r}_{ij}) + V_{\text{att}}(\vec{r}_{ij})\phi(\theta_i, \theta_j), \qquad (1)$$

where $\hat{p}_i$ and $\hat{p}_j$ are the attractive patch directions of the particles i and j, respectively, while θ_i and θ_j are their relative orientations with respect of their patch direction. This potential is composed by two short range potentials: one very short-range repulsive part $V_{\text{rep}}(\vec{r}_{ij})$ and an attractive term $V_{\text{att}}(\vec{r}_{ij})$, the range of the attractive potentials is a parameter we have studied in this investigation.

A sketch of the two main cases of Janus swimmer pairs can be seen in Fig. 1: when a particle swim in the direction of the attractive patch, it calls *with the patch* swimmer (WP), while a particle swimming against the patch, it is called *against the patch* swimmer (AP). Another important parameter we have studied is the nature of the orientational part of the potential $\phi(\theta_i, \theta_j)$, which models the amphiphilic feature of the swimmers. We have used two models: one with non-zero torque within the interaction range (blue curve of the bottom panel in Fig. 1) and another one with non-zero torque just around the maximum relative angle between a pair of swimmers (red curve of the bottom panel in Fig. 1).

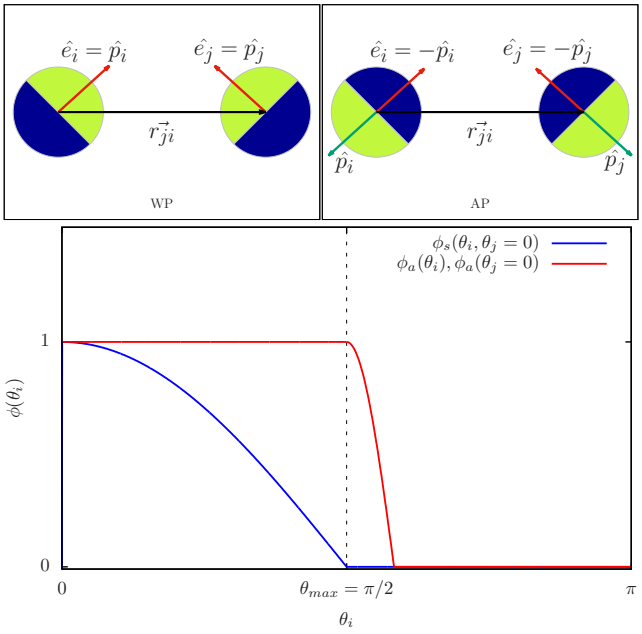

Fig. 1. Upper panels are sketches of the interaction between two Janus swimmers, attractive patch is in green, while non attractive patch is in blue. The direction of the swimming is represented by a red vector $\vec{e}$, the green vectors represent the direction of the attractive patch $\vec{p}$ and the black vector is the center-center distance between two swimmers $\vec{r}_{ij}$. Bottom panel is the graphic representation of the angular part of the Janus potential $\phi(\theta_i, \theta_j)$ in Eq. (1). Blue curve is used in Ref. [3], while red curve is used in Ref. [4].

We have carried out systematic simulations of Janus swimmer suspensions changing the parameters described above. We have characterized the morphology, alignment and dynamics of the self-assembled states and living clusters observed, in order to elucidate the fundamental ingredients needed to design better macroscopic assemblies that could help to design new materials and micro-robots.

[1] F. Alarcón, C. Valeriani, and I. Pagonabarraga, Soft Matter, **13**, 814-826 (2017).

[2] S. A. Mallory, F. Alarcon, A. Cacciuto, and C. Valeriani, New J. Phys. **19**, 125014 (2017).

[3] L. Hong, A. Cacciuto, E. Luijten, and S. Granick, Langmuir **24**, 621-625 (2008).

[4] W. L. Miller and A. Cacciuto, Phys. Rev. E **80**, 021404 (2009).

Exploring long range interactions in neural networks

Alejandro Tlaie[1], Inmaculada Leyva[2], and Irene Sendiña-Nadal[1]
[1]Rey Juan Carlos University, Madrid, Spain
[2]Center for Biomedical Technology, Technical University of Madrid, Madrid, Spain

Complex networks have attracted more and more interest during recent years. They have been used to describe a wide spectrum of physical processes (from gene manifestation [1] to power grid optimization [2]), human interactions (social networks [3], for example) or to describe the brain, among many other applications.

Usually, there are two main ingredients when working with complex networks: the structural part -and the graph theory-based tools used to describe them- and the dynamical part -usually studied by means of statistics and nonlinear dynamics. When studying the temporal dynamics of a network's nodes, the paradigm is to account for the interactions among closest-neighbours (meaning, only directly structurally connected nodes are able to interact).

A recent novel approach, proposed by Estrada *et al.* [4] was to characterize the dynamics in complex networks taking into account more subtle interactions (they propose the term 'indirect peer pressure' when dealing with social networks, for example). This is not only revolutionary because of the technique they introduced but also due to the paradigm shift it would imply.

Following his insights, we have delved into the study of a well known single cell model, the Morris-Lecar neuron [5]

$$C\dot{V}_i = \sum_j g_j \cdot f(V_j - E_{\text{ion}}) + I_{\text{syn},i} + D\xi, \tag{1a}$$

$$\dot{W}_i = \phi\, \tau_w(V_i) \cdot \Big[W_\infty(V_i) - W_i\Big], \tag{1b}$$

where V_i is the main variable (it represents the membrane potential of the cell) and W_i is the recovery one (taking into account that there is a refractary period for the neuron to spike after having done so). This model is used to reproduce the variety of oscillatory behavior in relation to different conductances (for different ions) in the membrane potential of a neuron. Specifically, we compare the results we have already attained with the classical (short range) interactions [6] with these obtained when introducing higher order functional links.

This work is a pioneering one because it is a potential solution to the irreconcilable problem of not modelling the role of glia cells (in particular, astrocytes) in neuronal activity. As different physiological measures have shown [7], these cells not only serve as glue and maintenance cells for neurons but they also participate in the modulation and release of neurontransmitters.

The first promising results in this line of research are that we can achieve a greater synchronization (Fig. 1) when using higher-order interactions than when we don't, a possible –and suggestive– explanation for this being that astrocytes make the neuronal signal more synchronous with less coupling strength (i.e., neurons need less neurotransmitter release to achieve synchronization).

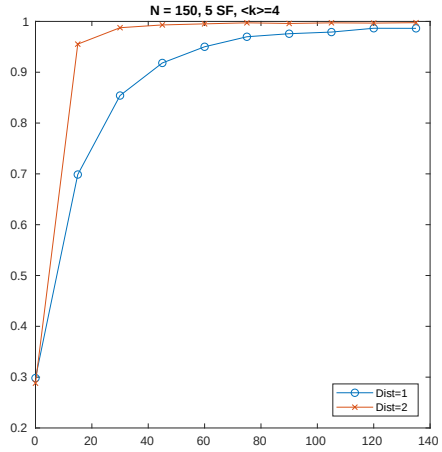

Fig. 1. Synchronization values for different coupling strengths. This is the result of averaging five different realizations of a Scale-Free network of 150 nodes with $\langle k \rangle = 4$. We see that a greater synchronizations is achieved before in the case that we let higher-order interactions take place.

[1] F. M. Lopes, R. M. CesarJr., and L. Da F. Costa, Gene expression complex networks: synthesis, identification, and analysis, J. Comput. Biol. **18** 1353-1367 (2011).

[2] S. Arianos, E. Bompard, A. Carbone, and F. Xue, Power grid vulnerability: A complex network approach, Chaos **19**, 013119 (2009).

[3] M. Grandjean, A social network analysis of Twitter: Mapping the digital humanities community, Cogent Arts Humanit. **3**, 1171458 (2016).

[4] E. Estrada and G. Silver, Accounting for the role of long walks on networks via a new matrix function, J. Math. Anal. Appl. **449**, 1581-1600 (2017).

[5] C. Morris and H. Lecar, Voltage oscillations in the barnacle giant muscle fiber, Biophys. J. **35**, 193-213 (1981).

[6] A. Tlaie, I. Leyva, and I. Sendiña-Nadal, Is it complex to be a hub?, (Submitted).

[7] G. Perea, M. Navarrete, and A. Araque, Tripartite synapses: astrocytes process and control synaptic information, Trends Neurosci. **32**, 421-431 (2009).

Buoyant forces in active Brownian particles?

Joan Codina[1,2] and Ignacio Pagonabarraga[1,2,3]
[1]Departament de la Matèria Condensada, Universitat de Barcelona, c. Martí i Franquès 1, Barcelona, Spain
[2]Institute of Complex Systems (UBICS), Universitat de Barcelona, c. Martí i Franquès 1, Barcelona, Spain
[3]Centre Européen de Calcul Atomique et Moléculaire, Ecole Polytechnique Fédérale de Lausanne, 1015 Lausanne, Switzerland

Active Brownian Particles (ABP) are known to accumulate close to walls [1], how do passive particles behave in such dense fluids? The ABP model introduces particles with spherical symmetry, and diameter σ_a, diffusing in a thermal bath with an out-of-equilibrium characteristic: ABPs have the intrinsic ability to self-propel in a given direction. The orientation of the propulsion diffuses in time, and thus defines a dimensionless number that compares propulsion to rotational diffusion the so called 'Péclet' number, Pe.

It has been previously reported that ABPs propelling towards a wall find themselves an increase of their residence time in contact to the wall. Active particles keep propelling towards the wall until their orientations are diffused so that ABPs can escape, the higher the Pe the higher the residence time.

This increase of the residence time close to walls leads to the formation of a dense layers of ABPs for high enough density, and activity [2]. We have characterized the layer thickness, and fluctuations in terms of the activity and introduced probe particles, passive particles or inclusions, to study the emergent forces. This technique has previously been used [3] to study the emergence of forces between pairs of inclusions in diluted suspensions of ABPs. Here we present a series of measures of emergent forces in the interior of the dense phase, and reveal the appearance of buoyant forces even though no gravity intervenes in such microscopic systems.

We define a computational model to simulate the emergence vertical forces of interactions, F_y, between probe particles and the confining walls of the system. In addition, we introduce forces in the centre-to-centre direction between inclusions F_r, see Fig. 1 for a schematic representation of the system.

Measures of the normal force F_y for fixed probes at different heights reveal the emergence of a force that expels the probe particles from the dense phase to the gas phase. In Fig. 2 we present the normal force for pairs of particles separated a surface-to-surface distance either 1.5, or 3 ABP's diameters, and for a sole inclusion $F_y^{(1)}$. Force computations reveal the emergence of a large wall-repulsion force that extends to the whole layer of particles and reaches a long plateau of constant normal force F_y^{est}. Then at distances beyond the average thickness of the layers the repulsion decreases, and finally disappears. A detailed analysis of the density field of ABPs close to the inclusion pairs reveals a deformation, and vertical pull of the interface between the dense, and gas fluid ABPs phases mediated by the inclusions. Measures for $d = 3\sigma_a$ reveal minor deviations from results on one particle, while in $d = 1.5\sigma_a$ we report an additional two-body contribution to the normal forces.

In the talk I will introduce a simple calculation to capture the constant vertical force for sole inclusions in the system, and numerically extract the two-body contributions to the buoyant force between pairs. Finally, I will extend this calculations to the relative force between pairs and discuss the effect of the coupling with Z in the emergent pair interactions.

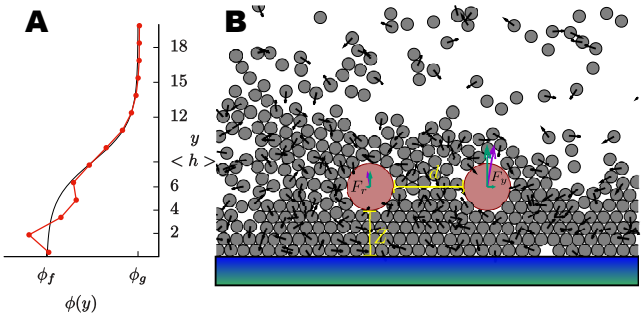

Fig. 1. Accumulation of ABPs close to a wall. (a) Local density of ABPs at a distance y from the wall, the interface is located at $\langle h \rangle$. (b) Sketch of the system with a pair of probe particles in the dense layer of ABPs, in yellow the surface-to-surface distances d for probe-probe distances, and Z for the wall-probe distance. In arrows the radial force F_r, and the normal force F_y on each particle.

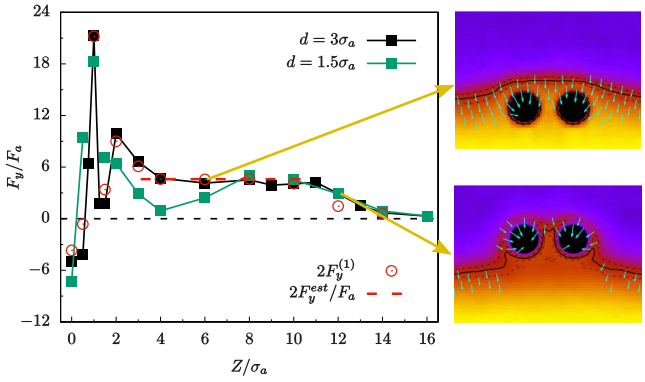

Fig. 2. A pair of inclusions different heights from the surface of the wall for $d = 1.5\sigma_a$, $d = 3\sigma_a$, and two sole inclusions in red dots. The right panels depict the average density field of active particles with arrows pointing in average direction.

[1] J. Elgeti and G. Gompper, Wall accumulation of self-propelled spheres, Europhys. Lett. **101**, 48003 (2013).

[2] D. Levis, J. Codina, and I. Pagonabarraga, Active Brownian equation of state: metastability and phase coexistence, Soft matter **13**, 8113-8119 (2017).

[3] J. Harder, S.A. Mallory, C. Tung, C. Valeriani, and A. Cacciuto, The role of particle shape in active depletion, J. Chem. Phys. **141**, 194901 (2014).

To remember or not to remember? An account of memory random walks

Daniel Campos and Vicenç Méndez
Grup de Física Estadística, Universitat Autònoma de Barcelona, 08193 Bellaterra, Spain

From an evolutionary point of view, an important innovation that emerged at some moment of history is active adaptation, i.e., the capacity of living systems to use their cognitive systems to sense the environment and react to their changes correspondingly. While this capacity can exhibit different levels of complexity (from microorganisms to humans), it is clear that one essential ingredient it requires is memory (for pattern recognition, decision making, etc.).

A basic function of living systems that can be used to explore this active adaptation is spatial exploration for foraging. Actually, spatial exploration of Y-mazes by animals with reward is a recurrent experimental case of study for cognitive biologists and neuroscientists, one which has recently provided the first evidence of mental simulations prior to execution in cognitive processing of rats [1], a result which challenges the classical stimulus-response paradigm in biology.

The elementary toy models statistical physicists have to explore such spatial processes are random walks [2, 3]. So, introducing and analyzing the possibility of memory (as well as prospective simulations) on the behavior of random walkers, even at a very basic level, represents a topic of major interest in the frontier between physics and biology. In the present contribution we will try to (i) present a very brief account on the field of random walks with memory and/or with nonlocal time effects (e.g., 'elephant walks', 'reinforced walks', among other) that our group and others have recently explored [4, 5], and (ii) discuss what are the main challenges we face nowadays in order to take such models progressively to a level where direct comparison with biological data is possible [6, 7].

[1] B. E. Pfeiffer and D. J. Foster, Hippocampal place-cell sequences depict future paths to remembered goals, Nature **497**, 74-79 (2013).

[2] E. A. Codling, M. J. Plank, and S. Benhamou, Random walks models in biology, J. R. Soc. Interface **5**, 813-834 (2008).

[3] V. Méndez, D. Campos, and F. Bartumeus, *Stochastic Foundations of Movement Ecology* (Springer-Verlag, Berlin, 2014).

[4] D. Boyer and C. Solis-Salas, Random walks with preferential relocations to places visited in the past and their application to biology, Phys. Rev. Lett. **112**, 240601 (2012).

[5] D. Campos, F. Bartumeus, and V. Méndez, Nonstationary dynamics of encounters: Mean valuable territory covered by a random searcher, Phys. Rev. E **96**, 032111 (2017).

[6] J. A. Merkle, D. Fortin, and J. M. Morales, A memory based foraging tactic reveals an adaptive mechanism for restricted space use, Ecol. Lett. **17**, 924-931 (2014).

[7] F. Bartumeus, D. Campos, R. Lloret-Cabot, V. Méndez, and J. Catalan, Foraging success under uncertainty: search tradeoffs and optimal space use, Ecol. Lett. **19**, 1299-1313 (2016).

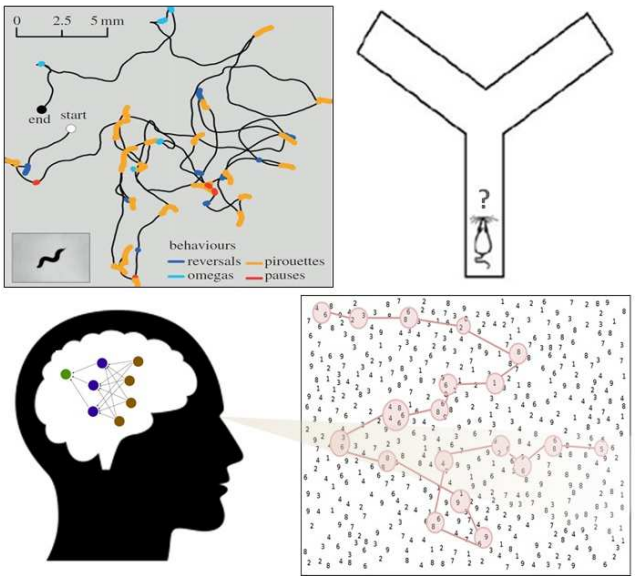

Fig. 1. Different levels of biological complexity in the use of memory for spatial exploration.

Nonlinear population dynamics in a bounded habitat

E. H. Colombo[1,2] and C. Anteneodo[2,3]
[1]IFISC, CSIC-UIB, Campus Universitat Illes Balears, 07122 Palma de Mallorca, Spain
[2]Departament of Physics, PUC-Rio, Rio de Janeiro, Brazil
[3]Institute of Science and Technology for Complex Systems, Rio de Janeiro, Brazil

Population dynamics is constrained by the environment, which needs to obey certain conditions to support individual's survival. Through the last decades, theoretical developments have been made to identify the environment spatiotemporal structures for which the population is sustainable. These advances comes in crucial times where habitats have been suffering drastic transformations, from degradation of the landscape to climate changes.

In order to understand this issue, one typically looks for the critical line in the environment parameter space that separates the population survival and extinction phases. In the classical work by Skellam [1], a single population lives in a static habitat domain of size L. In this minimal case, simple laws for individual behavior are considered, assuming, for instance, random motion and density independent reproduction rates. In terms of the balance between the spatial scales present, it is straightforward to find that exists an L_c above which the population survives. In Fig. 1 we show the temporal evolution of the population density distribution for habitat size below, at and above L_c. Since then, many improvements have been made considering different habitat boundary conditions, individual behavior and time variability. Nevertheless, despite the fact that L_c is sensitive to the modeling details, it is a common feature that L_c is always a lower bound to habitat size.

In this work [2], we investigate an extension of this problem, proposing a general formulation that introduces density-dependent feedbacks in organisms' mobility and reproduction rate. Explicitly, we address the class of dynamics given by $\partial_t \rho = \partial_x(\rho^{\nu-1}\partial_x\rho) + \rho^{\mu} + \mathcal{O}(\rho^{\mu+\varepsilon})$, where μ and ν are real parameters that regulate the degree of nonlinearity present. We obtained exact expressions for the critical habitat size L_c and the profiles for the steady states. Together with numerical simulations, we show that depending on the region in the parameter space $\mu - \nu$, the population survival can occur for either for $L \geq L_c$, $L \leq L_c$ or even for any L (see Fig. 2). This generalizes the common statement that L_c represents the minimum habitat size. In addition, nonlinearities introduce dependence on the initial conditions, affecting L_c. We show that, despite the counterintuitive changes in the stability on the critical line L_c, as more individuals are introduced the survival phase is always increased.

[1] J. G.Skellam, Random dispersal in theoretical populations, Biometrika **38**, 196-218 (1951).

[2] E. H. Colombo and C. Anteneodo, Nonlinear population dynamics in a bounded habitat, J. Theor. Biol. **446**, 11-18 (2018).

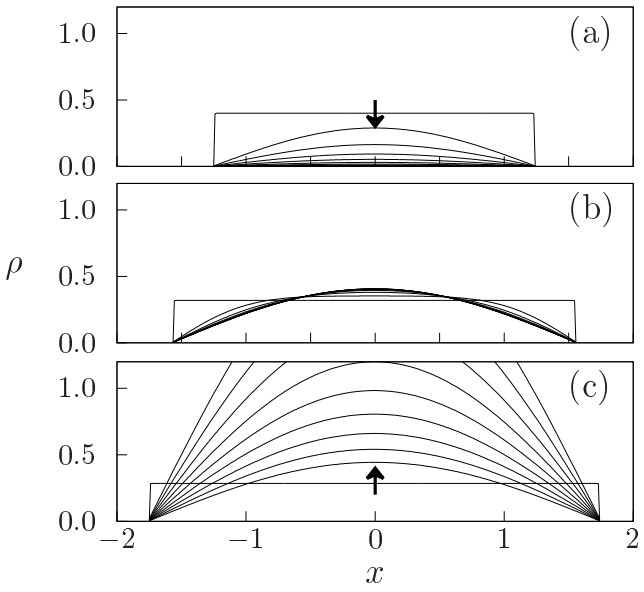

Fig. 1. Temporal evolution of the density distribution profile for the linear case in a one-dimensional habitat domain with harsh boundary condition. For (a) $L < L_c$, (b) $L = L_c$ and (c) $L > L_c$, the population becomes extinct, attains a steady state or blows up, respectively. The lines are produced by the analytical solutions. The arrows indicate the direction of time.

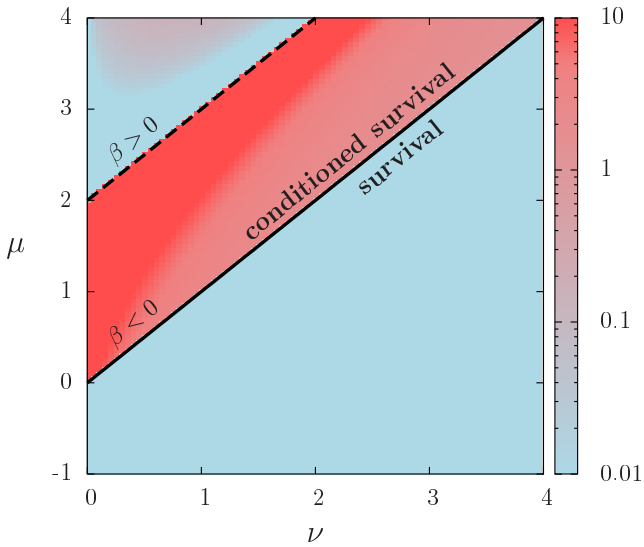

Fig. 2. Color map of the habitat size L_c in the plane (ν, μ), for initial condition $N_0 = 1$. The solid line $\mu = \nu$ separates the phases where survival always occurs (below) or it is conditioned (above). The dotted line separates where survival occur for $L > L_c$ (below) or $L < L_c$ (above). The parameter $\beta = 1 + 2/(\mu - \nu - 2)$, rules the scaling relation between $L_c \sim N_0^{\beta}$, where N_0 is the initially introduced population size. At the dotted line, $L_c \to \infty$.

Effect of time-to-collision in the interaction between pedestrians

Javier Cristin and Daniel Campos
Department of Physics, Universitat Autonoma de Barcelona, 08193 Bellaterra, Barcelona, Spain

According to the experimental results obtained in Ref. [1], pedestrians walking in two directions show a time-to-collision interaction, apparently disregarding the spatial distance between individuals, unlike most of the best-known physical systems. This temporal dependance implies a processing of the information, i.e., a calculus of how much time the pedestrian has to avoid the collisions for given conditions. Furthermore, the interaction potential obtained with the experimental data presents a very interesting behavior

$$U(\tau) = \frac{k}{\tau^2} e^{\frac{-\tau}{\tau_0}}. \quad (1)$$

Intuitively, an interaction which produces a bigger force when the collision is very close in time is expectable, but what is the cause of a power law with that certain exponent? To undergo the question, we analyse a system with non-intelligent pedestrians, which means they repel each other uniquely with a spatial and repulsive potential.

We observe that the combination of a repulsive potential and a forcing to go in a certain direction (cross the street in one of the two possible senses) enhances an effective interaction based in the time-to-collision distance obeying the law presented in Ref. [1].

[1] I. Karamouzas, B. Skinner, and S. J. Guy, Phys. Rev. Lett. **113**, 238701 (2014).

Stochastic animal foraging models with resets: General approach and new ingredients

Axel Masó-Puigdellosas, Daniel Campos, and Vicenç Méndez
Grup de Física Estadística, Departament de Física, Universitat Autònoma de Barcelona, 08193 Bellaterra, Barcelona, Spain

In the last decades a lot of effort has been put into the description of the territorial motion of animals [1]. Among the models that have been proposed, diffusion-based models, Lévy flights and Lévy walks are three of the most used. Nevertheless, in the vast majority of these approaches, only the foraging process of the animals was described (i.e., their motion while they are collecting) and it had not been attempted to study their overall behaviour, including the return to the nest after their search is completed.

On this direction, in 2011 Evans and Majumdar [2] studied the properties of a model consisting on a diffusive process subject to resets with constant rate (i.e., the reset times are exponentially distributed). For this process, the mean first passage time (MFPT) is finite and the mean square displacement (MSD) collapses to a stationary value unlike a simple diffusive process which has infinite MFPT and the MSD scales linearly with time. The fact that the system achieves a stationary state allows us to define the territoriality of a given species being a quantitative measure of the region that the animals occupy around its nest.

From then on, multiple processes have been studied when they are subject to resets but no general study of the robustness of the properties found in [2] has been done. In this work we address this issue by analysing general properties of foraging processes with resets from a continuous-time random walk (CTRW) perspective. Moreover, we use a Mittag-Leffler distribution for the reset times, a generalisation of the exponential distribution which can also take the form of a long-tailed distribution.

On one hand, we derive a general equation for the MSD of the process with resets in terms of the MSD of the intrinsic process. From it, we conclude that all the processes whose MSD is Laplace-transformable and finite reach a stationary value when exponentially distributed resets are applied to them. On the other hand, we study the finiteness of the mean first arrival time (MFAT) of the process. We derive the conditions under which it is finite for a general power-law asymptotic behaviour of the intrinsic survival probability $Q_x(t) \propto t^{-q}$ and study some cases of particular interest as the diffusive process or the Lévy flights.

With the aim of adjusting the present formulation to real cases, we also propose a new model for the description of the movement of the animals consisting in the introduction of a new element to the CTRW with resets: a retention mechanism at the origin. This novel ingredient is motivated by the fact that when animals return to their nest after a collecting trip, they rest there some time before starting another trip. For this model we also study the MSD and the MFAT for general intrinsic processes and reset and retention time distributions, studying more deeply some cases of particular interest in ecology.

[1] F. Bartumeus, M. G. E. Da Luz, G. M. Viswanathan, and J. Catalan, Animal search strategies: a quantitative random-walk analysis, Ecology **86**, 3078-3087 (2005).

[2] M. R. Evans and S. N. Majumdar, Diffusion with stochastic resetting, Phys. Rev. Lett. **106**, 160601 (2011).

Mechanics, thermodynamics, and kinetics of ligand binding to biopolymers

Javier Jarillo[1], José A. Morín[2], Elena Beltrán-Heredia[1], Juan P. G. Villaluenga[1], Borja Ibarra[2], and Francisco J. Cao[1,2]

[1]Departamento de Estructura de la Materia, Física Térmica y Electrónica, Facultad de Ciencias Físicas, Universidad Complutense de Madrid, pl. Ciencias 1, 28040 Madrid, Spain

[2]Instituto Madrileño de Estudios Avanzados en Nanociencia (IMDEA Nanociencia), c. Faraday 9, 28049 Madrid, Spain

Ligands binding to polymers regulate polymer functions by changing their physical and chemical properties. This ligand regulation plays a key role in many biological processes.

We propose here a model to explain the mechanical, thermodynamic, and kinetic properties of the process of binding of small ligands to long biopolymers. These properties can now be measured at the single molecule level using force spectroscopy techniques. Our model performs an effective decomposition of the ligand-polymer system on its covered and uncovered regions, showing that the elastic properties of the ligand-polymer depend explicitly on the ligand coverage of the polymer (i.e., the fraction of the polymer covered by the ligand). The equilibrium coverage that minimizes the free energy of the ligand-polymer system is computed as a function of the applied force. We show how ligands tune the mechanical properties of a polymer, in particular, its length and stiffness, in a force dependent manner. In addition, it is shown how ligand binding can be regulated applying mechanical tension on the polymer.

Moreover, the binding kinetics study shows that, in the case where the ligand binds and organizes the polymer in different modes, the binding process can present transient shortening or lengthening of the polymer, caused by changes in the relative coverage by the different ligand modes. Our model will be useful to understand ligand-binding regulation of biological processes, such as the metabolism of nucleic acid. In particular, this model allows estimating the coverage fraction and the ligand mode characteristics from the force extension curves of a ligand-polymer system.

We illustrate the power of the method based in this model with the analysis of experimental results of Human mitochondria SSB (HmtSSB) binding to single stranded DNA (ssDNA), which has allowed to characterize the binding modes and coverage of HmtSSB-ssDNA complexes in several configurations, including ssDNA generated during DNA replication.

[1] J. Jarillo, J. A. Morín, E. Beltrán-Heredia, J. P. G. Villaluenga, B. Ibarra, and F. J. Cao, Mechanics, thermodynamics, and kinetics of ligand binding to biopolymers, PLoS ONE **12**, e0174830 (2017).

[2] J. A. Morín, F. Cerrón, J. Jarillo, E. Beltrán-Heredia, J. R. Arias, G. L. Ciesielski, L. S. Kaguni, F. J. Cao, and B. Ibarra, DNA synthesis determines the binding mode of the human mitochondrial single-stranded DNA-binding protein, Nucleic Acids Res. **45**, 7237-7248 (2017).

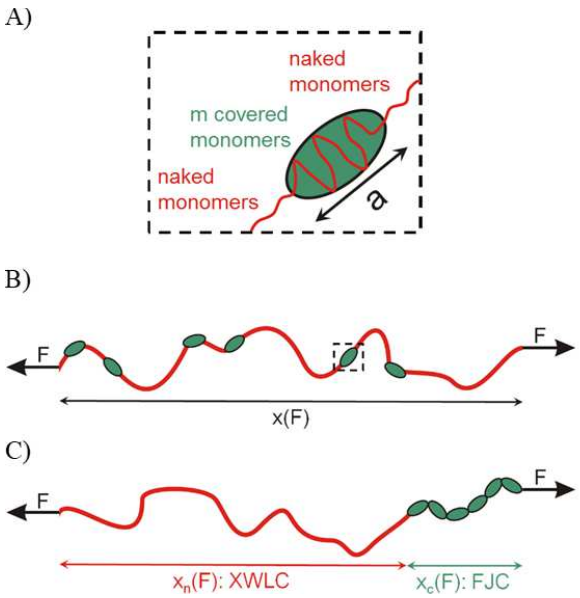

Fig. 1. (a) Zoom of a ligand bound to a polymer. Each ligand covers m monomers, and the end-to-end distance of the DNA segment covered by one ligand is given by the parameter a. (b) Scheme of a polymer (red), partially covered by ligands (green), under a tension F. (c) Effective mechanical decomposition of the partially covered polymer in two chains: one chain corresponds to the naked region and the other chain corresponds to the covered region. Note that distribution of ligands along the polymer is important for thermodynamic properties, this effective mechanical decomposition was done to effectively compute the extension. An extensible worm-like chain (XWLC) model is considered for the naked region, while a freely-jointed chain (FJC) model is assumed for the covered region.

Selection, folding, stability, and aggregation of proteins in a water-protein coarse grain model

Valentino Bianco[1], Giancarlo Franzese[2], Christoph Dellago[3], and Ivan Coluzza[4]
[1]Universidad Complutense de Madrid, Madrid, Spain
[2]Universitat de Barcelona, Barcelona, Spain
[3]Universität Wien, Vienna, Austria
[4]CIC biomaGUNE Research Institute, San Sebastian, Spain

Proteins are molecules made of a sequence of amino acids that fold into the native structures. Such a structure is usually stable within a certain range of temperatures and pressures, beyond which a protein denaturate. Such a phenomenon is well known at higher temperatures, where the thermal fluctuations disrupt the native conformation. However, similar phenomena are observed by decreasing the temperature or by increasing the pressure, respectively known as cold- and pressure-denaturation. Moreover, in order to guarantee the correct biological functions, proteins have evolved to have a low enough propensity to aggregate within a range of protein expression required for their biological activity, but with no margin to respond to external factors increasing/decreasing their expression/solubility.

Indeed, protein aggregation is mostly unavoidable when proteins are expressed at concentrations higher than the natural ones. Water and the hydrophobic effect play a major role in these phenomena, affecting the hydrophilic/hydrophobic composition of stable sequences, driving the folding of the proteins and contributing to their stability.

Here, using a coarse-grain model on lattice [1, 2, 3, 4, 5], which includes the protein effects on the water properties in the hydration shell and accounts explicitly for the thermodynamic properties of water, we investigate the folding [2, 3], the stability [4] and the aggregation [5] of proteins.

[1] V. Bianco, S. Iskrov, and G. Franzese, Understanding the role of hydrogen bonds in water dynamics and protein stability, J. Biol. Phys. **38**, 27-48 (2012).

[2] V. Bianco and G. Franzese, Contribution of water to pressure and cold denaturation of proteins, Phys. Rev. Lett. **115**, 108101 (2015).

[3] V. Bianco, N. Pagès-Gelabert, I. Coluzza, and G. Franzese, How the stability of a folded protein depends on interfacial water properties and residue-residue interactions, J. Mol. Liq. **245**, 129-139 (2017).

[4] V. Bianco, G. Franzese, C. Dellago, and I. Coluzza, The role of water in the selection of stable proteins in extreme thermodynamic conditions, Phys. Rev. X **7**, 021047 (2017).

[5] V. Bianco and I. Coluzza, Pathways on protein aggregation, (in preparation).

Globule-like conformation and enhanced diffusion of active polymers

Valentino Bianco[1], Emanuele Locatelli[2], and Paolo Malgaretti[3]
[1]Universidad Complutense de Madrid, Madrid, Spain
[2]Universität Wien, Vienna, Austria
[3]Max Planck Institute for Intelligent Systems, Stuttgart, Germany

We study the dynamics and conformation of polymers composed by active monomers. By means of Brownian dynamics simulations we show that when the direction of the self-propulsion of each monomer is aligned with the backbone, the polymer undergoes a coil-to-globule-like transition, highlighted by a marked change of the scaling exponent of the gyration radius.

Concurrently, the diffusion coefficient of the center of mass of the polymer becomes essentially independent of the polymer size for sufficiently long polymers or large magnitudes of the self-propulsion. These effects are reduced when the self-propulsion of the monomers is not bound to be tangent to the backbone of the polymer.

Our results, rationalized by a minimal stochastic model, open new routes for activity-controlled polymer and, possibly, for a new generation of polymer-based drug carriers [1].

[1] V. Bianco, E. Locatelli, and P. Malgaretti, Globule-like conformation and enhanced diffusion of active polymers, arXiv: 1805.08879.

Identification of protein functional regions

Francesca Nerattini[1], Luca Tubiana[1], Chiara Cardelli[1], Valentino Bianco[1], Christoph Dellago[1], and Ivan Coluzza[2]
[1]Faculty of Physics, University of Vienna, Boltzmanngasse 5, 1090 Vienna, Austria
[2]CIC biomaGUNE, po. Miramon 182, 20014 San Sebastian, Spain

Functional regions of proteins have evolved to have specific patterns of amino acids tailored to the activity of the biomolecule. The identification of the functional region of such protein families was obtained with large scale mutation experiments where the effect on the protein function was tested against each alteration [1]. The information obtained with such experiments can have important implications for the mapping of the proteome interactions, as well as for many pharmaceutical applications, e.g., by identifying ligand binding regions for targeted pharmaceutical protein design. However, the experimental determination of the functional regions is generally time consuming and require extensive resources, hence a computational approach could help towards the final goal.

In this work we propose an approach to identify functional regions of proteins to distinguish between residues that have a strictly functional role from the one that are important for the protein structural stability. The methodology that we propose here is based on the hypothesis that an artificial evolution process based on protein design, in the absence of any functional constraints, would lead only to co-evolution events of the structural type.

Using Direct Coupling Analysis (DCA) [2] we identify conserved and co-evolved residues both in natural and artificial evolution processes. Simply by subtracting the list of structural residues form the natural correlated and conserved ones, we show that we identify the functional residues.

[1] M. E. Cusick, N. Klitgord, M. Vidal, and D. E. Hill, Interactome: Gateway into systems biology, Hum. Mol. Genet. **14**, R171-R181 (2005).

[2] M. Weigt, R. A. White, H. Szurmant, J. A. Hoch, and T. Hwa, Identification of direct residue contacts in protein-protein interaction by message passing, Proc. Natl. Acad. Sci. USA, **106**, 67-72 (2009).

Heteropolymer design and folding of arbitrary topologies reveals an unexpected role of alphabet size on the knot population

Chiara Cardelli[1], Luca Tubiana[1], Valentino Bianco[1], Francesca Nerattini[1], Christoph Dellago[1], and Ivan Coluzza[2]
[1]Faculty of Physics, University of Vienna, Boltzmanngasse 5, 1090 Vienna, Austria
[2]CIC biomaGUNE, po. Miramon 182, 20014 San Sebastian, Spain

Obtaining complex topological micro- and nano-materials in a controlled way is an open challenge for material science and chemistry. Recent experimental and computational studies have demonstrated the feasibility of self-assembling knots with up to 8 crossings starting from small, identical building blocks.

In this work, we investigate computationally a different pathway for knot production. By performing extensive computer simulations of hetero patchy polymers with different patch geometries, we show that it is possible to obtain both torus and twist knots, up to knots with more than 12 crossings.

Our results indicate that with patchy-polymers it is possible to exploit the bending rigidity of the backbone, the specific geometry of the patches and the alphabet size to control the spectra of knots of the polymer. In particular, we find that increasing the alphabets to 20 letters tends to suppress knots, a finding that points to a new hypothesis to explain the rarity of knots in proteins.

Finally, we demonstrate the ability to fold specific knotted conformations with high precision by designing the heteropolymer sequence. These include both diffuse and highly localised knots as well as two topologies which have not yet been synthesised by self-assembly, the 5_2 and the 10_{124} knot.

Effects of species interactions on the spatial scales of population synchrony: Competition and predation

Javier Jarillo[1], Bernt-Erik Sæther[2], Steinar Engen[3], and Francisco J. Cao[1,4]

[1]Dept. de Estructura de la Materia, Física Térmica y Electrónica, Universidad Complutense de Madrid, Madrid, Spain

[2]Dept. of Biology, Centre for Biodiversity Dynamics, Norwegian University of Science and Technology, Trondheim, Norway

[3]Dept. of Mathematical Sciences, Centre for Biodiversity Dynamics, Norwegian University of Science and Technology, Trondheim, Norway

[4]Instituto Madrileño de Estudios Avanzados en Nanociencia (IMDEA Nanociencia), Madrid, Spain

In virtually all major taxa it has been observed that the population fluctuations around the equilibrium at different locations are usually correlated over large geographical scales [1]. This spatial synchronization of the species population dynamics is an extremely important characteristic, since it has been found that the degree of population synchrony tends to be correlated with the regional extinction risk of the species [2]. It has been found that the population synchrony can be affected by inter–species interactions (e.g., [3]). Here, we employ two-species models to analyze how interspecific interactions affects the characteristic spatial scales of population synchrony.

First, we employ spatial two-competitor models to analyze the effects of competition [4]. In such models, we assume that species are able to disperse between locations of the habitat. When the environmental fluctuations affecting the competitors are uncorrelated, competition generally increases the spatial scales of population synchrony of both competitors (Fig. 1). When the environmental fluctuations affecting the competitors are correlated, competition generally increases the spatial scale of population synchrony of at least one, but often both species.

Second, we study the effects of predation in the spatial scales of population synchrony, employing predator-prey models. On the one hand, the spatial scale of population synchrony of the predator is greater than (or, at least, similar to) the spatial scale of the prey (Fig. 2). On the other hand, the presence of the predator increases the spatial scale of synchrony of the prey. These results point that in real ecosystem the spatial scaling of population synchrony is expected to increase with the trophic level.

Finally, harvesting can modify the degree of population synchrony of the harvested species [5], and also of the other interacting unharvested cohabitants [4]. Hence, since a higher synchronization on the species dynamics would increases the regional extinction risk, our results are relevant for the development of improved sustainable harvesting strategies.

[1] A. Liebhold, W. D. Koenig, and O. N. Bjørnstad, Spatial Synchrony in Population Dynamics, Annu. Rev. Ecol. Evol. Syst. **35**, 467 (2004).

[2] M. Heino, V. Kaitala, E. Ranta, and J. Lindstrom, Synchronous dynamics and rates of extinction in spatially structured populations, Proc. Natl. Acad. Sci. USA **264**, 481 (1997).

[3] B. Blasius, A. Huppert, and L. Stone, Complex dynamics and phase synchronization in spatially extended ecological systems, Nature **399**, 354 (1999).

[4] J. Jarillo, B.-E. Sæther, S. Engen, and F. J. Cao, Spatial scales of population synchrony of two competing species: effects of harvesting and strength of competition, Oikos (in press), DOI: 10.1111/oik.05069

[5] S. Engen, F. J. Cao, and B.-E. Sæther, The effect of harvesting on the spatial synchrony of population fluctuations, Theor. Popul. Biol. (in press), DOI: 10.1016/j.tpb.2018.05.001

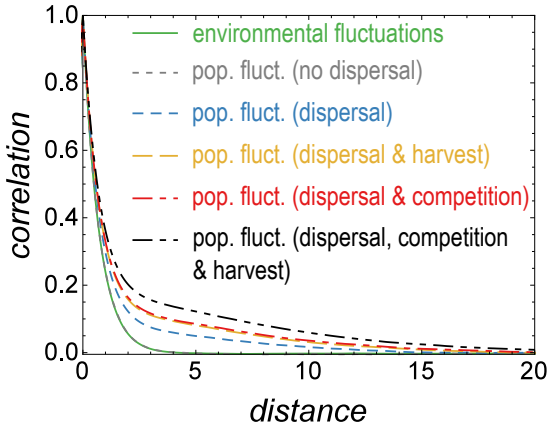

Fig. 1. Autocorrelation functions for environmental (green solid line) and population fluctuations (dashed lines): for no-harvested and no-dispersing species (grey); for dispersing species (blue); for harvested dispersing species (yellow); for dispersing species in the presence of a competitor (red); and for harvested dispersing species in the presnce of a competitor (black).

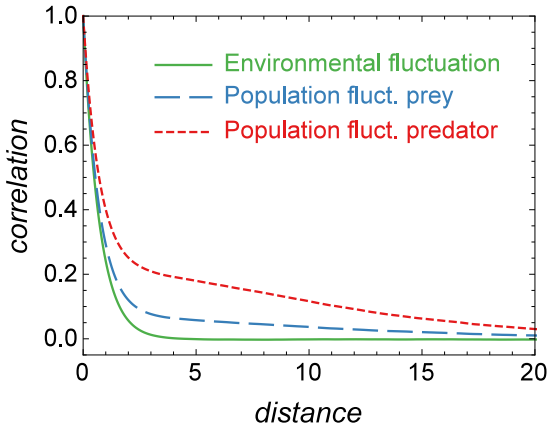

Fig. 2. Autocorrelation functions for environmental and population fluctuations in a predator-prey model. In green solid line, autocorrelation function of the environmental conditions affecting the prey. In blue dashed line, autocorrelaton function of the population fluctuations of the prey. In red dashed line, autocorrelation function of the population fluctuations of the predator.

Stokes's law in a bath of colloidal hard spheres

Antonio M. Puertas[1], F. Orts[2], G. Ortega[3], and E. M. Garzón[2]
[1]Group of Complex Fluids Physics, Dpt. of Applied Physics, Univ. of Almería, ctra. Sacramento s/n, 04120 Almería, Spain
[2]Supercomputation-Algorithms Group, Dpt. of Informatics, Univ. of Almería, ceiA3, ctra. Sacramento s/n, 04120 Almería, Spain
[3]Computer Architecture Dpt., Universidad de Málaga, ETSI. Informática, Campus Teatinos, 29071 Málaga, Spain

Stokes's law provides the friction force experienced by a spherical particle inmersed in a Newtonian fluid. This force is proportional to the particle radius, external force, and solvent viscosity and a geometrical factor. Stokes's law is valid for small Peclet numbers, namely, small external forces. Within the Navier-Stokes description of the bath, different works have extended this law to the case of compressible fluids, or viscoelastic ones, but the same relation is obtained between the friction force and viscosity when a constant force is applied, in the stationary regime.

In this work, we present simulations of a fluid colloidal hard spheres where a large colloidal tracer has been introduced (see the snapshot in Fig. 1). All particles, including the intruder, undergo microscopic Langevin dynamics, and a small constant external force acts only onto the tracer. Its stationary (long-time) velocity is used to obtain the effective friction coefficient γ_{eff}. A finite size analysis must be performed, as the large size of the tracer induces strong finite size effects. It is found that the inverse friction coefficient depends linearly on the inverse simulation box size, as expected from theoretical arguments based on the Navier-Stokes equation, only for small sizes. Contrary to this prediction, for large systems the friction coefficient becomes independent on the system size.

The ratio of γ_{eff} to the solvent friction coefficient, included in the microscopic dynamics, grows for increasing size of the tracer and reaches a plateau for large sizes (tracer size to bath particle size above six), apparently reaching the limit where the bath is described as a continuous medium. The value of the friction coefficient, however, does not agree with the result from Stokes's law. The origin of the discrepancy is traced back to the dissipative character of the microscopic Langevin dynamics.

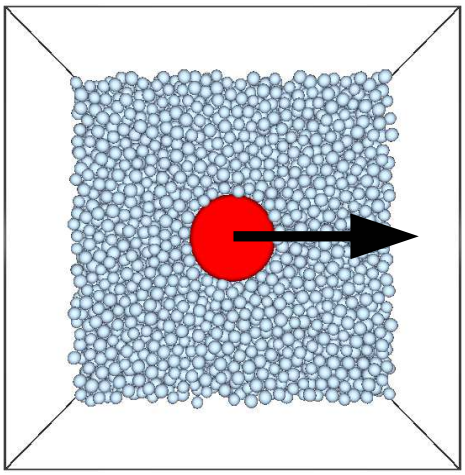

Fig. 1. Snapshot of the system with a large tracer (marked in red). The arrow indicates the external force. The particles in front of the tracer have been removed.

Structural properties of the Jagla fluid

A. Rodríguez-Rivas[1], M. López de Haro[2], S. B. Yuste[1], and A. Santos[1]
[1]Departamento de Física and Instituto de Computación Científica Avanzada (ICCAEx), Universidad de Extremadura, Badajoz E-06071, Spain
[2]Instituto de Energías Renovables, Universidad Nacional Autonoma de México (UNAM), Temixco, Morelos 62580, Mexico

The structural properties of the Jagla fluid [1] are studied by Monte Carlo (MC) simulations, numerical solutions of integral equation theories, and the (semi-analytic) rational-function approximation (RFA) method [2, 3, 4].

The Jagla intermolecular pair potential is a spherically symmetric potential consisting of a short-range hard core, a repulsive linear shoulder, and a linear attractive well. It belongs to a family of so-called core-softened potentials and has been invoked to cope with thermodynamic anomalies, such as reentrant melting and the density anomaly, and in connection with liquid-liquid phase transitions in water and other substances [5, 6, 7]. Moreover, the Jagla potential includes as interesting particular cases the ramp and the triangle-well potentials.

The RFA results of the present work [8] are obtained from the assumption (supported by our MC simulations) that the Jagla potential and a potential with a hard core plus an appropriate piecewise constant function lead to practically the same cavity function. The predictions obtained for the radial distribution function $g(r)$ from the RFA method are compared against MC simulations and integral-equation theories for the Jagla model, and also for the limiting cases of the triangle-well potential and the ramp potential, with a general good agreement.

The analytic form of the RFA in Laplace space allows us to describe the asymptotic behavior of $g(r)$ in a clean way and compare it with MC simulations for representative states with oscillatory or monotonic decay, as shown in Fig. 1. The RFA predictions for the Fisher-Widom and Widom lines [9] of the Jagla fluid confirms that this approach is both simple and useful. The RFA produces very reasonable estimates of the damping coefficients for either the monotonic or oscillatory behavior and, in this latter instance, it even leads to an excellent theoretical prediction of the wavelength.

All of the above provides support to the idea that a similar approach to the one followed here for the Jagla fluid may be profitably employed to compute the structural properties of fluids whose molecules interact with other continuous potentials.

[1] E. A. Jagla, J. Chem. Phys. **111**, 8980 (1999).

[2] A. Santos, S. B. Yuste, and M. López de Haro, Condens. Matter Phys. **15**, 23602 (2012).

[3] A. Santos, S. B. Yuste, M. López de Haro, M. Bárcenas, and P. Orea, J. Chem. Phys. **139**, 074503 (2013).

[4] A. Santos, *A Concise Course on the Theory of Classical Liquids. Basics and Selected Topics*, Lecture Notes in Physics, Vol. 923 (Springer, New York, 2016).

[5] E. Velasco, L. Mederos, G. Navascués, P. C. Hemmer, and G. Stell, Phys. Rev. Lett. **85**, 122 (2000).

[6] G. Franzese, G. Malescio, A. Skibinsky, S. V. Buldyrev, and H. E. Stanley, Nature **409**, 692 (2001).

[7] L. Xu, F. Mallamace, Z. Yan, F. W. Starr, S. V. Buldyrev, and H. E. Stanley, Nat. Phys. **5**, 565 (2009).

[8] M. López de Haro, A. Rodríguez-Rivas, S. B. Yuste, and A. Santos, Structural properties of the Jagla fluid, Phys. Rev. E (in press) [arXiv:1805.06874].

[9] M. E. Fisher and B. Widom, J. Chem. Phys. **50**, 3756 (1969).

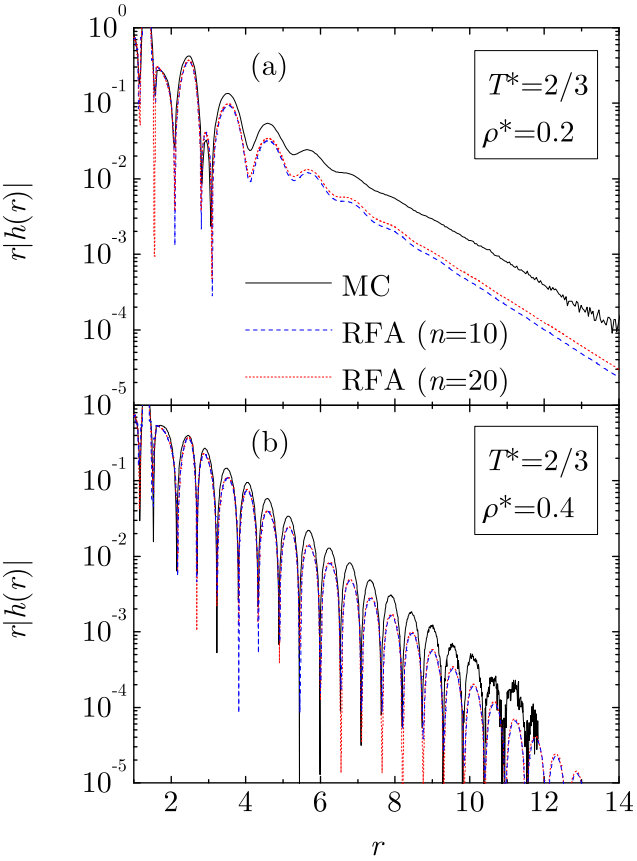

Fig. 1. Semilogarithmic plot of $r|h(r)|$ for a fluid with a Jagla potential ($\lambda_1 = 1.3$, $\lambda_2 = 1.6$, $\epsilon_1/\epsilon_2 = 1$) at (a) $(T^*, \rho^*) = (2/3, 0.2)$ and (b) $(T^*, \rho^*) = (2/3, 0.4)$. The solid, dashed, and dotted lines correspond to MC simulations, and to the RFA with $n = 10$ and $n = 20$ steps, respectively.

Thermal convection in granular gas of hard disk with dissipative lateral walls under zero gravity

Álvaro Rodríguez-Rivas[1], Miguel Ángel López-Castaño[1], and Francisco Vega Reyes[1,2]
[1]Departamento de Física, Universidad de Extremadura, av. Elvas s/n, 06071 Badajoz, Spain
[2]Instituto de Computación Avanzada (ICCAEx), Universidad de Extremadura, av. Investigación s/n, 06071 Badajoz, Spain

We study in this work the properties of thermal convection in a granular system with no gravity (i.e., $g = 0$). As it is known, Rayleigh-Bénard convection results from the competition of a thermal gradient against gravity volume [1]. Usually, this thermal gradient is caused by temperature sources. In the present work, however we specifically analyze the role of thermal gradients caused by the action of dissipative walls. More specifically, we study thermal convection in a low density granular gas enclosed by four walls when there is no gravity. Some previous studies suggest that dissipative walls (DW, lateral in the sense that they are perpendicular to gravity, if present) are the direct cause of the automatic appearance of convection cells, in a granular under the action of a gravity field [2].

In this work, we show that *this dissipative-wall-driven convection is present also when there is no gravity*. For this, we present event-driven MD simulations of granular gas composed of identical smooth hard disks. As we said, the system is enclosed by four walls, and there no gravitational field (i.e., $g = 0$). In Fig. 1 we can see the shape of the convection generated in this kind of configuration. The walls delimit a rectangular region and the rotational degrees of freedom of particles are ignored (our discs are spinless). The kinetic energy loss upon a particles pair is characterized by a constant coefficient of normal restitution, denoted as α. The system is also provided a pair of walls (in Fig 1, the horizontal walls) with a kinetic energy source. We denote the other two walls as "lateral" walls. The lateral walls-particle collisions are characterized by a constant coefficient of normal restitution denoted as α_{w}.

When the lateral walls are elastic (wall-particle collisions preserve kinetic energy), the system shows a steady base state that is hydrostatic, but if the α_{w} parameter decreases, i.e., the lateral walls act as a surface energy sink, the steady state becomes convective [3]. Dissipation at the lateral walls generates an additional gradient that is perpendicular to thermal gradient from temperature sources.

In order to clarify the role of the walls in the generation of the new convection steady state, it is necessary to characterize completely the transition from hydrostatic state to convective state, for different system parameters values. We present a complete analysis of the behavior of the DW convection with $g = 0$. We have studied the effect of the parameter α_{w} for different temperatures of the horizontal walls and constant coefficient of normal restitution α to characterize the transition to the steady convection convective at zero gravity.

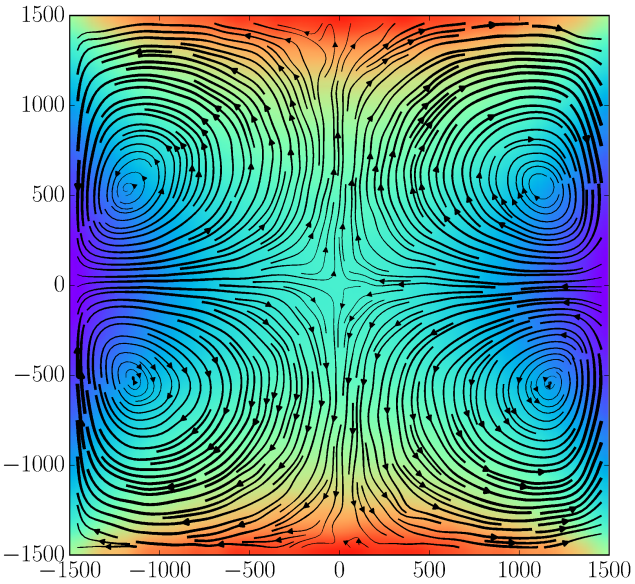

Fig. 1. Convection lines for the velocity field superimposed on the temperature field, evaluated on 2500 MFT of the granular gas with $\rho = 0.0016$. Thickest stream lines correspond to higher values of the velocity field $3 \times \sqrt{u_x^2 + u_y^2}/v_{\max}$ (in our dimensionless units). The relevant parameters are: $T = 1$ for horizontal walls, $\alpha_{\mathrm{w}} = 0.4$ for laterals, and $\alpha = 0.9$.

[1] F. H. Busse, Rep. Prog. Phys. **41**, 1929-1967 (1978).

[2] G. Pontuale, A. Gnoli, F. V. Reyes, and A. Puglisi, Phys. Rev. Lett. **117**, 098006 (2016).

[3] F. V. Reyes and A. R. Rivas, (unpublished).

[4] F. V. Reyes and J. S. Urbach, J. Fluid Mech. **636**, 279-283 (2009).

Viscous fingering instability triggered by a pH chemical reaction

D. M. Escala[1], J. Carballido-Landeira[2], A. De Wit[3], and A. Pérez Muñuzuri[1]
[1]Nonlinear Physics Group, University of Santiago de Compostela, Santiago de Compostela, Spain
[2]Departamento de Física, Facultad de Ciencias, Universidad de Oviedo, Oviedo, Spain
[3]Nonlinear Physical Chemistry Unit, Univeristé Libre de Bruxelles (ULB), Brussels, Belgium

A pH-changing chemical reaction is used to induce changes in a pH-sensitive polymer and induce a fingering instability in a liquid system otherwise stable. The formaldehyde-sulfite (FS) reaction is an example of a complex chemical reaction where pH varies according to the reaction parameters. On the other hand, poly(acrylic acid) is an organic polymer which exhibit large viscosity changes in aqueous solutions when the pH increases from acidic to basic. Results on the coupling between the FS reaction and the poly(acrylic acid) show that it is possible to obtain changes in both pH and viscosity that are strongly modulated by the reaction kinetics. We exhaustively analyzed the influence of the involved species by using rheological techniques and optimized the reaction initial conditions in order to maximize the differences between the initial and final pH/viscosity values [1].

Once obtained suitable conditions, we adapted the described system in order to study the occurrence of fingering instability driven by the chemistry in a radial Hele-Shaw cell experimental arrangement. The reaction reagents were separated into two independent solutions with different viscosities that only react where in contact. However, even if the liquids were injected in an initially stable configuration, fingering instability was obtained due to changes in the pH that strongly modified the local viscosity. At the interface the FS reaction occurs increasing the viscosity. The instability was also characterized and numerically modeled. Both experimental and numerical results show a very good agreement [2].

[1] D. M. Escala, A. P. Muñuzuri, A. De Wit, and J. Carballido-Landeira, Temporal viscosity modulations driven by a pH sensitive polymer coupled to a pH-shifting chemical reaction, Phys. Chem. Chem. Phys. **19**, 11914-11919 (2017).

[2] D. M. Escala, J. Carballido-Landeira, A. De Wit, and A. P. Muñuzuri, pH induced viscous fingering instability, (in preparation).

On the origin of complex memory effects in a granular gas

Francisco Vega Reyes[1], Antonio Lasanta[2], Antonio Prados[3], and Andrés Santos[1]
[1]Departamento de Física and Instituto de Computación Científica Avanzada (ICCAEx), Universidad de Extremadura, 06071 Badajoz, Spain
[2]Gregorio Millán Institute of Fluid Dynamics, Nanoscience and Industrial Mathematics, Department of Materials Science and Engineering and Chemical Engineering, Universidad Carlos III de Madrid, 28911 Leganés, Spain
[3]Física Teórica, Universidad de Sevilla, apdo. correos 1065, 41080 Sevilla, Spain

We study in this theoretical work the physical origin of the emergence of surprisingly complex memory effects in a granular gas of identical rough hard spheres. The granular gas, usually defined as a low density set of particles that suffer instantaneous and binary inelastic collisions, is in this case driven by a stochastic force in the form of a white noise and the particles have uniform mass density [1].

If the stochastic force intensity suddenly changes, the system undergoes a time evolution through a series of non-hydrodynamic states, allowing for the emergence of memory effects. We show that, in this case, the granular temperature may display —for certain values of the relevant physical parameters— successive changes in the temperature trend. More specifically, this can occur when, after a sudden heat pulse at a given instant t_0, the white noise intensity ξ^2 is set so that the corresponding stationary granular temperature $T_{\rm s}(\xi^2)$ (i.e., the temperature for $t \to \infty$) coincides with the instantaneous granular temperature produced by the heat pulse $T(t_0)$, i.e., $T_{\rm s}(\xi^2) = T(t_0)$.

This kind of intricate memory effects are displayed in Fig. 1. As we can see, three consecutive changes in the time derivative show up here. In order to characterize the degree of complexity of this kind of memory effect, we define the magnitude

$$\mathcal{S} = \mathrm{sg}(T_{\rm s} - T_1)\frac{\min\{\mathcal{H}_1,\, \mathcal{H}_2\}}{\max\{\mathcal{H}_1,\, \mathcal{H}_2\}}, \qquad (1)$$

where here T_1 is the temperature of the earliest extremum (maximum or minimum) and $\mathcal{H}_1 \equiv |T_1/T_{\rm s} - 1|$, $\mathcal{H}_2 \equiv |T_2/T_{\rm s} - 1|$ are the heights of the earliest and second earliest extrema. In Fig. 2 we observe, however, that at least in the case of uniform mass density particles this complex behavior is constrained to very narrow regions in the system parameter space. Out of the complex colored regions, the memory effect behavior resembles to the well known Kovacs effect [2], except that by comparison the magnitude of the effect is now giant [3].

In an accompanying work [4], we propose a laboratory set-up designed specifically for the production of a homogeneously excited granular gas. In this way, we intend to achieve the experimental detection of memory effects in a homogeneous granular gas eventually similar to the one described in the present work.

This work has been supported by the Spanish Government, through grants no. FIS2016-76359-P (F.V.R. and A.S.), no. MTM2017-84446-C2-2-R (A.L.), by *Junta de Extremadura*, grant no. GR15104, partially funded by the ERDF (F.V.R., A.L., A.S.), and by *Universidad de Sevilla*, through grant no. PP2018/494 *VI Plan Propio de Investigación* (A.P.).

[1] F. Vega Reyes and A. Santos, Steady state in a gas of inelastic rough spheres heated by a uniform stochastic force, Phys. Fluids **27** 113301 (2015).

[2] A. Prados and E. Trizac, Kovacs-like memory effect in driven granular gases, Phys. Rev. Lett. **112** 198001 (2014).

[3] A. Lasanta, F. Vega Reyes, A. Prados, and A. Santos, On the emergence of large and complex memory effects in non-equilibrium fluids, (in preparation).

[4] M. A. López-Castanño, A. Rodríguez-Rivas, and F. Vega Reyes, Experimental results on a granular gas driven by an air-generated stochastic force, in *XXII Congreso de Física Estadística (FisEs'18) – Libro de Resúmenes/Book of Abstracts, Madrid, 2018* (Universidad Politécnica de Madrid, Madrid, 2018), p. 51.

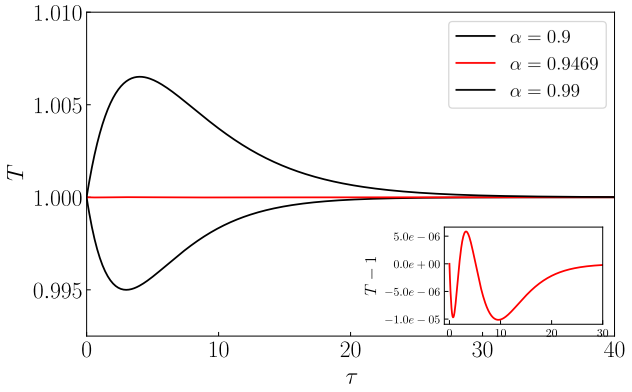

Fig. 1. Complex time evolution in the granular temperature after a sudden heat pulse from a white noise thermostat. α and β (here, $\beta = -0.65$) are the coefficients of normal and tangential restitution, respectively (see [1] for more detail).

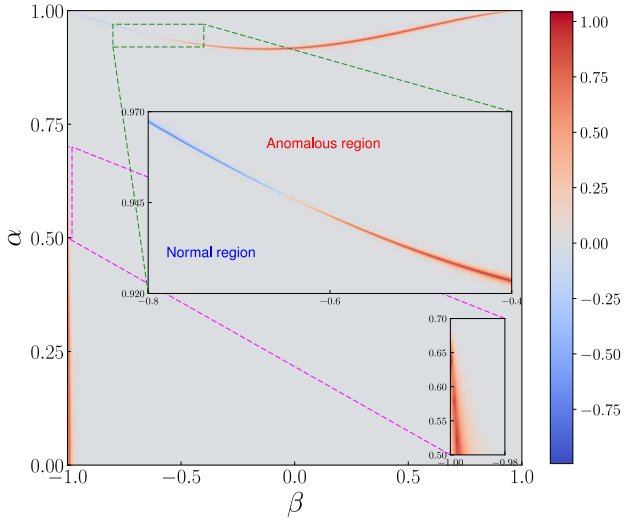

Fig. 2. Behavior of the memory effects complexity in the driven granular gas, when subject to a heating pulse. Two complex regions are detected, through definition of the magnitude $\mathcal{S}$ as it appears in Eq. (1).

Ordering and dynamics in a thin vibrated granular layer

Francisco Vega Reyes[1] and Jeffrey S. Urbach[2]
[1]Departamento de Física and Instituto de Computación Científica Avanzada (ICCAEx), Universidad de Extremadura, 06071 Badajoz, Spain
[2]Department of Physics, Georgetown University, Washington DC 20057, USA

We present in this work a review of past and recent advances on the granular dynamics of a thin granular layer that is vibrated vertically (in the presence of a gravitational field with acceleration $g = 9.8$ m/s^2). Since the work by the group at Texas Austin [1] and others, it has been shown that a granular layer vibrated vertically can display a number of patterns and cells. These phenomena can be understood and explained theoretically, in some cases, as a thermal convection, that has some peculiarities with respect to thermal convection in molecular fluids.

However, the granular layer, if sufficiently dense, can display ordering phenomena with an essentially different nature, as a series of experiments have shown. In Fig. 1 we can see a sketch of the experimental system. What we see now in this kind of confined system can be regarded as phase transitions instead. For instance, the granular layer can spontaneously come to an arrest state (from a previously disordered state) for a low enough vibration acceleration ($\Gamma \leq 1$) with a hexagonal symmetry in a variant of the sketch shown in Fig. 1, without the top lid. This kind of phase was shown two decades ago [2]. For the confined system depicted in Fig. 1, it was shown in experiments that a cubic symmetry phase can appear for a system with $h \sim 1.75\sigma$ [3]. Later on, the phase map was completed by means of molecular dynamics simulations [4], for a range of different values of the system width h and density, showing that the set of ordered phases that appear in the confined granular layer is essentially analogous to the phases observed in colloidal systems (particles with elastic collisions) [5].

And yet, contrary to what happens in colloids, these ordered phases may melt for sufficiently high acceleration input [6]. Moreover, the melting point depends dramatically of the degree of inelasticity in the collisions [6]. To the point that very inelastic collisions can completely suppress ordering in the whole phase map, in complete disagreement with classical results for equilibrium systems. No theoretical explanation has been conveyed for this fact so far. And additional experimental results have deepened later in the description of this important effect either.

We now focus on the role of inelasticity in the phase behavior of the thin vibrated granular layer, showing results specifically for the hexatic phase, that has already been observed in a granular system [7]. As it is known, the hexatic phase forms part of the description of the liquid to solid crystal transition as a continuous transition in molecular 2D materials. We analyze also the limits of the agreement and the aspects that depart from the KTHNY description of this phase transition [8, 9, 10], when dealing with a thin granular layer.

We will also review the results on this kind experimental setup reported by other groups. The reader may find a comprehensive review in the recent work by Mujica & Soto [11].

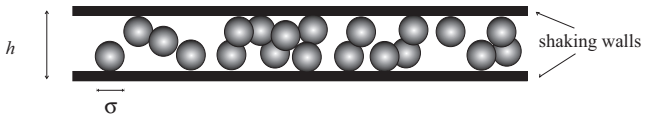

Fig. 1. We study a thin vibrated granular layer that is densely packed. The system width (distance between the two vibrating horizontal walls) is denoted as h and the particles diameter is σ (all particles are identical). The input acceleration $\Gamma \equiv A\omega^2/g$, where g is the gravitational acceleration. The vibration has sinusoidally-shaped, with amplitude A and angular frequency ω.

This work has been supported by the Spanish Government through grant no. FIS2016-76359-P.

[1] C. Bizon, M. D. Shattuck, J. R. de Bruyn, J. B. Swift, W. D. McCormick, and H. L. Swinney, Convection and diffusion patterns in oscillated granular media, J. Stat. Phys. **93**, 449-465 (1998).

[2] J. S. Olafsen and J. S. Urbach, Clustering, order, and collapse in a driven granular monolayer, Phys. Rev. Lett. **81**, 4369-4372 (1998).

[3] A. Prevost, P. Melby, D. A. Egolf, and J. S. Urbach, Nonequilibrium two-phase coexistence in a confined granular layer, Phys. Rev. E **70**, 050301(R) (2004).

[4] P. Melby, F. V. Reyes, A. Prevost, R. Robertson, P. Kumar, D. A. Egolf, and J. S. Urbach, The dynamics of thin vibrated granular layers, J. Phys.: Condens. Matter **17**, S2689-S2704 (2005).

[5] M. Schmidt and H. Löwen, Phase diagram of hard spheres confined between two parallel plates, Phys. Rev. E **55**, 7228-7241 (1997).

[6] F. V. Reyes and J. S. Urbach, Effect of inelasticity on the phase transitions of a thin vibrated granular layer, Phys. Rev. E **78**, 051301 (2008).

[7] J. S. Olafsen and J. S. Urbach, Two-dimensional melting far from equilibrium in a granular monolayer, Phys. Rev. Lett. **95**, 098002 (2005).

[8] J. M. Kosterlitz and D. J. Thouless, Ordering, metastability and phase transitions in two-dimensional systems, J. Phys. C **6**, 1181-1203 (1973).

[9] A. P. Young, Melting and the vector Coulomb gas in two dimensions, Phys. Rev. B **19**, 1855-1866 (1979).

[10] D. R. Nelson and B. I Halperin, Dislocation-mediated melting in two dimensions, Phys. Rev. B **19**, 2457-2484 (1979).

[11] N. Mujica and R. Soto, Dynamics of noncohesive confined granular media, in *Recent Advances in Fluid Dynamics with Environmental Applications*, edited by J. Klapp, L. Sigalotti, A. Medina, A. López, and G. Ruiz-Chavarría (Springer, 2016).

Flow field data processing for the oscillating conical bob rotational rheometer

Pablo Sánchez-Puga[1], Javier Tajuelo Rodríguez[1,2], Juan Manuel Pastor[3], and Miguel Ángel Rubio[1]

[1]Dpto. Física Fundamental, Fac. Ciencias, Universidad Nacional de Educación a Distancia, po. Senda del Rey 9, 28040 Madrid, Spain

[2]Dpto. Física Aplicada, Fac. Ciencias, Universidad de Granada, av. Fuente Nueva s/n, 18071 Granada, Spain

[3]Grupo de Sistemas Complejos, ETSIAAB, Universidad Politécnica de Madrid, av. Puerta de Hierro 2-4, 28040 Madrid, Spain

Rotational bulk rheometers may be used as interfacial shear rheometers (ISR) by supplementing them with proper accessories that allow one to impose a shear on a fluid-fluid interface in a controlled manner. Actually, most rotational rheometer manufacturers sell fixtures for interfacial shear rheometry measurements, such as the bicone, the Du Nouy ring, or the double-wall ring (DWR) fixtures.

However, recovering the proper values of the dynamic moduli from the torque and angular displacement data is far from trivial due to the coupling between the subphase and the interfacial flow fields. Moreover, a low viscosity fluid is usually chosen for the subphase, and the low interfacial pressure regimes usually have low interfacial viscosity. Therefore, fluid inertia very often comes into play, which results in nonuniform shearing profiles both at the interface and the subphase, further complicating then the data analysis.

Successful strategies to cope with these problems have been devised for the DWR interfacial rheometer [1] and the magnetic rod ISR [2, 3, 4, 5, 6]. The basic ingredients of the strategy are: (i) to find numerically the flow fields at, both, the subphase and the interface, (ii) to separately calculate the drags exerted on the probe by the interface and the subphase, taking into account the flow field solutions obtained, and (iii) to use the equation of the probe dynamics (the rotor in the DWR and the rod in the magnetic rod ISR) to build up an iterative scheme that, upon convergence, allows to recover the proper values of the complex Boussinesq number $\mathrm{Bo}^* = \eta_\mathrm{s}^*/L\eta$, where L is a characteristic length scale related to the probe size. Then, the viscoelasticity data can be recovered directly solving for η_s^* in the previous expression. Such an approach includes, and allows to properly account for, the inertia effects corresponding to the probe, the subphase, and the interface, yielding a much better separation of the elastic and viscous components of the interface response.

We will illustrate how such a scheme can be implemented in the case of the old bicone bob rotational rheometer configuration. First, we assume that the interface is flat and horizontal, that the flow is axisymmetric, and that the respective rheological properties of the subphase and the interface can be described by a newtonian viscosity η, and a complex viscosity $\eta_\mathrm{s}^* = \eta_\mathrm{s}' - i\eta_\mathrm{s}''$, which are uniform across the whole sample. Then we are left with a simplified version of the Navier-Stokes equations regarding only the azimuthal component of the velocity field. The boundary conditions are the Boussinesq-Scriven condition for the stress field at the interface, and no-slip elsewhere. The Navier-Stokes equation is solved by a second order centered differences method. An ansatz is made for the steady oscillatory rotational motion of the rotor+fixture assembly, assuming that the torque on the rotor and its angular displacement have the same frequency and a constant phase lag. Such an ansatz allows us to write down the torque balance equation in terms of the drags due to the interface and the subphase, the rotor inertia term, and a complex torque/angle amplitude ratio. Solving for the complex Boussinesq number in the torque balance equation allows us to devise an iterative scheme that, starting from a suitable seed for Bo^*, obtains the flow field solutions at the interface and subphase, uses the flow field to compute the hydrodynamic drags, and obtains a new corrected value for Bo^* out of the torque balance equation. Iterating such a scheme convergence is achieved and the value of Bo^* that accounts for the complex torque/angle amplitude ratio is found.

We will illustrate the performance of this scheme through, both, extensive numerical benchmarking and dynamic measurements with a rotational rheometer and a homemade bicone fixture [7] on several interfacial experimental systems.

[1] S. Vandebril, A. Franck, G. G. Fuller, P. Moldenaers, and J. Vermant, Rheol. Acta **49**, 131 (2010).

[2] C. F. Brooks, G. G. Fuller, C. W. Frank, and C. R. Robertson, Langmuir **15**, 2450 (1999).

[3] S. Reynaert, C. F. Brooks, P. Moldenaers, J. Vermant, and G. G. Fuller, J. Rheol. **52**, 261 (2008).

[4] T. Verwijlen, P. Moldenaers, H. A. Stone, and J. Vermant, Langmuir **27**, 9345 (2011).

[5] J. Tajuelo, J. M. Pastor, F. Martínez-Pedrero, M. Vázquez, F. Ortega, R. G. Rubio, and M. A. Rubio, Langmuir **31**, 1410 (2015).

[6] J. Tajuelo, J. M. Pastor, and M. A. Rubio, J. Rheol. **60**, 1095 (2016).

[7] J. Tajuelo, M. A. Rubio, and J. M. Pastor, J. Rheol. **62**, 295 (2018).

Brownian particle moving in a back-and-forth traveling periodic potential subjected to a temporal external excitation

Ricardo Chacón[1,2] and Pedro J. Martínez[3,4]
[1]Departamento de Física Aplicada, EII, Universidad de Extremadura, apdo. correos 382, E-06006 Badajoz, Spain
[2]Instituto de Computación Científica Avanzada (ICCAEx), Universidad de Extremadura, E-06006 Badajoz, Spain
[3]Departamento de Física Aplicada, EINA, Universidad de Zaragoza, E-50018 Zaragoza, Spain
[4]Instituto de Ciencia de Materiales de Aragón, CSIC-Universidad de Zaragoza, E-50009 Zaragoza, Spain

The physical properties characterizing the directed ratchet transport of a driven overdamped particle subjected to a back-and-forth periodic potential [1] are explained theoretically from the degree-of-symmetry-breaking mechanism [2, 3] and confirmed by numerical experiments. We demonstrate that the universality scenario holds regardless of the waveform of the periodic vibratory excitations involved, while optimal directed ratchet transport occurs when their impulse transmitted (temporal integral over a half-period) is maximum.

Remarkably, we find that the present universality scenario remains effective even when the external periodic excitation is substituted by a chaotic signal having the same underlying main frequency in its Fourier spectrum. Specifically, we investigate the directed ratchet transport of a driven Brownian particle moving in a back-and-forth traveling periodic potential described by the overdamped model

$$\dot{x} + \sin\left[x - \gamma\eta f\left(t\right)\right] = \sqrt{\sigma}\xi\left(t\right) + \gamma\left(1-\eta\right)g\left(t\right), \quad (1)$$

where $f(t)$ is a $(2\pi/\omega)$-periodic function, $g(t)$ is a temporal signal having its main Fourier component at the frequency 2ω, γ is an amplitude factor, and the parameters $\eta \in [0,1]$ and φ account for the relative amplitude and initial phase difference of the two temporal signals, respectively, while $\xi\left(t\right)$ is a Gaussian white noise with zero mean and $\langle \xi\left(t\right)\xi\left(t+s\right)\rangle = \delta\left(s\right)$, and $\sigma = 2k_{\mathrm{B}}T$ with k_{B} and T being the Boltzmann constant and temperature, respectively. Figure 1 shows an illustrative example for the standard case where $f\left(t\right)$ and $g\left(t\right)$ are harmonic functions.

R.C. acknowledges financial support from the *Ministerio de Ciencia e Innovación (MICINN)*, Spain, through project FIS2012-34902 cofinanced by FEDER funds, and from the *Junta de Extremadura (JEx)*, Spain, through Project No. GR18081 cofinanced by FEDER funds. P.J.M. acknowledges financial support from the MINECO, Spain, through project FIS2017-87519-P cofinanced by FEDER funds.

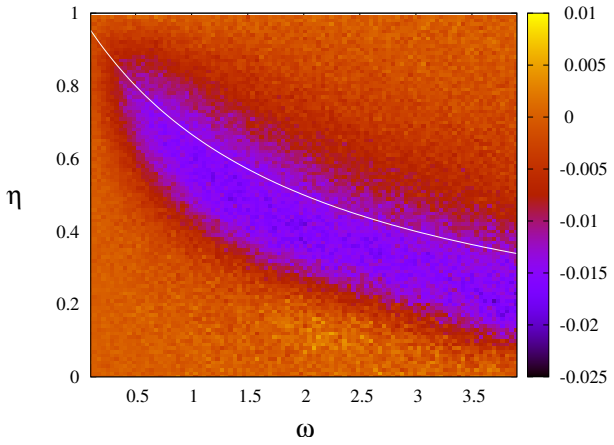

Fig. 1. Average velocity $\langle\langle \dot{x} \rangle\rangle$ *versus* relative amplitude η and frequency ω for the case $f\left(t\right) \equiv \cos\left(\omega t\right)$, $g\left(t\right) \equiv \cos\left(2\omega t + \varphi\right)$, and the parameters $\varphi = 0, \sigma = 10, \gamma = 15$. Also plotted is the theoretical prediction for the maximum average velocity (solid line).

[1] P. Reimann, Phys. Rep. **361**, 57 (2002).

[2] R. Chacón, J. Phys. A **40**, F413 (2007); **43**, 322001 (2010).

[3] P. J. Martínez and R. Chacón, Phys. Rev. E **87**, 062114 (2013); **88**, 019902(E) (2013); **88**, 066102 (2013).

Análisis de la estabilidad en una comunidad de mutualistas

Juan P. G. Villaluenga[1], Javier Galeano[2] y Rafael Vida[2]
[1]Departamento de Estructura de la Materia, Física Térmica y Electrónica, Universidad Complutense de Madrid, Spain
[2]Grupo de Sistemas Complejos, Universidad Politécnica de Madrid, Spain

García-Algarra *et al.* [1] estudian una comunidad de mutualistas cuya dinámica de poblaciones está descrita por la ecuación

$$\frac{dX_i}{dt} = X_i\left(r_i - s_i X_i\right), \tag{1}$$

donde el índice i denota la especie i-ésima ($i = 1, \ldots, S$). Los coeficientes r_i y s_i se definen como

$$r_i = r_i^\circ + \sum_{j=1, j\neq i}^{S} b_{ij} X_j, \tag{2}$$

$$s_i = s_i^\circ + c_i \sum_{j=1, j\neq i}^{S} b_{ij} X_j, \tag{3}$$

donde los elementos b_{ij} forman una matriz de dimensiones $S \times S$, cuyos valores caracterizan el tipo de interacción entre especies. La ecuación general puede escribirse de una manera más compacta como sigue

$$\frac{dX_i}{dt} = X_i\left[r_i^\circ - s_i^\circ X_i + (1 - c_i X_i)\sum_{j=1, j\neq i}^{S} b_{ij} X_j\right]. \tag{4}$$

Los puntos fijos del sistema son

$$r_i^\circ - s_i^\circ X_i^* + (1 - c_i X_i^*)\sum_{j=1, j\neq i}^{S} b_{ij} X_j^* = 0, \tag{5}$$

siendo X_i^* un vector de dimensión $S \times 1$. Los elementos de la matriz jacobiana evaluada en el punto de equilibrio son

$$M_{ii} = -X_i^*\left(s_i^\circ + c_i \sum_{j=1, j\neq i}^{S} b_{ij} X_j^*\right), \tag{6a}$$

$$M_{ij} = X_i^*\left(1 - c_i X_i^*\right) b_{ij}. \tag{6b}$$

Para simplificar la notación, definimos

$$\alpha_i = s_i^\circ + c_i \sum_{j=1, j\neq i}^{S} b_{ij} X_j^*, \tag{7}$$

$$B_{ij} = \left(1 - c_i X_i^*\right) b_{ij}. \tag{8}$$

En consecuencia, la matriz jacobiana puede escribirse como

$$M_{ii} = -\alpha_i X_i^*, \tag{9a}$$

$$M_{ij} = B_{ij} X_i^*. \tag{9b}$$

Este resultado sugiere que si se define una variable $Y_i = X_i / X_i^*$ (el punto fijo sería la unidad), la matriz jacobiana resultante A tendría los siguientes elementos

$$A_{ii} = -\alpha_i, \tag{10a}$$

$$A_{ij} = B_{ij}. \tag{10b}$$

Además, si definimos una nueva matriz $N = A/\beta$, donde $\beta = \sqrt{C\sigma^2} = \sqrt{S\,\mathrm{Var}(A_{ij})}$, esta nueva matriz satisfaría los requisitos de Sommers [2], esto es,

$$\mathrm{E}(N_{ij})_{i\neq j} = 0, \tag{11}$$

$$\mathrm{Var}(N_{ij}) = \frac{1}{S}, \tag{12}$$

y podríamos afirmar que los autovalores de N estarían contenidos en una elipse con semieje mayor $a^* = 1 + \tau$ y semieje menor $b^* = 1 - \tau$, donde

$$\begin{aligned}\tau &= \mathrm{E}(N_{ij}N_{ji})_{i\neq j} \\ &= \frac{\mathrm{E}(A_{ij}A_{ji})_{i\neq j}}{\beta^2}.\end{aligned} \tag{13}$$

En consecuencia, los autovalores de A estarían dentro de una elipse con semieje mayor $a = \beta(1 + \tau)$ y semieje menor $b = \beta(1 - \tau)$. Finalmente, el estado de equilibrio sería estable si se cumpliera [3]

$$\sqrt{S\,\mathrm{Var}(A_{ij})}\left[1 + \frac{E(A_{ij}A_{ji})}{\mathrm{Var}(A_{ij})}\right] < d, \tag{14}$$

donde d se calcula como sigue

$$\begin{aligned}d &= \frac{1}{S}\sum_{i=1}^{S} \alpha_i \\ &= \frac{1}{S}\sum_{i=1}^{S}\left(s_i^\circ + c_i \sum_{j=1, j\neq i}^{S} b_{ij} X_j^*\right).\end{aligned} \tag{15}$$

Si la interacción es mutualista, los elementos b_{ij} de la matriz comunitaria pueden calcularse a partir de los valores de una variable aleatoria X con distribución gaussiana. En este caso, se tiene que $\mathrm{E}(b_{ij})_{i\neq j} = 0$, $\mathrm{Var}(b_{ij})_{i\neq j} = C\sigma^2$ y $\mathrm{E}(b_{ij}b_{ji})_{i\neq j} = C\,\mathrm{E}(|X|)^2$. La conectividad C representa la probabilidad de que se produzca la interacción entre dos especies ($C \in [0, 1]$). Una vez generada la matriz comunitaria, conocidos los valores del resto de parámetros del sistema (r_i°, s_i° y c_i), se puede analizar la estabilidad del estado de equilibrio en términos de los parámetros de complejidad.

[1] J. García-Algarra, J. Galeano, J. M. Pastor, J. M. Iriondo, and J. J. Ramasco, Rethinking the logistic approach for population dynamics of mutualistic interactions, J. Theor. Biol. **364**, 332 (2014).

[2] H. J. Sommers, A. Crisanti, H. Sompolinsky, and Y. Stein, Spectrum of large random asymmetric variables, Phys. Rev. Lett. **60**, 1895 (1988).

[3] S. Allesina and S. Tang, Stability criteria for complex ecosystems, Nature **483**, 205 (2012).

3D AFM in dense fluids: What can we infer of their results?

Jose Hernandez-Munoz[1], Enrique Chacón[2], and Pedro Tarazona[1,3]
[1]Departamento de Física Teorica de la Materia Condensada, Condensed Matter Physics Center (IFIMAC), Universidad Autónoma de Madrid, 28049 Madrid, Spain
[2]Instituto de Ciencia de Materiales de Madrid, Consejo Superior de Investigaciones Científicas, 28049 Madrid, Spain
[3]Instituto Nicolás Cabrera de Ciencia de Materiales, Universidad Autónoma de Madrid, 28049 Madrid, Spain

Atomic Force Microscopy (AFM) has been a powerful tool to measure the structure of non-metallic surfaces. Normally, it operates in ultra high vacuum and low temperatures. In order to achieve high resolution, this is performed due to the direct interaction cantilever substrate. However, the use of AFM within a dense liquid has to take into account also the interaction between the structure of the liquid profile generated by cantilever and substrate. This kind of interaction is typically of long range, hence may mask direct cantilever substrate interaction and loose high resolution. On the other hand, we can measure directly the structure of the fluid performing 3D maps of phase shift and amplitude [1]. In Ref. [1] was found a spatial dependence in phase shift similar to the profile derivative of the liquid in contact with the surface. But, is this general? How we should interpret the results? Which framework will reproduce the results?

To answer this open question we develop a close framework. As usually done, we will model the dynamics of the AFM cantilever as a mass-point like forced and damped oscillator, given its classical dynamics by

$$m_{\text{eff}}\frac{\partial^2 x_p}{\partial t^2} + b\frac{\partial x_p}{\partial t} + k_0 x_p^2 = F_0\cos(\omega t) - \left\langle \vec{\nabla}\Omega[\rho(\vec{x})]|_{\rho_{\text{eq}}} \right\rangle (x_p), \quad (1)$$

where the effective mass takes into account the drag force relative to the acceleration of the cantilever, while b is related to the part proportional to the velocity. In other words, contrast and also quality factor are mainly given by the hydrodynamics of the system. On the other hand, the force which gives the spatial structure of the phase shift and amplitude corresponds to the differences in the grand potential of the fluid. This could be computed as the minimum of the grand potential Ω at an instantaneous position of the cantilever x_p, due to the several orders of differences between the characteristic times of the cantilever and relaxation of the fluids. The grand potential used here includes DIFMT to reproduce entropy contribution, and mean field theory of different interactions (Yukawa and Lennard-Jones).

Hence, our description assumes that contrast is given by the hydrodynamic contribution, while the spatial variations are mainly due to different profile structure of the fluids, which correspond a grand potential minimum of each cantilever spatial configuration.

A remarkable result obtained from these assumptions is that $\Omega[\vec{x}_p]$ presents the same decays that equilibrium profile of the substrate, i.e., the characteristics complex poles given by the bulk correlation. Which gives, as can be seen in Fig. 1, the oscillatory-exponential decay of the phase shift of the cantilever. This is also in amplitude results, but in a complex way that depends strongly of the regime used in measurements of the AFM.

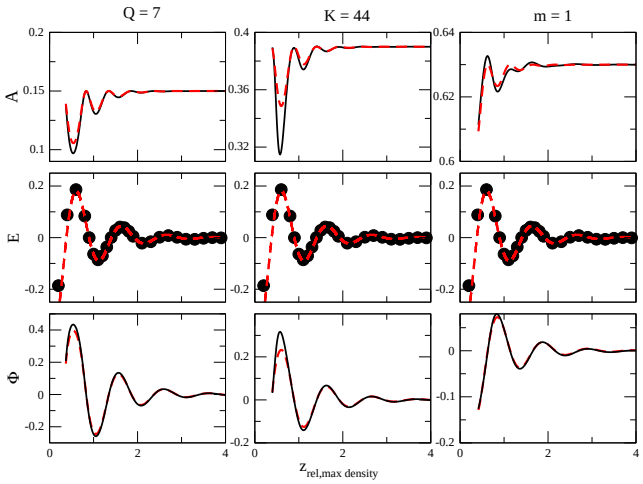

Fig. 1. The first row corresponds to the amplitude obtained, while the third row represents the phase shift. In both the straight line corresponds to the numerical results, while the dashed line (red) corresponds to a theoretical approach. The second row shows the values of $\Omega[\vec{x}]$ obtained by minimization (black points), while the dashed lines represents the fit using the decays of the bulk correlation.

The results can be understood by the interference between the structure generated by the cantilever with that corresponding to the substrate. This interference is induced by the boundary layers of cantilever and substrates, which generate a strong first density peak in the cantilever which its relative position to it is nearly fixed. Then, as long as you move the cantilever, this first peak performs a kind of topography of the density profile generated by the substrate. Which is traduced in the oscillatory-exponential decay observed in the energy excess of this system, and explain why the decays are given by the characteristic poles of the bulk correlation. Hence, only two parameters, phase shift and interaction strength of the energy, depend given a bulk density of the external interaction and geometry of the cantilever, which are related with how strong is the structure generated over the profile. In order to characterize both parameters, we refer the energy to the distance of the first peaks of cantilever and substrate.

[1] D. Martin-Jimenez, E. Chacon, P. Tarazona, and R. Garcia, Atomically resolved three-dimensional structures of electrolyte aqueous solutions near a solid surface, Nat. Commun. **7**, 12164 (2016).

The space of genotypes is a network of networks: Implications for evolutionary and extinction dynamics

Pablo Yubero[1], Susanna Manrubia[1,2], and Jacobo Aguirre[1,2]
[1] Centro Nacional de Biotecnología, CSIC, c. Darwin 3, 28049 Madrid, Spain
[2] Grupo Interdisciplinar de Sistemas Complejos (GISC), Madrid, Spain

The forcing that environmental variation exerts on populations causes continuous changes with only two possible evolutionary outcomes: adaptation or extinction. In this work we address this topic by studying the transient dynamics of populations on complex fitness landscapes.

There are three important features of realistic landscapes of relevance in the evolutionary process: fitness landscapes are rough but correlated, their fitness values depend on the current environment, and many genotypes do not yield viable phenotypes. We capture these properties by defining time-varying, holey, NK fitness landscapes.

We show that the structure of the space of genotypes so generated is that of a network of networks: in a sufficiently holey landscape, populations are temporarily stuck in local networks of genotypes. Sudden jumps to neighbouring networks through narrow adaptive pathways (connector links) are possible, though strong enough local trapping may also cause decays in population growth and eventual extinction.

In summary, a combination of analytical and numerical techniques to characterize complex networks and population dynamics on such networks permits to derive quantitative relationships between the topology of the space of genotypes and the fate of evolving populations.

[1] J. Aguirre, P. Catalán, José A. Cuesta, and S. Manrubia, On the networked architecture of genotype spaces and its critical effects on molecular evolution, Open Biol. **8**, 180069 (2018).

[2] P. Yubero, S. Manrubia, and J. Aguirre, The space of genotypes is a network of networks: implications for evolutionary and extinction dynamics, Sci. Rep. **7**, 13813 (2017).

[3] J. Aguirre and S. Manrubia, Tipping points and early warning signals in the genomic composition of populations induced by environmental changes, Sci. Rep. **5**, 9664 (2015).

[4] J. Aguirre, D. Papo, and J. M. Buldú, Successful strategies for competing networks, Nat. Phys. **9**, 230 (2013).

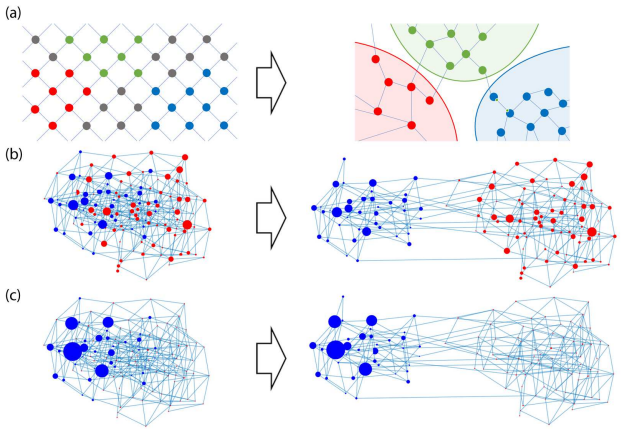

Fig. 1. Can the space of genotypes be viewed as a network of networks in competition for population?

Quantum approach to opinion dynamics

Daniele Vilone[1,2] and Mario Paolucci[1]
[1]Laboratory of Agent Based Social Simulation (LABSS), ISTC-CNR, Rome, Italy
[2]Grupo Interdisciplinar de Sistemas Complejos (GISC), Departamento de Matemáticas, Universidad Carlos III de Madrid, Spain

Binary-state models have been widely used to study the emergence of collective phenomena. In particular, Voter Model (VM) [1, 2] is a binary-state model based on local interactions. In VM, just as in an Ising model, nodes can have two states, that we can call spin up (1) or spin down (-1). In a single event, a randomly chosen node copies the state of one of its neighbours, also chosen at random. The Voter model has an analogue in quantum mechanics, the Heisenberg Model that is the quantum version of the classical Ising model. As it is well known, at $T = 0$ the Ising Model reduces exactly to the Voter Model in one dimension, while for higher dimensions the main difference is the absence of surface tension at the domain boundaries in the Voter Model.

We would like to define a "quantum-like" version of the pure VM. In the classical version, the key feature is the imitation dynamics: When an individual evolves, it simply copies the state of a neighbor. Therefore, let us consider a system where the only quantum entities are the opinions inside individuals' minds: An opinion really exists only when the agent has to express it based on its actual mental state. On the other hand, such mental state is the generic set of the thoughts, beliefs, views owned by the individual, which can be communicated and shared interacting with the others. In fact, we consider the state of mind $|\psi_i\rangle$ as a quantum object regarding internal dynamics, but treat it classically for what concerns the external dynamics. This would not make any sense for a real quantum system, yet for this very reason we call this model "pseudo-quantum" Voter Model (PQVM).

The Model – we consider a system of N agents whose state of mind is determined by their state ket $|\psi_i\rangle$ ($i \in \{1, N\}$). Since we are dealing with a two-opinion problem, such states belong to the Hilbert space of the $\frac{1}{2}$spin systems (spinors). Let $|u\rangle$ and $|d\rangle$ be the base kets, representing the positive and negative opinions, respectively, along a certain direction z (which can be seen as a particular binary question, i.e., yes or no in a referendum, the choice between two candidates, etc.), so that

$$|\psi_i\rangle = \alpha_i|u\rangle + \beta_i|d\rangle, \tag{1}$$

with $\alpha_i^*\alpha_i + \beta_i^*\beta_i = 1$. The other directions represent different questions, decreasingly related to the z-axis one as the angle increases. By constructions, the x and y directions, in a three dimensional space, should represent opinions that are completely independent from the studied one.

The dynamics takes place analogously to the classical Voter Model: At each elementary time step an agent is picked up at random and imitates the state of one of its neighbours, also randomly selected. The simplest assumption is independence: in the basic model, the states of different individuals cannot be directly correlated (unless one has just imitated a neighbor), so that the global state of the system will be a product-state

$$|\Psi\rangle = \Pi_i|\psi_i\rangle. \tag{2}$$

We expect the phenomenology of the PQVM to be much richer than the VM, and depends even more heavily on initial conditions.

Preliminary results – Analogously to the VM, the final state of the system is necessarily the one where all the individuals share the same state

$$|\psi_i^{\text{fin}}\rangle = |\phi^{\infty}\rangle, \ \forall i. \tag{3}$$

By definition of the model, that works by copying neighbours' states, $|\phi^{\infty}\rangle$ is necessarily one of the initial states which finally survived to the dynamics and the frozen configuration is reached following a power law of time with exponent $1/2$, exactly as in the CVM, even though with infinitely larger number of available states. If we are interested only in the final state, forcing a little bit the formalism, we can write down an Hamiltonian whose ground level (which is infinitely degenerate) is exactly the frozen state of the PQVM

$$\hat{H} = -J \sum_{\langle i,j \rangle} \|\langle\psi_j|\psi_i\rangle\|^2 \hat{I}, \tag{4}$$

where $\hat{I}$ is the identity operator and J the coupling constant, which can be assumed equal to 1. Similarly to the classical Ising Model, the system described by this Hamiltonian at zero temperature is perfectly equivalent to the PQVM in one dimension, differing for the absence of surface tension in higher dimensions [3].

As confirmed by simulations, differently from the classical version, the fact that the system finally reaches uniformity (i.e., all the agents are in the same state) does not imply that when they express their opinions, the population will be in a consensus state: since expressing an opinion on a given topic is equivalent to accomplishing a measurement of the spin along a given direction, in general every single opinion will depend in a probabilistic way from the mental state of the agent which expresses it. Moreover, the actual opinion distribution will also depend heavily from the initial conditions. Deeper and more systematic studies will be soon accomplished.

[1] P. Clifford and A. Sudbury, A model for spatial conflict, Biometrika **60**, 581-588 (1973).

[2] A. Carro, R. Toral, and M. San Miguel, The noisy voter model on complex networks, Sci. Rep. **6**, 24775 (2016).

[3] I. Dornic, H. Chaté, J. Chave, and H. Hinrichsen, Critical coarsening without surface tension: The universality class of the voter model, Phys. Rev. Lett. **87**, 045701 (2001).

Limited role of spatial self-structuring in emergent trade-offs during pathogen evolution

V. Buendía[1,2], M. A. Muñoz[1], and S. Manrubia[3,4]

[1]Departamento de Electromagnetismo y Física de la Materia e Instituto Carlos I de Física Teórica y Computacional, Universidad de Granada, 18071 Granada, Spain

[2]Dipartimento di Fisica e Scienza della Terra, Università di Parma, via G. P. Usberti 7/A, 43124 Parma, Italy

[3]Grupo Interdisciplinar de Sistemas Complejos (GISC), Madrid, Spain

[4]Programa de Biología de Sistemas, Centro Nacional de Biotecnología, CSIC, 28049 Madrid, Spain

Pathogen transmission and virulence are main evolutionary variables broadly assumed to be linked though trade-offs. In well-mixed populations, these trade-offs are often ascribed to physiological restrictions, while populations with spatial self-structuring might evolve emergent trade-offs.

Here, we reexamine a model of the latter kind proposed by Ballegooijen and Boerlijst [1] with the aim of characterising the mechanisms causing the emergence of the trade-off and its structural robustness. Using invadability criteria, we establish the conditions under which an evolutionary feedback between transmission and virulence mediated by pattern formation can poise the system to a critical boundary separating a disordered state (without emergent trade-off) from a self-structured phase (where the trade-off emerges), and analytically calculate the functional shape of the boundary in a certain approximation.

Beyond evolutionary parameters, the success of an invasion depends on the size and spatial structure of the invading and invaded populations. Spatial self-structuring is often destroyed when host are mobile, changing the evolutionary dynamics to those of a well-mixed population. In a metapopulation scenario, the systematic extinction of the pathogen in the disordered phase may counteract the disruptive effect of host mobility, favour pattern formation and therefore recover the emergent trade-off [2].

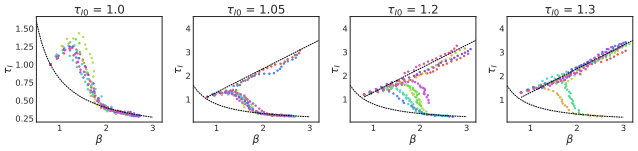

Fig. 1. Evolutionary trajectories of realizations with finite diffusion and fixed initial transmission rate β, for different values of the initial infection period τ_{I0}. The dashed black line shows the expected behaviours: No diffusion $\tau_I = R_0^{\text{ev}}/(8\beta)$ and mean-field $\tau_I = \beta +$ constant. The system either displays a behaviour indistinguishable from the $D = 0$ case or follows a curve of steady increase in R_0, as predicted in the mean-field theory. The region where stochastic fluctuations can lead the system to any of the two states stretches to a point in the limit $L \to \infty$.

[1] W. M. Ballegooijen and M. C. Boerlijst, Emergent trade-offs and selection for outbreak frequency in spatial epidemics, Proc. Natl. Acad. Sci. USA **101**, 18246-18250 (2004).

[2] V. Buendía, M. A. Muñoz, and S. Manrubia, Limited role of spatial self-structuring in emergent trade-offs during pathogen evolution, Sci. Rep. **8**, 12476 (2018).

Analytical solution of extensible freely jointed chain model

Alessandro Fiasconaro[1] and Fernando Falo[1,2]
[1]Department of Condensed Matter Physics, University of Zaragoza, Zaragoza, Spain
[2]Institute for Biocomputation and Physics of Complex Systems, University of Zaragoza, Zaragoza, Spain

Based on classical statistical mechanics, we calculate analytically the length extension under a pulling force of a polymer modeled as a freely jointed chain (FJC) with extensible bonds, the latter being considered as harmonic springs. We obtain an highly approximated formula for the extension curve, as well as an independent one for high force. These formulas can reproduce with high precision force-extension curves also at low values of the elastic constant of the spring, where previous proposals differ substantially. We successfully validate the analytical results together with the phenomenological expressions used in the literature by analysing the precision of their fit on data obtained from Langevin simulations.

Force-extension curve for rigid bond FJC model is given by the well known Langevin function $\xi = \mathcal{L}(\beta f l_0) = \coth(\beta f l_0) - 1/\beta f l_0$, where ξ is the normalised extension. To take into account a bond finite elastic constant k, two different corrections have been proposed in literature. The first one [1] is $\xi_{\rm N} = \mathcal{L}(\beta f l_0) + f/k l_0$ and the second [2] $\xi_{\rm M} = \mathcal{L}(\beta f l_0)(1 + f/k l_0)$. Both are phenomenological and not based in any first principle statistical mechanics calculation.

In this work [3], we make use of the Weiestrass transform to obtain a very precise expression for the partition function of the extensible FJC model and thus derive an extension-force formula given by

$$\xi_{\rm E} = \mathcal{L}(\beta f l_0) + \frac{f}{k l_0} \times \left[1 + \frac{1 - \mathcal{L}(\beta f l_0)\coth(\beta f l_0)}{1 + \frac{f}{k l_0}\coth(\beta f l_0)}\right]. \quad (1)$$

The same expression was also obtained by a different method in [4].

Another approximation, only valid at high forces can be also derived as [3]

$$\xi_{HF} = \mathcal{L}(\beta f l_0) + \frac{f}{k l_0} + \frac{1}{\beta l_0 (k l_0 + f)} + 1 - \coth(\beta f l_0). \quad (2)$$

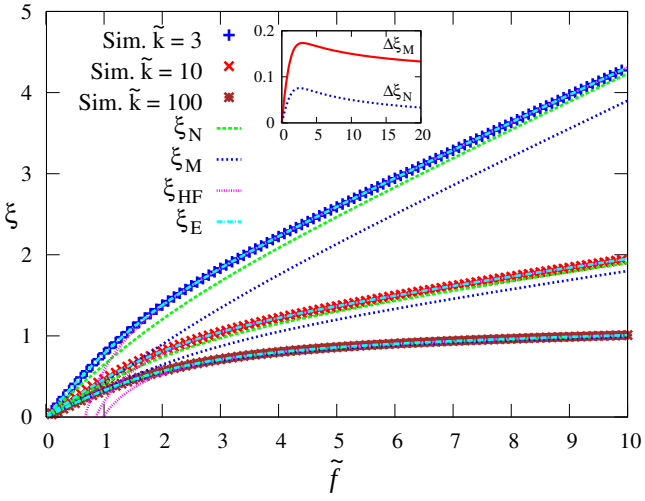

Fig. 1. Normalized extension ξ as a function of the dimensionless force $\tilde{f} = \beta f l_0$ for three values of the dimensionless elastic constant $\tilde{k} = \beta l_0^2 k$ in the extensible FJC model. The symbols represent the data from the simulations, and the lines the analytical expressions defined in the text.

A comparison with Langevin molecular dynamics simulations of the model are shown in the figure. Expression from Eqs. (1) and (2) reproduce very accurately the simulations whereas phenomenological approximations clearly deviate.

We will also discuss the fit of simulations to different models as well other interesting effects as the contribution of the extensibility to model fluctuations.

[1] T. Odijk, Macromolecules **28**, 7016-7018 (1995).

[2] S. B. Smith, Y. Cui, and C. Bustamante, Science **271**, 795-799 (1996).

[3] A. Fiasconaro and F. Falo, bioRxiv:315051.

[4] N. K. Balavaev and T. N. Khazanovich, Russ. J. Phys. Chem. B **3**, 242-246 (2009).

DFT and molecular dynamics simulations of a Langmuir monolayer

O. Toledano[1], O. Gálvez[1], M. A. Rubio[2], and P. Español[2]
[1]Dep. Física Interdisciplinar, Universidad Nacional de Educación a Distancia (UNED), po. Senda del Rey 9, 28040 Madrid, Spain
[2]Dep. Física Fundamental, Universidad Nacional de Educación a Distancia (UNED), po. Senda del Rey 9, 28040 Madrid, Spain

A Langmuir monolayer is a mono-molecular film formed at the air-water interface, usually composed of organic molecules like amphiphilic compounds. In this study, we have focused on a monolayer composed of palmitic acid molecules ($C_{15}H_{31}COOH$). In the formation of a Langmuir monolayer, the polar head group of amphiphilic molecules will be oriented towards the water-face, leaving the hydrophobic hydrocarbon tail tilted a certain angle (β) with respect to the normal surface.

The dominant interactions involved in this type of compounds are dispersive forces, which arises from the formation of dihydrogen bonds (-C-H$\cdots$H-C-) between neighboring molecules. Despite dihydrogen bond are one of the weakest intermolecular forces in the nature, the accumulation of many of them makes the total interaction appreciable. Dihydrogen bonding is highly anisotropic, and the strength of the interaction depends not only on the distance between the molecules but also on the orientation of the participating atoms [1]. It is therefore necessary to characterize this force by means of an accurate DFT method, since, for example, a Lennard-Jones type potential approximation would not adequately reproduce this behavior. In this context, different Van der Waals (VdW) exchange-correlation functionals (available in the DFT SIESTA package) have been tested to compare the geometries and interaction energy values of different dimers of alkanes molecules with that obtained by *ab initio* perturbative methods MP2 at a high level of calculation [2]. As a result of this study, we have obtained the most adequate VdW functional for this system, as well as optimized convergence parameters. It has been proved in this work that the interaction between several molecules can be approximated as the sum of the pairwise interactions and the monomers can be assumed as a rigid solid in the dimer formations, since the structures obtained before or after this formation are virtually identical.

To describe the different structures adopted by monomers relative to the water-air interface, three parameters have been established that define, in an univocal way, the relative position of them (see Fig. 1). In this study, we have assumed that the chains are aligned according to the normal to the aqueous interface ($\beta = 90°$), which occurs in all phases of high pressure. The rest two parameters will refer to the relative displacement between the molecules and the relative orientation of both chains. By varying these two parameters, the potential energy surface (PES) of the intermolecular interaction of a dimer of palmitic acid has been calculated, including the basis set superposition error (BSSE) correction, which is relevant for this system.

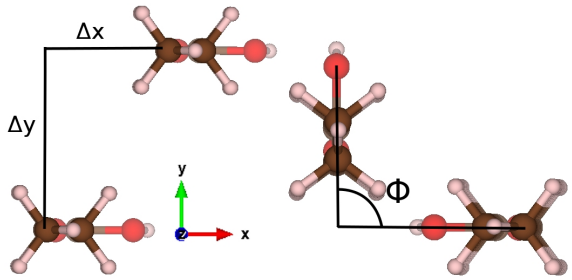

Fig. 1. Relevant parameters of the relative position of the molecules in the dimer.

Using the calculated PES, molecular dynamics simulations have been carried out to find both dynamic and equilibrium properties of this system. By varying the temperature controlled by a thermal bath to the simulation, as well as the concentration of the molecules in the surface, we have obtained different equilibrium structures corresponding to the different phases of the monolayer. Using the Green-Kubo expressions, we have also calculated the shear viscosity of this system at different temperatures. In addition, we compare the calculated value with experimental results, in which an anomalous behavior of the shear viscosity is observed.

[1] J. Echeverría, G. Aullón, D. Danovich, S. Shaik, and S. Alvarez, Dihydrogen contacts in alkanes are subtle but not faint, Nat. Chem. **3**, 323-330 (2011).

[2] S. Tsuzuki, K. Honda, T. Uchimaru, and M. Mikami, Magnitude of interaction between n-alkane chains and its anisotropy: High-level *ab initio* calculations of n-butane, n-pentane, and n-hexane dimers, J. Phys. Chem. A **108**, 10311-10316 (2004).

Engineering non-local correlations in fermionic systems

Hernán Santos[1], José Enrique Alvarellos[2], and Javier Rodríguez-Laguna[2]
[1]Departamento de Física de la Materia Condensada, Universidad Autónoma de Madrid, Cantoblanco, 28049 Madrid, Spain
[2]Departamento de Física Fundamental, Universidad Nacional de Educación a Distancia (UNED), 28040 Madrid, Spain

Large correlations and entanglement constitute two fundamental elements in quantum many-body physics, which are basic resources in quantum communications and computation. As example, the ground states of quantum systems are known to present very interesting entanglement properties indicating by the *area-law* which describes the entanglement entropy of a certain block for gapped systems. Nevertheless, this *area-law* can be maximally violated when systems are gapless. In these cases the entanglement presents a volumetric entanglement, doing it difficult to implement in actual quantum devices. Therefore, for attractive applications a large entanglement preserved by a gapped systems is traced to do real devices in quantum computation [1].

In this work, we have studied large correlations between distant locations and entanglement properties in 1D deformed systems that maximally the gap. The systems studies are mainly finite fermionic chains (top view of Fig. 1). Then, we have established the properties of different systems derived from the previous one (inset in the bottom graph of Fig. 1).

From the Su-Schrieffer-Heeger (SSH) model, we have used machine-learning techniques to obtain the trade-off line between the end-to-end correlations and the energy gap for open chains at half-filling [2]. We find that edge-dimerized chains, where the second and penultimate hoppings are reinforced, are very often close to the optimal configuration.

This pattern is then generalized to provide strongly correlated superlattices on a fermionic chain, characterizing the strongly correlated subsystem via its entanglement properties. From these studies we have introduced the concept of entanglement detachment, i.e., enlarging a few couplings of a Hamiltonian can effectively detach a block within the ground state [3]. Lastly, we show that edge-dimerized legs can induce strong correlations among the extremal sites of a star-graph with a central ring. In this last case, a magnetic flux through the ring can alter significatively the correlations [3], via an analogue of the Aharonov-Bohm effect (see bottom panel of Fig. 1).

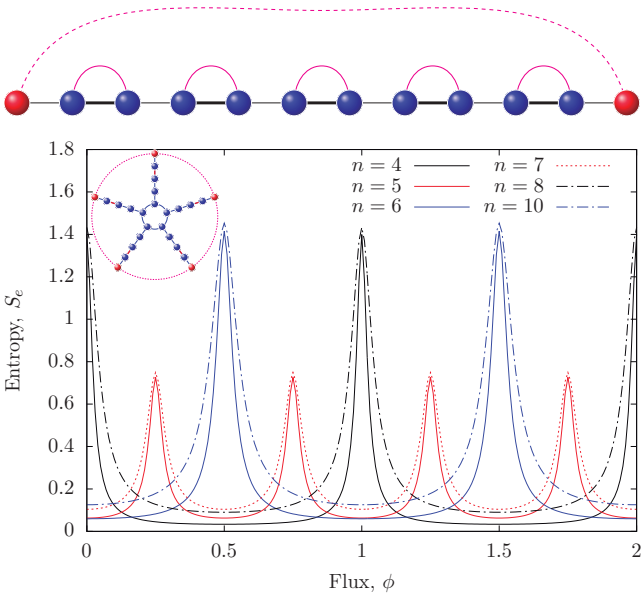

Fig. 1. (Top) Illustration for dimerized fermionic chain with alternate lighter and stronger links. Dashed line represents a large distance correlation between end-to-end sites. (Bottom) Entropy of star-graph system (shown at the upper left corner) as a function of the flux traversing the central ring.

[1] M. A. Nielsen and I. L. Chuang, *Quantum Computation and Quantum Information* (Cambridge University Press, 2018).

[2] H. Santos, J. E. Alvarellos, and J. Rodríguez-Laguna, arXiv:1809.06246.

[3] H. Santos, J. E. Alvarellos, and J. Rodríguez-Laguna, Eur. Phys. J. D (in press) [arXiv:1809.06793].

Correlations between vegetation index and soil moisture index in pasture areas

Ana M. Tarquis[1,2,†], Carmelo Alonso[3], Juan J. Martín-Sotoca[4], and Rosa M. Benito[1]
[1]Grupo de Sistemas Complejos, Universidad Politécnica de Madrid (UPM), Madrid, Spain
[2]Research Center for the Management of Agricultural and Environmental Risks (CEIGRAM), UPM, Madrid, Spain
[3]Earth Observation Systems, Indra Sistemas S.A., Madrid, Spain
[4]Dpto. de Ciencia, Computación y Tecnología, Universidad Europea de Madrid, Villaviciosa de Odón, Spain

The study of the dynamics of the vegetation cover, such as pasture, is the result of a complex interaction between vegetation, soil and climate and man activity. In south Europe, drought has severe consequences in these areas. One aspect to understand it is to characterize the spatial patterns of pasture along the seasons and their relation with soil moisture content.

The normalized difference vegetation index (NDVI) has been used in drought assessment during the last decade. However, some authors question the correlation between NDVI and the soil moisture content measured with the normalized soil moisture index (NSMI). The objectives of this study were to determine whether there are spatial correlations of NDVI with NSMI and how the scales affect them.

To study these correlations, monthly Sentinel-2A images, from July 2015 till August 2016, were processed to extract NDVI and NSMI, with a resolution of 20×20 m. An area was selected, approximately 6.55 km^2 (2.56×2.56 km), and located in a pasture landscape at the north of the Community of Madrid (Spain) between the municipalities of *Soto del Real* and *Colmenar Viejo*.

Correlations of NDVI and the corresponding NSMI pixels were calculate with a resolution of 20×20 m with and without any segmentation. Then, these correlations were up scaling to the whole image. The results showed a different behaviour depending on the NDVI set and the scale used for the correlations.

† E-mail: anamaria.tarquis@upm.es

Lista de participantes

List of Participants

A

1. **Abad Jarillo, Enrique**
Universidad de Extremadura
eabad@unex.es

2. **Aguirre Araujo, Jacobo**
Consejo Superior de Investigaciones Científicas
jaguirre@cnb.csic.es

3. **Alarcón Oseguera, Francisco**
Universidad Complutense de Madrid
franalar@ucm.es

4. **Alcázar Cano, Nerea**
Universidad Autónoma de Madrid
nerea.alcazar@uam.es

5. **Allen-Perkins Avendaño, Alfonso**
Universidad Politécnica de Madrid
alfonso.allen@hotmail.com

6. **Alonso Muñoz, Sergio**
Universitat Politècnica de Catalunya
s.alonso@upc.edu

7. **Arenas, Àlex**
Universitat Rovira i Virgili
alexandre.arenas@urv.cat

8. **Arola Fernández, Lluís**
Universitat Rovira i Virgili
lluis.arolaf@urv.cat

9. **Arranz Saiz, Francisco Javier**
Universidad Politécnica de Madrid
fj.arranz@upm.es

10. **Artime, Oriol**
Universitat de les Illes Balears-CSIC
oriol@ifisc.uib-csic.es

11. **Astillero Vivas, Antonio**
Universidad de Extremadura
aavivas@unex.es

B

12. **Bauzá Mingueza, Francisco**
Universidad de Zaragoza
fbm.prof@hotmail.com

13. **Beltrán de Heredia Rodríguez, Elena**
Universidad Complutense de Madrid
elenabel@ucm.es

14. **Benito Zafrilla, Rosa María**
Universidad Politécnica de Madrid
rosamaria.benito@upm.es

15. **Bianco, Valentino**
Universidad Complutense de Madrid
vbianco283@gmail.com

16. **Borondo Rodríguez, Florentino**
Universidad Autónoma de Madrid
f.borondo@uam.es

17. **Bravo Yuste, Santos**
Universidad de Extremadura
santos@unex.es

18. **Brey Abalo, José Javier**
Universidad de Sevilla
brey@us.es

19. **Brito, Ricardo**
Universidad Complutense de Madrid
brito@ucm.es

20. **Buendía Ruiz-Azuaga, Víctor**
Universidad de Granada
vbuendiar@onsager.ugr.es

21. **Buldú, Javier Martín**
Universidad Rey Juan Carlos
jmbuldu@gmail.com

22. **Burguete, Javier**
Universidad de Navarra
javier@unav.es

C

23. **Calero Borrallo, Carlos**
Universitat de Barcelona
carles.calero@ub.edu

24. **Calero Sanz, Jorge**
Universidad Politécnica de Madrid
jorge.calero.sanz@alumnos.upm.es

25. **Calleja Solanas, Violeta**
Universidad de Zaragoza
violeta.vics@gmail.com

26. **Camargo Trillos, Diego**
Universidad Pontificia Bolivariana
diego.camargo@upb.edu.co

27. **Campo Moreno, Rosa del**
Hospital Universitario Ramón y Cajal
rosacampo@yahoo.com

28. **Campos Moreno, Daniel**
Universitat Autònoma de Barcelona
daniel.campos@uab.cat

29. **Cao García, Francisco Javier**
Universidad Complutense de Madrid
francao@ucm.es

30. **Casanova Ferrer, Pau**
Universidad Carlos III de Madrid
pau.casanova25@gmail.com

31. **Castro Ponce, Mario**
Universidad Pontificia Comillas
marioc@comillas.edu

32. **Català Sabaté, Martí**
Universitat Politècnica de Catalunya
marti.catala@upc.edu

33. **Catalán Fernández, Pablo**
Universidad Carlos III de Madrid
pablocatalanfdez@gmail.com

34. **Cerdà Pino, Joan Josep**
Universitat de les Illes Balears
jj.cerda@uib.cat

35. **Chacoma, Andrés**
Universitat de les Illes Balears-CSIC
andres.chacoma@gmail.com

36. **Chacón García, Ricardo**
Universidad de Extremadura
rchacon@unex.es

37. **Codina Sala, Joan**
Universitat de Barcelona
jocodina@gmail.com

38. **Colet, Pere**
Universitat de les Illes Balears-CSIC
pere@ifisc.uib-csic.es

39. **Colombo, Eduardo Henrique**
Universitat de les Illes Balears-CSIC
ecolombo@ifisc.uib-csic.es

40. **Coluzza, Ivan**
CIC biomaGUNE
icoluzza@cicbiomagune.es

41. **Corbett, Daniel**
University of Manchester
daniel.corbett@manchester.ac.uk

42. **Crespo Miguel, Rodrigo**
Universidad Complutense de Madrid
rodrigocrespo_14@hotmail.com

43. **Cristín Redondo, Javier**
Universitat Autònoma de Barcelona
javier.cristin@uab.cat

44. **Cruz Hidalgo, Raúl**
Universidad de Navarra
raulcruz@unav.es

45. **Cuerno Rejado, Rodolfo**
Universidad Carlos III de Madrid
cuerno@math.uc3m.es

46. **Cuesta, José**
Universidad Carlos III de Madrid
cuesta@math.uc3m.es

D

47. **Delgado Buscalioni, Rafael**
Universidad Autónoma de Madrid
rafael.delgado@uam.es

48. **Díaz de Armas, Ariel**
Universidad Carlos III de Madrid
ardiaza@math.uc3m.es

49. **Díez López, Ángel Luis**
Universidad Complutense de Madrid
angediez@ucm.es

50. **Dinis Vizcaíno, Luis Ignacio**
Universidad Complutense de Madrid
ldinis@ucm.es

51. **Doldán Martelli, Victoria**
Universidad Carlos III de Madrid
vl.doldan@gmail.com

52. **Domínguez Álvarez, Álvaro**
Universidad de Sevilla
dominguez@us.es

53. **Domínguez García, Pablo**
Universidad Nacional de Educación a Distancia
pdominguez@fisfun.uned.es

54. **Duque Zumajo, Diego**
Universidad Nacional de Educación a Distancia
d.duque@fisfun.uned.es

E

55. **Echebarría Domínguez, Blas**
Universitat Politècnica de Catalunya
blas.echebarria@upc.edu

56. **Echeverría Huarte, Iñaki**
Universidad de Navarra
inaki.echeverria.ihs@gmail.com

57. **Escala Vodopivec, Darío Martín**
Universidade de Santiago de Compostela
dmescala@gmail.com

F

58. **Faci Lázaro, Sergio**
Universidad de Zaragoza
sergiofacilazaro@gmail.com

59. **Falo Forniés, Fernando**
Universidad de Zaragoza
fff@unizar.es

60. **Fernández Gallén, Andreu**
Universitat de Barcelona
fdzgallen@gmail.com

61. **Fernández Sánchez, Julio Juan**
Universidad Nacional de Educación a Distancia
jjfernandez@fisfun.uned.es

62. **Fiasconaro, Alessandro**
Universidad de Zaragoza
afiascon@unizar.es

63. **Floría Peralta, Luis Mario**
Universidad de Zaragoza
mario.floria@gmail.com

64. **Fonceca Junior, José Ilberto**
Universidad de Navarra
jfonceca@alumni.unav.es

65. **Franzese, Giancarlo**
Universitat de Barcelona
gfranzese@ub.edu

66. **Fuente Marañón, Rebeca de la**
Universitat de les Illes Balears-CSIC
rebeca@ifisc.uib-csic.es

G

67. **Galeano Prieto, Javier**
Universidad Politécnica de Madrid
javier.galeano@upm.es

68. **Gálvez González, Óscar**
Universidad Nacional de Educación a Distancia
oscar.galvez@ccia.uned.es

69. **García Barreales, Beatriz**
Universidad de Extremadura
beatrizgb@unex.es

70. **García Regueiro, Lucía**
Universidad Politécnica de Madrid
lucia.garcia.regueiro@alumnos.upm.es

71. **García Selfa, David**
Universidade de Santiago de Compostela
david.garcia@usc.es

72. **García Villaluenga, Juan Pedro**
Universidad Complutense de Madrid
jpgarcia@ucm.es

73. **Garcimartín Montero, Ángel**
Universidad de Navarra
angel@unav.es

74. **Gella Bitrián, Diego**
Universidad de Navarra
dgella@alumni.unav.es

75. **González González, Miguel Ángel**
Universidad Complutense de Madrid
miguelangel.gonzalez@ucm.es

76. **González Torre, Iván**
Universidad Politécnica de Madrid
ivan.gonzalez.torre@upm.es

77. **Granell Martorell, Clara**
Universitat de Barcelona
claragranell@gmail.com

78. **Guerrero Borges, Bruno Valdemar**
Universidad de Navarra
bguerrero.3@alumni.unav.es

79. **Gutiérrez, Ricardo**
Universidad Rey Juan Carlos
ricardo.gutierrez@urjc.es

H

80. **Halpaap, Donatus**
Universitat Politècnica de Catalunya
donatus.halpaap@upc.edu

81. **Heras, Daniel de las**
Universität Bayreuth
delasheras.daniel@gmail.com

82. **Hernández, José**
Universidad Autónoma de Madrid
josehermu93@gmail.com

83. **Hernández Delfin, Dariel**
Universidad de Navarra
dhernandezd@alumni.unav.es

84. **Hernández García, Emilio**
Universitat de les Illes Balears-CSIC
emilio@ifisc.uib-csic.es

85. **Hernández Machado, Aurora**
Universitat de Barcelona
a.hernandezmachado@gmail.com

86. **Hurtado Fernández, Pablo Ignacio**
Universidad de Granada
phurtado@onsager.ugr.es

I

87. **Ibañes, Marta**
Universitat de Barcelona
mibanes@ub.edu

J

88. **Jarillo Díaz, Javier**
Universidad Complutense de Madrid
jjarillo@ucm.es

K

89. **Kameke, Alexandra von**
Hamburg University of Technology
alexandra.vonkameke@tuhh.de

90. **Korutcheva, Elka**
Universidad Nacional de Educación a Distancia
elka@fisfun.uned.es

L

91. **Le Vot Granado, Felipe**
Universidad de Extremadura
felipe.levot@gmail.com

92. **Llombart González, Pablo**
Consejo Superior de Investigaciones Científicas
pablollombart@hotmail.es

93. **López Castaño, Miguel Ángel**
Universidad de Extremadura
malopez00@unex.es

94. **López Rodríguez, Diego**
Universidad de Navarra
dlopez.14@alumni.unav.es

95. **López Sánchez, Cristóbal**
Universitat de les Illes Balears-CSIC
clopez@ifisc.uib-csic.es

96. **Losada González, Juan Carlos**
Universidad Politécnica de Madrid
juancarlos.losada@upm.es

M

97. MacDowell, Luis González
Universidad Complutense de Madrid
lgmac@quim.ucm.es

98. Manrubia, Susanna
Consejo Superior de Investigaciones Científicas
smanrubia@cnb.csic.es

99. Manzano, Daniel
Universidad de Granada
manzano@onsager.ugr.es

100. Marchena, Miquel
Universitat Politècnica de Catalunya
miquel.marchena@upc.edu

101. Martín Conde, María
Universidad Complutense de Madrid
mmconde@ucm.es

102. Martínez Fernández, Raúl
Universidad Complutense de Madrid
raumar05@ucm.es

103. Martínez Pedrero, Fernando
Universidad Complutense de Madrid
fernandm@ucm.es

104. Martínez Ratón, Yuri
Universidad Carlos III de Madrid
yuri@math.uc3m.es

105. Masó Puigdellosas, Axel
Universitat Autònoma de Barcelona
axel.maso@uab.cat

106. Masoliver Vila, María
Universitat Politècnica de Catalunya
maria.masoliver@gmail.com

107. Masoller, Cristina
Universitat Politècnica de Catalunya
cristina.masoller@upc.edu

108. Massana Cid, Helena
Universitat de Barcelona
massana@ecm.ub.edu

109. Matias, Manuel Alberto
Universitat de les Illes Balears-CSIC
manuel@ifisc.uib-csic.es

110. Maynar Blanco, Pablo
Universidad de Sevilla
maynar@us.es

111. Maza Ozcoidi, Diego
Universidad de Navarra
dmaza@unav.es

112. Mazo Torres, Juan José
Universidad de Zaragoza
juanjo@unizar.es

113. Mazzoli, Mattia
Universitat de les Illes Balears-CSIC
mattia@ifisc.uib-csic.es

114. Megías Fernández, Alberto
Universidad de Extremadura
albertomegf@gmail.com

115. Meléndez Schofield, Marc
Universidad Autónoma de Madrid
marc.melendez@uam.es

116. Mercadal Melià, Josep
Universitat de Barcelona
josepmercadal@ub.edu

117. Miguel López, María del Carmen
Universitat de Barcelona
carmenmig@gmail.com

118. Montero de Hijes, Pablo
Universidad Complutense de Madrid
pamonter@ucm.es

119. Montes Maldonado, Javier
Universidad Politécnica de Madrid
jmontes.m.163@gmail.com

120. Moreno Ramos, Eduardo
Universitat Politècnica de Catalunya
emr_lalo04@hotmail.com

121. Muñoz García, Javier
Universidad Carlos III de Madrid
javiermunozgarcia@gmail.com

122. Muñoz Martínez, Miguel Ángel
Universidad de Granada
mamunoz@onsager.ugr.es

123. Mussa Juane, Mariamo
Universidade de Santiago de Compostela
mariamomussa@hotmail.com

N

124. Nerattini, Francesca
Universität Wien
francesca.nerattini@univie.ac.at

O

125. Orozco Gámez, Víctor
Universidad Carlos III de Madrid
100373884@alumnos.uc3m.es

126. Ortiz Ambriz, Antonio
Universitat de Barcelona
aortiza@ecm.ub.edu

127. Ortiz de Zárate, José María
Universidad Complutense de Madrid
jmortizz@ucm.es

128. Otero Cacho, Alberto
Universidade de Santiago de Compostela
alberto.otero.cacho@usc.es

P

129. Panzuela Pérez, Sergio
Universidad Autónoma de Madrid
sergio.panzuela@uam.es

130. Parry, Andrew
Imperial College London
a.o.parry@imperial.ac.uk

131. Pastor Ruiz, Juan Manuel
Universidad Politécnica de Madrid
juanmanuel.pastor@upm.es

132. Pérez Espigares, Carlos
Universidad de Granada
cpespigares@gmail.com

133. Pérez Muñuzuri, Alberto
Universidade de Santiago de Compostela
alberto.perez.munuzuri@usc.es

134. Pérez Muñuzuri, Vicente
Universidade de Santiago de Compostela
vperezm.usc@gmail.com

135. Pérez Peláez, Raúl
Universidad Autónoma de Madrid
raul.perez@uam.es

136. Puertas López, Antonio Manuel
Universidad de Almería
apuertas@ual.es

R

137. Ramasco, José Javier
Universitat de les Illes Balears-CSIC
jramasco@ifisc.uib-csic.es

138. Rascón Díaz, Carlos
Universidad Carlos III de Madrid
carlos.rascon@uc3m.es

139. Rebollo Pedruelo, Miguel
Universitat Politècnica de València
mrebollo@upv.es

140. Reguera, David
Universitat de Barcelona
dreguera@ub.edu

141. Revuelta Peña, Fabio
Universidad Politécnica de Madrid
fabio.revuelta@upm.es

142. Riádigos Sánchez, Irma
Universidade de Santiago de Compostela
irma.riadigos@rai.usc.es

143. Rodríguez Díaz, Miguel Ángel
Universidad de Cantabria-CSIC
rodrigma@ifca.unican.es

144. Rodríguez Fernández, Enrique
Universidad Carlos III de Madrid
enrodrig@math.uc3m.es

145. Rodríguez Parrondo, Juan Manuel
Universidad Complutense de Madrid
parrondo@fis.ucm.es

146. Rodríguez Quintero, Niurka
Universidad de Sevilla
niurka@us.es

147. Rodríguez Rivas, Álvaro
Universidad de Extremadura
digitalfis@gmail.com

148. Rogel Rodríguez, Diego
Universidad Complutense de Madrid
drogel@ucm.es

149. Romero Enrique, José Manuel
Universidad de Sevilla
enrome@us.es

150. Rosales Peláez, Pablo
Universidad Complutense de Madrid
pabros01@ucm.es

151. Rubio Álvarez, Miguel Ángel
Universidad Nacional de Educación a Distancia
mar@fisfun.uned.es

152. Ruiz Lorenzo, Juan Jesús
Universidad de Extremadura
ruiz@unex.es

153. Ruiz Reynés, Daniel
Universitat de les Illes Balears-CSIC
druiz@ifisc.uib-csic.es

S

154. San Miguel, Maxi
Universitat de les Illes Balears-CSIC
maxi@ifisc.uib-csic.es

155. Sánchez, Ángel
Universidad Carlos III de Madrid
anxo@math.uc3m.es

156. Sánchez Puga, Pablo
Universidad Nacional de Educación a Distancia
p.sanchez@fisfun.uned.es

157. Sancho, José María
Universitat de Barcelona
josemsancho@gmail.com

158. Santos, Andrés
Universidad de Extremadura
andres@unex.es

159. Santos Expósito, Hernán
Universidad Autónoma de Madrid
hernan.santos@uam.es

160. Sendiña Nadal, Irene
Universidad Rey Juan Carlos
irene.sendina@urjc.es

161. Sintes Olives, Tomás
Universitat de les Illes Balears-CSIC
tomas@ifisc.uib-csic.es

162. Soriano Paños, David
Universidad de Zaragoza
sorianopanos@gmail.com

163. Steinegger, Benjamin
École Polytechnique Fédérale de Lausanne
benjaminsteinegger@gmail.com

T

164. Tamarit, Ignacio
Universidad Carlos III de Madrid
ignacio.tamarit@uc3m.es

165. Tarazona Lafarga, Pedro
Universidad Autónoma de Madrid
pedro.tarazona@uam.es

166. Tarquis Alfonso, Ana María
Universidad Politécnica de Madrid
anamaria.tarquis@upm.es

167. Tejedor Reyes, Andrés
Universidad Complutense de Madrid
andretej@ucm.es

168. Tiana Alsina, Jordi
Universitat Politècnica de Catalunya
jordi.tiana.alsina@gmail.com

169. Tlaie Boria, Alejandro
Universidad Rey Juan Carlos
alejandro.tboria@urjc.es

170. Toledano Sanz, Óscar
Universidad Nacional de Educación a Distancia
otoledano@ccia.uned.es

171. Toral, Raúl
Universitat de les Illes Balears-CSIC
raul@ifisc.uib-csic.es

V

172. Valeriani, Chantal
Universidad Complutense de Madrid
cvaleriani@ucm.es

173. Vázquez Quesada, Adolfo
Universidad Autónoma de Madrid
adolfo.vazquez@uam.es

174. Vega Reyes, Francisco
Universidad de Extremadura
fvega@unex.es

175. Vida Delgado, Rafael Ángel
Universidad Politécnica de Madrid
ra.vida@alumnos.upm.es

176. Villarrubia Moreno, Daniel
Universidad Complutense de Madrid
danvilla@ucm.es

177. Vilone, Daniele
Consiglio Nazionale delle Ricerche
daniele.vilone@gmail.com

W

178. Witt, Annette
Max-Planck-Institut
annette.witt@ds.mpg.de

Z

179. Zappalà, Dario
Universitat Politècnica de Catalunya
dario.a.zappala@gmail.com

180. Zaragoza de Lorite, Alberto
Universidad Complutense de Madrid
azlorite@ucm.es

181. Zuriguel, Iker
Universidad de Navarra
iker@unav.es

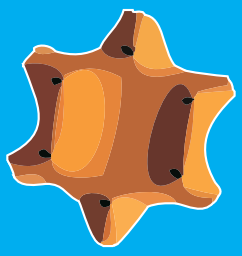

Organizado por/*Organized by*

GRUPO DE SISTEMAS COMPLEJOS
UNIVERSIDAD POLITÉCNICA DE MADRID

POLITÉCNICA

ETSI Agronómica, Alimentaria
y de Biosistemas

Bajo el auspicio de/*Under the aegis of*

GEFENOL
Grupo especializado en Física Estadística y no Lineal

R.S.E.F.